# ION PROCESSES AND EFFECTS IN $CO_2$ LASER DISCHARGES

Henry Shields

A Thesis Submitted for the Degree of PhD
at the
University of St Andrews

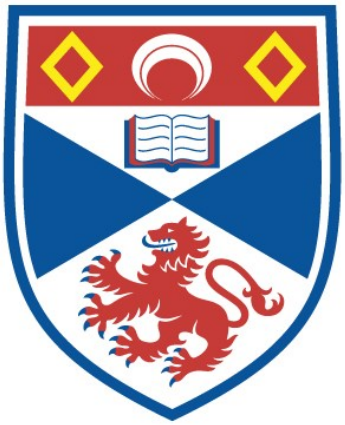

1987

# ION PROCESSES AND EFFECTS IN $CO_2$ LASER DISCHARGES

A thesis

presented by

H Shields, BSc

to the

University of St Andrews

in application for the Degree

of Doctor of Philosophy.

Th 9235

ABSTRACT

Presently, a major factor restricting the achievement of higher power outputs from the $CO_2$ laser is the occurrence of plasma instability. This instability may manifest itself in two forms causing either discharge striations (ionisation instability) or, more importantly, discharge arcing (thermal instability). Recent experimental and theoretical work has identified these instabilities with the electron and ion kinetics of the $CO_2$ laser discharge.

The $CO_2$ laser discharge, its development for high power output and the conditions leading to the two types of instability are reviewed. The requirement for full data on electron and ion processes for discharge modelling is clearly established.

The techniques involved in mass spectrometric analysis of ions in gas discharge plasmas are reviewed and subsequently applied to the $CO_2$ laser discharge. The major processes affecting the positive ion species in $CO_2$ laser plasmas are determined in this way.

The important negative ion species in the $CO_2$ laser plasma are most easily and comprehensively determined by computational methods. These methods have allowed considerable insight into the dominant negative ion processes of the $CO_2$ laser discharge. By application to specific laser situations correlation has been shown to exist between ion densities and the onset of experimentally observed discharge instability.

The elucidation of the main ion processes, both by mass spectrometer and computer, has contributed detailed information for modelling of the $CO_2$ laser discharge, and its instabilities, in a variety of configurations.

ACKNOWLEDGEMENTS

I wish to express my thanks to Dr A L S Smith for his careful supervision of the work presented herein, and for his invaluable help, advice and criticism during the preparation of this thesis. Also I am indebted to Mrs Norma Pacholek for her care in typing the manuscript. Finally, thanks are due to my wife, Miranda, for her encouragement and patience while writing was in progress.

## CAREER

Henry Shields was born in Glasgow, Scotland on 23 June 1952. He received secondary education at Whitehill School, Glasgow and in 1973 was awarded a BSc degree with First Class Honours in Physics by Strathclyde University. After completion of the experimental work for this thesis at St Andrews University, he worked as a Research Fellow at St Andrews on waveguide $CO_2$ lasers. He is now with the Laser Development Group, at Ferranti, Dundee.

## DECLARATION

I hereby certify that this thesis has been composed by me, and is a record of work done by me, and has not previously been presented for a Higher Degree.

This research was carried out in the Physical Science Laboratory of St Salvator's College, in the University of St Andrews, under the supervision of Dr A L S Smith.

H Shields

CERTIFICATE

I certify that H Shields, BSc, has spent nine terms at research work in the Physical Science Laboratory of St Salvator's College, in the University of St Andrews, under my direction, that he has fulfilled the conditions of Ordinance No 16 (St Andrews) and that he is qualified to submit the accompanying thesis in application for the Degree of Doctor of Philosophy.

Dr A L S Smith
Research Supervisor

CONTENTS

# CHAPTER ONE

# THE DEVELOPMENT OF HIGH-POWER CARBON DIOXIDE LASERS

## 1.1 INTRODUCTION

Laser operation using carbon dioxide gas was first demonstrated by Patel (1964(a) and (b)). Infra-red radiation was produced at a power of ∿1mW continuous-wave (c w ) and an electrical to optical power conversion efficiency of $\sim 10^{-3}$%. Since then advances in laser design and technology have realised output powers >10kW and efficiencies up to ∿25%. $CO_2$ lasers have found applications in cutting, drilling and welding of materials, optical ranging and radar, communications, laser surgery, isotope separation, laser fusion, pollution monitoring and spectroscopy. The diversity of these applications indicates the versatility and importance of the $CO_2$ laser.

The most commonly used transition of the $CO_2$ molecule for laser action is that occurring between the 001 asymmetric stretching vibrational level and the 100 symmetric stretching vibrational level, at ∿10.6μm . The vibrational energy levels of the $CO_2$ molecule are illustrated in figure 1.1.1 which omits the rotational substructure for simplicity.

Population inversion, such that the number of molecules in the 001 upper laser level is greater than that in the 100 lower laser level, may be produced by several means but is usually achieved by excitation in an electrical discharge. As the $CO_2$ laser has developed, so too has the understanding of the various discharge configurations used to excite the gas.

The development of the laser for high power and efficiency has depended on the design of discharge configurations capable of allowing high electrical power densities being deposited in the gas at the highest possible pressure and minimum increase in gas temperature. Discharge configurations commonly used in $CO_2$ laser design are discussed in section 1.2, while the physical principles involved in producing high

power and efficiency are discussed in section 1.3.

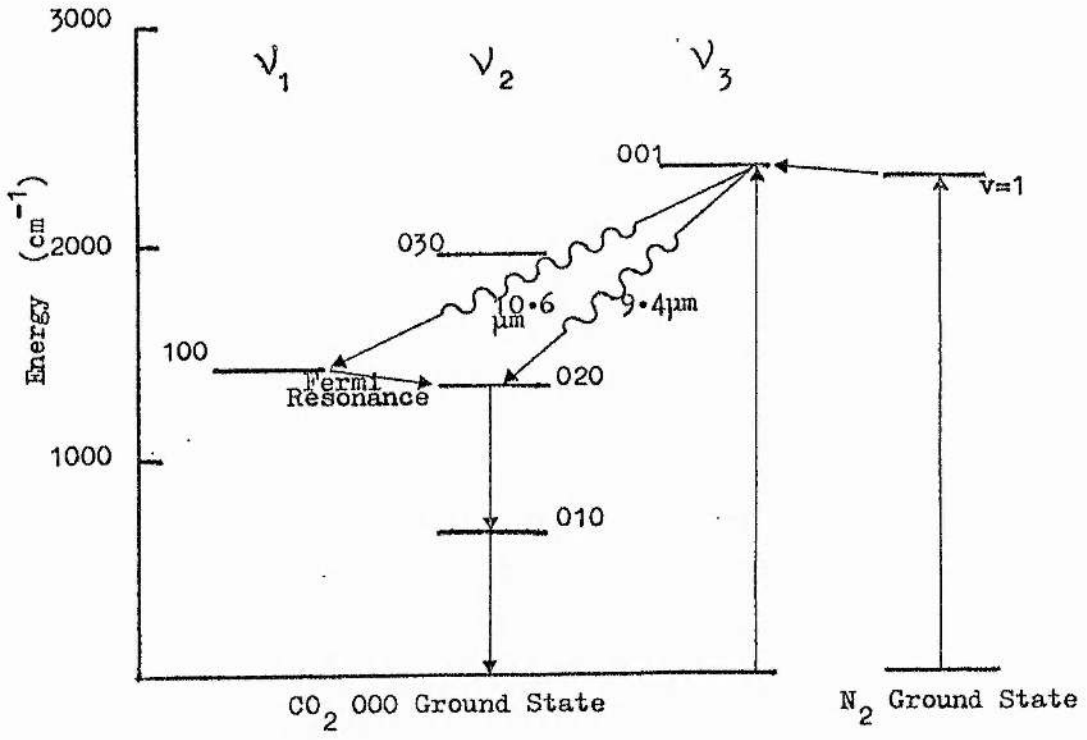


Figure 1.1.1 Energy level diagram of important vibrational levels in $CO_2$ and $N_2$ for laser action.

In practice it is found that even though a particular laser design allows the use of high gas pressure, and provides adequate gas cooling, the electrical input power density may not be increased to the limit predicted by theory. When large quantities of power are delivered to the laser gas, the discharge becomes unstable, limiting the input power density to levels which allow uniform electrical excitation of the gas. Such input power levels are considerably greater than those encountered in traditional glow discharge physics, although they are common in arc discharges. Thus, techniques to maintain stable glow

discharges at high input power densities as in high power $CO_2$ lasers, have had to be investigated and developed. In section 1.4 the operation of a steady-state, stable $CO_2$ laser discharge is described. Discussion of the two plasma instabilities of greatest importance to the high power $CO_2$ laser - the ionisation instability and the thermal instability - is presented in section 1.5.

It will become apparent that the efficiency and electrical stability of the $CO_2$ laser are determined by processes associated with the electron kinetics in the discharge (eg. elastic and inelastic electron - molecule collisions, ionisation, etc) and are thus characterised by a scale size of the order of an electron mean free path. This may be contrasted with the considerable size of a high power laser including gas handling equipment, electrical power source, laser cavity, etc. Nevertheless, as will be shown in this chapter, it is the understanding and control of the fundamental electron and ion processes which have greatest influence on laser performance.

## 1.2 CARBON DIOXIDE LASER DISCHARGE CONFIGURATIONS

### 1.2.1 Conventional Axial Flow Lasers

The initial $CO_2$ laser of Patel (1964(b)) producing $\sim$1 mW cw power used a dc electrical discharge to excite "pure" $CO_2$ gas. The laser gas flowed along a cooled cylindrical discharge tube and conventional dc glow discharge excitation techniques were employed. Subsequent $CO_2$ lasers were based on this design and a typical laser of this type is shown schematically in figure 1.2.1. Operating characteristics of these devices depend on the dimensions of the discharge tube and the gas mixture used but for a 2.5 cm diameter tube of 1m length, a gas pressure of $\sim$10 torr, discharge current density $\sim$10mA $cm^{-2}$ and voltage of $\sim$10kV are typical.

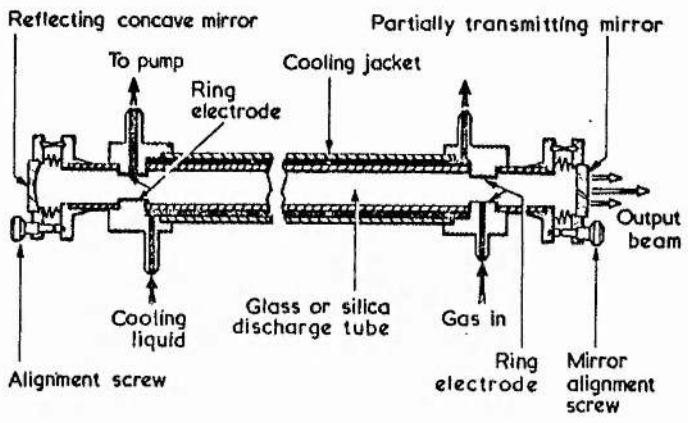


Figure 1.2.1 The conventional $CO_2$ laser - dc electrical excitation in a cooled cylindrical tube and slow axial gas flow (from Foster (1972)).

After the initial experiment of Patel nitrogen was added to the flowing $CO_2$ (Patel (1964(b)), Legay-Sommaire et al (1965)). The v = 1 vibrational level of the $N_2$ molecule has a wave number of 2330.7 $cm^{-1}$ which is only $\sim$ 18 $cm^{-1}$ less than the 001 asymmetric stretch upper laser level and this difference is much less than the average molecular thermal energy (kT $\sim$ 210 $cm^{-1}$ at 300K). Thus these two levels are effectively in resonance and since the nitrogen molecule has no permanent dipole moment the transition from the v = 1 level to the ground state (v = 0) is forbidden (Herzberg (1960)). The nitrogen (v = 1) level can enhance the 001 upper laser level population by resonant energy transfer to ground state $CO_2$ molecules (Figure 1.1.1). The increase in population inversion produced by this means led to much improved performance, giving $\sim$ 10W cw output from a 2m long laser at a conversion efficiency of $\sim$ 3% (Patel (1965)).

The next advance in $CO_2$ laser development was the addition of helium to the $CO_2$-$N_2$ mixture. Moeller and Rigden (1965) found that addition of He to pure $CO_2$ gave greater power increase than did $N_2$ addition. However, Patel et al (1965) obtained even better performance from a 3-component,

$CO_2$-$N_2$-He mixture, achieving a cw power of 106W from a 2.3m long device at 6% efficiency.

It has been established that He performs several beneficial functions in the $CO_2$ laser gas mixture. First, He assists the achievement of population inversion by collisionally depopulating the lower laser levels (Figure 1.1.1). The collisional de-excitation of the $CO_2$ 010 and 020 levels by He has been shown to be an efficient process (Taylor and Bitterman (1969)). Second, the high thermal conductivity of He improves heat conduction from the gas to the cooled walls and a correspondingly reduced thermal population of the 010 level (Laderman and Byron (1971)). Finally, and most importantly, He lowers the E/N (electric field to gas density ratio) at which the discharge operates and improves the excitation efficiency of the upper laser level (see section 1.3). Thus a gas mixture of $CO_2$, $N_2$ and He is now widely used as the laser medium for high power $CO_2$ lasers.

In early devices, the flowing gas minimised loss of $CO_2$ by electron impact dissociation, forming CO and $O_2$ in the process.

$$CO_2 \rightleftharpoons CO + \tfrac{1}{2}O_2$$

Advances in understanding of plasma chemical processes, particularly those resulting in reformation of $CO_2$ from CO and $O_2$, led to long-life sealed lasers (Carbone (1967), Witteman (1967), Dumitras et al (1976)).

The application of discharge scaling laws has resulted in the development of waveguide $CO_2$ lasers operating in a discharge configuration similar to conventional lasers but at tube diameters of $\sim$1-2 mm and pressures of $\sim$100 - 200 torr (Bridges et al (1972), Degnan (1976)). These lasers offer the attractions of compactness and larger tuning range resulting from the increase in pressure-broadened linewidth at the higher pressures.

$CO_2$ lasers of the conventional longitudinal discharge type discussed

in this section have the property that the output power scales approximately with the discharge length, assuming gas temperature and $CO_2$ dissociation equilibria exist over most of the discharge. Thus a cw power output of 1 kW requires a discharge of $\sim$ 30m. While this power may be produced with a conventional design of laser, other techniques have been developed specifically for high power, relatively compact devices. Lasers using convective cooling of the gas and volume excitation mechanisms are described in the next section. Such lasers have achieved many kilowatts output from comparatively small discharge volumes.

1.2.2 Convection Cooled Lasers

The conventional, axial flow discharge configuration suffers from two serious disadvantages when used as a high power laser source.

Firstly, since the transition from the 100 lower laser level to the $CO_2$ ground state takes place via the 010 level (Figure 1.1.1), significant thermal population of this level at high gas temperature causes a "bottlenecking" effect which limits the achievable population inversion between the 001 and the 100 laser levels. In the conventional $CO_2$ laser gas cooling is achieved by thermal diffusion to the cooled walls, mainly by high thermal conductivity helium. In order to achieve high power output it is necessary to input high electrical powers, and since the thermal conductivity is, to a first approximation, independent of power input, the temperature of the laser medium increases degrading the population inversion and limiting the output power.

The second deficiency of the conventional design is that at the low flow rates employed the down-stream penetration of fresh, cool gas is minimal. Most of the gas has reached a thermal equilibrium such that the thermal "bottlenecking" effect limits the output power. However this

second effect indicates how the problem of achieving very high output powers can be solved. Since the requirement is essentially to maintain a sufficiently low gas temperature that significant thermal population of the 010 level does not occur, then rapidly flowing the gas through the discharge zone, such that gas is expelled from the discharge before reaching thermal equilibrium, minimises the thermal influence on the lower laser level population. This is the principle of the Electric Discharge Convection Laser (EDCL).

Many designs producing multikilowatt cw power using convective cooling have been reported in the literature (eg. Tiffany et al (1969), Eckbreth and Davis (1971), Hill (1971), Brown and Davis (1972)). Figure 1.2.2 shows the configuration employed by Eckbreth and Davis (1971) to produce ∿2kW cw power. This system uses a rectangular discharge design (60 cm x 2.5 cm area , 1 m length), multiple pass optics and gas flow velocity of ∿ 100m $s^{-1}$. Similar techniques, but with larger volumes, faster gas flow and higher power inputs, have been demonstrated by Hill (1971), and Brown and Davis (1972) , yielding ∿20 kW cw power.

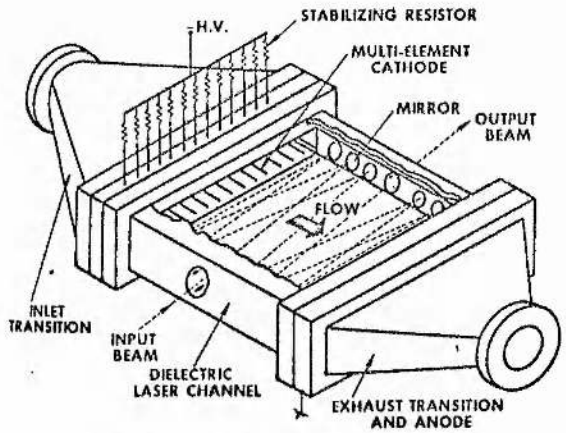


Figure 1.2.2 The convectively cooled $CO_2$ laser design of Eckbreth and Davis (1971) which has produced ∿2kW cw power.

De Maria (1973) has developed a two-level model which illustrates the advantages of using convective gas cooling for high power lasers. This simplified model applies to a pressure-broadened pair of vibrational levels with populations $N_1$ and $N_2$ in the lower and upper levels, respectively. These levels are pumped by the discharge at volumetric rates $R_1$ and $R_2$. Collisional relaxation times for the two levels are $\tau_1$ and $\tau_2$, and the flow of gas through the discharge takes a time $\tau_F$. $N_{10}$ and $N_{20}$ are the lower and upper level populations in the absence of stimulated emission and $(N_{20} - N_{10})$ represents the population inversion before stimulated emission has depleted the upper level and filled the lower. The thermal "bottlenecking" is thus described by the increase of the lower level population from $N_{10}$ to $N_1$ due to stimulated emission. The laser intensity in the gas is I, $h\nu$ is the energy of a laser photon and $\sigma$ is the stimulated emission cross-section. When little thermal population of the levels occurs (gas temperature $\lesssim$ 400K for the $CO_2$ laser - see section 1.3.3), the rates of change of populations are,

$$\frac{dN_1}{dt} = R_1 - \frac{N_1}{\tau_1} + (N_2 - N_1)\frac{\sigma I}{h\nu} + \frac{(N_{10} - N_1)}{\tau_F}$$

$$\frac{dN_2}{dt} = R_2 - \frac{N_2}{\tau_2} - (N_2 - N_1)\frac{\sigma I}{h\nu} + \frac{(N_{20} - N_2)}{\tau_F} \qquad (1.2.1)$$

The terms represent pumping by the discharge, collisional relaxation, stimulated emission and the flow of fresh gas through the laser.

Under equilibrium conditions with constant output intensity, gas flow rate and pumping rate, $\frac{dN_1}{dt} = \frac{dN_2}{dt} = 0$. Hence, noting that the population of level 1 in the absence of stimulated emission is $R_1\tau_1$ in equilibrium, (ie. $N_{10} = R_1\tau_1$) and $N_{20} = R_2\tau_2$, then

$$\alpha = \sigma(N_2 - N_1) = \frac{\sigma(R_2\tau_2 - R_1\tau_1)}{1 + \frac{I\sigma}{h\nu}\left[\frac{\tau_2\tau_F}{(\tau_2+\tau_F)} + \frac{\tau_1\tau_F}{(\tau_1+\tau_F)}\right]} \qquad (1.2.2)$$

where $\alpha$ is the gain coefficient of the medium.

When there is no stimulated emission intensity then

$$\alpha = \alpha(0) = \sigma(N_{20} - N_{10}) = \sigma(R_2\tau_2 - R_1\tau_1), \qquad (1.2.3)$$

and $\alpha(0)$ is the small signal gain coefficient. Defining the saturation intensity, $I_s$, as

$$I_s = \frac{h\nu}{\sigma} \cdot \frac{1}{\left[\frac{\tau_2\tau_F}{(\tau_2+\tau_F)} + \frac{\tau_1\tau_F}{(\tau_1+\tau_F)}\right]}, \qquad (1.2.4)$$

then,

$$\alpha = \frac{\alpha(0)}{1 + I/I_s} \quad . \qquad (1.2.5)$$

Thus, for slow flow ($\tau_F \gg \tau_1, \tau_2$),

$$I_s \simeq \frac{h\nu}{\sigma(\tau_2+\tau_1)} \quad . \qquad (1.2.6)$$

and, for fast flow ($\tau_F \ll \tau_1, \tau_2$),

$$I_s \simeq \frac{h\nu}{2\sigma\tau_F} \quad , \qquad (1.2.7)$$

which results in an increase in saturation intensity by a factor of $(\tau_1+\tau_2)/2\tau_F$, and shows that saturation intensity increase is proportional to gas flow velocity for fast flows.

As equation (1.2.5) shows the gain coefficient increases as the saturation intensity increases resulting in a large potential output from a fast flow device.

The most serious restriction on the development of the E.D.C.L. has been the tendency for the uniform glow excitation discharge to collapse to

one, or more, high current density arcs (Eckbreth and Davis (1971)). Detailed analysis of the fundamental electron and ion processes in the discharge has led to an understanding of the cause of this "thermal" instability (Nighan and Wiegand (1974(a)) and of other discharge instabilities (Nighan and Wiegand (1974(b)), Haas (1973)). Hence techniques have been developed which have improved discharge stability over a wide range of operating conditions. These include rf augmentation of the discharge (Brown and Davis (1972)) and electron beam irradiation (see section 1.4.2).

The fast gas flows required for convective cooling and the relatively large volume of the EDCL result in large quantities of gas being used in these devices. In order to avoid the excessive cost of constantly replenishing the gas, gas recirculation is employed. Thus, previously discharged gas is flowed through heat exchangers and pumps and re-injected to the discharge. In this way, contaminants created by plasma chemical reactions in the discharge accumulate in the laser gas, until an equilibrium is established.

These contaminants can have a considerable effect on the electrical properties of the discharge (see sections 1.4 and 1.5) and it has been experimentally observed that recycled gas must flow more rapidly through the discharge than fresh, clean gas if the onset of plasma instability is to be avoided (Hill (1971), Eckbreth and Owen (1972)).

### 1.2.3 High Pressure Pulsed Lasers

As the EDCL was being developed, so too were techniques for obtaining laser action from $CO_2$-$N_2$-He gas mixtures in a pulsed mode at, or near, atmospheric pressure. The attractions of high pressure operation are the higher output powers resulting from increased $CO_2$ density and the increase in the pressure-broadened linewidth giving greater wavelength tunability. However the increase in the discharge gap breakdown voltage

with pressure, and the difficulties encountered in maintaining a stable glow discharge at high pressure, have dictated a design where the inter-electrode spacing is relatively small (∿ few cms) and the discharge is pulsed. Figure 1.2.3 shows a common design of TEA laser (Transverse Electric excitation, Atmospheric pressure).

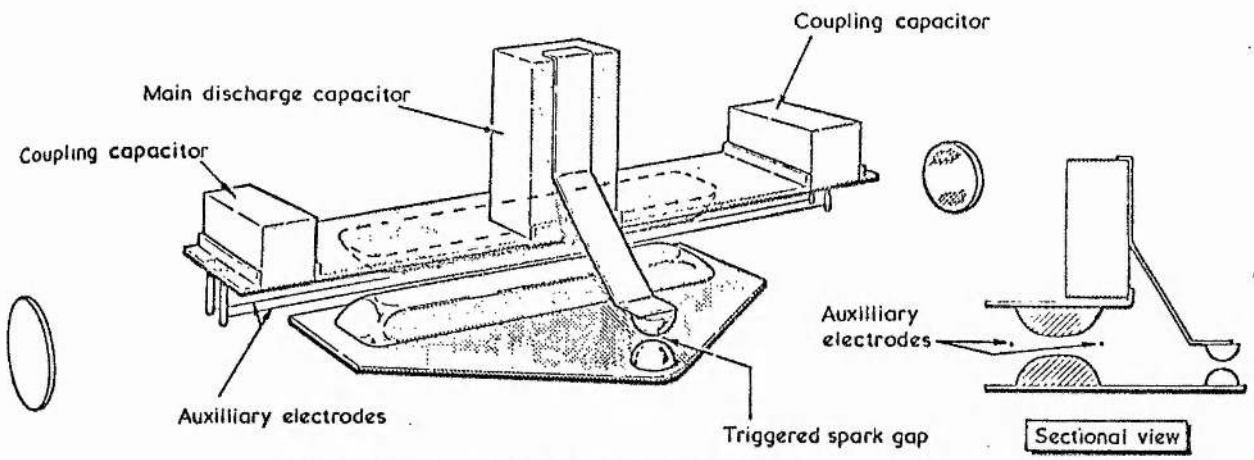


Figure 1.2.3 Schematic diagram of the TEA laser design of Lamberton and Pearson (1971) (from Foster (1972)).

Early designs for high pressure operation used multi-component electrode structures to produce a quasi-glow discharge (eg Beaulieu (1970)) however a greater volume of gas can be excited using solid electrodes. Successful use of solid electrodes was first reported by Lamberton and Pearson (1971) who achieved glow discharges of ∿100 ns duration using electrodes profiled for electric field uniformity and trigger wires to provide preionisation of the discharge gap (see figure 1.2.3).

As with the EDCL one advantage of the TEA laser is the increase in saturation intensity which it offers over that obtainable with the conventional laser design (section 1.2.1). From equation (1.2.6)

$$I_s = \frac{h\nu}{\sigma(\tau_1+\tau_2)} \qquad (1.2.8)$$

for slow, or zero gas flow. The stimulated emission cross-section, $\sigma$, decreases with increasing pressure for the case when the laser line is pressure-broadened (Bullis et al (1972)). Also collisions occur more frequently at high pressure resulting in shorter $\tau_1$ and $\tau_2$, thus the saturation intensity increases with pressure. The gain coefficient $\alpha = \sigma(N_2 - N_1)$ is approximately constant for a pressure-broadened line, and the optical power density of the medium ($\alpha I_s$) is increased at high pressure. Thus a high output power is potentially available from an atmospheric pressure device. For reasons concerned with the electrical discharge stability, this type of laser cannot be operated in a cw mode, nevertheless pulsing the discharge at frequencies $\sim$100 pulses per second, with rapid gas flow cooling, has enabled mean output powers of $\sim$2k W to be produced. This is considerably less than the single pulse peak power of $\sim$ 100MW of the same device (Dumanchin et al (1972)).

In order to prevent the uniform glow discharge required for laser excitation from rapidly degenerating into high current density arcs, several design features have become characteristic of TEA lasers. These include the use of profiled electrodes, shaped for uniform electric field in the discharge gap (Rogowski (1923), Bruce (1947), Chang (1973)), and the provision of some means of preionisation of the discharge medium. Palmer (1974) has shown that a preionisation electron density of $\sim 10^4$ cm$^{-3}$ is necessary before the main discharge can occur in the glow discharge form. Techniques successfully used to preionise the gas have included uv induced photo-emission from a solid cathode (Pearson and Lamberton (1972)), volumetric uv photoionisation where the uv radiation is produced by an array of spark discharges (Richardson et al (1973)) and electron-beam ionisation of the laser medium (section 1.4.2). Wood (1974) has reviewed these and other similar techniques for operation of TEA lasers.

The electron-beam technique has been most successful in extending the duration of the discharge pulse while still maintaining discharge stability. However it is also by far the most expensive means of stabilizing the glow discharge. The role of external ionisation is discussed in detail in sections 1.4.2 and 1.5.

## 1.3 LASER OUTPUT AND EFFICIENCY

### 1.3.1 Pumping Efficiency

The maximum attainable efficiency of the $CO_2$ laser operating on the 10.6μm transition is 41% - the quantum efficiency, defined as the ratio of the laser photon energy to the energy required to excite the upper laser level of a molecule. In practice such an efficiency cannot be achieved since input electrical energy not only pumps the upper laser level but also is dissipated in gas heating, electronic excitation of gas molecules and ionisation. Indeed it is necessary that a fraction of the electrical energy results in sufficient ionisation to sustain the discharge.

Present knowledge of the electron kinetic processes relevant to an electrically excited $CO_2$-$N_2$-He gas mixture is sufficiently advanced that numerical solution of the Boltzmann equation yielding the electron energy distribution has been possible (Nighan (1970), Judd (1974)). These processes include electron-neutral collisions (resulting in elastic scattering, rotational, vibrational and electronic excitation, ionisation and electron attachment), electron-ion interactions (resulting in recombination) and electron-electron scattering. The resulting non-Maxwellian electron energy distribution for a particular gas mixture reflects the complexity of the electron kinetics resulting from the atomic and molecular energy levels of the laser gas mixture.

The relative importance of the various electron interaction processes as the discharge E/N (E = electric field, N = gas density) is varied has

been calculated by Nighan (1970) for a 10-10-80, $CO_2$-$N_2$-He mixture by averaging the appropriate cross-sections over the electron energy distribution - see figure 1.3.1. Similar calculations have been performed by Judd (1974). Since the energy gained from the electric field, by an electron between collisions is $eE\lambda$ (where e is the electronic charge and $\lambda$ is the mean free path), and since $\lambda$ is inversely proportional to gas density, N, the parameter E/N is a measure of the average energy gained by the electrons from the electric field.

Figure 1.3.1 shows that as much as 70% of the electrical energy input to the gas can be channelled into the $CO_2$(001) upper laser level and the $N_2$ (v = 1-8) vibrational levels at E/N $\sim$ 1 x $10^{-16}$ V $cm^2$, in a 10-10-80, $CO_2$-$N_2$-He mixture. The $N_2$ vibrational levels can efficiently populate the upper laser level by

$$CO_2\ (000) + N_2\ (v) \longrightarrow CO_2\ (001) + N_2\ (v-1),$$

thus $\sim$ 70% efficient population of the upper laser level is possible. Given the corresponding excitation efficiency of the $CO_2$ (100) lower laser level of $<$ 10% and the quantum efficiency of 41%, then an overall optimum laser efficiency of $\sim$25% is possible at optimum E/N.

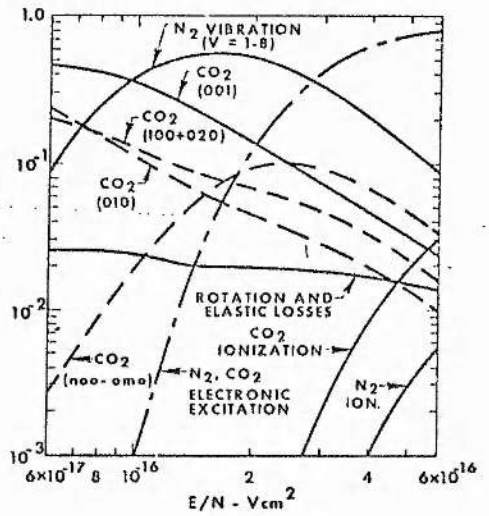


Figure 1.3.1 Fractional transfer of electrical input power as a function of E/N, calculated for a 10-10-80, $CO_2$-$N_2$-He gas mixture (Bullis et al, (1972)).

However, as figure 1.3.1 shows, the fraction of input energy which is deposited in the ionisation process is extremely small at values of E/N where vibrational pumping of the upper laser level is efficient, and the discharge can only sustain itself at higher E/N values. This difficulty may be overcome by providing the ionisation by some means other than from the pumping electric field, eg. electron-beam assisted lasers (see section 1.4.2). Thus a discharge which provides its own ionisation - a self-sustained discharge - results in a laser efficiency of less than the optimum 25%.

The increase in laser efficiency made possible by using an external ionisation source and operating at the optimum E/N for vibrational pumping may be offset by the additional energy required to drive the external source. However, when very high output powers are required, large power input densities must be deposited in the gas. Section 1.5 shows that high input power densities can result in discharge instabilities but that additional stability may be achieved using an external source of ionisation. The scaling of discharge input power density for high power devices is discussed in the next section.

1.3.2 Input Power Density

The efficiency of a high power $CO_2$ laser has been demonstrated to remain $\sim$ 10-20% at high input powers, provided adequate gas cooling exists (Brown and Davis (1972)). This has enabled power outputs exceeding 20 kW cw to be achieved from electrical input powers of $\sim$ 150 kW. The factors which determine the scaling of power input and hence, at constant efficiency, power output are considered in this section.

For a discharge current density of J and an electric field intensity E, the input power density of the discharge is

$$JE = n_e \, e \, v_d \, E$$

$$= \left[\frac{n_e}{N} \, e \, v_d \, \frac{E}{N}\right] N^2, \qquad (1.3.1)$$

where $n_e$ is the electron density, e is the electronic charge, $v_d$ is the electron drift velocity and N is the neutral particle number density. As discussed in the previous section (1.3.1) the E/N value will be fixed such that sufficient ionisation occurs in a self-sustained laser discharge or such that optimum vibrational pumping occurs in an ionisation assisted device (see section 1.4 for discussion of the operating E/N of the discharge). Lowke et al (1973) have found the electron drift velocity to be approximately proportional to E/N, and for a fixed gas mixture is thus constant for a fixed E/N.

Experimentally it is found that for a given operating pressure of a laser (ie. a given number density, N) output power is optimised for a particular discharge current density (ie. a particular electron density, $n_e$). This occurs, since at low currents, electron pumping of the upper laser level is weak while at high currents electron pumping is strong but gas heating significantly populates the lower laser level (section 1.3.3). Similarly, low pressures result in slow collisional depopulation of the lower laser level while high N values require high electric fields to maintain the same E/N value. The increase in E results in greater power input and higher gas temperature. Thus, for a given pressure, gas mixture and flow rate the optimum $n_e/N$ value is fixed for the laser discharge usually in the range $10^{-7} - 10^{-8}$.

Hence, when the gas mixture is specified all the parameters in square brackets in equation (1.3.1) are approximately constant, and the input power density scales with the square of the gas pressure. Brown and Davis (1972)

in depositing 160 kW power in their discharge configuration, producing a laser output power of 27 kW, achieved a power density of 2W $cm^{-3}$ at 30 torr. At atmospheric pressure, this would enable an input power density of $\sim$ 1.2 kW $cm^{-3}$ to be attained and a corresponding increase in output power. However such feats are limited by the onset of discharge instabilities (section 1.5).

The scaling indicated by equation (1.3.1) predicts high input power density and thus a high output power from a laser assuming the laser efficiency is unchanged as the input power is increased. As the next section shows this assumption is one of constant gas temperature and is not always valid. Nevertheless equation (1.3.1) indicates the desirability of operation at high gas pressure for the attainment of high laser power.

1.3.3 Gas Temperature Effects

Preceding sections have shown that high power output and efficiency require both high input power and optimisation of the discharge E/N for efficient pumping of the appropriate vibrational energy levels in $CO_2$ and $N_2$. However the $CO_2$ laser is known to be highly sensitive to gas temperature, and the population inversion that is produced in a device depends not only on efficient vibrational pumping and deposition of input energy in the upper laser level but also on the efficiency of gas cooling.

The most important effect of gas cooling arises from the exponential dependence of vibrational populations on gas temperature. De Maria (1973) has computed the temperature variation of the populations of the vibrational levels of $CO_2$ (figure 1.3.2). The calculation assumes that all levels except the 001 upper laser level are in thermal equilibrium with the gas and that 3% of the $CO_2$ molecules are maintained in the 001 level by collisions with $N_2(v=1)$. The Fermi resonance between the 100 and 020 levels

(figure 1.1.1) and the rapid decay from the 020 level to the 010 level allow these three levels to be described by the same temperature. However they may only be considered to be in thermal equilibrium with the 000 ground state if efficient collisional relaxation of the 010 level occurs (eg. by He or $H_2O$). Assuming this condition to be satisfied, De Maria computes a sharp decrease in the population inversion ($N_{001} - N_{100}$) at temperatures above $\sim$ 500K.

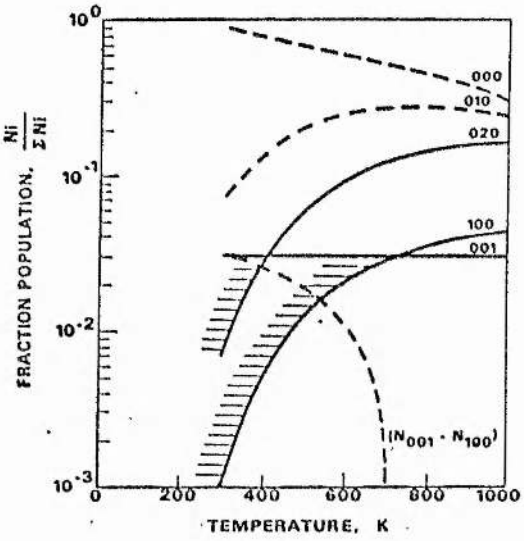


Figure 1.3.2 Fractional populations of the lower $CO_2$ vibrational levels by gas heating. Collisions with $N_2(v=1)$ are assumed to maintain a 30% fractional population of the $CO_2$ (001) level. (from De Maria (1973)).

A similar estimate of the maximum allowable gas temperature has been made by Fowler (1972) from considerations of the temperature dependence of the small signal gain $\alpha_o$, the saturation intensity $I_s$ and the maximum optical power density of the medium $\alpha_o I_s$. The small signal gain is proportional to the population inversion (equation 1.2.2) and rapidly decreases above temperatures of $\sim$ 500-600K. The saturation intensity increases due to decreased collisional depopulation times and stimulated emission cross-section (Bullis et al (1972)) as temperature increases (equation 1.2.6)). However the saturation intensity is much less sensitive

than $\alpha_o$ to temperature variation and thus the effect of gas temperature on optical power density $\alpha_o I_s$ is as shown in figure 1.3.3 (from Fowler (1972)). Thus $T \lesssim 600K$ is required for efficient laser action.

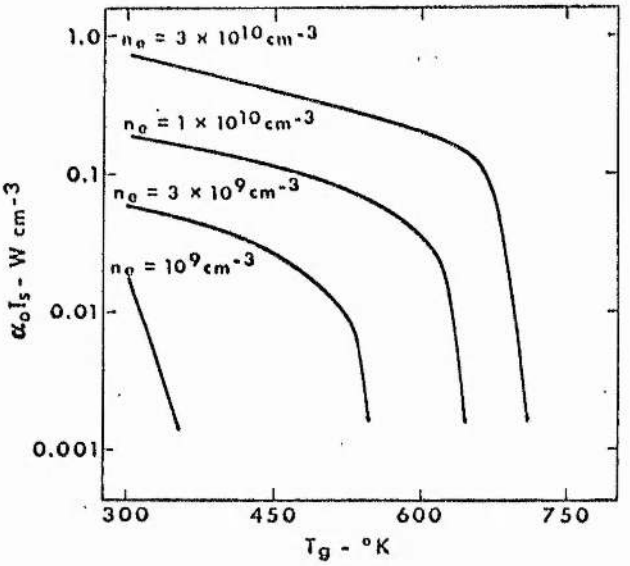


Figure 1.3.3 Calculation of optical power density $\alpha_o I_s$ as a function of $T_g$ and $n_e$ for a gas mixture of 1 torr $CO_2$, 1 torr $N_2$ and 8 torr He. The electron temperature is 1.0 eV (from Fowler (1972)).

Calculations of the population of the 100 lower laser level, and of pumping efficiency of the 001 upper laser level, $N_2$ (v = 1-8) levels and the 100 lower laser level (section 1.3.1), enable an estimate of the laser output power and efficiency to be made for a given gas mix, temperature, $n_e/N$ and E/N. Provided these parameters remain constant the input power density, and thus output power will scale as the square of the gas pressure. Since the discharge configuration has little effect on pumping efficiency, for a fixed gas mix, $n_e/N$ and E/N, the performance of a laser depends only on the cooling mechanism.

Thus in the conventional, axial flow laser increase of pressure and input power density will only result in increased output power when the thermal population of the lower laser level (and the 020 and 010 states) is small.

As the gas temperature rises to $\sim$ 500-600K the population inversion decreases, as does the laser efficiency. Thus scaling of input power density with pressure, and hence output power scaling (at constant laser efficiency) is only possible up to $\sim$ 30-40 torr for the conventional device.

The EDCL employs convective (fast gas flow) cooling such that the laser gas is exhausted from the discharge region before the gas temperature rises to $\sim$ 600K. Such lasers thus allow pressure scaling as long as gas through-put is sufficient to satisfy this temperature restriction. Large quantities of energy may be deposited in the high pressure TEA device where the gas temperature rise is small for the short duration discharge pulse. However high repetition rate TEA devices do require flowing gas to assist cooling. (Dumanchin et al (1972)).

The preceding sections show that very high power, either cw or pulsed, may be obtained when the E/N is optimised and adequate cooling is incorporated in the laser design. However experiments on both the EDCL and the TEA laser configurations have shown that, even when both these requirements are satisfied, the performance of devices is limited by plasma instabilities. Thus the theoretical emphasis in recent years has changed from a study of excitation properties of the electrical discharge to an analysis of the plasma stability.

## 1.4 THE STEADY-STATE PLASMA

### 1.4.1 Self-Sustained Discharges

In a steady state gas discharge the discharge parameters (neutral particle and electron temperature, densities, and electric field) are temporally invariant at all points. The maintainance of a constant electron density in the plasma requires a balance of electron production

and loss processes. These processes include,

(a) direct, electron impact ionisation of neutral species,

$$e + AB \longrightarrow AB^+ + 2e \qquad (k_i)$$

(b) dissociative attachment of electrons to neutral molecules,

$$e + AB \longrightarrow A^- + B \qquad (k_a)$$

(c) dissociative recombination of electrons and positive ions,

$$e + AB^+ \longrightarrow A + B \qquad (k_r^e)$$

(d) associative detachment of electrons from negative ions,

$$A^- + B \longrightarrow AB + e \qquad (k_d)$$

where k represents the rate coefficient for the appropriate process. Other possible processes such as multi-step ionisation, Penning ionisation, radiative recombination, three-body attachment, etc, are less important in the $CO_2$ laser plasma (Nighan and Wiegand (1974(b))). However, one process not directly affecting the electron density, but necessary to complete the major processes affecting positive and negative ion densities, is the ion-ion recombination process which may be two-body or three-body, ie

$$A^+ + B^- \longrightarrow A + B \qquad (k_{2r}^i)$$

or

$$A^+ + B^- + M \longrightarrow AB + M \qquad (k_{3r}^i)$$

Processes (a) and (d) above result in electron production while (b) and (c) result in electron loss, so that the time dependence of the electron density may be described by

$$\frac{dn_e}{dt} = k_i n_e N + k_d n_- N - k_a n_e N - k_r^e n_e n_+, \qquad (1.4.1)$$

where $n_e$, $N$, $n_-$ and $n_+$ are the electron, neutral particle, negative ion and positive ion densities, respectively. It should be appreciated that the rate coefficients $k_i$, $k_d$, $k_a$ and $k_r^e$, refer to <u>mixture weighted</u> values. For example, in a $CO_2$-$N_2$-He mixture, the appropriate $k_i$ value is the sum of the ionisation rate coefficients for $CO_2$, $N_2$ and He, weighted according to the proportions of these gases in the mixture. Thus, in order to

correctly weight the detachment and recombination coefficients, it is necessary to know the densities of the various species of positive and negative ions in the discharge since these will react at different rates. (ie the species have different reaction cross-sections).

Also it should be noted that the loss of electrons by diffusion is omitted from equation (1.4.1). The diffusion loss term ($= D_a \nabla^2 n_e$, where $D_a$ is the ambipolar diffusion coefficient (see section 2.2)) is often the dominating electron loss term for conventional, axial flow lasers where the pressure is $\sim$ 30 torr, and the discharge tube is $\sim$ 2cm diameter. However for EDCL's and TEA lasers diffusion is insignificant compared with attachment and recombination loss processes. In the EDCL the discharge typically occurs in a large volume enclosure and with a gas flow velocity sufficiently rapid that the gas residence time in the discharge is less than the characteristic ambipolar diffusion time. In the TEA laser the high pressure and short duration electrical pulse are such that electron diffusion to the walls has a characteristic time longer than the discharge pulse duration. Thus equation (1.4.1) refers specifically to discharges where the electrons are produced and lost in bulk processes.

In the steady state $d n_e/dt = 0$ and equation (1.4.1) yields

$$k_i + k_d \frac{n_-}{n_e} = k_a + k_r^e \frac{n_+}{N} . \qquad (1.4.2)$$

While the processes of ionisation, attachment and recombination are always present in the $CO_2$ laser discharge, the influence of detachment on the steady-state depends on the stability of the negative ions. This, in turn, depends on the nature of the negative ion species. Thus, in the absence of prior knowledge of the negative ion species and their stability it is necessary to consider cases where no detachment occurs (stable

negative ions) and where detachment is efficient (unstable negative ions). Nighan and Wiegand (1974(b)) have considered such situations and the results of their analysis are discussed below.

(A) No detachment ($k_d \approx 0$)

In order to understand the steady state operating conditions for a self-sustained discharge with no detachment, Nighan and Wiegand have determined the dependence of the ionisation, attachment and recombination coefficients on E/N. Previous calculations by Nighan (1970) have provided electron energy distribution curves for various gas mixtures with E/N as a variable parameter. Thus the variation of the rate coefficients with E/N may be found by averaging the appropriate cross-section Q(u) (where Q is a function of the electron energy u, expressed in electron volts) over the distribution of electron energies. Hence for process j,

$$k_j(E/N) = \left(\frac{2e}{m}\right)^{\frac{1}{2}} \int_0^\infty u\, f(u, E/N) Q_j(u)\, du, \qquad (1.4.3)$$

where $k_j$ is the rate coefficient, e and m are the electron charge and mass and f(u,E/N) is the distribution function.

Figure 1.4.1 shows the variation of the rate coefficients for a 5-35-60, $CO_2$-$N_2$-He mixture, when j refers to ionisation, attachment and recombination (weighted by a factor $n_+/N$), as computed by Nighan and Wiegand (1974(b)). The fractional ionisation ($n_+/N$) is assumed to be $10^{-7}$ and the species $O^-$ and $CO_2^+$ are assumed to be the products of attachment and ionisation respectively. The gas temperature is not specified.

As can be seen from the figure $k_r^e\, n_+/N$ is much smaller than $k_i$ and $k_a$ for E/N values above $\sim 2 \times 10^{-16}$ V cm$^2$. Thus when no detachment is present, the operating point of a discharge which sustains itself against electron loss by attachment by providing its own ionisation is given by the E/N

corresponding to $k_i = k_a$ (point 'a' in figure 1.4.1).

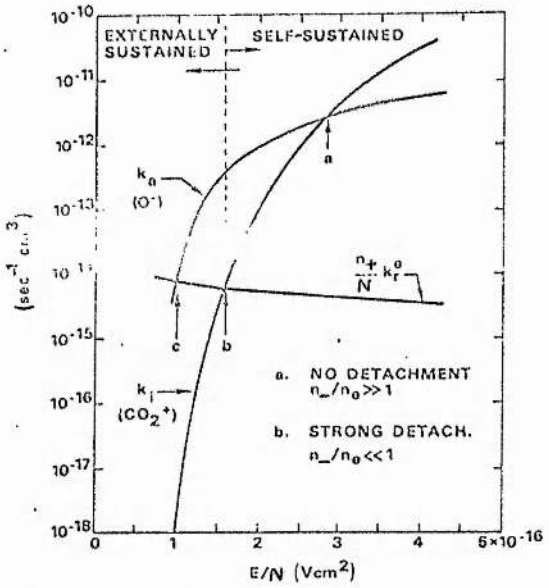


Figure 1.4.1 Variation of ionisation, attachment and recombination coefficients with E/N, computed by Nighan and Wiegand (1974(b)) for typical $CO_2$ laser discharge conditions (see text for details).

In the case of Nighan and Wiegand's 5-35-60, $CO_2$-$N_2$-He mix this would result in an operating E/N of $\sim 3 \times 10^{-16}$ V cm$^2$, a value which is higher than optimum for vibrational level pumping (cf figure 1.3.1 for a 10-10-80, $CO_2$-$N_2$-He mixture).

(B) Strong detachment ($k_d$ large)

In considering the effect of detachment on the operation of the laser discharge Nighan and Wiegand (1974(b)) have assumed the process

$$O^- + CO \longrightarrow CO_2 + e$$

to be operative, with CO as the detaching agent. The gas mixture is thus composed of four constituents ($CO_2$, $N_2$, He and CO). With sufficient CO present, the dissociative attachment reaction

$$e + CO_2 \longrightarrow O^- + CO$$

becomes nullified. Thus, from equation (1.4.2) the operating value of E/N is given by the intersection of the $k_i$ and $k_r^e\, n_+/N$ curves (point 'b' in figure 1.4.1), corresponding to an E/N of $\sim 2 \times 10^{-16}$ V cm$^2$. This is the

lowest E/N value at which the discharge can sustain itself and shows that even when attachment loss of electrons does not occur the discharge cannot be operated under conditions corresponding to the optimum for vibrational pumping (E/N $\sim$ 1 x $10^{-16}$ V $cm^2$, see section 1.3.1).

When the effect of detachment is not sufficient to cancel electron attachment (small quantities of CO) then the operating point will occur between points 'a' and 'b' in figure 1.4.1.

Hence, with sufficient knowledge of electron production and loss processes, the operating E/N of a self-sustained discharge may be accurately predicted.

1.4.2 Externally Sustained Discharges

As discussed in section 1.3.1 the optimum E/N value for vibrational pumping in a $CO_2$-$N_2$-He discharge is insufficient to sustain the ionisation of the gas. A commonly employed method of providing electrons for the discharge, so that the E/N can be lowered to optimise vibrational pumping, is the use of a high energy electron beam ($\sim$ 150 keV) injected through a metal foil uniformly into the discharge region (Fenstermacher et al (1972)). The metal foil is usually one of the discharge electrodes. The purpose of the beam is to provide a controllable secondary electron population in the gas by ionisation of the neutral species by the primary electron beam. These secondary electrons can then be accelerated to the energy optimising vibrational pumping, by application of a suitable E/N. In this way the electron density $n_e$ and the laser discharge E/N are decoupled.

The technique has been successfully applied to TEA lasers (Daugherty et al (1972)) and to EDCL's (Hoag et al (1974)). However the provision of a high energy electron source considerably increases the size of the laser. For many applications sufficient decoupling of the electron density and E/N may be achieved by use of volume photoionisation by uv radiation (Richardson et al (1973), Seguin et al (1973)). The uv

radiation is normally provided by spark discharges and is only suitable for the pulsed TEA systems at present.

Describing the externally provided electron production rate as S electrons per molecule per second, equation (1.4.2) becomes

$$k_i + k_d \frac{n_-}{n_e} + \frac{S}{n_e} = k_a + k_r^e \frac{n_+}{N} , \qquad (1.4.4)$$

However Nighan and Wiegand (1974(b)) point out that for efficient decoupling of $n_e$ and E/N then the external ionisation rate exceeds the ionisation rate (ie in figure 1.4.1, $k_i$ is small at E/N $\lesssim 1.5 \times 10^{-16}$ V cm$^2$). Thus when detachment is unimportant and attachment is the dominant electron loss process, the operating E/N is such that $k_a = S/n_e$. From Figure 1.4.1, such a point will lie between points 'a' and 'c' and E/N values below the self-sustained lower limit (point 'b') become accessible.

If an E/N below point 'c' is required for optimisation of vibrational pumping then electron-ion recombination is the dominant electron loss process and the E/N is such that

$$k_r^e \frac{n_+}{N} = \frac{S}{n_e} \qquad (1.4.5)$$

for no detachment.

When strong detachment occurs (sufficient CO present) the attachment and detachment processes can be considered to cancel in equation (1.4.4) and the equality of recombination and external ionisation determines the operating point as in equation (1.4.5).

1.4.3 The Discharge Characteristic

Computation of the electron energy distribution function, from the relevant cross-section data, as a function of E/N enables the subsequent computation of ionisation, attachment and electron-ion recombination rate constants for a given gas mixture.

The detachment process depends more strongly on the gas temperature

than the discharge E/N and may be considered constant with E/N for a given density of detaching species (Massey (1976) ch 12). In a steady state discharge the equality of electron production and loss by these processes (and external ionisation, if present) enables the operating discharge E/N to be predicted for a given gas mix. When this E/N is known, vibrational population efficiency may be estimated (section 1.3.1). Also the electron density may be found by solving the steady state simultaneous equations for electrons, positive and negative ions, ie.

$$k_i + k_d \frac{n_-}{n_e} + \frac{S}{n_e} = k_a + k_r^e \frac{n_+}{N}$$

$$k_i = k_r^e \frac{n_+}{N} + k_{2r}^i \frac{n_+ n_-}{n_e N} \qquad (1.4.6)$$

$$k_a = k_d \frac{n_-}{n_e} + k_{2r}^i \frac{n_+ n_-}{n_e N}$$

- assuming two-body recombination of positive and negative ions to dominate over the three-body process.

Accurate solution of the simultaneous equations (1.4.6) depends on knowledge of the ion-ion recombination and detachment processes. The rate coefficients of these processes should be weighted according to the concentrations of the various positive and negative ion species in the discharge. Since this knowledge is not presently available, calculations of ion and electron densities from equations (1.4.6) must be speculative.

Lowke et al (1973) and Judd (1974) have calculated electron drift velocities as a function of E/N for several gas mixtures. Thus, if it were possible to estimate $n_e$ accurately from equations (1.4.6) the current density could be determined. This would enable a comparison to be made between voltage-current characteristics measured experimentally, and those computed from calculations of the operating E/N, $n_e$ and drift velocity. At present

such comparisons cannot be made since the electron and ion loss processes are not sufficiently well understood.

## 1.5 PLASMA INSTABILITIES

### 1.5.1 The Ionisation Instability

The first plasma instability to be theoretically investigated for high power gas laser discharge conditions was the ionisation instability (Nighan et al (1973)). This type of instability manifests itself in the form of striations - spatial and temporal fluctuations in discharge electric field and charged particle density - observed in the cw EDCL discharge. Experimental observations of the fluctuations in voltage and current in a volume-dominated discharge have been made by Nighan and Wiegand (1974(b)), while Douglas-Hamilton and Mani (1974) have extensively investigated electron-beam sustained discharges where the ionisation instability occurs. (These authors refer to the instability as an "attachment" instability, but the mechanism is identical to that described by Nighan et al (1973)).

This type of instability, and its theoretical analysis apply specifically to volume-dominated plasmas where all processes affecting charged particle kinetics are bulk processes and wall effects (eg diffusion, wall recombination) are negligible. It should not be confused with the striations observed in diffusion-dominated low pressure (usually < 5 torr) glow discharges which have been theoretically treated by Pekarek and Krejci (1961,1962).

The fluctuations in electric field and charged particle density move rapidly through the discharge such that no visible striation of the glow discharge occurs. However, they may be easily detected by electrostatic probes inserted into the discharge. Thus, although the laser medium

appears uniform, the optical quality of the discharge will be diminished. More seriously, the maximum input power density is not limited by gas heating or gas pressure (section 1.3) but by the onset of instability. Douglas-Hamilton and Mani (1974) have observed this discharge power limitation in a 1-1, He-$CO_2$ pulsed discharge at 760 torr which is sustained by an electron beam providing $\sim 10^{17}$ electrons $cm^{-3}$ $s^{-1}$. Increase of the sustainer electric field above $\sim$ 3600 V $cm^{-1}$ produces irregular fluctuations in the sustainer current density monitored at the discharge anode. The current density is uniform at $\sim$100 mA $cm^{-2}$ at sustainer electric fields below $\sim$ 3600 V $cm^{-1}$.

The nature of the ionisation instability has been comprehensively analysed by Nighan and Wiegand (1974(b)) and the following discussion is based on their work. The equations describing the conservation of electrons and negative ions constitute the basis of the analysis, and are

$$\frac{dn_e}{dt} = k_i N n_e - k_a N n_e + k_d N n_- - k_r^e n_+ n_e + NS$$

$$\frac{dn_-}{dt} = k_a N n_e - k_d N n_- - k_r^i n_+ n_- \qquad (1.5.1)$$

where the terms have been defined in section 1.4.1. Two body ion-ion recombination is assumed to be more important than the three body mechanism. S is the volumetric electron production rate from an external source.

In the steady state both time derivatives are zero. But, to analyse the effect of a fluctuation in charged particle density, a small amplitude, time dependent component $\delta n_e \sim n_{ek}\, e^{i\omega t}$ will be assumed in the steady-state electron density $n_e$. The complex wave frequency, $\omega$, is such that if $R_e(i\omega) > 0$, then the disturbance $\delta n_e$ will grow exponentially in time, ie the plasma will be unstable. Appendix I shows that the condition

$R_e(i\omega) > 0$ is equivalent to

$$N\left[k_i\hat{k}_i - k_a\hat{k}_a\right]\frac{\delta E}{E}\cdot\frac{n_e}{\delta n_e} - \left[\frac{n_e}{n_+}n_+ k_r^e \pm \frac{n_-}{n_e}Nk_d \pm \frac{NS}{n_e}\right.$$

$$\left.\frac{n_-}{n_+}n_+ k_r^i \pm \frac{n_e}{n_-}N\,k_a\right] > 0 \qquad (1.5.2)$$

where $\hat{k}$ denotes the logarithmic derivative of k with respect to the electric field, E, ie

$$\hat{k} = \frac{\partial(\ell n\ k)}{\partial(\ell n\ E)} \qquad (1.5.3)$$

(see Appendix I).

In the derivation of (1.5.2) constant gas density is assumed so that the ionisation and attachment coefficients vary with electric field (see figure 1.4.1) but both recombination coefficients, the detachment coefficient and the ionisation source term are assumed to be constant with electric field.

The instability condition, equation (1.5.2), consists of two, square-bracketed, terms. The first reflects the E/N dependence of the ionisation and attachment rate constants, or at constant pressure and temperature, the electric field dependence. The second term, in which all coefficients are positive, must always be positive, and thus contributes to discharge stability. Thus discharge stability depends on the magnitude and sign of the first term. In order to determine the effect of this term it is necessary to examine the relationship between fluctuations in the electric field and the electron density.

This relationship has been examined in considerable detail by Haas (1973) and Nighan and Wiegand (1974(b)) in terms of electron momentum and energy exchange with the electric field. Douglas-Hamilton and Mani (1974) and Kovalev et al (1974) have adopted a simpler approach and arrived at a

qualitatively similar result. The relationship is based on the current density,

$$J = n_e \, e \, \mu_e \, E \qquad (1.5.4)$$

where e is the electron charge and $\mu_e$ is its mobility which is assumed to a first approximation to be electric field independent. The positive and negative ion contributions to the current density are neglected. The change in current density arising from perturbations in $n_e$, and E is then,

$$\delta J = e \, \mu_e \, E \, \delta n_e + e \, \mu_e \, n_e \, \delta E. \qquad (1.5.5)$$

In the absence of sources or sinks of current in the bulk discharge, current density will be constant, ie $\delta J = 0$. Thus, perturbations in electron density and electric field are related by

$$\frac{\delta E}{E} \cdot \frac{n_e}{\delta n_e} = -1. \qquad (1.5.6)$$

In deriving a detailed relationship between electron density and electric field fluctuations (or, equivalently, electron temperature) Nighan and Wiegand (1974(b )) have determined a phase difference of 180° between perturbations, as in equation (1.5.6). The coefficient relating the perturbations derived by these authors depends on the electron momentum and energy transfer frequencies and the angle between the initial perturbation and the electric field. However, a value of $\sim -1$ is predicted for typical $CO_2$ laser conditions.

Substitution of equation (1.5.6) into equation (1.5.2) shows that, for the instability to occur, the term $\left[k_i \hat{k}_i - k_a \hat{k}_a\right]$ must be negative, ie.

$$\frac{k_a \hat{k}_a}{k_i \hat{k}_i} > 1. \qquad (1.5.7)$$

However even if this inequality is satisfied the stabilising influence of the second square -bracketed term may prevent the ionisation

instability from occurring.

Calculations by Nighan et al (1973) for a 5-35-60, $CO_2$-$N_2$-He gas mixture, have shown that equation (1.5.7) is satisfied for values of electron temperature $\lesssim$ 1.1 eV (corresponding to a E/N $\lesssim$ 2 x $10^{-16}$ V $cm^2$ for this gas mixture). Consideration of figure 1.4.1 (computed for the same gas mixture) shows that maintenance of the discharge below E/N = 2 x $10^{-16}$ V $cm^2$ requires strong detachment and/or external ionisation. Thus the occurrence of ionisation instability does not automatically imply a large negative ion density. However, without the formation of negative ions, equation (1.5.7) cannot be satisfied, and clearly a large loss of electrons in attachment must be counterbalanced in a stable discharge. At the relatively low E/N values where the criterion of equation (1.5.7) is satisfied, ionisation is not sufficient to compensate for electron loss. Thus either strong detachment and/or external ionisation is required to offset the high attachment rate. The stabilising influence of these processes is verified by their appearance in the second, square-bracketed term of equation (1.5.2).

Based on calculations of the range of E/N values over which the instability criterion, equation (1.5.2), is satisfied, Nighan and Wiegand (1974(b )) have computed the ratio of negative ion density to electron density, $n_-/n_e$, for a 5-35-60, $CO_2$-$N_2$-He mixture. Knowledge of the variation of ionisation, attachment, detachment and recombination coefficients over this E/N range make it possible to solve the steady state charged particle equations (1.4.6) resulting in the variation of $n_-/n_e$ with E/N. Thus Nighan and Wiegand have found that $n_-/n_e \sim 1$ for the 5-35-60, $CO_2$-$N_2$-He mixture when the instability criterion is satisfied.

However, calculations of discharge stability, $n_-/n_e$ ratio, etc for a particular gas mixture require assumptions of the dominant ion species participating in recombination and detachment (eg Nighan and Wiegand assume $CO_3^-$ to dominate the negative ion species). Thus the development of the theory of ionisation instability is restricted by inadequate knowledge of ion species densities.

1.5.2 The Thermal Instability

When large power densities are supplied to electrical discharges, the power is usually intended to be dissipated uniformly throughout the gas. However, at fast gas flow velocities (eg in the EDCL) localised heating of the gas may occur at points in the discharge where relatively slower gas velocities exist. Such points may be close to inlet and exhaust ducts, near electrodes, or they may exist in the bulk gas due to a non-uniform velocity profile. This local change in gas temperature will affect the local gas density and electron density (since the local value of E/N will change). The important question from the viewpoint of discharge stability is "Will the local temperature fluctuation be reinforced by the plasma kinetic processes?".

Consideration of the processes resulting from a gas temperature, or gas density fluctuation have led many authors to the conclusion that such fluctuations are responsible for the glow-arc transition often observed in high power density volume-controlled discharges. The filamentary nature of the arc is a manifestation of the reinforcement of the initial disturbance.

The cause of the thermal instability was first analysed for atomic gases by Ecker at al (1964) and subsequently adapted by Nighan and Wiegand (1974(a)) and Jacob and Mani (1975) to explain glow-arc transitions

in molecular gases where vibrational temperatures (ie the temperature characterising a Boltzmann distribution of molecules amongst the vibrational energy levels) will also fluctuate. Nighan (1977) has considered the effect of gas temperature and density fluctuations in discharges where the electron loss processes are dominated by either recombination, attachment or three-body attachment. He has shown, as will be discussed, that the coupling of electron density and gas temperature disturbances depends critically on the electron loss processes. Additionally, when the detachment process is included, the electron production by this mechanism also contributes significantly to reinforcement of the initial disturbance.

Nighan and Wiegand (1974(a)) have shown that a fluctuation in gas temperature will be temporally amplified when the inequality,

$$b = (N\ C_p\ T)^{-1}\left[Kk'^2T + \frac{NC_pT}{\tau_{VT}} + F_V JE(2 + \hat{\tau}_{VT}) + F_T JE\ (\frac{\delta n_e}{n_e}\frac{N}{\delta N})\right] < 0 \qquad (1.5.8)$$

is satisfied (see Appendix 2 for derivation of the above instability criterion and definition of symbols). In the inequality (1.5.8) the first term in square brackets $\{Kk'^2T\}$ describes damping of a localised thermal inhomogeneity by thermal conduction over a distance $1/k'$. ($\frac{1}{k'}$ is the distance over which perturbations in steady state plasma properties are assumed to extend - the perturbation scale size).

The terms $(\frac{NC_pT}{\tau_{VT}} + F_V JE(2 + \hat{\tau}_{VT}))$ describe the vibrational - translational energy relaxation process, where vibrationally excited molecules are collisionally de-excited, thus increasing the kinetic energy of the neutral gas particles. The final term $F_T JE(\frac{\delta n_e}{n_e}\frac{N}{\delta N})$ in (1.5.8) refers to the coupling between electron heating by the discharge and gas

heating by subsequent electron-neutral particle elastic collisions.

Nighan and Wiegand (1974(a)) have derived the instability growth rate, $\omega$, in the form

$$\omega = -\frac{b}{2} \pm \frac{1}{2}\sqrt{b^2 - 4c} \qquad (1.5.9)$$

where b is given by equation (1.5.8) and

$$c = \frac{(N\, C_p\, T)^{-1}}{\tau_{VT}} \left[ K\, k'^2\, T + JE\left(\frac{\delta n_e}{n_e} \cdot \frac{N}{\delta N}\right) \right] \qquad (1.5.10)$$

The term $JE\left(\frac{\delta n_e}{n_e} \cdot \frac{N}{\delta N}\right)$ in equation (1.5.10) describes the coupling of electron heating by the electric discharge to neutral particle heating. Thus it includes both translational heating (elastic collisions) and vibrational heating (inelastic collisions). However under typical $CO_2$ laser conditions the excitation of vibrational levels dominates (see figure 1.3.1) and thus the term $JE\left(\frac{\delta n_e}{n_e} \cdot \frac{N}{\delta N}\right)$ describes mainly electron-molecule vibrational excitation.

Nighan and Wiegand (1974(a)) have constructed a qualitative diagram describing the development of the thermal instability (figure 1.5.1). The initial coupled disturbances in gas density and temperature are such that the decrease in gas density (ie increase in E/N) leads to an increase in the electron density due to an increase in the ionisation rate and/or a decrease in the electron loss rate (see figure 1.4.1). This initial disturbance will affect the vibrational temperature $T_V$ by locally adjusting the collisional de-excitation rate of vibrationally excited species. However the influence of increased local electron density resulting from the ionisation rate increase will itself increase the vibrational excitation rate, ie increase $T_V$.

It is the processes by which the above local increases in $n_e$ and $T_V$ subsequently affect the local gas density and temperature which determine

the discharge stability. Both electron-gas heating and vibrational-translational relaxation tend to reinforce the initial disturbance which will then grow unless the process of heat conduction is rapid enough to compensate for the additional local heating.

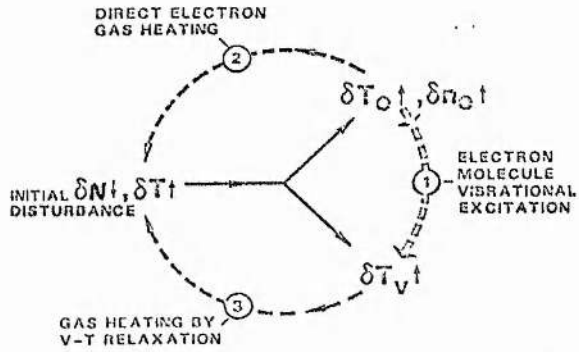


Figure 1.5.1 Development of the thermal instability. The initial disturbance in gas density leads directly to disturbances in electron density and vibrational temperature. The feedback processes are indicated by broken lines (Nighan and Wiegand 1974(a)).

As figure 1.5.1 indicates, for the growth of the thermal instability it is necessary that the disturbance in gas density produces a negative response in electron density

ie. $$\frac{\delta n_e}{n_e} \cdot \frac{N}{\delta N} < 0. \qquad (1.5.11)$$

Also, equation (1.5.8) shows that the necessary condition for thermal instability to develop is that either equation (1.5.11) holds, or $\tau_{VT} \lesssim -3$, or both. Only then can the inequality (1.5.8) be satisfied since the terms $K k'^2 T + \frac{NC_p T}{\tau_{VT}}$ are always positive. The condition that $\tau_{VT} \lesssim -3$ requires that the vibrational-translational relaxation rate $(1/\tau_{VT})$ be proportional to $T^3$ or some higher power. If such a sensitive temperature dependence of the V-T relaxation rate does not exist, then the instability growth depends critically on the coupling of electron and gas densities.

A situation where inequality (1.5.11) is satisfied can occur in a self-sustained discharge where electron production in ionisation is balanced by loss in attachment. Any local increase in gas density (ie a decrease in E/N) will reduce the rate of electron loss by attachment (Figure 1.4.1).

However, electron production by ionisation will be reduced even more, resulting in an overall decrease in electron density. The same negative response in electron density to gas density fluctuations can be shown to accompany a decrease in local gas density, ie. $\delta n_e$ is positive when $\delta N$ is negative, for the self sustained discharge. Also since the values of $k_i$ and $k_a$ are sensitive to changes in E/N the resulting change in electron density due to gas density perturbations can be large. Nighan and Wiegand (1974(a)) have calculated a fractional change in electron density of 100 times the accompanying change in gas density in a 5-35-60, $CO_2$-$N_2$-He gas mixture at 20 torr pressure.

When an external source of ionisation is employed the discharge may be operated in an E/N regime where the ionisation coefficient is small (section 1.4.2). Under these conditions fluctuations in electron density due to changes in ionisation rate are negligibly small (assuming a stable external ionisation source). However, the electron density may still fluctuate as a result of the electron loss processes, which cannot be externally controlled.

Nighan (1977) has comprehensively analysed the influence of electron loss processes in externally sustained discharges. For conditions typical of an externally sustained $CO_2$ laser electron-ion recombination is likely to be the dominant electron loss process (see section 1.4.2 and figure 1.4.1). Since the rate of this process ($k_r^e$) decreases with increasing E/N values (figure 1.4.1) the local sequence of events satisfying the inequality (1.5.11) necessary for thermal instability is

$$N \downarrow \quad ; \quad E/N \uparrow \quad ; \quad k_r^e \downarrow \quad ; \quad n_e \uparrow \quad ,$$

or vice-versa. By assuming a dependence of $k_r^e$ on electron temperature $T_e$ (effectively the E/N of the discharge) of $k_r^e \propto T_e^{-3/2}$, Nighan has computed the growth rate ($\omega$) of the thermal instability for a 5-35-60, $CO_2$-$N_2$-He mixture at a pressure of 190 torr and initial temperature of

300K in an externally sustained discharge. Figure 1.5.2 shows the instability growth rates for both thermal and ionisation instabilities (see section 1.5.1) as a function of distance travelled through the discharge by the gas at a flow velocity of 100 m $s^{-1}$. For $x < 5$cm the corresponding gas dwell time is < 0.5 ms. Since the thermal instability growth time $(1/\omega)$ is > 2ms in this region, no thermal instability is likely. However, for 5 cm < x <18 cm attachment instability is highly probable. Conditions where thermal instability becomes possible develop around x = 20 cm, ie. gas dwell time = 2 ms, growth time ∿ 2 ms. Clearly, thermal instability, due to recombination alone creating the negative response in electron density to gas density fluctuations is not likely.

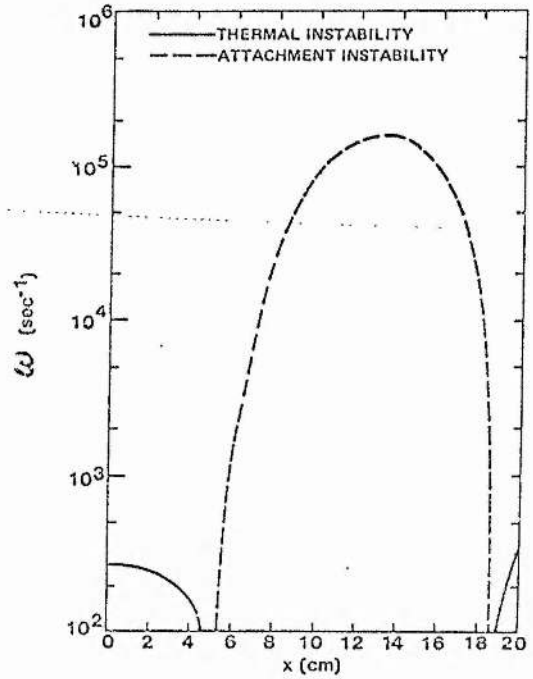


Figure 1.5.2 Calculated growth rates ($\omega$) for thermal and ionisation instabilities as a function of downstream distance (x) in the discharge. Recombination is the dominant electron loss mechanism ($k_r^e \propto T_e^{-3/2}$). Discharge conditions are given in the text (from Nighan, (1977)).

Nighan (1977) goes on to consider the role of detachment in $CO_2$ laser discharges where CO is produced and can cause considerable detachment of electrons from negative ions,

ie. $$CO + O^- \longrightarrow CO_2 + e,$$

Unfortunately, as Nighan points out, the dependence of the detachment rate coefficient, $k_d$, on gas and electron temperature is only known in any detail for oxygen discharges, where detachment from $O_2^-$ occurs. Since the reactants in the detachment process are negative ions and neutral particles, the electron temperature dependence of $k_d$ is expected to be small, while its gas temperature dependence may be considerable {as is the case for oxygen (Pack and Phelps (1966))}. The importance of gas temperature dependent detachment has been stressed by Nighan (1977), since a local increase in gas temperature could lead to a local increase in the detachment coefficient and a corresponding increase in electron density. The decrease in local gas density accompanying the gas temperature increase (assuming constant pressure) will thus enable the inequality (1.5.11) to be satisfied, as is necessary for instability.

Assuming a highly sensitive dependence of the detachment coefficient on gas temperature ($k_d \sim T^{20}$), Nighan has recalculated the thermal instability growth rate for the same discharge conditions as for figure 1.5.2. Figure 1.5.3 shows his results, and clearly, while thermal instability is unlikely for $x < 8$ cm (gas dwell time $< 0.8$ ms), such an instability is highly probable for $x \geq 10$ cm. For example, when $x = 10$ cm (gas dwell time = 1 ms) the growth time is $\sim$ 1 ms.

The agreement between the typical instability growth rates for thermal instability, with gas temperature dependent attachment, predicted by Nighan's theory, and the onset times of the glow-arc transition in EDCL's (Eckbreth and Davis (1971), Hill (1971)), is excellent. However, reported glow-arc transitions in EDCL's have occurred at lower pressures ($\sim$ 50 torr) than used in Nighan's calculations, but without the aid of external ionisation. Nevertheless, considering the lack of basic data

concerning ion-molecule, and electron processes in $CO_2$ discharges (eg. precise determination of principle ion species, detachment rate temperature dependence, etc) thermal instability seems the most plausible explanation of the glow-arc transition observed in EDCL's.

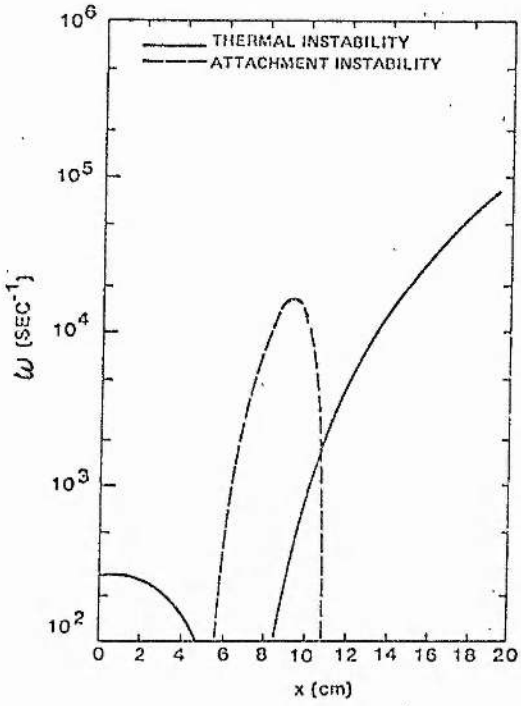


Figure 1.5.3 Calculated growth rates for thermal and ionisation instabilities as a function of downstream distance (x) when detachment is highly temperature sensitive ($k_d \sim T^{20}$) (from Nighan (1977))

Although no calculations of thermal instability growth rate have been performed for the atmospheric pressure, pulsed discharge of the TEA lasers, the thermal instability is the probable explanation of the glow-arc transition observed in these devices (Johns and Nation (1972), Dyer and James (1975), Pearson and Lamberton (1972)). The high input power density of the TEA laser augments the destabilising term $\{F_T JE\ (\frac{\delta n_e}{n_e} \cdot \frac{N}{\delta N}) + F_V JE\ \hat{\tau}_{VT}\}$ in equation (1.5.8) such that the instability growth rate, $\omega$, may be sufficiently large to allow the thermal instability

to cause glow collapse before the termination of the discharge pulse.

The preceding discussion of thermal instability development illustrates the influence of negative ions on the instability mechanism. In self-sustained discharges the disturbance in the balance of ionisation and attachment due to gas density and temperature fluctuations may result in the instability criterion (equation (1.5.11)) being satisfied. Also, in both self-sustained and externally-sustained discharges, the influence of gas temperature dependent detachment can contribute to discharge instability. Thus, some investigaton of negative ion processes is necessary before the thermal instability can be quantitatively analysed for the $CO_2$ laser discharge. Additionally, the destabilising influence of electron-ion recombination in externally sustained lasers indicates a requirement for knowledge of positive ion processes in $CO_2$ laser discharges.

## 1.6 CONCLUSIONS

Since laser action in the $CO_2$ molecule was first demonstrated by Patel in 1964, the development of the $CO_2$ laser has proceeded at a rate as impressive as the performance which has been obtained from these devices. This development has naturally divided into three distinct classes of $CO_2$ laser. The first type is a small scale device capable of several watts of infra-red output (cw) at an efficiency which may be as high as 25% for conversion of electrical to optical energy. The second type is a much larger device, intended for generation of high power infra-red radiation and capable of several tens of kilowatts output power (cw). Third, a laser design intended for pulsed output has realised output powers ranging from megawatts to tens of gigawatts in pulses of $\sim$ 1μs to tens of nanoseconds duration. Thus the $CO_2$ laser has found application in many fields as diverse

as eye surgery and thermonuclear fusion.

However, all three types of laser design have the common feature that they depend on an electrical discharge in the laser gas mixture for excitation of the appropriate laser levels. A complete understanding of this electrical discharge is thus essential if the potential of the $CO_2$ laser is to be fully exploited.

Section 1.2 of this chapter has described the development of the three basic $CO_2$ laser types referred to above. The inability of the conventional axial flow design (section 1.2.1) to provide adequate gas cooling for high power generation has resulted in the EDCL design (section 1.2.2) for high power cw output and the TEA laser design (section 1.2.3) for high power pulsed output. Both these latter types allow high electrical power input while still maintaining a low gas temperature but both suffer from discharge instabilities which ultimately limit the power input.

Theories of laser efficiency, power output and power input scaling have been discussed in section 1.3. Modelling of the laser discharge shows good qualitative agreement with experiment, but calculations for a particular laser discharge environment required detailed knowledge of gas temperature, gas mixture, electrode configuration, etc.

Similarly, calculations of the electrical characteristics of the discharge (E/N, electron density, etc) yield results in acceptable agreement with experiment but once again lack of data has limited the applicability of such calculations. In this case, greater knowledge of plasma kinetic processes is required, so that, for a given gas mixture, the operating E/N of the discharge, and other dependent parameters (eg. electron drift velocity, electron and ion densities, etc) may be

accurately predicted (section 1.4).

Detailed plasma kinetic information is possibly even more important if the theories of plasma instabilities (section 1.5) are to be closely related to experimental lasers. This includes detachment and recombination rates for the ion species present in the discharge. Section 1.5 shows that both these processes are particularly important in determining discharge stability.

Reaction rate constants and cross-sections for the ionisation and attachment processes involving the major and minor species in the $CO_2$ laser discharge are well known, having been extensively studied in recent years by physicists interested in the earth's upper atmosphere. Understanding of these processes, the resultant ions, and the rates of detachment, recombination and ion-molecule reactions are enabling atmospheric physicists to obtain good agreement between measured ion species densities in the upper atmosphere and theories based on the plasma kinetics.

In principle the $CO_2$ laser discharge may be modelled as successfully as the upper atmosphere, using similar techniques. However, three factors presently limit the detailed modelling of the $CO_2$ laser discharge. First, the plasma chemical processes controlling the densities of minority species (notably the oxides of nitrogen) in the discharge are not well understood. Second, experimentally measured or theoretically predicted densities of positive and negative ions in the plasma are both scarce and lacking in detailed analysis. This makes predictions of the major ions species in a given discharge environment little better than guesswork and leads to corresponding uncertainties in recombination, detachment and ion-molecule reaction rates. Third, the rates of plasma kinetic processes depend on gas and electron temperature. While these rates are usually well known for typical atmospheric physics conditions ($T_{gas} \sim$ 200-500K, $T_e \sim T_{gas}$) this

is not the case for the $CO_2$ laser discharge ($T_{gas} \sim$ 300-700K, $T_e \sim$ 0.7-2.0 eV).

The intention of this thesis is to provide detailed information concerning the positive and negative ion species present in $CO_2$ laser discharges. This data may be used in discharge modelling and plasma instability computations.

The theory of positive ion sampling from a glow discharge plasma with subsequent mass-spectrometric ion identification is given in chapter 2. This indicates how positive ion species densities might be reliably measured by using a $CO_2$ laser discharge coupled to a mass spectrometer system. Chapter 3 describes an experimental system which has been constructed specifically for positive ion analysis of gas laser discharges. The results produced by the system are compared with the theory of chapter 2 and are shown to be reliable.

Results of the analysis of positive ions in $CO_2$ laser discharges are presented in chapter 4. This chapter takes the form of a published paper, "Positive ion processes in the positive column of $CO_2$ laser electrical discharges" by A L S Smith and H Shields (J. Chem Phys, 67, p1594-1604 (1977)). By variation of the discharge conditions (current, pressure and gas flow rate) some insight into positive ion kinetics has been possible. This should be particularly useful in discharge modelling.

Chapter 5 indicates the inadequacy of the mass-spectrometric approach in determining negative ion densities in the laser discharge. An alternative approach, based on computational techniques, is employed yielding results of particular significance to instability modelling in high power EDCL's and TEA lasers. Calculations of negative ion species densities for the discharge conditions of a TEA laser have been performed and results are presented in chapter 6, which is, once again, a published paper, "Negative ion effects in TEA $CO_2$ lasers" by H Shields, A L S Smith and B Norris, (J Phys D, 9, p1587-1603 (1976)). These calculations are

correlated with the onset of discharge arcing observed in an experimental laser. Similar calculations for EDCL conditions have enabled comparison between the build-up of negative ions in the discharge and published results of instabilities in these discharges. These results are given in chapter 7, a published paper entitled "Negative ion effects in $CO_2$ convection laser discharges" by H Shields and A L S Smith (Appl. Phys, 16, p111-118 (1978)). Finally, in the concluding chapter the results of this study and their relevance to $CO_2$ laser discharges and discharge models are reviewed.

## References


Beaulieu A J, 1970, Appl Phys Lett, 16, 504.

Bridges T J, Burkhardt E G and Smith P W, 1972, Appl Phys Lett, 20, 403.

Brown C O and Davis J W, 1972, Appl Phys Lett, 21, 480.

Bruce F M, 1947, J Inst Elect Eng, 94, 138.

Bullis R H, Nighan W L, Fowler M C and Wiegand W J, 1972, AIAA Jnl, 10, 407.

Carbone R J, 1967, IEEE J Quant Electron, QE-3, 373.

Chang T Y, 1973, Rev Sci Instrum, 44, 405.

Daugherty J D, Pugh E, House D A and Douglas-Hamilton D, 1972, Phys Today, 25, 18.

Degnan J J, 1976, Appl Phys, 11, 1.

De Maria A J, 1973, Proc IEEE, 61, 731.

Douglas-Hamilton D and Mani S A. 1974, J Appl Phys, 45, 4406.

Dumanchin R, Michon M, Farcy J C, Boudinet G and Rocca-Serra J, 1972, IEEE J Quant Electron, QE-8, 163.

Dumitras D C, Dutu D C, Comaniciu N and Draganescu V, 1976, Rev Roum Phys, 21, 559.

Dyer P E and James D J, 1975, J Appl Phys, 46, 1679.

Eckbreth A C and Davis J W, 1971, Appl Phys Lett, 19, 101.

Eckbreth A C and Owen F S, 1972, Rev Sci Instrum, 43, 995.

Ecker G, Kroll W and Zoller O, 1964, Phys Fluids, 7, 2001.

Fenstermacher C A, Nutter M J, Leland W T and Boyle K, 1972, Appl Phys Lett, 20, 56.

Foster H, 1972, Optics and Laser Tech, 4, 121.

Fowler M C, 1972, J Appl Phys, 8, 3480.

Haas R A, 1973, Phys Rev, A8, 1017.

Herzberg G, 1960, "Molecular Spectra and Molecular Structure", Vol II, Van Nostrand-Reinhold, Princeton, New Jersey.

Hill A E, 1971, Appl Phys Lett, 18, 194.

Hoag E, Pease H, Staal J and Zar J, 1974, Appl Optics, 13, 1959.

Jacob J H and Mani S A, 1975, Appl Phys Lett, 26, 53.

Johns T W and Nation J A, 1972, Appl Phys Lett, 20, 495.

Judd O P, 1974, J Appl Phys, 45, 4572.

Kovalev A A, Persiantsev I G, Pismenny V D and Rakhimov A T, 1974, Phys Lett, 49A, 29.

Laderman A J and Byron S R, 1971, J Appl Phys, 42, 3138.

Lamberton H M and Pearson P R, 1971, Electron Lett, 7, 141.

Legay-Sommaire N, Henry L and Legay F, 1965, C R Acad Sci, 206B, 3339.

Lowke J J, Phelps A V and Irwin B W, 1973, J Appl Phys, 44, 4664.

Massey H, 1976, "Negative Ions" Cambridge University Press, Cambridge.

Moeller G and Rigden J D, 1965, Appl Phys Lett, 7, 274.

Nighan W L, 1970, Phys Rev, A2, 1989.

Nighan W L, 1977, Phys Rev, A15, 1701.

Nighan W L and Wiegand W J, 1974(a), Appl Phys Lett, 25, 633.

Nighan W L and Wiegand W J, 1974(b), Phys Rev, A10, 922.

Nighan W L, Wiegand W J and Haas R A, 1973, Appl Phys Lett, 22, 579.

Pack J L and Phelps A V, 1966, J Chem Phys, 45, 4316.

Palmer A J, 1974, Appl Phys Lett, 25, 138.

Patel C K N, 1964(a), Phys Rev, 136, 1187.

Patel C K N, 1964(b), Phys Rev Lett, 13, 617.

Patel C K N, 1965, Appl Phys Lett, 7, 15.

Patek C K N, Tien P K and McFee J H, 1965, Appl Phys Lett, 7, 290.

Pearson P R and Lamberton H N, 1972, IEEE J Quant Electron, QE-8, 145.

Pekarek L and Krejci V 1961, Czech J Phys, B11, 729.

Pekarek L and Krejci V, 1962, Czech J Phys, B12, 451.

Richardson M C, Leopold K, Alcock A J and Burtyn P, 1973, IEEE J Quant Electron, QE-9, 236.

Rogowski W, 1923, Arch Elektrotech, 12, 1.

Seguin H J, Tulip J and McKen D, 1973, Appl Phys Lett, 23, 344.

Taylor R L and Bitterman S, 1969, Rev Mod Phys, 41 26.

Tiffany W B, Targ R and Foster J D, 1969, Appl Phys Lett, 15, 91.

von Engel A, 1965, "Ionized Gases", Oxford University Press, London.

Witteman W J, 1967, Appl Phys Lett, 11, 337.

Wood O R , 1974, Proc IEEE, 62, 355.

# CHAPTER TWO

## POSITIVE ION SAMPLING FROM THE POSITIVE COLUMN OF A DC GLOW DISCHARGE PLASMA

## 2.1 INTRODUCTION

The technique of measuring positive ion species in dc gas discharges using a mass spectrometer is well developed and several reviews of the principles of such experiments exist (Drawin (1968), Mark and Helm (1974), Hasted (1974)). This method has been adopted to determine the nature and relative abundances of positive ions in $CO_2$ laser discharges. As discussed in chapter 1 (sections 1.4 and 1.5), this knowledge is essential for comprehensive and accurate computer modelling of these discharges. In order to determine the reliability of these positive ion measurements, a complete understanding of the ion sampling process is required. Thus, in this chapter factors likely to influence positive ion mass spectra and lead to erroneous interpretation of results are considered.

The mass spectrometer is a versatile instrument which can be used for quantitative gas analysis in a wide variety of applications. Normally gas particles are ionised by electron emission from a hot filament and the ions produced are analysed according to their charge-to-mass ratio.

Alternatively, the positive column of a low pressure gas discharge may be used as a source of ions. The resulting mass spectrum is representative of the ions in the discharge environment. This mass spectrum may bear little resemblance to the neutral gas composition in the discharge tube since the ions produced in low pressure gas discharges are often the end products of a series of ion-molecule reactions. Ions produced by electron impact of the neutral gas in the discharge undergo subsequent reactions with other neutral species to produce secondary ions. Since the ratio of ion to neutral density is $\sim 10^{-7}$ in such discharges, impurities present in the gas, even in a few parts per million concentration, can have considerable

influence on the ion mass spectrum. A quantitative analysis is necessary if the reaction mechanisms operating are to be correctly interpreted. The mechanisms and interpretation of ion-molecule reactions are discussed by McDaniel et al (1970) and Knewstubb (1969).

There are many effects occurring both in the discharge and the sampling process which can lead to misinterpretation of mass spectra. These effects should be understood and accounted for before results can be considered quantitative. Several types of gas discharge ion sources are available for study and each type presents its own problems. For example, either rf or dc excitation may be employed with sampling of ions either from the active plasma or from the afterglow of a decaying discharge.

A typical experiment involves sampling of a constant or time-varying ion current through a small orifice from a glow discharge at a few torr pressure into a low pressure ($p \lesssim 10^{-4}$ torr) chamber where the mass spectrometer is situated. The orifice is normally positioned in the discharge tube wall. It should be large enough to allow a useful quantity of ions and neutral gas particles to effuse to the mass spectrometer for analysis while sufficiently small that the background pressure in the mass spectrometer chamber is kept below $\sim 10^{-4}$ torr. Ion sampling may be achieved using either a small metallic disc with an orifice at its centre, or an orifice in the dielectric wall confining the discharge.

The discussion of the factors which can influence or modify a positive ion current flowing from the positive column of a dc gas discharge through a sampling orifice to a mass spectrometer may be conveniently divided into three parts (ignoring instrumental effects which are characteristic of particular systems):-

(i) the influence of the bulk plasma on ion currents to the discharge wall where the orifice is situated,

(ii) the effect of the positive ion wall sheath which exists at the plasma-wall boundary,

(iii) the effect of the nature of the orifice and its dimensions on ion currents. These factors have been discussed or commented on in previous reviews of mass-spectrometric analysis of ions produced in gas discharge plasmas (Drawin (1968), Smith and Plumb (1973), Mark and Helm (1974), Hasted (1974, 1975)).

In the following discussion of mass-spectrometric positive ion analysis from the positive column of a dc gas discharge, the three topics above are treated in separate sections. Thus in section 2.2 the ion wall currents arising from radial diffusion are considered. Possible modification of these wall currents by negative ion effects and volume recombination are included. The effects of discharge current, pressure, electron and gas temperatures and tube radius on the positive ion wall current are evaluated.

In section 2.3 the passage of ions across the wall sheath from plasma to orifice is discussed for cases where collisions in the sheath occur and where the sheath is collisionless. The consequences of sheath collisions are considered in terms of ion-molecule reactions and the energy of effusing ions.

Section 2.4 discusses the characteristics of metallic orifices and compares this type of orifice with the dielectric type. Also the distortion of the equipotentials in the vicinity of the orifice leading to an ion lens effect and the limitations on orifice tube length and diameter are examined.

Hence the factors likely to effect the positive ion current as it flows from the plasma, across the sheath and through the orifice to the mass spectrometer are considered sequentially as encountered by the positive ions.

## 2.2 PLASMA EFFECTS ON POSITIVE ION SAMPLING

### 2.2.1 Diffusion in the Positive Column

When the motion of electrons and positive ions in a plasma is controlled by diffusion (at pressures $> 5 \times 10^{-3}$ torr) the equations describing the radial flux of particles across unit area per second in a cylindrical discharge are (Oskam (1958)),

$$\begin{aligned} \underline{\Gamma}_+ &= - D_+ \nabla n_+ \pm \mu_+ n_+ \underline{E}_s \\ \underline{\Gamma}_e &= - D_e \nabla n_e - \mu_e n_e \underline{E}_s \end{aligned} \qquad (2.2.1)$$

$\Gamma$ represents the particle flux of a particular species, D and $\mu$ are the appropriate diffusion coefficient and mobility, n is the species density and $E_s$ is the radial electric field. Equations (2.2.1) apply to the case where there are no externally applied electric or magnetic fields and for one type of positive ion. When there are several different positive ion species present, as in the usual mass spectrometric analysis, then the total positive particle flux is given by

$$\underline{\Gamma}_+ = \sum_{i=1}^{m} \{ - D_{+i} \nabla n_{+i} + \mu_{+i} n_{+i} \underline{E}_s \} \qquad (2.2.2)$$

where each of the m positive ion species has its own diffusion coefficient $D_{+i}$ and mobility $\mu_{+i}$.

In a cylindrical dc positive column, the potential at any point on the dielectric discharge confining wall is constant in time. This means that the rate at which positive ions reach the wall is equal to that for electrons,

$$\underline{\Gamma}_+ = \underline{\Gamma}_e = \underline{\Gamma} \, . \qquad (2.2.3)$$

Using this relation in (2.2.1) together with plasma neutrality, $n_+ = n_e = n$ leads to

$$\underline{E}_s = - \left[ \frac{D_e - D_+}{\mu_e + \mu_+} \right] \frac{\nabla n}{n} , \qquad (2.2.4)$$

Equation (2.2.4) gives the magnitude of the radial electric field and shows that it depends on the radial distribution and density of charged particles in the discharge, being largest where the gradient of the charged particle distribution is greatest and the density is smallest. Later in this section the radial dependence of the charged particle density will be approximately deduced assuming production of electrons and positive ions by electron impact ionisation of neutral particles and loss by diffusion to the discharge wall. This theory assumes, also, that the charged particle density is zero at the wall. Although this is not strictly true, the approximation is sufficiently good that the charge particle distribution derived agrees well with experimentally determined radial profiles for the bulk discharge.

The non-zero charge density near the wall arises from the conditions prevailing at the initiation of the discharge and the nature of the wall. When the discharge is initiated, electrons, having greater mobility than positive ions in the gas ($\mu_e \gg \mu_+$), diffuse quickly to the wall. Since the wall is dielectric, a negative space charged is established there, impeding further electron flow. Thus in the steady state a space charge sheath forms at the wall and the potential of the wall with respect to the plasma - the floating potential, $V_f$ - inhibits electron flow such that both electron and positive ion wall currents are equal. The significance of the wall sheath for positive ion sampling from a dc positive column is discussed in detail in section 2.3.

Substitution of equation (2.2.4) into (2.2.1) allows the radial charged particle currents to be expressed in terms of density gradients, alone. Thus,

$$\underline{\Gamma} = - \left[ \frac{\mu_e D_+ + \mu_+ D_e}{\mu_+ + \mu_e} \right] \nabla n. \qquad (2.2.5)$$

Putting $$D_a = \left[\frac{\mu_e D_+ + \mu_+ D_e}{\mu_+ + \mu_e}\right], \qquad (2.2.6)$$

yields $$\underline{\Gamma} = - D_a \nabla n. \qquad (2.2.7)$$

$D_a$ is the ambipolar diffusion coefficient, the value of which ensures that both positive ions and electrons diffuse to the wall at the same rate. Equation (2.2.7) resembles the free diffusion equation for both positive ions and electrons in the absence of space charge fields. Einstein's relationship $D = \frac{\mu kT}{e}$ (Oskam (1958) p367) is now used, where k is Boltzmann's constant, e is the electronic charge and T is the temperature appropriate to the diffusing particle. (This substitution is only strictly applicable when T is independent of radius. In a glow discharge this is not the case (Laderman and Byron (1971)) but such an assumption will not affect the principles of the argument to be presented). With the inequalities $\mu_e \gg \mu_+$, and $T_e \gg T_+$ in an active discharge (von Engel (1965)), equation (2.2.6) becomes

$$D_a \simeq \frac{\mu_+ kT_e}{e} = \frac{D_+ T_e}{T_e} = \frac{D_e \mu_+}{\mu_e} \qquad (2.2.8)$$

Thus $D_a$ is much less than $D_e$ and much greater than $D_+$. Hence in a dc positive column the effect of the negative charge at the wall and its associated field, $E_s$, is to enhance positive ion diffusion by a factor $(\frac{T_e}{T_+})$ and hinder electron diffusion by a factor $(\frac{\mu_+}{\mu_e})$. The positive ion wall current density $\Gamma_+$ is given by (2.2.7) and (2.2.8) as

$$\underline{\Gamma}_+ = - D_+ \frac{T_e}{T_+} \nabla n. \qquad (2.2.9)$$

Typically in a glow discharge $kT_e \sim 1eV$ ($T_e \sim 10^4 K$) while $T_+$ is similar to the temperature of the gas molecules ($\sim$ 500K). Thus the positive ion wall

current density is increased by a factor of $\sim 20$ over the free diffusion case (no space charge fields) and the discharge assists in obtaining positive ion mass spectra.

When there are several types of positive ion effusing to the wall, the wall current density of the i'th species is given by

$$\Gamma_{+i} = - D_{+i} \frac{T_e}{T_+} \nabla n, \qquad (2.2.10)$$

where the density gradient and ion temperature are approximately the same for all ions. The theory of ionic diffusion (eg. Loeb (1961) chs I,II) shows that when the masses of ion and neutral molecules are approximately equal, $D_+ \propto (m_+)^{-\frac{1}{2}}$ where $m_+$ is the ion mass. Thus the wall current densities, $\Gamma_{+i}$ are proportional to $m_+^{-\frac{1}{2}}$ and lower mass ions diffuse to the wall more quickly than the more massive ions, introducing a mass discrimination against heavy mass ions in the ion beam effusing from the discharge (Drawin (1968)).

In a steady state dc positive column, the diffusion loss of charged species is balanced by their production in ionisation. The rate of production is then given by $k_i nN$, where $k_i$ is the rate coefficient for ionisation and N is the neutral gas density. Equating this production rate with the diffusion loss rate expressed in cylindrical coordinates (von Engel (1965) p240) results in the zero order Bessel equation,

$$\frac{d^2n}{dr^2} + \frac{1}{r}\frac{dn}{dr} + \left[\frac{k_i N}{D_a}\right] n = 0. \qquad (2.2.11)$$

Although, as will be discussed in section 2.3, there is a finite charge density at the wall of the discharge (the wall sheath), it is normal to set $n = 0$ at the wall as a boundary condition, enabling equation (2.2.11) to be solved. The solution is the zero order Bessel function having a value of unity at $r = 0$, and zero at $r = R$ (where R

is the tube radius), ie

$$n(r) = n_o J_o (2.405 \frac{r}{R}). \qquad (2.2.12)$$

This distribution of charged particles is based on the assumptions that

(i) the gas temperature, $k_i$ and N are independent of radial position in the discharge tube,

(ii) there are no negative ions in the discharge,

(iii) $n(R) = 0$.

Using the property of Bessel functions,

$$\frac{d}{dr} [J_o(\alpha r)] = - \alpha J_1(\alpha r),$$

the radial variation of charged particle flux, obtained from equations (2.2.7) and (2.2.12), is

$$\Gamma(r) = \frac{2.405\ D_a\ n_o}{R} J_1 (2.405 \frac{r}{R}) = \Gamma_o J_1(2.405 \frac{r}{R}) \qquad (2.2.13)$$

Curves representing the radial variation in n(r) (equation (2.2.12)) and $\Gamma(r)$ (equation (2.2.13)) are shown in figure 2.2.1.

An expression relating the number of positive ions effusing through a sampling orifice of area A, per second, may be derived from equation (2.2.13) in terms of experimental variables. Thus,

$$i_+ = A\ \Gamma(R)$$
$$= \frac{1.25\ D_a\ n_o\ A}{R} \qquad (2.2.14)$$

This assumes that the sampling orifice is sufficiently small not to affect the natural plasma processes in its vicinity (see section 2.4). From equation (2.2.8),

$$i_+ = \frac{1.25\ D_+\ T_e\ n_o A}{T_+\ R} \qquad (2.2.15)$$

When ion and neutral molecule masses are approximately equal then

(see eg Loeb (1961) p202) $D_+ \propto \lambda_i \bar{v}$, where $\lambda_i$ is the ion mean free path (inversely proportional to gas density N) and $\bar{v}$ is the root mean square thermal velocity of gas molecules (proportional to $(T_g/m)^{\frac{1}{2}}$). Since $T_+ \simeq T_g$, the gas temperature, equation (2.2.15) yields

$$i_+ \propto \frac{n_o A T_e}{(T_g m)^{\frac{1}{2}} RN}, \qquad (2.2.16)$$

In addition to the previously mentioned mass discrimination, the sampled current of positive ions depends on $n_o$ (ie on the discharge current), the gas temperature, the discharge tube radius and the gas number density (ie discharge pressure).

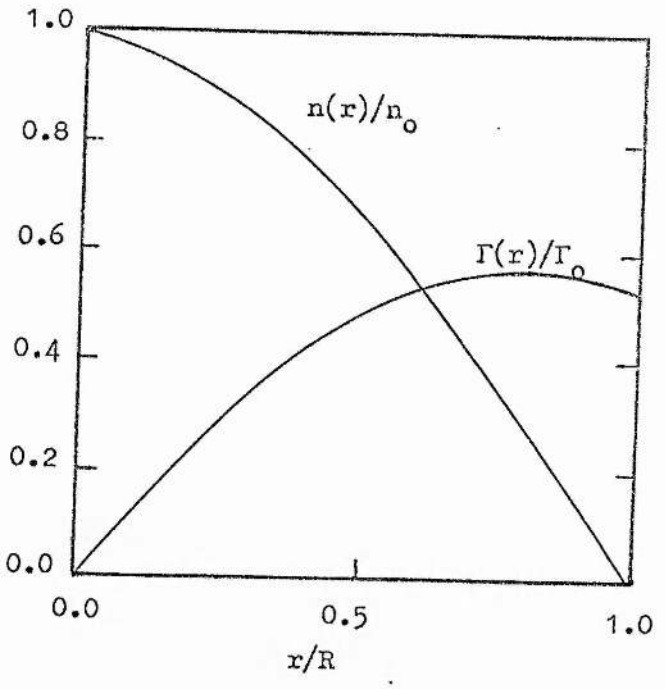


Figure 2.2.1 Radial variation of charge density (n) and charged-particle flux (Γ) calculated from equations (2.2.12) and (2.2.13).

The relation (2.2.16) has been derived in a form which has been found to be useful in analysis of experimental results of sampling of positive ions from discharges typical of carbon dioxide laser gases

(see chapter 3). Most literature reports of positive ion sampling are presented in terms of relative variations in ion densities with varying discharge conditions and do not consider the overall variation of sampling efficiency with discharge current, pressure, tube radius, etc. For this reason comparison of the predictions of equation (2.2.16) with published experimental results of absolute ion effusion currents is limited by lack of information.

Kuehn and Chanin (1972) have published absolute measurements of ion currents effusing from He-$SO_2$ mixtures as a function of discharge current and pressure. They find a decrease in ion current by two orders of magnitude as pressure increases from 1 torr to 6 torr in a 15 mA dc discharge. At 1 torr pressure, the same authors find an increase in total ion signal of $\sim$ 2.5 times when discharge current is increased from 5 mA to 30 mA. Both these results are qualitatively predicted by relation (2.2.16). Similarly, a decrease in total positive ion effusion current with increasing pressure has been observed by Evans and Jennings (1965) and Pahl (1963). Evans and Jennings have measured reductions in total positive ion current by greater than an order of magnitude in rf discharges in $CO_2$ (0.2-2 torr pressure range) and CO (0.4-1.25 torr pressure range). Similar large reductions in the number of ions effusing from a dc discharge have been reported by Pahl in pure Ar, Ar-He and Ar-$H_2$ mixtures over the 0.05-1.6 torr pressure range.

Some difficulty may arise in using relation (2.2.16) in analysis of rf discharges. Schildcrout et al (1970) have measured a severe drop in the total ion signal observed from an rf $CO_2$ discharge when the pressure is increased from 0.1- 0.5 torr, which they have attributed to decreasing power input efficiency at the higher pressures. This results in a drop in

electron and ion densities in the discharge. In such a situation it is likely that variations in $n_o$, $T_e$ and $T_g$ in equation (2.2.16) occur simultaneously with pressure increase, all contributing to the observed decrease in positive ion effusion current.

Although published variations in ion current with pressure and current are qualitatively as predicted by equation (2.2.16) over the limited ranges of parameters treated in the literature, it should be noted that equation (2.2.16) is of limited validity. It does not include the effects of molecular dissociation leading to gas composition changes, or volume recombination of ions and electrons (see section 2.2.3). These effects vary in importance as discharge current, tube radius and pressure change. Also changes in gas and electron temperatures are intrinsically linked to changes in pressure and current, and the effect of varying a single parameter cannot be isolated. The limitations on the use of equation (2.2.16) are discussed in chapter 3 (section 3.2) in an analysis of ion currents effusing from discharges typical of $CO_2$ lasers.

The usefulness of equation (2.2.16) is that it indicates the regime of operating conditions where positive ion currents effusing from gas discharges should be easily detected. Thus the low pressure (0-5 torr) and moderate current region ($\sim$10-50 mA) has been particularly favoured as a gas discharge positive ion source (eg Pahl (1963), Knewstubb and Tickner (1962(a)), Dawson and Tickner (1963), Kuehn and Chanin (1972,1973), Tannen et al (1974) and Keren et al (1976)). However, as previously stated, relative peak heights rather than absolute ion currents are generally reported in the literature.

## 2.2.2 The Effect of Negative Ions on Positive Ion Diffusion

The ambipolar diffusion theory applicable to the positive column in an electronegative gas has been derived by Thompson (1959). This theory is analogous to that developed in section(2.2.1) but contains an additional negative ion wall current density,

$$\begin{aligned} \underline{\Gamma}_+ &= - D_+ \nabla n_+ + \mu_+ n_+ \underline{E}_s \\ \underline{\Gamma}_- &= - D_- \nabla n_- - \mu_- n_- \underline{E}_s \\ \underline{\Gamma}_e &= - D_e \nabla n_e - \mu_e n_e \underline{E}_s \end{aligned} \qquad (2.2.17)$$

In equilibrium, when charge neutrality holds in the plasma, then $\underline{\Gamma}_+ = \underline{\Gamma}_- + \underline{\Gamma}_e$ and $n_+ = n_- + n_e$. Proceeding as before $E_s$ is eliminated to yield

$$\begin{aligned} \underline{\Gamma}_+ &= - D_{a+} \nabla n_+ \\ \underline{\Gamma}_- &= - D_{a-} \nabla n_- \\ \underline{\Gamma}_e &= - D_{ae} \nabla n_e \end{aligned} \qquad (2.2.18)$$

where

$$\begin{aligned} D_{a+} &= D_+ \left[ \frac{(1 + \gamma + 2\alpha\gamma)(1 + \alpha\mu_-/\mu_e)}{(1 + \alpha\gamma)\{1 + \mu_+(1 + \alpha)/\mu_e + \alpha\mu_-/\mu_e\}} \right] \\ D_{a-} &= D_+ \left[ \frac{\mu_-(1 + \gamma + 2\alpha\gamma)}{\gamma \mu_e \{1 + \mu_+(1 + \alpha)/\mu_e + \alpha\mu_-/\mu_e\}} \right] \\ D_{ae} &= D_+ \left[ \frac{(1 + \gamma + 2\alpha\gamma)}{1 + \mu_+(1 + \alpha)/\mu_e + \alpha\mu_-/\mu_e} \right] \end{aligned} \qquad (2.2.19)$$

In these equations $\gamma$ is the ratio of the electron temperature to the ion temperature (assuming $T_+ = T_-$), ie $\gamma = T_e/T_+$. The ratio of the negative ion to electron concentration is $\alpha$. These theoretical ambipolar diffusion coefficients are plotted as a function of $\alpha$ in figure 2.2.2 (taken from Bletzinger et al (1975)) for a mixture of $CO_2$, $N_2$ and He in the ratio 5-15-80, and are the only published results for a typical $CO_2$ laser mixture.

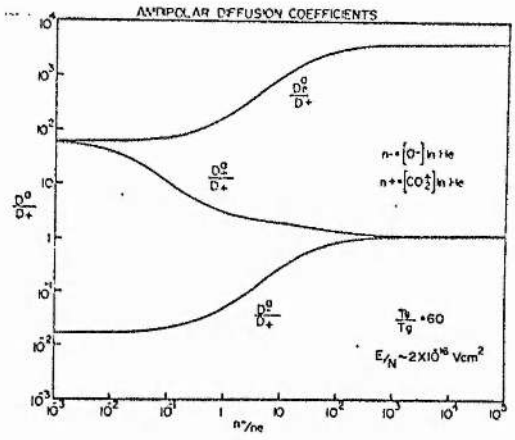


Figure 2.2.2 Ambipolar diffusion coefficients in a 5-15-80, $CO_2$-$N_2$-He mixture, calculated as a function of $n_-/n_e$ (from Bletzinger et al(1975)).

When the negative ion density is much less than the electron density ($\alpha < 10^{-1}$) $D_{a+} \simeq D_{ae}$, and the situation is identical to that described in section 2.2.1. At large negative ion densities ($\alpha > 10^2$) the electron ambipolar diffusion coefficient is large and electron loss is great. The plasma is mainly composed of positive and negative ions both having approximately the same diffusion coefficient, $D_+$. In the intermediate regime ($10^{-1} < \alpha < 10^2$) the ambipolar coefficient for positive ions, $D_{a+}$, decreases from a value of $\sim 2OD_+$ to $\sim D_+$. The effect of this variation in diffusion coefficient on positive ion effusion currents is demonstrated in the decay of afterglow plasmas (Fite and Rutherford (1964), Puckett et al (1971), Smith and Plumb (1973)).

Simultaneous observation of positive and negative ions from afterglow plasmas shows that, in the early afterglow , positive ion densities decay at a rate determined by positive ion - electron ambipolar diffusion (see section 2.2.1) while no negative ions are detected.

In the early afterglow, the plasma contains positive and negative ions

and electrons. Assuming a value of $\alpha(n_-/n_e)$ of $\sim 10^{-1}$, figure 2.2.2 predicts approximately equal diffusion coefficients for positive ions and electrons, with a very low negative ion diffusion rate. (Although figure 2.2.2 refers to a $CO_2$-$N_2$-$N_2$-He gas mixture, the situation will be, at least, qualitatively the same for other electronegative gas mixtures, for which no similar calculation exists.) The result is approximately equal diffusive decay of positive ions and electrons (figure 2.2.3).

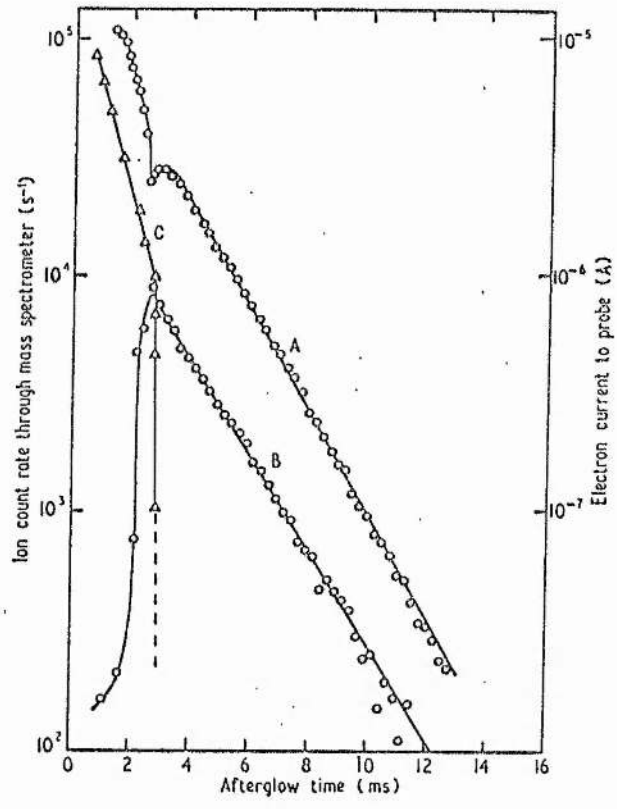


Figure 2.2.3 Dependence of ion and electron currents in a stationary afterglow in a krypton-oxygen mixture. A-positive ions (32 amu); B-negative ions (16 amu); C-electrons; (from Smith and Plumb (1973)).

However, as the electrons decay, the value of $\alpha$ increases. This has two effects. First, when $\alpha \sim 10^2$, electron diffusion is rapid and the electron density falls quickly to zero, as illustrated in figure 2.2.3. Second, as the electrons decay positive ion-electron ambipolar diffusion breaks down and ambipolar diffusion of positive and negative ions takes over. The positive ion diffusion coefficient is reduced from $\sim 2OD_+$ to $\sim D_+$ while the negative ion diffusion coefficient increases from $\sim 10^{-1} D_+$ to $\sim D_+$. Thus positive ions decay more slowly, while negative ions, no longer trapped in the positive ion-electron ambipolar diffusion field, are now detected and decay at the same rate as the positive ions (figure 2.2.3).

Hence the decaying afterglow represents a time-dependent variation in $\alpha$, with the corresponding variations in diffusion coefficients. However in a steady state discharge only one value of $\alpha$ will persist and the positive ion, negative ion and electron wall currents will be determined accordingly.

An important effect occurring in discharges in electronegative gases is the positive ion - negative ion recombination process. The rate at which this process proceeds depends on the nature of both positive and negative ion types (Olsen (1972)). The process is part of the natural behaviour of the plasma and the resulting positive ion spectrum is typical of the plasma. However, in afterglow plasmas this ion-ion recombination can lead to a more rapid loss of positive and negative ions than would be expected from ambipolar diffusion. This will occur when the characteristic recombination time is shorter than the ambipolar diffusion time in the afterglow and can lead to difficulties in ion sampling (positive or negative ions) in these plasmas (see section 5.2).

## 2.2.3 Positive Ion Wall Currents in the Presence of Volume Recombination

When electrons and positive ions are lost by volume recombination as well as diffusion, the steady state charged particle conservation equation is (Francis (1956) p128),

$$D_a \nabla^2 n + k_i N n - \beta n^2 = 0, \qquad (2.2.20)$$

where $\beta$ is the two-body positive ion-electron recombination coefficient and $n = n_e = n_+$. This equation is non-linear and the radial distribution of n can only be found by numerical methods. This type of solution has been performed for argon by Hatori and Shioda (1976) for the case when both $\beta$ and $k_i$ depend on the gas and electron temperatures radial distributions. Results, reproduced in figure 2.2.4, show that for low values of n ($n_e \sim 10^{11}$ cm$^{-3}$ on the discharge axis) the discharge profile is broader than the Bessel distribution derived in section 2.2.1. Assuming diffusion to be less important than volume recombination, equation (2.2.20) predicts a value of $n \sim \frac{k_i N}{\beta}$. This value is independent of radial position in the discharge, but since charged particle densities are assumed to be zero at the wall, the gradient in charged particle densities near the wall is large and the diffusion term becomes important here. Thus the broad distribution of figure 2.2.4(a) is explained.

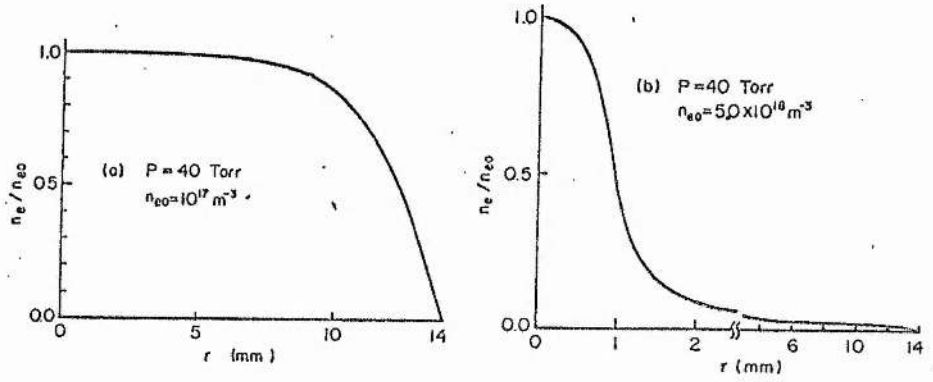


Figure 2.2.4 Radial profiles of electron density in argon discharges computed by Hatori and Shioda (1976), (a) diffuse discharge, (b) constricted discharge.

Figure 2.2.4(b) shows that when the discharge current is increased ($n_e \sim 5 \times 10^{12}$ cm$^{-3}$ on the axis) the discharge contracts to a much narrower radial distribution of charged particles. The explanation of this phenomenon lies in the dependence of $\beta$ and $k_i$ on gas and electron temperatures. Both these temperatures will be higher on the discharge axis than at the wall. Since the recombination coefficient has been experimentally shown to decrease with increasing gas temperature and ionization increases with electron temperature increase (Brown (1959)) then on the axis charged particle loss will be smaller as the gas temperature is raised. Such an increase in gas temperature occurs when the discharge current is increased corresponding to the situation of figure 2.2.4(b) where volume recombination is more effective near the cooler walls than at the centre of the discharge.

Similar results have been experimentally found by Kenty (1962) for a $X_e + N_2$ discharge. This discharge broadens relative to the Bessel distribution for currents up to 10 mA, but a 15 mA discharge has a filamentary form. Kenty has also noted a decrease in the average radial electric field, which decreases from a value of 1.4V cm$^{-1}$ at 1 mA to 0.5V cm$^{-1}$ at 10 mA.

The effect of volume recombination on the charged particle radial distribution will only be important when the recombination term, $\beta n^2$, outweighs the diffusion loss term, $D_a \nabla^2 n$. When this is not so, the radial distribution is diffusion controlled and the theory is that of section 2.2.1. Thus contraction of the positive column may be expected at high currents (large $\beta n^2$) or at high pressures where diffusion is slow (small $D_a \nabla^2 n$). Von Engel (1965 p253) compares the diffusion time, $\tau_D$, with the characteristic time for volume recombination, $\tau_{rec}$. He shows

that since $\tau_D \gtrsim R^2/D_a$ and $\tau_{rec} \simeq 1/n\beta$, contraction becomes important when $\tau_D \gtrsim \tau_{rec}$

$$\text{ie} \quad np \gtrsim \frac{D_a p}{R^2 \beta} \quad , \tag{2.2.21}$$

where p is the discharge pressure. For a typical molecular gas $D_a p \sim 500$ cm$^2$ torr s$^{-1}$ while $\beta \sim 10^{-8}$ cm$^3$ s$^{-1}$. Thus for a 1 cm radius discharge tube $np \gtrsim 5 \times 10^{10}$ torr cm$^{-3}$ for contraction.

When contraction of the positive column occurs, the radial charged particle distribution and its gradient, $\nabla n$, are changed from their diffusion controlled values (section 2.2.1). Thus the positive ion wall current will be changed from its diffusion controlled value given by equation (2.2.13). Appreciable recombination of positive ions before they can diffuse to the wall results in a low positive ion effusion current. Thus the value of np should be kept below the limit indicated by equation (2.2.21). In most glow discharges $n \sim 10^9$ to $10^{10}$ cm$^{-3}$ and p is $\sim$1 to 10 torr giving $10^9 < np < 10^{11}$ torr cm$^{-3}$, thus volume recombination is usually not important.

The preceding discussion has a number of important consequences concerning mass-spectrometric analysis of positive ion currents effusing from the positive column of a dc glow discharge. First, in diffusing to the discharge wall, a mass-discriminatory effect proportional to $(m_+)^{-\frac{1}{2}}$ is introduced (see equation(2.2.16)), thus favouring lighter ions. Second, the ion effusion current depends on conditions prevailing in the discharge (eg current, pressure, tube radius). Equation (2.2.16) gives the predicted dependence for a discharge where ions are produced by direct electron impact ionisation, and are lost by ambipolar diffusion, only. However, the ion effusion currents are modified by the presence of negative

ions and/or volume recombination of electrons and positive ions as discussed in sections 2.2.2 and 2.2.3.

The presence of negative ions has been predicted to significantly change ambipolar diffusion coefficients when negative ion and electron densities are similar in magnitude. Volume recombination can lead to contraction of the discharge column when high currents and/or pressures are used ($np \geq 5 \times 10^{10}$ torr $cm^{-3}$) with a resulting change in positive ion effusion current.

Also, positive ions must cross a wall sheath between discharge and ion sampling orifice. Such a sheath results from different electron and positive ion mobilities, as discussed in section 2.2.1.

The consequences of the existence of the wall sheath are considered in the next section.

## 2.3 POSITIVE ION EXTRACTION THROUGH THE WALL SHEATH

### 2.3.1 The Wall Sheath at Low Pressure

As positive ions diffuse radially from the discharge axis to the wall, they enter the wall sheath. This is a transition region between the bulk plasma and the dielectric wall. Its effect on positive ion current to the wall must be understood so that sampling through an orifice located in the wall can be evaluated. The influence of the sheath on effusing ion currents depends on whether the orifice is dielectric or metallic and whether the ions pass through the wall sheath without collision. The simpler case of a low pressure, collisionless sheath and dielectric wall is considered first, with the higher pressure sheath and the comparison of dielectric and metallic orifices considered in later sections.

In the absence of a wall sheath the random thermal current of electrons to the wall is $\frac{1}{4}n_e v_e$, and that of positive ions is $\frac{1}{4}n_+ v_+$. But since the thermal velocity of electrons, $v_e$, is considerably greater than that of positive ions, $v_+$, and since $n_+ = n_e$ in the absence of negative ions in the plasma, the electron current to the wall would exceed the positive ion current. In order that current equality is preserved (ie $I_e = I_+$) a negative space charge accumulates on the dielectric wall and the potential at which the wall floats, $V_f$, impedes electron flow to the wall, as discussed in section 2.2.1. Thus, the sheath is a region over which the influence of the negative wall charge extends.

Assuming a mean electron density of $n_e$ in the bulk plasma and a Maxwell-Boltzmann distribution of electron energies, the number of electrons per unit volume with energy sufficient to cross the sheath is $n_e \exp(-eV_f/kT_e)$. The number of electrons incident on unit area of wall per second due to random thermal motion is then $\frac{1}{4}n_e v_e \exp(-eV_f/kT_e)$. Similarly the current of positive ions incident on unit area of wall per second is $\frac{1}{4}n_+ v_+$. Thus, in the steady state, since $n_+ \simeq n_e$,

$$v_e \exp\left[\frac{-eV_f}{kT_e}\right] = v_+, \qquad (2.3.1)$$

The mean thermal velocity of electrons is $v_e = (8kT_e/\pi m_e)^{\frac{1}{2}}$, while that of positive ions is $v_+ = (8kT_+/\pi m_+)^{\frac{1}{2}}$. Hence equation (2.3.1) yields the potential difference between the wall and the sheath edge as

$$V_f = \frac{kT_e}{2e} \cdot \ell n \left[\frac{T_e m_+}{T_+ m_e}\right], \qquad (2.3.2)$$

(von Engel (1965), p249).

In order to calculate the mean electric field in the sheath an estimate of the sheath thickness is required. This may be achieved by

treating the sheath as a space-charge limited diode of planar geometry, with $V = V_f$ at the plane plasma sheath boundary and $V = 0$ at the wall. If the electric field is zero outside the sheath, and if the mean charge density in the sheath is $n_+$ (ie no electrons or negative ions in the sheath), then the environment of a positive ion in the collisionless sheath is similar to that of an electron in a space-charge limited diode. Thus we can apply a suitably modified Child-Langmuir relation, (Hasted (1974))

$$d_s^2 = \frac{4\varepsilon_o}{9}\sqrt{\frac{2e}{m_+}} \cdot \frac{V_f^{3/2}}{J_+} , \qquad (2.3.3)$$

where $d_s$ is the sheath thickness, $\varepsilon_o$ is the permittivity of free space, $m_+$ is the ion mass and $J_+$ is the positive ion current density crossing the sheath to the wall.

Thus

$$J_+ = \tfrac{1}{4} n_+ e \, v_+ = \tfrac{1}{4} n_+ e \sqrt{\frac{8kT_+}{\pi m_+}} . \qquad (2.3.4)$$

Substitution of (2.3.4) into (2.3.3) yields

$$d_s^2 = \frac{8\varepsilon_o}{9n_+} V_f^{3/2} \sqrt{\frac{\pi}{ekT_+}} , \qquad (2.3.5)$$

showing that the sheath thickness is proportional to $V_f^{\frac{3}{4}}$.

In a theoretical analysis of the dependence of the sheath thickness on probe voltage, for spherical and cylindrical Langmuir probes, Bettinger and Walker (1965) derived the relationship

$$d_s \simeq 1.7 \, \lambda_D \left[\frac{eV_p}{kT_e}\right]^{\frac{3}{4}} , \qquad (2.3.6)$$

where $V_p$ is the probe voltage with respect to the plasma and $\lambda_D$ is the Debye length,

$$\lambda_D = \left[\frac{\varepsilon_o \, kT_e}{n_e \, e^2}\right]^{\frac{1}{2}} , \qquad (2.3.7)$$

From their analysis, equation (2.3.6) applies when the probe radius is much greater than the sheath thickness and when $eV_p/kT_e \gg 1$.

Thus, for the case of a dielectric orifice located in a discharge tube wall, the space-charge limited diode derivation (equation (2.3.5)) provides an estimate of $d_s$, while for the case of a pinhole in a metallic disc, the cylindrical probe theory leading to equation (2.3.6) may be more appropriate, especially at high probe voltages ($V_p > V_f$). However, despite the approximations involved in each derivation, the functional dependence of $d_s$ on voltage is the same, and both equations will be shown to give similar results.

For a plasma with $kT_e \simeq 4eV$, $T_+ \simeq T_g \simeq 400K$, $n_e = n_+ \simeq 10^{10}$ cm$^{-3}$, equations (2.3.2), (2.3.7), (2.3.5) and (2.3.6) give

$$V_f \simeq 30 \text{ V}$$

$$\lambda_D \simeq 2 \times 10^{-2} \text{ cm}$$

$$d_s \simeq 0.28 \text{ cm (from equation (2.3.5))}$$

$$d_s \simeq 0.20 \text{ cm (from equation (2.3.6))}$$

and

$$E_s \simeq \frac{V_f}{d_s} \simeq 130 \text{ V cm}^{-1}.$$

This electric field is approximately one order of magnitude greater than the axial electric field in the positive column of a dc glow discharge at low pressure. This estimate of the mean electric field is important in the analysis of ion lens effects considered in section 2.4.2.

It is also important to consider the energy acquired by ions in crossing the sheath when no collisions occur. In practice a collisionless sheath is only realised at pressures of less than $\sim 10^{-1}$ torr, where the ion mean free path, $\lambda_i$, is greater than the sheath thickness, $d_s$. Ideally the mass spectrometer used to analyse ions from a glow discharge will

have constant sensitivity and resolution over the complete range of ion energies sampled, thus the relative peak heights will be independent of the ion energy distributions of the effusing ions. The quadrupole mass spectrometer is noted for its constant transmission over a wide range of ion velocities through the quadrupole field and for this reason is favoured for ion sampling from glow discharges (Studniarz and Franklin (1968)). However, Kohout and Neiswender (1970) have observed that ions drifting through the quadrupole field must experience a minimum number of cycles of the radio-frequency field for a resolution R to be achieved.

If an ion of speed v travels through a quadrupole mass analyser of length L, where the electric field oscillates with frequency f, then the number of oscillations experienced by the ion is

$$N_o = \frac{Lf}{v} \qquad (2.3.8)$$

Experimentally, for a resolution R to be achieved (where R is defined as the ratio of a mass number, M, to the full width at half maximum peak height of a detected peak, $\Delta M$, at that mass number; ie $R = M/\Delta M$) $N_o \geq 3.5\ R^{\frac{1}{2}}$ oscillations must be experienced by the ions (Mathieson and Harris (1969)). Thus from (2.3.8)

$$v \leq \frac{Lf}{3.5R^{\frac{1}{2}}} \quad , \qquad (2.3.9)$$

or, expressed in terms of the ion energy

$$eV_{ion} = \tfrac{1}{2}m_+v^2 \leq \frac{L^2f^2m_+}{2(3.5)^2R} \qquad (2.3.10)$$

Typically, the ion energy must be less than a few tens of electron volts.

Equation (2.3.10) sets the upper limit to the ion energy for a required resolution. But if the ion energy is below this limit the instrument operation is independent of incident ion energy. Assuming L ≈ 15 cm,

$f \simeq 2$ MHz and the ion energy of the previously quoted example, ie $eV_f \simeq 30$ eV, equation (2,3.10) yields a resolution of $\sim 40$ (sufficient to resolve one mass unit at mass number 40).

The collisionless nature of the low pressure sheath has several important consequences. First, since no energy is lost in collisions with neutral molecules, the ions gain the full sheath energy $eV_f$ in crossing the sheath. Second, the spread in ion energies will be small ($\sim$ the ion thermal energy, $kT_+$) since only those few ions involved in collisions with neutral molecules in the sheath will not have energy $eV_s$. And finally, no ion-molecule reactions will occur in the sheath when the ion mean free path is greater than the sheath thickness, and so no modification of the ion mass-spectrum will result.

In general, literature reports of ion sampling refer to cases where the sheath is not collisionless. However, low pressure results have been published by Seguin et al (1972). The sampling orifice was located in a metallic probe (see section 2.4.1) allowing control of the sheath potential. $N^+$ and $N_2^+$ ions were sampled at pressures of 0.02 torr (where the sheath is collisionless, $\lambda_i > d_s$), 0.21 torr and 0.42 torr (where collisions occur in the sheath, $\lambda_i < d_s$). Figure 2.3.1 shows results obtained in measuring the energy of effusing $N^+$ ions (by applying a retarding field between orifice and mass spectrometer) as a function of sheath voltage. The slope of the line appropriate to 0.02 torr is 0.96 eV $V^{-1}$, indicating that $N^+$ ions sampled from a discharge at this low pressure have a most probable energy of 0.96 $V_s$ (where $V_s$ is the potential difference across the sheath, ie the difference between the plasma potential and the potential applied to the metallic sampling orifice).

The most probable energy of $N^+$ ions sampled from higher pressures is 0,90 $V_s$ at 0,21 torr and 0.83 $V_s$ at 0,42 torr the energy being lost in collisions in the sheath.

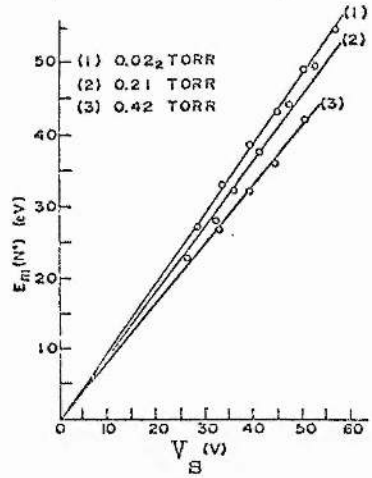


Figure 2.3.1 Most probable ion energy ($E_m$) versus sheath potential difference ($V_s$) for $N^+$ ions (Seguin et al (1972)).

The ion energy distribution was also measured by Seguin et al using the same ion retarding technique. Only ions with energy sufficient to overcome the retarding voltage are detected by the mass spectrometer. Since the number of ions of energy between E and E + dE is given by $dN = f(E)\,dE$, where f(E) is the ion energy distribution, and since the ion energy is proportional to its retarding voltage, the distribution is obtained from $f(E) \propto dN/dV$. Thus by differentiating the curve of number of ions sampled per second versus the applied retarding voltage, f(E) is obtained. The ion energy distribution of $N_2^+$ ions obtained by Seguin et al is shown in figure 2,3,2. The narrower spread at low pressure indicates few collisions in the sheath and thus most ions have an energy close to $eV_s$.

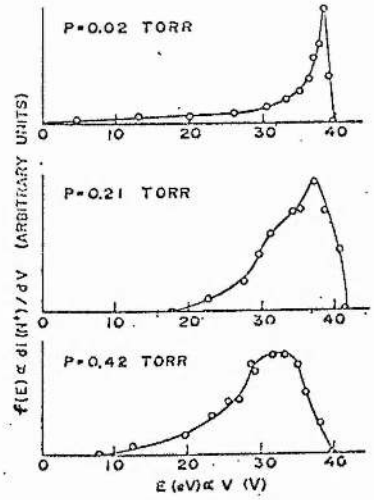


Figure 2.3.2 Ion energy distributions at three pressures. The sheath potential difference is 40 V in each case (Seguin et al (1972)).

## 2.3.2 The Wall Sheath at High Pressure

The region of pressure above 0.1 torr is of greater practical importance than the low pressure discharge since ionospheric reactions can be simulated in laboratory discharges in this pressure regime. However ion sampling is complicated by collisions occurring in the sheath prior to ion extraction from the discharge. The high pressure sheath is formed by precisely the same physical process as the low pressure sheath, that is the requirement for equal electron and positive ion currents to the wall. Thus the sheath potential is given by equation (2.3.2) as before. However energy acquired by ions from the sheath field will be lost in collisions with neutral molecules in the sheath, with the possible occurrence of ion molecule reactions, and very few ions will effuse from the discharge with energy $eV_s$. Before estimating the sheath thickness and ion energy gained in crossing the sheath, it is necessary to consider some ion mobility theory.

In a region of low electric field, the ion drift velocity in the field, $v_{d+}$, is much less than the mean thermal velocity of gas molecules and ions, $\bar{c}$. If the ion mean free path is $\lambda_i$, then $\tau = \lambda_i/\bar{c}$ is the mean time between collisions. In this time the ion moves under the acceleration due to the applied electric field, $a = eE/m_+$, and travels an extra distance, s, in the field direction, where

$$s = \tfrac{1}{2} a \tau^2 = \frac{eE}{2m_+} \tau^2. \tag{2.3.11}$$

Hence, the drift velocity is

$$v_{d+} = \frac{s}{\tau} = \frac{eE}{2m_+} \tau. \tag{2.3.12}$$

Defining the mobility as drift velocity per unit field, the positive ion mobility is

$$\mu_+ = \frac{e\tau}{2m_+}. \tag{2.3.13}$$

A more sophisticated theory due to Langevin (see Loeb (1961) ch.1) takes the velocity distribution of ions and gas molecules into account and possible differences in masses of ions and gas molecules. It yields

$$\mu_+ = \frac{0.75\ e\tau}{m_g} \sqrt{\frac{m_+ + m_g}{m_+}} \tag{2.3.14}$$

where $m_g$ is the mass of a gas molecule.

As previously shown for the low pressure sheath, the electric field is relatively high in the sheath, and this will be shown to be true at high pressure. Thus the low field mobility theory above does not apply to ions in the wall sheath field. At low fields $v_{d+}$ is much less than $\bar{c}$ and the mean time between collisions is determined by gas kinetic processes, only. Thus both $\tau$ and $\mu_+$ are independent of the applied field, E. But

when the field is increased to values typical of the sheath (ie a few hundred volts per cm) ions are more rapidly accelerated between collisions, and travel a mean free path in shorter time. The result is a mean time between collisions and mobility which depend on the electric field strength. For this situation $v_{d+} \sim \bar{c}$, and an approximate treatment has been considered by von Engel (1965, p118). This theory assumes that on average a constant fraction, $\kappa$, of the ion mean energy is lost in each collision with a gas molecule. This lost energy is then restored by acceleration in the electric field between collisions. Thus in equilibrium,

$$\tfrac{1}{2} \kappa m_+ \bar{c}^2 = eE\, v_{d+}\, \tau. \qquad (2.3.15)$$

Hence,

$$\tau = \frac{\kappa m_+ \bar{c}^2}{2eE\, v_{d+}} . \qquad (2.3.16)$$

But, since $\tau = \lambda/\bar{c}$, equation (2.3.16) becomes, on substitution for $\bar{c}$,

$$\tau = \left[\frac{\kappa m_+ \lambda^2}{2eE v_{d+}}\right]^{1/3} . \qquad (2.3.17)$$

Substitution for $\tau$, from equation (2.3.12), and solving for $v_{d+}$ yields

$$v_{d+} = \tfrac{1}{2}(\kappa)^{\frac{1}{4}} \left[\frac{eE\lambda}{m_+}\right]^{\frac{1}{2}} . \qquad (2.3.18)$$

Thus, the drift velocity is dependent on the square root of the electric field when the mean time between collisions is dependent on the field. The nature of the dependence of the mean time between collisions can be found from equations (2.3.12) and (2.3.18) giving,

$$\tau = \kappa^{\frac{1}{4}} \left[\frac{\lambda m_+}{eE}\right]^{\frac{1}{2}} \qquad (2.3.19)$$

revealing that the mean time between collisions is inversely proportional to the square root of the electric field in the high field case.

At a constant temperature, for a particular ion species moving through

a species of neutral gas molecules, using a simple hard sphere model (Loeb (1961) p41),

$$\lambda = \frac{1}{\sqrt{2}\,\sigma N} \quad , \tag{2.3.20}$$

where N is the neutral gas number density and $\sigma$ is the collision cross-section. Thus, equation (2.3.18) becomes

$$v_{d\pm} = \tfrac{1}{2}\,\kappa^{\frac{1}{4}} \left(\frac{e}{\sqrt{2}\,\sigma\, m_{\pm}}\right)^{\frac{1}{2}} \left(\frac{E}{N}\right)^{\frac{1}{2}} \quad , \tag{2.3.21}$$

or

$$v_{d\pm} = \mu_{\pm}' \left(\frac{E}{N}\right)^{\frac{1}{2}} \quad , \tag{2.3.22}$$

where $\mu_{\pm}' = \frac{\kappa^{\frac{1}{4}}}{2} \left(\frac{e}{\sqrt{2}\,\sigma\, m_{\pm}}\right)^{\frac{1}{2}}$ is a constant for a particular ion in a given neutral gas. Hence, the drift velocity of ions in a collision dominated wall sheath is dependent on the E/N in the sheath and the ion mass.

An expression for the thickness of the high pressure sheath has been found by Fette and Hesse (1970). In their derivation these authors assume an expression for the ion drift velocity similar to that of equation (2.3.21). They use

$$v_{d\pm} = \left[\frac{Ee\lambda}{2\, m_{\pm}}\right]^{\frac{1}{2}} , \tag{2.3.23}$$

which differs from (2.3.21) only by a numerical constant. The fraction of energy lost per collision, $\kappa$, depends on the nature of the colliding ion and neutral gas molecule, but according to von Engel (1965, p118) it is typically $\sim\frac{1}{2}$. Thus expression (2.3.23) gives a value of the ion drift velocity which is $\sim$ twice that obtained using (2.3.21). This is not a serious discrepancy as it is not possible to derive an exact value for $d_s$ in the high pressure sheath. In order to arrive at the same result as Fette and Hesse, it is preferable to use equation (2.3.23).

The derivation begins with Poisson's equation

$$\frac{dE}{dx} = \frac{e}{\varepsilon_o}(n_+ - n_e) \quad , \tag{2.3.24}$$

and the requirement of constant positive ion current flowing radially to the walls,

$$I_+(x) = I_+(o) = I_+(d) \tag{2.3.25}$$

where $x = 0$ represents the sheath edge ($V = V_s$) and $x = d_s$ represents the wall ($V = 0$). When the sheath thickness is much less than the discharge tube radius the problem can be treated in one dimension as expressed in equations (2.3.24) and (2.3.25). From (2.3.23),

$$I_+(x) = e\, n_+(x) \left[\frac{eE(x)\lambda}{2m_+}\right]^{\frac{1}{2}}, \tag{2.3.26}$$

thus, from (2.3.26) and (2.3.25) where $E = E_o$ and $n_+ = n_o$ at the sheath edge ($x = 0$),

$$n_+(x) = n_o\left[E_o/E(x)\right]^{\frac{1}{2}}, \tag{2.3.27}$$

The theory of Fette and Hesse assumes the existence of a pre-sheath region separating the sheath from the bulk plasma. However the values of $n_o$ and $E_o$ may be taken as those of the positive ion density and radial electric field in the bulk plasma without serious error, thus neglecting the modification of these parameters by the pre-sheath region.

In the sheath the density of positive ions is much greater than the electron density ($n_+ \gg n_e$). This follows since the density of electrons with sufficient energy to cross the sheath is reduced from the bulk plasma value by a factor $\exp(-eV_f/kT_e)$ which is typically $\sim 10^2$ to $5 \times 10^2$. Hence from equation (2.3.24) and (2.3.27), Poisson's equation becomes,

$$\frac{dE}{dx} = \frac{e}{\varepsilon_o}\, n_o\left[\frac{E_o}{E(x)}\right]^{\frac{1}{2}} \tag{2.3.28}$$

Integrating to obtain the spatial variation of electric field in the sheath gives,

$$E(x) = \left[\frac{3\, e\, n_o}{2\, \varepsilon_o} E_o^{\frac{1}{2}} x + E_o^{3/2}\right]^{2/3}. \tag{2.3.29}$$

Using the boundary conditions $V(x=d_s) = 0$ and $V(x = 0) = V_f$, further integration gives the spatial variation of potential in the sheath,

$$V_f - V_{(x)} = \frac{2\varepsilon_o}{5e\, n_o\, E_o^{\frac{1}{2}}} \left(E_{(x)}^{5/2} - E_o^{5/2}\right). \qquad (2.3.30)$$

Equation (2.3.29) shows that the maximum electric field in the sheath occurs when x is a maximum, ie $x = d_s$. Denoting this value of field by $E_{max}$ and setting the reference of potential $V = 0$ at the wall ($x = d_s$) we obtain from equation (2.3.30),

$$E_{max} = E_o \left[1 + \frac{5e\, n_o\, V_f}{2\, \varepsilon_o\, E_o^2}\right]^{2/5}. \qquad (2.3.31)$$

Fette and Hesse (1970) approximate the field at the sheath edge $E_o$ by,

$$E_o = \frac{1}{c}\frac{V_e}{\lambda_D}, \qquad (2.3.32)$$

where $V_e = k\, T_e/e$, the electron temperature expressed in volts, and c is a constant which has the value $\sqrt{2}$ for an highly non-isothermal plasma ($T_e \gg T_+$) and the value 2.32 for an isothermal plasma ($T_e = T_+$), ie $\sqrt{2} < c < 2.32$. Thus equation (2.3.32) is an empirical relation, assuming that electrons of mean energy $eV_e$ are able to penetrate a distance $\sim\lambda_D$ into a region of retarding field $E_o$ - consistent with the concept of Debye length.

Combining equations (2.3.32), (2.3.31) and using (2.3.7) for the Debye length, with $n_o = n_e$ and $kT_e/e = V_e$, we get

$$E_{max} = E_o \left[1 + \frac{5V_f}{2V_e}\, c^2\right]^{2/5}. \qquad (2.3.33)$$

Noting that $c > 1$ and for a non-isothermal plasma $V_f > V_e$ (from equation (2.3.2)), thus

$$E_{max} \simeq E_o \left[\frac{5}{2}\, c^2\, \frac{V_f}{V_e}\right]^{2/5}. \qquad (2.3.34)$$

From the form of equation (2.3.29) it can be seen that $E_{max}$ corresponds to the field at the maximum value of x, ie $x = d_s$.

Making the approximation that the transition from sheath to plasma occurs with a negligible pre-sheath region, the positive ion density, electric field and Debye length immediately outside the sheath are $n_o$, $E_o$ and $\lambda_D$ respectively. Assuming $E_{max} \gg E_o$, equations (2.3.29), (2.3.32), (2.3.34) and (2.3.7) combine to yield

$$d_s \simeq \left[\frac{5}{2}\frac{V_f}{V_e}\right]^{3/5} \frac{2}{3} c^{1/5} \lambda_D. \qquad (2.3.35)$$

Considering a typical high pressure (p $\sim$ few torr) plasma where $kT_e = eV_e \simeq 2eV$, $T_+ \simeq T_g \simeq 400^oK$, $n_e = n_+ \simeq 10^{10}$ cm$^{-3}$, and $c \simeq 2$, equations (2.3.2), (2.3.7) and (2.3.35) give,

$$V_f \simeq 14 \text{ V}$$

$$\lambda_D \simeq 10^{-2} \text{ cm}$$

$$d_s \simeq 4 \times 10^{-2} \text{ cm}$$

and $$E_s \simeq 350 \text{ V cm}^{-1}.$$

Thus the sheath is only a few Debye lengths thick and the average field is greater than the longitudinal electric field in the high pressure discharge ($\sim$ 100 V cm$^{-1}$). Also, from equations (2.3.32) and (2.3.34), the maximum electric field can be calculated as

$$E_{max} \simeq 600 \text{ V cm}^{-1}.$$

As in the case of the low pressure sheath, it is also possible to estimate the average energy of an ion effusing from the plasma, having crossed the collision-dominated sheath. Using equation (2.3.22) for the drift velocity in the high field of the sheath gives

$$e V_{ion} = \tfrac{1}{2} m_+ v_{d+}^2 = \frac{m_+ \mu_+'^2 V_f}{2 N d_s} , \qquad (2.3.36)$$

where the average sheath electric field $E \simeq V_f/d_s$. Noting that $\mu_+' \propto (\sigma m_+)^{-\frac{1}{2}}$, equation (2.3.36) shows that the ion energy will be independent of the ion mass when the ion crosses the sheath and enters the sampling orifice. However the ion energy will be inversely proportional to the collision cross-section $\sigma$. Consequently, ions with little probability of collision (small cross-section and long mean free path) gain greater energy from the sheath field than those with high collision probability, and thus have greater energy on leaving the plasma.

When ions move amongst their own neutral species resonant charge transfer occurs which increases the collision cross-section (Hasted (1972), ch 12). Hence ions in their own neutral gas will have low energies on effusing from the plasma.

Simultaneous ion mass and energy analysis has been performed by Knewstubb and Tickner(1962(b)) and Seguin et al (1972). Both groups found that the energy attained by ions in crossing the sheath depends on the ion species. This has been attributed to ion mobility differences where, as the preceding discussion has shown, the collision cross-section determines the ion energy.

Knewstubb and Tickner (1962(b)) used a magnetic sector mass spectrometer and electrostatic deflection energy analysis to show that lighter ions acquired greater energy from the sheath than heavy ions. For example, when sampling from a 3:1 - Kr:Ar mixture at 1 torr they find $H_3O^+$ (mass 19), which is present due to residual water vapour, has $\sim$2 eV more energy than $Ar^+$ (mass 40) on effusing through the sheath. Also, sampling from a krypton discharge at a similar pressure, they found the heavier

$Kr_2^+$ ion to have greater energy than the atomic $Kr^+$ ion. This is due to the atomic ion suffering resonant charge transfer collisions in the neutral gas.

In the preceding section (2.3.1) the experiments of Seguin et al (1972) illustrated the effect of the collisionless sheath on ion energy, showing that ions in a low pressure (0.02 torr) discharge in nitrogen leave the plasma with approximately the full sheath energy. These same experiments show that at higher pressure (0.42 torr) the slope of the mean ion energy versus sheath voltage is 0.83 eV $V^{-1}$ indicating a loss of 17% of the sheath energy in collisions (see figure 2.3.1). Also, figure 2.3.2 shows the greater spread in ion energies found by Seguin et al (1972) at the higher pressure. This arises from the greater variation in ion energies resulting from collisions.

A serious consequence of the high sheath electric field is that endoergic ion-molecule reactions may become possible. Evidence for such reactions in nitrogen has been found by Bohme and Goodings (1966). At high accelerating voltage ($\sim$ 50v between plasma and wall, most of which appears across the sheath) they observed the dissociative charge transfer reaction.

$$N_2^+ \text{ (fast)} + N_2 \longrightarrow N^+ + N + N_2.$$

Seguin et al (1972) have measured the energy distribution of $N^+$ ions produced in a nitrogen discharge similar to that of Bohme and Goodings. This showed a long low-energy tail indicating that much of the $N^+$ was produced in the sheath and hence did not undergo appreciable acceleration in the sheath field. This supports the theory that dissociative charge transfer in the sheath produces $N^+$ in the above reaction as most of the sheath energy acquired by the $N_2^+$ ion is lost in the inelastic dissociating collision with $N_2$.

Knewstubb and Tickner (1963), studying a glow discharge in water vapour, have observed the ions in the $H_3O^+$. $(H_2O)_n$ series (n = 0, 1.....5). These authors suggested that the high sheath fields can lead to collisional dissociation of one, or even two, of the water molecules from the cluster ion, thus biassing the mass spectrum in favour of the lighter (smaller n value) ions,

Clearly the use of high sheath fields is to be avoided wherever possible. When biassed metallic pinholes are used for positive ion sampling the negative bias should be small and if signal magnitudes permit, the pinhole should be allowed to float at wall potential (see section 2.4).

The influence of the wall sheath, which exists at the plasma-wall boundary, on positive ion currents sampled through an orifice in the discharge wall has been considered in this section. This sheath may either be collisionless ($\lambda_i > d_s$) or collisions between ions and neutral molecules may occur ($\lambda_i < d_s$). In either case the potential of the wall with respect to the plasma (the sheath potential) is given by equation (2.3.2) but the energy gained by positive ions in crossing the sheath will depend on whether collisions occur. Thus ions crossing a collisionless sheath gain approximately the full sheath energy, while ions undergoing collisions will gain less than the full sheath energy.

Calculations based on equations for sheath voltage (equation (2.3.2)) and sheath thickness (equation (2.3.35) for the collisionless case, and equation (2.3.5) when collisions occur in the sheath) show that the average electric field in the sheath is greater when the sheath is collision dominated. However the sheath field is considerably greater than the longitudinal electric field of the discharge, in both the collision-free and collision-dominated cases. This high field region which the ions must cross before mass-spectrometric analysis can be performed can

influence the ion effusion currents in two ways. First, endoergic ion-molecule reactions may occur in the high-sheath field producing ions which are not typical of the lower electric field of the bulk discharge. Such reactions include collisional break-up of cluster species. Second, rapid acceleration of ions can result in high ion velocities through the analysing region of the mass spectrometer. In the case of a quadrupole mass spectrometer the resolution will be limited according to equation (2.3.10).

## 2.4 INFLUENCE OF SAMPLING ORIFICE ON ION CURRENTS

### 2.4.1 Metallic sampling orifices

In the previous section the effects of the positive ion wall sheath on ion currents were discussed. The potential difference between the sheath edge and the discharge wall is determined by the prevailing conditions in the plasma (ie the gas and electron temperatures and ion species appropriate to equation (2.3.2)). This is the floating potential of the system. Alternatively, when a metallic sampling probe is used, direct biassing may be employed, allowing control of the sheath potential difference. Results of the previous section apply whether the sampling orifice floats or is directly biassed as long as the positive ion sheath is maintained (and $V_f$ is replaced by $V_p$ for a biassed metallic orifice). Additional effects introduced by using a metallic sampling probe are now considered.

Small biassed sampling orifices behave similarly to Langmuir probes when used for ion or electron collection. The use of such sampling probes allows greater control of the sheath around the sampling point and the potential at which the ions leave the discharge than can be achieved using dielectric orifices. A typical positive ion probe

characteristic obtained by Lindinger (reproduced from the review of Hasted (1974)) is shown in figure 2.4.1. The probe voltage is referred to the plasma potential of the discharge in this experiment and $V_f$ is the floating potential of the wall with respect to the plasma. There are a number of features appearing in this figure which will be discussed.

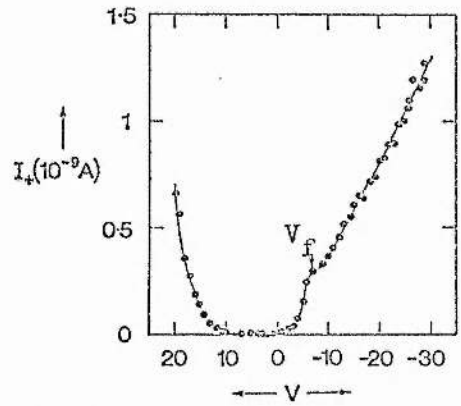


Figure 2.4.1 Metallic ion-sampling probe characteristic - total positive ion effusion current to mass spectrometer as a function of probe potential measured with respect to plasma potential in an argon discharge, p = 0.2 torr, 2 mA current (from Hasted (1974)).

First, at high negative voltages ($|V| > |V_f|$) simple Langmuir probe theory predicts saturation of the positive ion probe current. This is not observed in figure 2.4.1. A similar effect has been observed by Bohme and Goodings (1966), who failed to achieve positive ion saturation at voltages up to 80V negative with respect to the potential at which positive ion current is first detected. These authors attribute this phenomenon to an increase in the effective "collection area" of the probe and the orifice. Equation (2.3.5) for the low pressure sheath and equation (2.3.35) for the high pressure sheath show that the thickness of the sheath increases as the potential between probe and plasma (the sheath potential) is increased. For a perfectly planar sheath-plasma boundary, an increase in sheath thickness results only in an increase in sheath volume, but not in the area of the sheath at the boundary. However, in practice, small

sampling orifice discs are used to cause little disturbance to the electric field in the bulk plasma. Hence the nearness of the disc edge to the orifice results in non-planar equipotential surfaces above the orifice due to the influence of edge effects. Making the disc more negative relative to the plasma increases the area of the sheath-plasma boundary and the effective "collection area" of the probe and orifice, with a resulting increase in positive ion current with increasing sheath voltage.

Mark and Helm (1974) point out that saturation may be obtained when large diameter sampling probes are used. In this case the effect of the edge of the probe is small and an almost plane sheath edge exists, parallel to the probe. As the sheath thickness is increased the "collection area" is still approximately equal to the probe area. Hence no increase in collection of ions occurs after saturation. However the use of large metallic probes seriously distorts the electric field in the bulk plasma.

At more positive potentials than those corresponding to ion saturation, figure 2.4.1 shows that the ion current versus potential curve changes slope at $V_f$ and drops to zero at $V = 0$. When the probe is at floating potential $V_f$, a sheath exists which is similar to that existing between the plasma and a dielectric wall. The potential between probe and plasma is given by equation (2.3.2) and the positive ion current corresponds to a space charge limited current in the positive ion space charge sheath. This is given by the Child-Langmuir equation as

$$i_{+} = \frac{4\varepsilon_o}{9} \sqrt{\frac{2e}{m_{+}}} \frac{V_f^{3/2}}{d_s^2} \cdot A_o \qquad (2.4.1)$$

where $d_s$ is the sheath thickness and $A_o$ is the orifice area.

The current of positive ions at the sheath edge is simply the random thermal current of ions given by

$$i_+ = \tfrac{1}{4} e n_+ v_+ A_c \qquad (2.4.2)$$

where $v_+$ is the thermal velocity of positive ions ($v_+ = \sqrt{8kT_+/\pi m_+}$), $n_+$ is the density of positive ions in the bulk discharge and $A_c$ is the "collection area" for positive ions. For a plane sampling probe and sheath edge, $A_o \simeq A_c$, and the current arriving at the sheath edge will be equal to that reaching the probe in the steady state. In the absence of the sheath expansion previously discussed, the value of the positive ion probe current at $V_f$ is the saturation positive ion current.

At potentials more positive than the plasma potential the electric field in the region of the orifice is such that the orifice disc is more positive than the bulk plasma. Thus positive ions are repelled by the orifice disc and no positive ion current is observed. However, electrons are accelerated to the orifice probe under these conditions, and at high positive voltages the electron energy becomes sufficiently great to enable electron impact ionisation of neutral species to take place at the orifice. This is the explanation of the increase in positive ion current observed at high positive sampling probe potentials. This effect has been used to evaluate the result of collisions in the orifice leading to ion-molecule reactions (see section 2.4.3).

2.4.2 Ion Lens Effects

When a large diameter orifice is used (diameter > $\lambda_D$) distortion of the electric fields in the orifice vicinity is likely to occur. This phenomenon has been discussed by Hasted (1974,1975) who considers four possible configurations. These are reproduced for illustration in figure 2.4.2 which shows equipotential lines in the orifice region. Ideally the equipotentials in the sheath are undistorted (figure 2.4.2(c)) and ion lens effects are minimal. This only occurs if the orifice diameter

is less than $\lambda_D$. When the orifice diameter d exceeds the sheath thickness, $d_s$, the plasma penetrates into the orifice as shown in figure 2.4.2(d). Hence it is normal to have $d \lesssim d_s$.

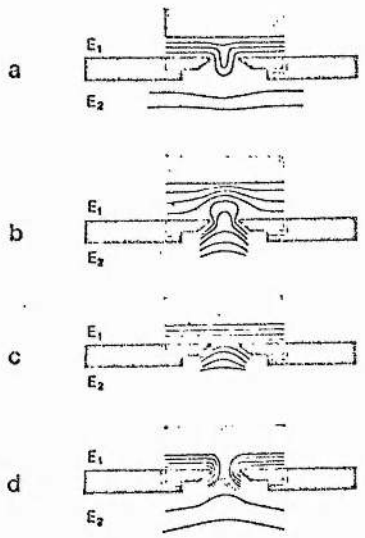


Figure 2.4.2 Equipotential planes at a metallic sampling orifice, (a) $E_2 < E_1$; (b) $E_2 \gtrsim E_1$; (c) $E_2 = E_1$; (d) collapse of sheath when $d > d_s$, (from Hasted (1974)).

Smith and Plumb (1973) have pointed out that the ion current densities incident on the sheath boundary (equation (2.2.10))can only be equated with those reaching the sampling orifice when there are no electrostatic lens effects altering the effective area of the orifice.

An example of the ion lens effect is given by Studniarz and Franklin (1968) who have used a metallic orifice probe of $\sim$ 500μm diameter to sample methane discharges with a Debye length $\lambda_D \sim$ 500 μm. These authors have estimated the potential at the probe orifice to be $\sim$ 50V more positive than that on the glass wall in the probe vicinity. This was done by calculating the potential of the glass wall with respect to the plasma (equation (2.3.2)) and measuring the probe-plasma potential. Since the

plasma will be positive with respect to the wall, the equipotentials will appear as in figure 2.4.2(a). Thus in Studniarz and Franklin's experiment ions were deflected away from the probe while electrons were accelerated towards it, resulting in a ratio of electron to positive ion current through the orifice of 100:1. Electron impact ionization of neutral particles at the probe was thus possible, and the mass spectrum displayed larger peaks due to direct ionisation than was representative of the stable ion species in the plasma.

Hasted (1974, 1975) has examined the operation of a biassed orifice probe for ion extraction through a thin orifice into a region of electric field $E_a$ which accelerates the ions towards the mass spectrometer. The requirement that the orifice should be thin (length of orifice tube < orifice radius) is necessary if the orifice is to be treated as a single aperture, electrostatic, ion lens of focal length f, according to the formula proposed by Davisson and Calbick (1932),

$$\frac{1}{f} = - \frac{(E_2 - E_1)}{4V} \quad , \qquad (2.4.3)$$

where $E_2$ is the field on the exit side of the lens (ie $E_2 = E_a$), $E_1$ is the field at the entrance to the lens(ie $E_1 = E_s$, the sheath field) and V is the orifice potential, referred to the plasma potential as zero. The characteristics of such an ion lens are given in figure 2.4.3 (taken from Hasted (1974)) showing that the ion current for each accelerating field behind the orifice exhibits a peak corresponding to the optimum value of the focal length, given by equation (2.4.3).

According to the high pressure sheath theory of Fette and Hesse, the sheath field near the probe is given by equation (2.3.34) as

$$E_{max} \simeq E_o \left[ \frac{5}{2} c^2 \frac{y_n}{y_e} \right]^{2/5}$$

where, from equation (2.3.32),

$$E_o = \frac{V_e}{c\,\lambda_D} .$$

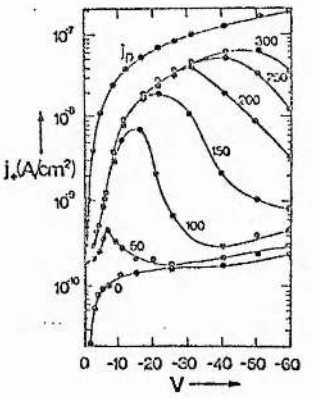


Figure 2.4.3 Focussing characteristics of a biassed sampling orifice for various accelerating voltages behind the orifice (marked against each curve). $j_p$ is the total orifice current density (from Hasted (1974)).

Substituting $E_{max}$ for $E_1$, and $E_a$ for $E_2$ in equation (2.4.3) and denoting the potential of the orifice with respect to plasma potential at which optimum focussing occurs as $V = V_m$(the optimum potential across the sheath), Hasted derived,

$$\frac{E_a}{4\,V_m} - \frac{V_e}{4\,V_m\,c\lambda_D}\left[\frac{5}{2}\,c^2\,\frac{V_m}{V_e}\right]^{2/5} = -\frac{1}{f} = \text{constant} \qquad (2.4.4)$$

The accelerating field behind the lens is given by

$$E_a = \frac{V_a - V_m}{d_a} \qquad (2.4.5)$$

where $V_a$ is the accelerating potential applied to the ion current and $d_a$ is the distance between the lens and the accelerating electrode.

The data of figure 2.4.3 were obtained with $d_a = 5$ cm, $V_e = 1$ eV, $n_e = 10^{10}$ cm$^3$ and $c = 2$. Hasted has calculated that this leads to a focal length of the ion lens which varies by no more than 15% for each of the peaks in ion current of figure 2.4.3.

The ion lens formula, equation (2.4.3) shows that the lens is only converging when $E_2 > E_1$. Referring to figure 2.4.2, this occurs in case b, while for case c no lens action takes place. Case a, that of Studniarz and Franklin (1968), corresponds to a diverging lens for positive ions, which is consistent with the high electron current through the orifice observed by these authors.

2.4.3 Effects Occurring In The Orifice Tube

In the preceding section, it was shown that in normal operating conditions, in order to avoid penetration of the plasma into the orifice, the orifice diameter should not exceed the sheath thickness ($d < d_s$). This requirement limits the maximum allowable orifice area. However, as yet, no limitation has been imposed on the orifice tube length used in sampling.

The orifice is used to sample the ions or neutral particles effusing from a discharge at a few torr pressure into a low pressure chamber ($p < 10^{-3}$ torr). Thus in the vicinity of the orifice there is a transition zone where the density of neutral gas particles decays from its value in the discharge to its value in the mass spectrometer chamber.

There is some possibility of ion-molecule reactions occurring in the orifice tube and immediately beyond where the neutral particle density is still considerable. There is also the possibility of elastic scattering of ions from unreactive neutral species. The consequences of these collisional effects are explained below.

The probability P of a particle (ion or neutral gas molecule) making a collision while moving a distance dx through a gas density N is,

$$P = N \sigma \, dx, \qquad (2.4.6)$$

where $\sigma$ is the cross-section for the collision which may be either elastic or inelastic. The occurrence of an ion-molecule reaction is a particularly important inelastic collision. Similarly if a beam of particles of current i pass through a neutral gas of density N, the change in the current due to collisions in the distance dx is given by (Hasted (1972) p11),

$$\begin{aligned} di &= - P\, i \\ &= - N\, \sigma\, i\, dx, \end{aligned} \qquad (2.4.7)$$

where the current is reduced by collisional scattering and reactions.

Thus the beam of particles is attenuated according to

$$i = i_o \exp(- N\sigma x). \qquad (2.4.8).$$

The attenuation of a positive ion beam by neutral gas molecules after effusion from a discharge through a sampling orifice may be described by equation (2.4.8). In this case, while scattering of ions out of the beam will result in attenuation, the occurrence of ion-molecule reactions will result in a change of relative species concentrations in the beam. Thus, some species may be severely attenuated in the beam while others increase in concentration as they are created in the effusing beam.

To account for the effect of collisions in and behind the orifice the neutral gas density variation in this region must be known. The geometry is illustrated in figure 2.4.4, where X is a point on the beam axis (ie on a line drawn through the centre of the orifice, perpendicular to the orifice plane) at a distance x from the orifice. Assuming an ideal zero-length orifice of radius R and an isotropic velocity distribution of gas molecules in the discharge, the density of effusing particles contained in solid angle $\Omega$ is

$$N' = \frac{N\,\Omega}{4\pi}, \qquad (2.4.9)$$

where N is the gas density in the discharge.

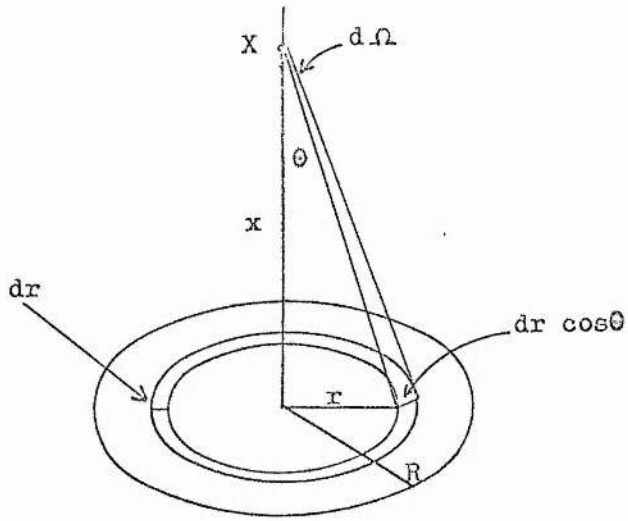


Figure 2.4.4 Solid angle dΩ subtended at X by annulus of thickness dr in sampling orifice of radius R.

Thus at point X on the axis the contribution to the density from an annulus in the orifice between radius r and r + dr is

$$dN' = \frac{N\ d\Omega}{4\pi} \quad . \tag{2.4.10}$$

The element of solid angle dΩ is given by

$$d\Omega = \frac{2\pi\ r\ dr}{r^2+x^2}\ \cos\Theta \tag{2.4.11}$$

and

$$\cos\Theta = \frac{x}{(r^2+x^2)^{\frac{1}{2}}} \tag{2.4.12}$$

Hence the neutral gas density at X, integrated over the orifice is, from equation (2.4.10) to (2.4.12)

$$N'(x) = \frac{N}{2}\int_0^R \frac{x\ r}{(r^2+x^2)^{3/2}}\ dr$$

$$= \frac{N}{2}\left[1 - \frac{x}{(R^2+x^2)^{\frac{1}{2}}}\right] \tag{2.4.13}$$

Equation (2.4.13) represents the variation of gas density on the axis that will be encountered by an effusing ion beam. Since the probability of collision in an element dx, on the beam axis is proportional to $N'(x)\,dx$ (equation (2.4.6)), integrating $N'(x)$ along the entire beam axis yields the probability of an ion making a collision after effusing through the orifice as

$$p = \sigma \int_0^\infty N'(x)\ dx = \sigma \frac{N}{2} R. \qquad (2.4.14)$$

Thus the attenuation of the ion current between the sampling orifice and the mass spectrometer (where collisions are negligible) is

$$i = i_o \exp(-\frac{N}{2} \sigma R). \qquad (2.4.15)$$

The density of gas molecules at the centre of the orifice can be obtained from equation (2.4.13) by letting $x \rightarrow 0$. Hence the effective gas density at the orifice centre is N/2. In the non-ideal situation where the orifice has a finite length L, taking the gas density as N/2 in the entire length of the orifice tube results in an ion current attenuation of

$$i = i_o \exp\{ - \frac{N}{2} \sigma (R + L)\} \qquad (2.4.16)$$

and the effective length for collisions in the region of the orifice is (L + R). Since the cross-section $\sigma$ will depend on the nature of the ions and neutral gas species, whether for scattering or ion-molecule reactions, the degree of attenuation of primary ion species effusing from the plasma will be different for the various ion species in the beam.

The attenuation mechanism of equation (2.4.16) has been considered by Helm et al (1974) and figure 2.4.5 shows their calculated attenuation of species X due to conversion to species X' in ion-molecule reactions for orifice dimensions of R + L = 30 μm, and R + L = 100μm as shown. These authors have used this attenuation of primary ions to measure ion-

molecule reaction cross-sections.

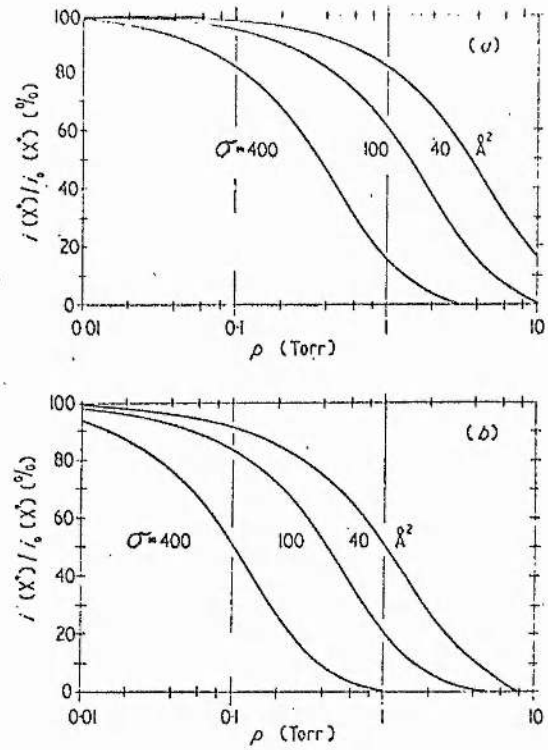


Figure 2.4.5 Attenuation of species $X^+$ by an ion-molecule reaction of cross-section $\sigma$ occurring in the effusing ion beam, calculated from equation (2.4.16) (a) R + L = 30μm (b) R + L = 100μm (from Helm et al (1974)).

They employed a metallic sampling orifice, biassed positively to attract electrons, and produce primary ions in the orifice region by electron bombardment of neutral gas as described at the end of section 2.4.1. Only ions produced between the ionisation region at the orifice and the mass spectrometer are measured since primary and secondary ions produced in the plasma are repelled by the positive sampling probe. Thus in sampling from a water vapour discharge, $H_2O^+$ was produced at the orifice and subsequently converted to $H_3O^+$ by

$$H_2O^+ + H_2O \longrightarrow H_3O^+ + OH.$$

By measuring the $H_2O^+$ and $H_3O^+$ ion currents to the mass spectrometer the reaction cross-section was measured as 0.85 $nm^2$.

When collisional scattering of ions out of the ion beam occurs, ions of low mass number are generally scattered more than heavy ions. Wellenstein and Robertson (1972) have sampled a helium discharge and observed the ratio of molecular to atomic ion currents, $i(He_2^+)/i(He^+)$, to increase with orifice length and pressure (figure 2.4.6). They attribute this to increased scattering of the lighter atomic ion, $He^+$, in the longer orifice and at higher pressures. Resonant charge transfer between $He^+$ and He atoms will occur in the orifice, and this will result in high scattering attenuation of the atomic ion.

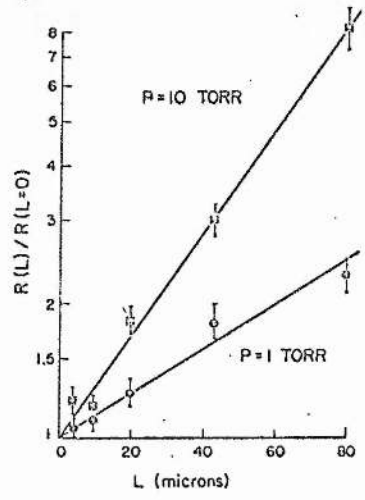


Figure 2.4.6 Normalised ratio of molecular ($He_2^+$) to atomic ($He^+$) ions versus thickness of sampling orifice (from Wellenstein and Robertson (1972))

Pahl (1963), sampling from an Ar discharge, and Franck and Ludemann (1972), sampling from an Hg discharge, have also noted the collisional scattering attenuation of lighter ions. The latter authors found the $Hg_2^+$ and $Hg^+$ ions to obey the relation,

$$\left.\frac{i(Hg_2^+)}{i(Hg^+)}\right]_{measured} = \left.\frac{i(Hg_2^+)}{i(Hg^+)}\right]_{true} \exp\left\{(L+R)\frac{p}{2}\left[\frac{1}{\lambda_o(Hg^+)} - \frac{1}{\lambda_o(Hg_2^+)}\right]\right\} \tag{2.4.17}$$

where p is the discharge pressure and $\lambda_o$ is the ion mean free path at 1 torr pressure. The true ion current ratio, typical of the ions in the discharge, is found by extrapolating the measured ratio to zero pressure.

The consequence of collisional scattering of ions to the orifice wall is of considerable importance when a dielectric orifice is used for ion sampling. Smith and Plumb (1973) have drawn attention to the possibility of accumulation of positive charge on the wall of the orifice tube. This would lead to an electric field which would oppose the flow of ions through the orifice. Ion currents would be reduced and only high energy ions could penetrate the fields in the orifice. The problem may be overcome to some extent by using a conductive coating on the mass spectrometer side of the orifice (Knewstubb and Tickner (1962(b)), provided that the coating does not interfere with the gas discharge (eg penetration of the discharge through the orifice to the coating). The use of a metallic orifice overcomes the space charge build up but ions will still be lost to the orifice tube wall. The most satisfactory solution is to use a thin orifice such that the orifice length is less than its diameter.

The design of the ion sampling orifice can have considerable effect, deliberate or accidental, on both the magnitude and relative composition of the total positive ion current to the mass spectrometer. The use of a metallic sampling orifice probe allows the probe to be biassed with respect to the plasma potential. Increasing negative bias on the probe increases the positive ion current. However large negative (or positive)

voltage applied at the orifice will result in distortion of the electric field around the probe, thus causing ion lens action. Similar distortion, with the same ion lens action result, will occur when the diameter of the sampling orifice is sufficiently large that the electric field penetrates through the orifice. This happens when the orifice diameter is greater than the Debye length characterising the plasma. The ion lens created by the distorted field may either focus or defocus the effusing ion current, thus enhancing or diminishing the mass-spectrometer signal.

Finally, the orifice length should be such that neither collisional scattering nor ion-molecule reactions occur in the orifice tube. Thus the condition that $L < R$ should be satisfied. If this is not the case then the scattering and ion-molecule processes can modify the positive ion densities observed mass spectrometrically from those representative of the discharge.

Thus careful design of the sampling orifice can minimise complications in the analysis of the mass spectrum arising from this source.

## 2.5 CONCLUSIONS

The preceding discussion has shown that positive ion mass spectra sampled from dc glow discharge plasmas can be influenced by many effects. These effects may be divided into two groups; those which arise from experimental design and those which are largely outwith experimental control. The most important design feature of an ion sampling experiment concerns the construction of the sampling orifice. Section 2.4 has shown that, ideally, such an orifice should have a diameter to length ratio greater than unity to avoid the possibility of reactions occurring in the orifice tube. Also, to minimise the effect of field penetration

through the orifice, the diameter should be less than the plasma Debye length. Whether a metallic or dielectric orifice is chosen largely depends on the object of the experiment. However, for straightforward ion monitoring, a dielectric orifice is more suitable since it disturbs the plasma least and avoids biassing problems.

The factors which cannot be controlled in an experiment are those which are part of the natural behaviour of the discharge, such as ion diffusion rates, negative ion influence, volume recombination effects and wall sheath collisions. Section 2.2 and 2.3 have indicated the experimental conditions where such effects will be important and, where necessary, how these may be estimated.

Chapter 3 describes a mass-spectrometric ion monitoring system which has been designed and constructed specifically to investigate plasmas used to excite $CO_2$ lasers. Many of the effects discussed in Chapter 2 are illustrated and evaluated for this system.

## References


Bettinger R T and Walker E H, 1965, Phys Fluids, 8, 748.

Bletzinger P, Laborde D A, Bailey W F, Long W H, Tannen P D and Garscadden A, 1975, IEEE J Quantum Electron, QE-11, 317.

Bohme D K and Goodings J M, 1966, Rev Sci Instrum, 37, 362.

Brown S C, 1959, "Basic Data of Plasma Physics", MIT Press, New York.

Davisson C J and Calbick C J, 1932, Phys Rev, 42, 580.

Dawson P H and Tickner A W, 1963, Proc 6th Intern Conf on Ioniz Phenom in Gases, Paris, 2, 79.

Drawin H W, 1968, in "Plasma Diagnostics", ed. Lochte-Holtgreven, North Holland, Amsterdam.

Evans H E and Jennings P P, 1965, Trans Faraday Soc, 61, 2153.

Fette K and Hesse J, 1970, Z Naturforsch, 25a, 518.

Fite W L and Rutherford J A, 1964, Discuss Faraday Soc, 37, 192.

Francis G, 1956, in "Handbuch der Physik," ed Flugge, Springer Verlag, Berlin.

Franck G and Ludemann H, 1972, Z Naturforsch, 27a, 1278.

Hasted J B, 1972, "Physics of Atomic Collisions," Butterworth, London.

Hasted J B, 1974, Advances in Mass Spectrom, 6, 901.

Hasted, J B, 1975, Int J Mass Spectrom and Ion Phys, 16, 3.

Hatori S and Shioda S, 1976, J Phys Soc Japan, 40, 1449.

Helm H, Howorka F, Handle F, Egger F, and Lindinger W, 1974, J Phys B, 7, 170.

Kenty C, 1962, Phys Rev, 126, 1235.

Keren H, Avivi P and Dothan F, 1976, IEEE J Quantum Electron, QE-12, 58.

Kohout F C and Neiswender D D, 1970, Int J Mass Spectrom and Ion Phys, 4, 21.

Knewstubb P F, 1969, "Mass Spectrometry and Ion-Molecule Reactions", Cambridge University Press, London.

Knewstubb P F and Tickner A W, 1962(a), J Chem Phys, 37, 2941.

Knewstubb P F and Tickner A W, 1962(b), J Chem Phys, 36, 674.

Knewstubb P F and Tickner A W, 1963, J Chem Phys, 38, 464.

Kuehn D G and Chanin L M, 1972, J Appl Phys, 43, 339.

Kuehn D G and Chanin L M, 1973, J Appl Phys, 44, 5288.

Laderman A J and Byron S R, 1971, J Appl Phys, 42, 3138.

Loeb L B, 1961, "Basic Processes of Gaseous Electronics", University of California Press, Berkeley.

McDaniel E W, Cermak V, Dalgarno A, Ferguson E E and Friedman L, 1970, "Ion-Molecule Reactions", Wiley, New York.

Mark T D and Helm H, 1974, Acta Phys Austr, 40, 158.

Mathieson E and Harris T J, 1969, Am J Phys, 37, 1054.

Olsen, R E, 1972, J Chem Phys, 56, 2979.

Oskam H J, 1958, Philips Research Reprints, 13, 335.

Pahl M, 1963, Z Naturforsch, 18a, 1276.

Puckett L J, Kregel M D and Teague M W, 1971, Phys Rev, A4, 1659.

Schildcrout S M, Collins J G and Franklin J L, 1970, J Chem Phys, 52, 5767.

Seguin J G, Dugan C H and Goodings J M, 1972, Int J Mass Spectrom and Ion Phys, 9, 203.

Smith D and Plumb I C, 1973, J Phys D, 6, 1431.

Studniarz S A and Franklin J L, 1968, J Chem Phys, 49, 2652.

Tannen P D, Bletzinger P and Garscadden A, 1974, IEEE J Quantum Electron, QE-10, 6.

Thompson J B, 1959, Proc Phys Soc, 73, 818.

von Engel A , 1965, "Ionized Gases", Oxford University Press, London.

Wellenstein H F and Robertson W W, 1972, J Chem Phys, 56, 1077.

# CHAPTER THREE

# DESCRIPTION AND ANALYSIS OF EXPERIMENTAL DETERMINATION OF POSITIVE IONS

## 3.1 GENERAL DISCUSSION OF EXPERIMENT

The carbon dioxide laser, whether of slow axial gas flow, convective gas flow or TEA design (see section 1.2) can attain electrical to optical conversion efficiencies approaching 25% for suitably optimised conditions. The discussion of Chapter 1 (section 1.3) has shown that the achievement of this high efficiency depends on both the laser gas temperature and electric discharge E/N. Section 1.4 has illustrated how, in theory, the discharge E/N may be calculated from knowledge of the plasma kinetics (ie attachment, ionisation etc). However, due to lack of knowledge of the precise nature of the ions species present, calculations of discharge E/N and other dependent parameters (eg laser efficiency, stability) based on presently available data can only be considered speculative.

An experimental system has been designed and constructed to mass-spectrometrically analyse the positive ion species present in the positive column of a typical $CO_2$ laser discharge. This experiment is based on the principles of positive ion sampling from glow discharge plasmas discussed in Chapter 2. The gas discharge source is intended to simulate electrical conditions occurring in the positive column of a conventional axial flow $CO_2$ laser. Variation of gas flow rate, discharge current and pressure has enabled a detailed understanding of the positive ion kinetics of $CO_2$ laser discharges, as will be discussed in Chapter 4. This knowledge enables projections of likely positive ion species in EDCL's and TEA lasers to be made in a more enlightened manner than has been possible in the past.

This chapter discusses the details of the positive ion sampling experiment used to determine positive ion species in $CO_2$-$N_2$-He discharges and with the aid of the theory of ion sampling (chapter 2) the reliability of the results is considered.

The experimental system is shown in figure 3.1.1 and consists of three chambers corresponding to different pressure regimes. The first is the discharge tube ($p \simeq 1$-$20$ torr) from which ions and neutral particles effuse to the intermediate pumping chamber ($p < 10^{-4}$ torr) through a primary sampling orifice of $\sim$ 100μm diameter. Particles effuse from this second chamber to the mass spectrometer chamber, where the pressure is $<10^{-6}$ torr, through a 1 mm diameter orifice at the apex of a stainless steel cone. The quadrupole mass spectrometer (VG-Micromass Q8K) is situated in this high vacuum environment.

The requirements of an ion monitoring system such as that of figure 3.1.1 have been considered by Mark and Helm (1974) and are:-

1. Adequate resolving power and high transmission. The resolving power is normally electronically variable and typical transmission efficiency is $\sim$ 90% for the quadrupole system.
2. High sensitivity and large dynamic range. These qualities allow very weak signals to be detected and compared with the major species in the mass spectrum.
3. Either minimum energy discrimination (over an energy range of at least 10 eV) or controlled, variable energy analysis. The latter allows the effect of ion energy discrimination to be evaluated.
4. High source pressure capabilities, enabling investigation of plasmas over a wide range of pressure.
5. Minimum influence of the mass spectrometer analysing field on the plasma. High magnetic fields associated with magnetic sector spectrometers can distort the plasma.
6. Bakeable system, especially when impurity phenomena are undesirable.

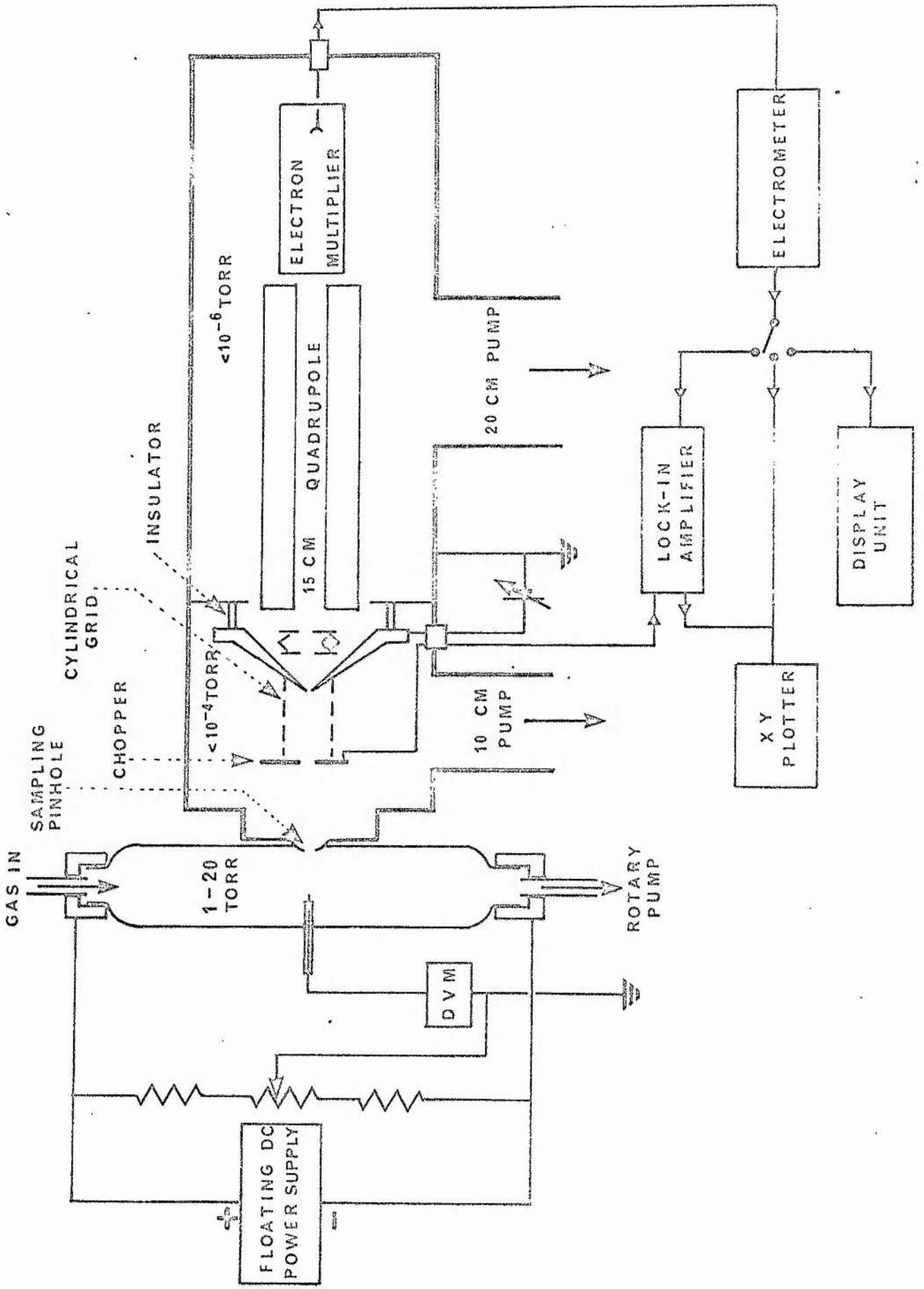


Figure 3.1.1 Experimental system for positive ion sampling from a dc positive colum

7. Uncritical ion injection angle. This simplifies alignment in ion beam experiments.

The "VG Quadrupoles" Q8K quadrupole mass spectrometer used in the experimental configuration described in this section satisfies all of these requirements although baking of the system was never carried out. Since all impurity effects observed in experiments resulted directly from the discharge gas, and not from residual contaminants in the vacuum system, baking was unnecessary.

Similar designs to that of figure 3.1.1 have been employed in the past to determine positive ion species in dc glow discharges in various gases. Knewstubb and Tickner have studied positive ions in rare gases (1962(a), 1962(b)), $N_2$-$H_2$-$O_2$ mixtures (1962(c)) and $H_2O$ (1963). Dawson and Tickner (1963) have investigated positive ions in $CO_2$ while Gaur and Chanin (1969) have examined Ne and Ar. Recent work on gas mixtures has included He-$SO_2$-CO-$CO_2$ (Kuehn and Chanin (1972,1973)), CO-He (Egorov et al (1975)) and He-CO-$O_2$ (Keren et al (1976(a), 1976(b))). Positive ion species in $CO_2$-$N_2$-He mixtures have been determined by Austin and Smith (1972) but only in the cathode region of the discharge. Tannen et al (1974) have measured relative concentrations of positive ions in a $CO_2$-$N_2$-He flowing afterglow. However these results for $CO_2$-$N_2$-He laser gas mixtures cannot be considered representative of typical positive ion species in $CO_2$ lasers since neither sample from the positive column of the discharge. The positive column accounts for almost all of the $CO_2$ laser discharge and it is desirable to make direct measurements from this region of the discharge.

Several modes of operation are possible with the system of figure 3.1.1. Analysis of neutral species alone can be performed by using an electron bombardment ionisation source at the mass spectrometer entrance

to ionise the neutral beam, and by arranging that the potential at the sampling orifice in the discharge tube prevents ions from the plasma reaching the mass spectrometer. An "ions only" mode can be achieved by suitable adjustment of potentials at the discharge tube, secondary pinhole/grid system and the mass spectrometer entrance aperture, and by switching off the electron bombardment ion source. A combination of these two modes of operation, simultaneously sampling both ions and neutral particles from the discharge, is also possible.

The beam of ions and neutral particles from the discharge tube to the mass spectrometer is defined by the primary and secondary orifices and is aligned with the quadrupole axis. Primary sampling orifices of both metallic (nickel and stainless steel) and dielectric (glass) materials have been used in experiments, but unless stated otherwise, results refer to the dielectric orifice type.

When operated in the neutral particle monitoring mode the spectrum detected by the mass spectrometer arises from two sources. First there is the spectrum due to species in the beam which is related to the abundances of neutral particles in the discharge. Second, there is a spectrum corresponding to "background" species. These arise from residual gas in the mass spectrometer chamber and from scattering of particles through the secondary orifice after collisions with the walls of the intermediate chamber (The pressure in this chamber is sufficiently low that the mean free path is greater than the dimensions of the chamber and collisional scattering from other particles is unimportant). This "background" signal is reduced by employing fast diffusion pumps to reduce the residual gas pressure in the mass spectrometer chamber and remove particles which effuse from the discharge to the intermediate chamber, except those in the beam.

When operating in conditions for detection of ions produced by the discharge, only the ions in the beam will be detected by the mass spectrometer. Those ions not in the beam are assumed to be lost in single collisions with the metallic walls of the apparatus.

When the ion current to the mass spectrometer is very weak, eg. in the case of minority ion species, the ion signal-to-noise ratio can be improved by beam modulation. This is achieved by using the chopper situated in the intermediate chamber and phase sensitive detection of the modulated electron multiplier output, as shown in figure 3.1.1.

Control of potentials applied at various points in the system is exceedingly important for positive ion analysis. Complete loss of ion signal will occur if a retarding or deflecting electric field of sufficient intensity exists between the discharge sampling orifice and the mass spectrometer, while degradation of the ion signal will result from poor ion focussing.

Typical potentials between discharge and mass spectrometer are shown in figure 3.1.2. The potential at the sampling orifice is monitored directly by an insulated probe inserted into the discharge at the sampling point (see figure 3.1.1). This probe is connected to earth via a high impedance voltmeter and thus assumes floating potential with respect to the plasma. The rear surface of the sampling orifice is aluminium-coated to prevent accumulation of space charge and is fixed at earth potential. Thus the potential difference across the orifice length is that measured by the probe.

Positive ions cross the wall sheath gaining some fraction of the sheath potential, $V_f$ (equation (2.3.2)), depending on collisions in the sheath. They are then accelerated through the orifice by the earthed coating on the rear surface. On entering the drift region between orifices the

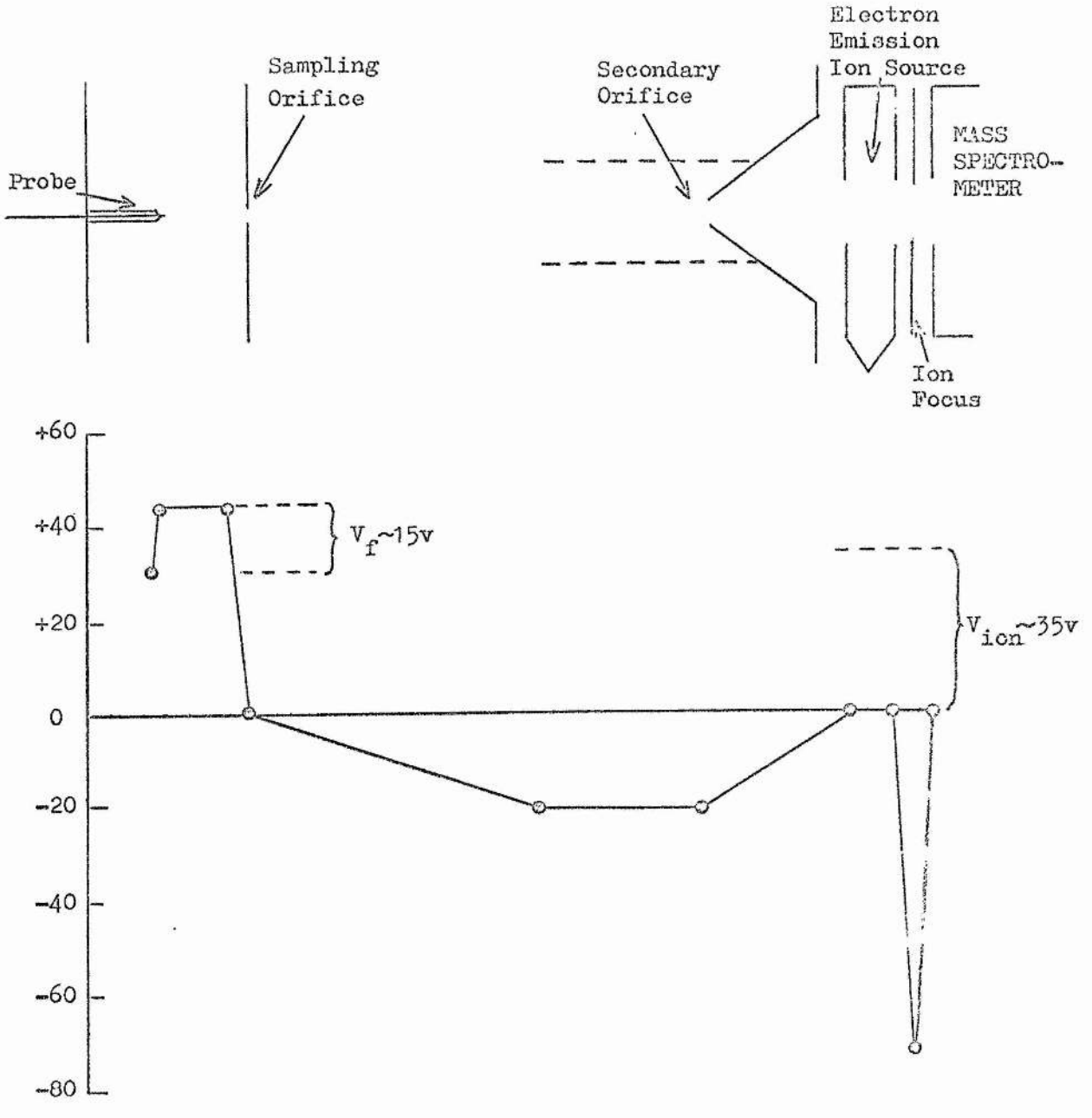


Figure 3.1.2 Typical potentials at various points in the sampling system (not to scale).

Sheath potential difference $V_f \simeq$ 15V

Sampling probe-earth potential $\simeq$ + 30V

Secondary orifice-earth potential $\simeq$ - 20V

Ion focussing lens $\simeq$ - 70V

ions have an energy equal to the sum of that gained on acceleration through the orifice (as determined by the insulated probe voltage) plus whatever fraction of the sheath potential, $V_f$, they have gained.

Focussing by the ion lenses at the secondary orifice and the mass spectrometer entrance in figure 3.1.2 enables the ion signal to be optimised, but does not affect the ion energy on entering the analyser region of the mass spectrometer. Figure 3.1.2 shows that ions will have $\sim$ 30-40 eV energy through the quadrupole analyser.

It was noted in section 2.3.1 that the optimum resolution which could be achieved by the mass spectrometer decreased as the ion energy increased. This arises from the shorter time for which fast moving ions experience the analysing fields of the quadrupole mass filter. The effect of increasing the ion energy from $\sim$40 eV to $\sim$70 eV on the resolution of the mass spectrometer is shown in figure 3.1.3. The peak at mass 32 is barely resolved at the higher energy. According to equation (2.3.10) the optimum resolving power is one mass unit in thirty ($R \simeq 30$) at 40eV ion energy but only one mass unit in twenty ($R \simeq 20$) at 70 eV for the quadrupole mass spectrometer employed. This predicts slightly better resolution than is experimentally observed in figure 3.1.3, but this may be due to the spread in energies of ions drifting through the analyser.

Three features of the quadrupole mass spectrometer are particularly useful in analysis of ions produced in the gas discharge source. The first is the ability to vary the potential at the mass spectrometer entrance aperture, thus excluding ions of insufficient energy to overcome the retardation introduced. This ion energy analysis is discussed in connection with the effect of the wall sheath in section 3.3.

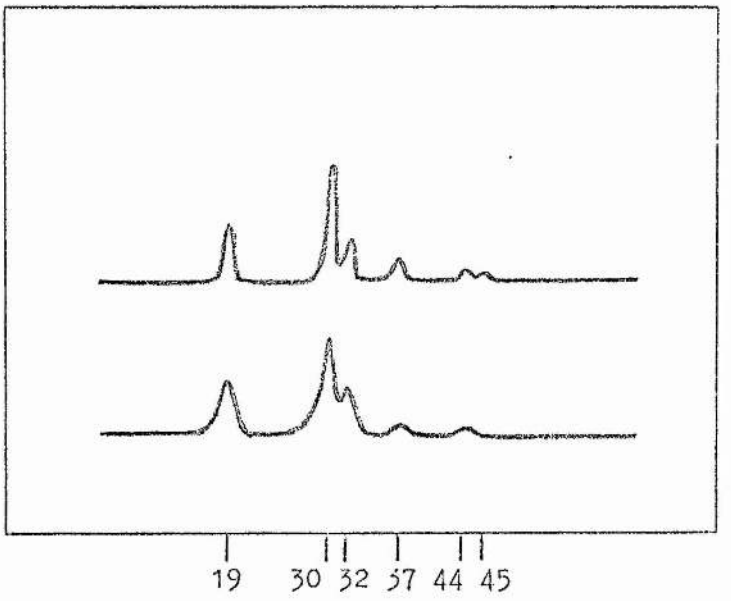


Figure 3.1.3 Positive ion mass spectra from a 6-12-82, $CO_2$-$N_2$-He discharge at 10 torr, 10 mA. Upper trace, ∿40 eV ion energy; lower trace, ∿ 70 eV ion energy. Ions are $H_3O^+$ (mass 19), $NO^+$ (mass 30), $O_2^+$ (mass 32), $H_3O^+.(H_2O)$ (mass 37), $CO_2^+$ (mass 44) and $HCO_2^+$ (mass 45).

The second useful feature is the ability to vary the potential of the quadrupole analyser region by ± 15V with respect to earth. This has the effect of accelerating or decelerating the ions towards the quadrupole region thus altering the drift velocity of the ions through the analyser. This allows an improvement in resolution for fast moving ions by slowing them down so that they experience the analysing fields of the quadrupole for a longer time. However resolution is ultimately limited by the design of the mass spectrometer.

By mounting the system of sampling orifices, focussing lenses, quadrupole analyser and electron multiplier coaxially, not only ions but photons and metastable neutral particles can effuse from the discharge to the

multiplier. Only the charged ion species are mass analysed but both the photons and the metastables can eject electrons from the first dynode of the multiplier and can thus give rise to a noisy background in the ion mass spectrum. To avoid this, the third useful feature of the mass spectrometer is the provision of an off-axis electron multiplier. Due to their charge, ions can be deflected by an electric field on to the first dynode of the off-axis multiplier after analysis, while photons and metastables are not deflected and do not strike the multiplier.

A well resolved mass spectrum of positive ions in a 1½% $H_2$, 6% $CO_2$, 12% $N_2$, 80½% He mixture at 10 torr and 10 mA, in a 1 cm radius tube - conditions similar to a cw laser discharge - is shown in the upper trace of figure 3.1.3. For reasons to be discussed in subsequent sections of this chapter, spectra such as this are believed to be representative of the ion species actually present in the plasma.

## 3.2 THE GAS DISCHARGE

With the development of high power $CO_2$ lasers, much data relevant to $CO_2$-$N_2$-He and pure $CO_2$ gas discharges has recently been obtained, both theoretically and experimentally. This includes knowledge of electron energy distributions and electron temperatures (Nighan (1970), Judd (1974)), electron drift velocities (Lowke et al (1973)), ionisation and dissociative attachment coefficients (Nighan and Wiegand (1974), Bletzinger et al (1975)), the $CO_2$ electron impact dissociation process (Smith and Austin (1974), Corvin and Corrigan (1969)), and the gas temperature (Laderman and Byron (1971)).

This data is insufficient to allow detailed plasma modelling, as the plasma instability computations discussed in chapter 1 illustrated. Nevertheless many of the available parameters are useful in describing the

electrical and chemical conditions of the discharge. This avoids the inconvenience of the determination of required data by separate experiment.

Parameters appropriate to the gas discharge of the present experiment are given in Table 3.1. Also, the sheath parameters (voltage, thickness and average field) have been calculated for the discharge and are given in Table 3.1.

TABLE 3.1

| | |
|---|---|
| Gas mixture | 6% $CO_2$, 12% $N_2$, 82% He |
| Discharge pressure | 1 - 20 torr |
| Discharge current | 10 - 60 mA |
| Gas flow rate | 0.1 - 1.5 $\ell\ s^{-1}$ |
| Discharge tube radius | 1 cm |
| Discharge length | 20 cm |
| Gas temperature | 400-600 K (1) |
| Electron temperature | 1 - 2 eV (2) |
| Discharge E/p (longitudinal field /pressure) | 10-20 V $cm^{-1} torr^{-1}$ |
| Electron density | $5 \times 10^9$ - $3 \times 10^{10}$ $cm^{-3}$ (3) |
| Debye length (equation 2.3.7) | $\sim$ 100 $\mu$m |
| Ion mean free path (equation 2.3.20) | 40-800 $\mu$m |
| Sheath voltage, $V_f$ (equation 2.3.2) | $\sim$ 15-20 V |
| Sheath thickness, $d_s$ (equation 2.3.35) | $\sim$500 $\mu$m |
| Average sheath field ($V_f/d_s$) | $\sim$ 300 V $cm^{-1}$ |

(1) Laderman and Byron (1971)

(2) Nighan (1970)

(3) Calculated from the discharge current and using drift velocity from Lowke et al (1973).

The total positive ion current reaching the mass spectrometer as a function of discharge current, gas pressure and gas flow rate is given in figures 3.2.1, to 3.2.3. These curves refer to a $CO_2$-$N_2$-He mixture in the proportions 6% $CO_2$ - 12% $N_2$ -82% He with a potential of + 30V with respect to earth at the sampling orifice and - 20V with respect to earth at the secondary orifice. The shape of these curves is now discussed in conjunction with the relation (2.2.16).

$$i_{+-} \propto \frac{n_o A T_e}{(T_g m)^{\frac{1}{2}} R N} \qquad (3.2.1)$$

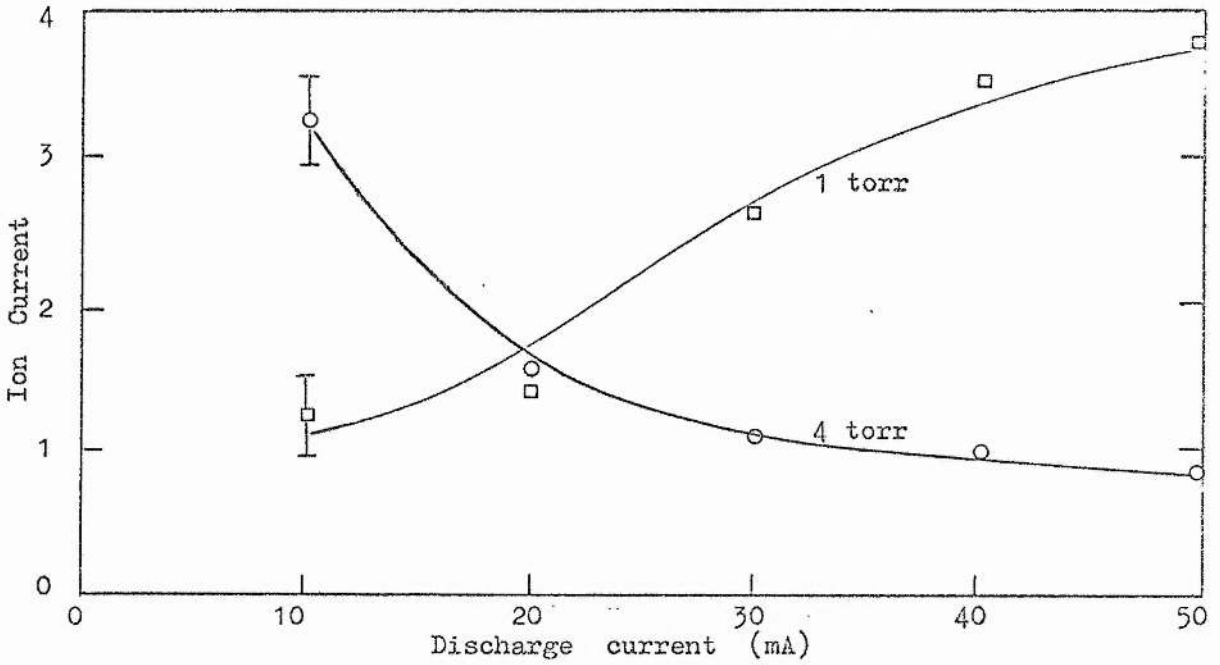


Figure 3.2.1. Variation of total ion current to mass spectrometer (arbitrary units) with discharge current in a 6-12-82, $CO_2$-$N_2$-He mix at 1 torr (E/p=30V $cm^{-1}torr^{-1}$) and 4 torr (E/p= 12V $cm^{-1}$ $torr^{-1}$). The gas flow rate is 1·3 l $s^{-1}$.

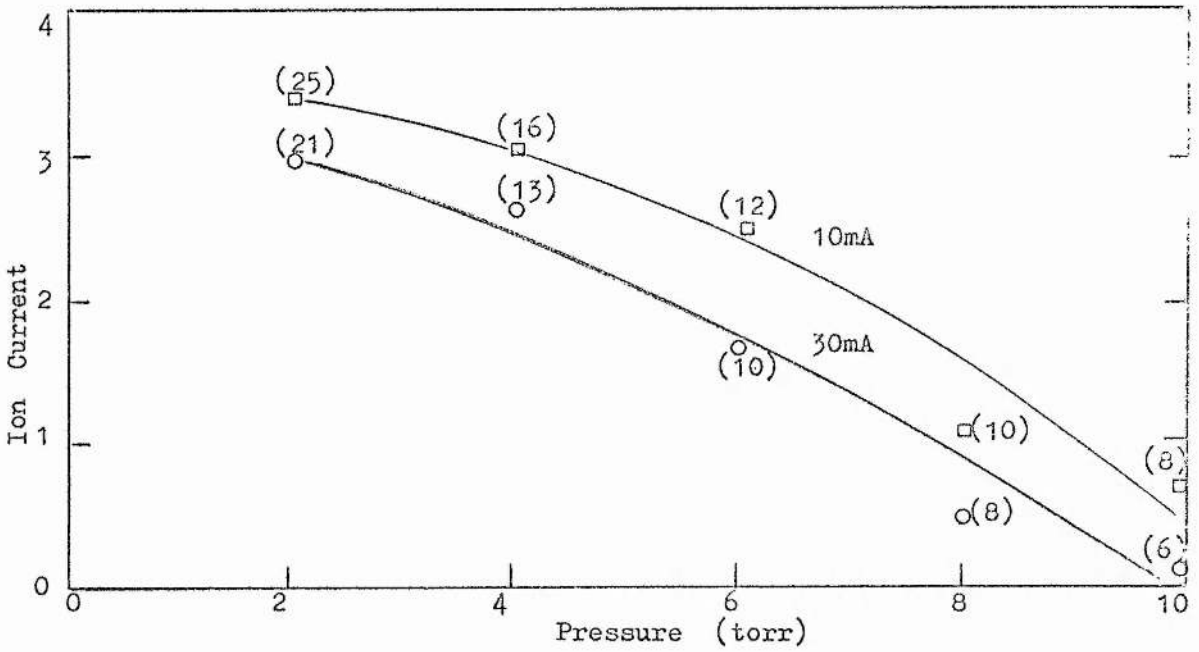


Figure 3.2.2. Variation of total ion current to mass spectrometer (arbitrary units) with pressure for a 6-12-82, $CO_2$-$N_2$-He mix at 10mA and 30 mA. The E/p for each point is given in brackets and the gas flow rate is 1·3 l $s^{-1}$

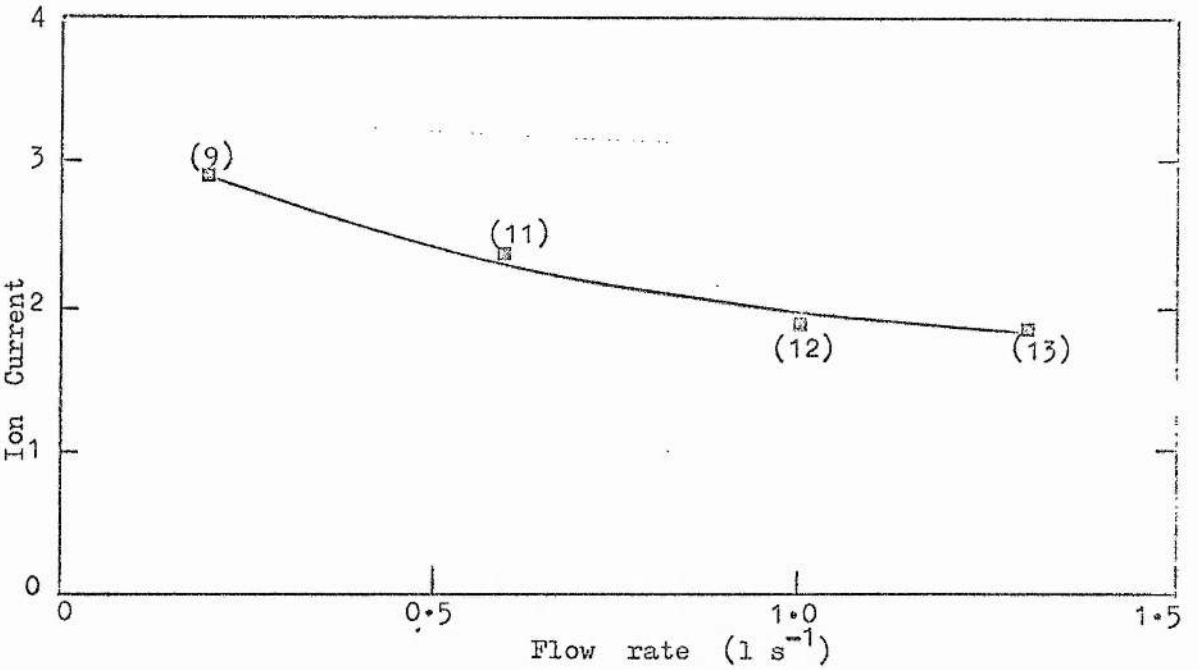


Figure 3.2.3. Variation of total ion current to mass spectrometer (arbitrary units) with gas flow rate for a 6-12-82, $CO_2$-$N_2$-He mix at 4 torr, 30mA. The E/p for each point is given in brackets.

First, in figure 3.2.1, the total ion peak height is found to decrease with increasing discharge current at 4 torr pressure. This is contrary to the prediction of equation (3.2.1) above, which gives a six-fold rise in peak height as the discharge current (ie $n_o$) is raised from 10 mA to 60 mA. The increase in gas temperature arising from this current increase will not result in more than a factor of 1.5 reduction in ion peak height from relation (3.2.1) (ie the gas temperature will not be greater than 650K). The curve for p = 1 torr is in qualitative agreement with equation (3.2.1).

Second, from figure 3.2.2, the ion peak height decays with increasing source pressure, in approximate agreement with equation (3.2.1). The E/p decreases as the pressure increases from 2 torr to 10 torr as shown in the figure. Finally, the variation of ion current with flow rate is shown in figure 3.2.3. Although equation (3.2.1) does not explicitly include gas flow rate, this parameter affects the gas temperature. The gas is hotter at low flow rates and consequently a lower ion peak height is expected from equation (3.2.1). This is contrary to experimental observation. Once again, the E/p varies in this figure from 9 V $cm^{-1}$ $torr^{-1}$ at 0.2 $\ell$ $s^{-1}$ to 13 V $cm^{-1}$ $torr^{-1}$ at 1.3 $\ell$ $s^{-1}$.

Thus, unfortunately, the variation of the positive ion current effusing from a discharge typical of a $CO_2$ laser is not as simple as predicted by equation (3.2.1). There are three important complicating factors which may account, to some extent, for the discrepancies between equation (3.2.1) and experimental observation.

The first complication arises from changes in the gas composition due to dissociation of $CO_2$, and subsequent plasma-chemical reactions

resulting in the presence of CO, $O_2$, and traces of the oxides of nitrogen (ie $N_2O$, NO and $NO_2$, Tannen et al (1974)). The degree of dissociation depends on discharge current, gas pressure and time spent by the gas in the discharge (ie flow rate) (Smith and Austin (1974)). Thus, although the initial gas composition in figures 3.2.1 to 3.2.3 is 6% $CO_2$-12% $N_2$-82% He, the change in gas mixture between the gas inlet and the sampling point can result in production of up to 2% CO, 1% $O_2$ and $\sim$ 0.1% oxides of nitrogen under present experimental conditions (see Chapter 4). This means that all experimental points in figures 3.2.1 to 3.2.3 correspond to slightly different gas mixtures. The change in gas composition is the most likely explanation of the changing E/p in figure 3.2.3.

Secondly, the change in E/p in figure 3.2.2 (due mainly to changing pressure) and figure 3.2.3 (due to gas composition changes) has two consequences. The first is that, since the average energy gained by an electron between collisions is e E $\lambda_e$ (where e = electronic charge and $\lambda_e$ = electron mean free path) and since $\lambda_e \propto p^{-1}$, the quantity E/p is a convenient expression of average electron energy, similar in this respect to the electron temperature, $T_e$. Thus increasing E/p results in greater average electron energy and a higher value of $T_e$. The second consequence of varying E/p is that the electron drift velocity in $CO_2$-$N_2$-He mixtures increases monotonically with E/p (Lowke et al (1973)). Thus, under constant current conditions, an increase in E/p gives an increase in the electron drift velocity, and a corresponding drop in the electron density, $n_o$. Hence, consideration of the effect of increasing the E/p in equation (3.2.1) shows that the positive ion current to the mass spectrometer will increase due to increasing $T_e$, but will drop due to decreasing $n_o$.

The final factor complicating the analysis of figures 3.2.1 to 3.2.3 is the influence of volume recombination of positive ions and electrons. As discussed in section 2.2.3 this can lead to constriction of the positive column when the diffusion time of positive ions to the wall is longer than the characteristic time for recombination. Thus constriction occurs, to some degree, when the inequality (2.2.31) is satisfied, ie

$$np \gg \frac{D_a p}{R^2 \beta} \quad . \tag{3.2.2}$$

Using approximate values of $D_a p \sim 500$ cm$^2$ torr s$^{-1}$, and $\beta \sim 10^{-8}$ cm$^3$ s$^{-1}$ at a few torr (Von Engel (1965, p144 and p 163)), in a discharge tube of 1 cm radius, constriction begins at a value of $np \sim 5 \times 10^{10}$ torr cm$^{-3}$. Comparing this value with values of electron density and pressure in Table 3.1 shows that constriction of the discharge is likely at the higher values of current and pressure used in the experiment. Since the sampling orifice is located in the discharge wall, it will no longer be adjacent to the plasma, and equation(3.2.1) will not apply in the constricted discharge. Recombination will occur between the plasma and the orifice resulting in a reduced ion current to the mass spectrometer.

It would appear that constriction of the discharge is the cause of the drop in ion peak height with increasing discharge current, for $p = 4$ torr shown in figure 3.2.1. A value of $np \gtrsim 5 \times 10^{10}$ torr cm$^{-3}$ occurs for a current $\gtrsim$ 20 mA at 4 torr, and a current $\gtrsim$ 80 mA at 1 torr. Thus the higher pressure curve ($p = 4$ torr) in figure 3.2.1 is strongly influenced by constriction while the lower pressure curve ($p = 1$ torr) is not. This constriction was visible in experiments; the discharge radius was $\sim$ 80% of the tube radius at 4 torr and 50 mA. Thus the application of equation (3.2.1) to the higher pressure case is not appropriate.

In figure 3.2.2, the influence of recombination (ie plasma constriction) is important at values of Ip $\gtrsim$ 80 mA torr, as discussed above. In this case the effects of varying E/p may also contribute. The combination of the effects of E/p variation and constriction are difficult to predict theoretically and it is fortuitous that the ion peak height varies with gas pressure approximately as predicted by equation (3.2.1).

The variation in ion peak height with gas flow rate in figure 3.2.3 shows less than 50% decrease between 0.2 $\ell\ s^{-1}$ and 1.3 $\ell\ s^{-1}$. This may be explained by the greater change in gas composition occurring at the slower flow rate, and the resulting lower E/p at which the discharge runs. In this case, it would appear that the decrease in $n_o$ resulting from the rise in E/p as flow increases outweighs the increase in electron temperature in affecting the positive ion wall current. Thus the ion current decreases with increasing flow rate and E/p. The degree of discharge constriction is assumed to be approximately independent of gas flow rate, although the axial electron density $n_o$ varies with E/p, as discussed.

The variation of total ion currents to the mass spectrometer with discharge current, gas pressure and flow rate discussed above indicates the need for care in the analysis of the dependence of individual ion concentrations, determined from the mass spectrum. For example, a study of the effect of varying discharge current on the mass spectrum will not only contain information on the relative changes in ion peak heights, but also the variation in total ion current to the mass spectrometer, as shown in figure 3.2.1. The analysis is simplified by normalising the peak height of individual ion peaks to the total ion concentration. Thus a particular ion current, $i_A$, is normalised by

$$i_A \text{ (normalised)} = \frac{i_A(\text{measured})}{i(\text{total})} \qquad (3.2.3)$$

In this way only relative changes in ion peak heights are considered. This procedure of allowing for variations in the efficiency of the ion source is adopted by almost all workers in the field of ion sampling from gas discharges.

## 3.3 THE WALL SHEATH

The previous section suggests that, when charged particle loss is greater by volume recombination than by ambipolar diffusion, constriction of the plasma will preclude the formation of a wall sheath. In order to produce conditions representative of conventional axial flow $CO_2$ lasers, while avoiding the regime of high current and pressure where volume recombination leads to considerable constriction ($I > 20$ mA, $p > 20$ torr) most experiments have been performed at relatively low currents ($\sim 10$ mA) and at pressures up to 20 torr. The experimental evidence that ions are sampled through a wall sheath is discussed. This indicates that ambipolar diffusion is important in determining the charged particle radial profile.

The potential across the sheath calculated according to equation (2.3.2) is shown in Table 3.1 to be $\sim$ 15-20 V. Assuming a sheath thickness of a few Debye lengths (see Table 3.1), an approximate average electric field in the sheath of $\sim 300$ V cm$^{-1}$ may be calculated. Assuming, initially, that the low field mobility theory applies, then the drift velocity $v_{d\pm}$ of positive ions is given by

$$v_{d\pm} = \mu_{\pm} E. \qquad (3.3.1)$$

E is the average electric field in the sheath and $\mu_{\pm}$ is the ion mobility given by equation (2.3.14) as

$$\mu_+ = \frac{0.75\ e\ \lambda_i}{\bar{c}\ m_g} \sqrt{\frac{m_+ + m_g}{m_+}} \quad , \tag{3.3.2}$$

where $\lambda_i$ is the ion mean path (see Table 3.1), $m_+$ and $m_g$ are the ion and neutral gas molecule masses respectively and $\bar{c}$ is the average thermal velocity of ions, given by (Hasted (1972) p35)

$$\bar{c} = \sqrt{\frac{8k\ T_g}{\pi\ m_+}} \quad . \tag{3.3.3}$$

Taking a gas temperature, $T_g$, of 500K (Table 3.1) gives $\bar{c} \sim 5 \times 10^4$ cm $s^{-1}$, which when substituted into equation (3.3.2), with $m_+ \simeq m_g$ and $\lambda_i \simeq 80$ μm at 10 torr yields $\mu_+ \sim 5 \times 10^3$ $cm^2\ V^{-1}\ s^{-1}$. {Brown (1959) p63 provides an experimentally determined value of $\mu_+ \sim 23$ $cm^2\ V^{-1}\ s^{-1}$ for mass 30 ions in He gas at 760 torr, corresponding to $\mu_+ \sim 2 \times 10^3$ $cm^3\ V^{-1}\ s^{-1}$ at 10 torr.} Thus for a field of 300 V $cm^{-1}$, equation (3.3.1) yields a drift velocity of $\sim 10^6$ cm $s^{-1}$; greater than the average thermal velocity. Hence the high field mobility theory discussed in section 2.3.2 applies, and the sheath thickness and average sheath field are shown for this situation in Table 3.1.

Evidence to support the existence of the wall sheath under conditions typical of cw $CO_2$ lasers (~ 10 torr, 10 mA, 1 cm radius discharge tube) comes from an analysis of the energy of the ions effusing from the discharge and entering the mass spectrometer. The entrance of the mass spectrometer (ie. at the electron emission ion source in figure 3.1.2) is normally at earth potential. By adjusting the potential at this entrance aperture to $+V_o$, only ions of energy greater than $eV_o$ can reach the quadrupole analysing region of the mass spectrometer. While all ions are transmitted by the aperture at $V_o = 0V$, the low energy ions are progressively excluded from

analysis as $V_o$ is increased. Figure 3.3.1 shows the variation of the $NO^+$ ion signal (the dominant species under the experimental conditions) at the mass spectrometer as $V_o$ is increased. Ions are sampled through a metallic orifice which assumes the floating potential, $V_f$, with respect to the plasma. The potential at the insulated probe inserted into the discharge at the sampling point is +20V with respect to earth. Thus ions leave the discharge with $\sim (V_f + 20)$ volts energy (cf figure 3.1.2, where V probe-earth = + 30 V).

The ion energy distribution, f(E), also shown in figure 3.3.1, is obtained by differentiation of the ion current with respect to retarding voltage (see section 2.3.1). Due to collisions in the sheath very few ions gain the full sheath energy $eV_f$ ($\sim$20 eV, see Table 3.1) and so only a small number of ions are found at 40V retardation. Ions of low energy ($<$ 20 eV) are those which suffer a collision as they effuse from the plasma, losing most of the energy they have gained in the sheath. These ions only have the $\sim$20 eV energy due to the potential difference between plasma and mass spectrometer. The broadness of this energy distribution is an indication of collisions dominating the ion energy in the sheath.

If appreciable constriction of the plasma were occurring under the conditions of figure 3.3.1, then a layer of neutral gas might be expected between the plasma and the sampling orifice. Since the ion mean free path is $\sim$80μm at 10 torr, collisions between ions and gas molecules in this layer would thermalise the ion energies. Thus, if constriction occurred, the ion energy distribution would be heavily biassed to low ion energies.

Further evidence for the existence of an ion sheath at the wall comes from a comparison of the ion energy distributions. Figure 3.3.2 shows

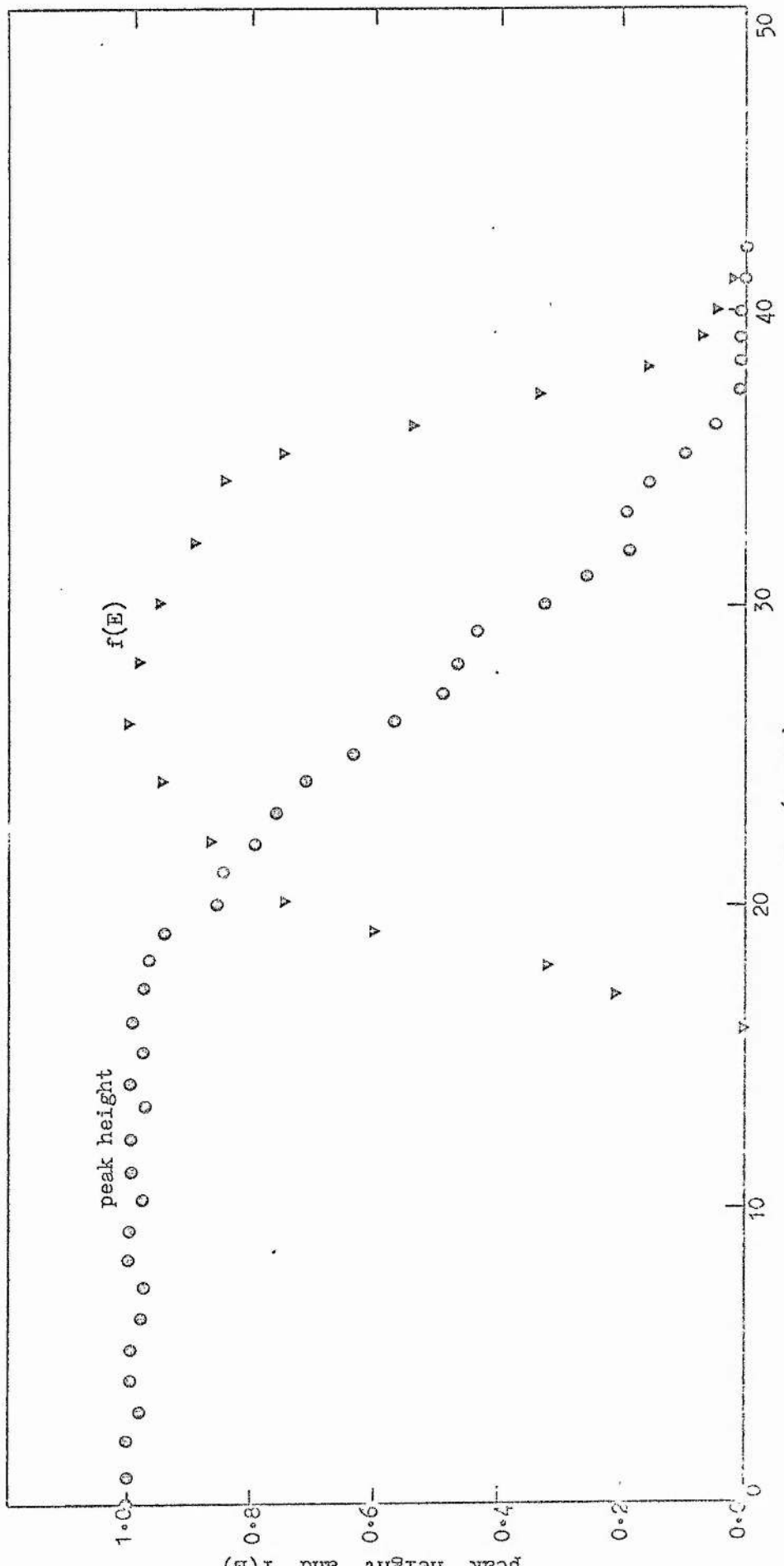


Figure 3.3.1 Variation of $NO^+$ ion peak height and energy distribution, f(E), with ion energy (retarding potential, $V_0$). Sampling conditions are: nickel orifice (at floating potential), 6% $CO_2$ - 12% $N_2$ - 82% He, 10 mA, 10 torr, 0·1 $ls^{-1}$, V probe-earth = +20V. Both curves are normalised to unity at their maximum values.

Figure 3.3.2 Ion energy distributions for $NO^+$ ions sampled from a 6% $CO_2$ - 12% $N_2$ - 82% He discharge through a nickel orifice at floating potential. $V_0$ is the ion retarding potential, excluding ions with energy less than $eV_0$ from analysis. Curve A; 2 torr, 10mA, V probe-earth = +8V. Curve B; 10 torr, 10mA, V probe- earth = +20V. Curve C; 10 torr, 50 mA, V probe-earth = +20V.

these distributions for three cases. These correspond to conditions where the criterion for volume recombination dominating ambipolar diffusion as a loss process (equation (3.2.2)) is not satisfied (2 torr, 10 mA), is marginally satisfied (10 torr, 10 mA) and is easily satisfied (10 torr, 50 mA). Due to the setting of the probe - mass spectrometer (earth) potential difference, ions sampled at 10 torr receive 20 V acceleration after effusion, while those sampled at 2 torr receive only 8 V acceleration. The similarity in the shape of the 2 torr, 10 mA and 10 torr, 10 mA distributions indicates that the transition from sheath-controlled sampling to sampling through a neutral gas layer in a constricted discharge has not taken place. However the distribution for the 10 torr 50 mA conditions is biassed towards the lower energy tail, as would be expected if most ions made collisions with neutral gas molecules in the undischarged gas surrounding the constricted discharge.

Discharge conditions where a considerable degree of constriction occurs (Ip $\gtrsim$ 200 mA torr) have been avoided in the determination of positive ion species in $CO_2$ laser discharges discussed in chapter 4. By operating in a regime where constriction is not an important influence on ion effusion currents, the reliability of ion sampling is improved.

## 3.4 THE ORIFICE

The sampling orifice may take two forms depending on whether the ions are sampled through the naturally occurring wall sheath, or the wall sheath and ion current are modified by application of potentials. Where signal levels permit, it is preferable to extract ions through an orifice in the discharge wall at a potential equal to that of the wall with respect to the plasma at that point, ie. the floating potential $V_f$. This minimises ion lens effects and ion-molecule reactions caused by accelerating the ions

towards the orifice (see sections 2.3.2 and 2.4.2), while avoiding signal attenuation due to ion retardation. Also, sampling at $V_f$ represents no disturbance to the naturally occurring electric fields and charged particle gradients in the discharge.

Sampling at the natural wall potential, $V_f$, may be achieved either by using a dielectric orifice in the discharge wall or by sampling through an orifice in a small metallic disc, allowed to assume the wall potential. Both methods have been employed in the present work and their performances are discussed in this section.

The metallic orifice employed in the ion sampling experiments is a 100μm diameter pinhole in the centre of a 3mm diameter nickel disc. The thickness of the disc is 40 μm, and it is fixed to a Pyrex substrate (part of the discharge tube wall) by means of Techkits E7 epoxy adhesive. The dielectric orifice is a pinhole of ∿120μm diameter blown in a small dome in the Pyrex discharge tube wall. It is ∿500μm in length. The surface of the glass at the rear of each orifice type is aluminium coated to prevent accumulation of space charge.

As a consequence of the considerable length of the dielectric orifice (length ∿ 4 x diameter) it might be expected that ion-molecule reactions and scattering of light ions would occur in the orifice tube, as discussed in section 2.4.3. However comparison of spectra obtained with this orifice and those obtained with the metallic orifice (length ∿ 0.4 x diameter) for the same conditions shows good agreement (see figure 3.4.1). The slight discrepancies between the spectra of figure 3.4.1 can be adequately explained in terms of uncertainties in flow rate, pressure, current, potential settings and water vapour impurity concentration. These uncertainties lead to a day-to-day variation of ± 15% in the ion peak heights observed for similar experimental conditions.

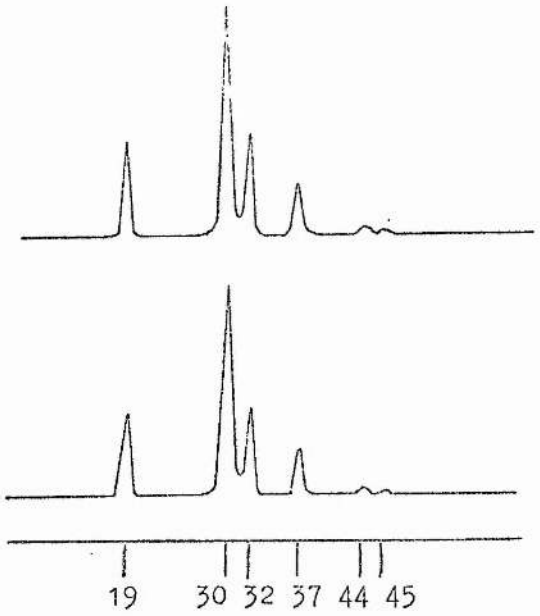


Figure 3.4.1 Positive ion mass spectra obtained from a 10 torr, 10 mA discharge in a 6-12-82, $CO_2$-$N_2$-He gas mixture. Upper trace- nickel sampling orifice; lower trace - Pyrex orifice. Ions are $H_3O^+$ (mass 19), $NO^+$ (mass 30), $O_2^+$ (mass 32), $H_3O^+$ ($H_2O$) (mass 37), $CO_2^+$ (mass 44), and $HCO_2^+$ (mass 45).

All ion species over the relatively small range of interest (15-60 amu) have similar masses and they may be assumed to have similar scattering cross-sections. Thus the effect of ion scattering by neutral species in the orifice vicinity will not lead to undue discrimination against any of the ion species. Also the ion-molecule reactions occurring in the sampling orifice will, in the absence of high electric fields in this region, be identical to those occurring in the bulk plasma since the two environments are similar. Possible endoergic ion-molecule reactions (eg dissociative charge transfer) would only occur in high electric field gradients and there is no evidence of these in observed mass spectra.

Thus, despite its considerable length, the use of the dielectric orifice yields similar spectra to a thin metallic orifice.

The similarity of a biassed metallic orifice to a Langmuir

probe may be exploited to yield information on the sampling conditions prevailing in the discharge. Figure 3.4.2 shows the variation of total positive ion current to the mass spectrometer as a function of voltage applied to the orifice (measured with respect to the plasma). The shape of this type of characteristic has already been discussed in section 2.4.1. No ion saturation region is observed but a decrease in slope of the characteristic is observed at $V \simeq -15V$. Assuming that, in the absence of sheath expansion (see section 2.4.1), the ion current would saturate at this value of potential, then the floating potential of the sampling probe with respect to the plasma is $V_f \simeq -15V$. This is in agreement with the approximate value calculated from equation (2.3.2) and given in Table 3.1. Hence the biassed metallic orifice can be used to experimentally estimate the sheath voltage, and the agreement between the experimental and calculated values indicates that there are no serious electric field distortions created by the sampling orifice.

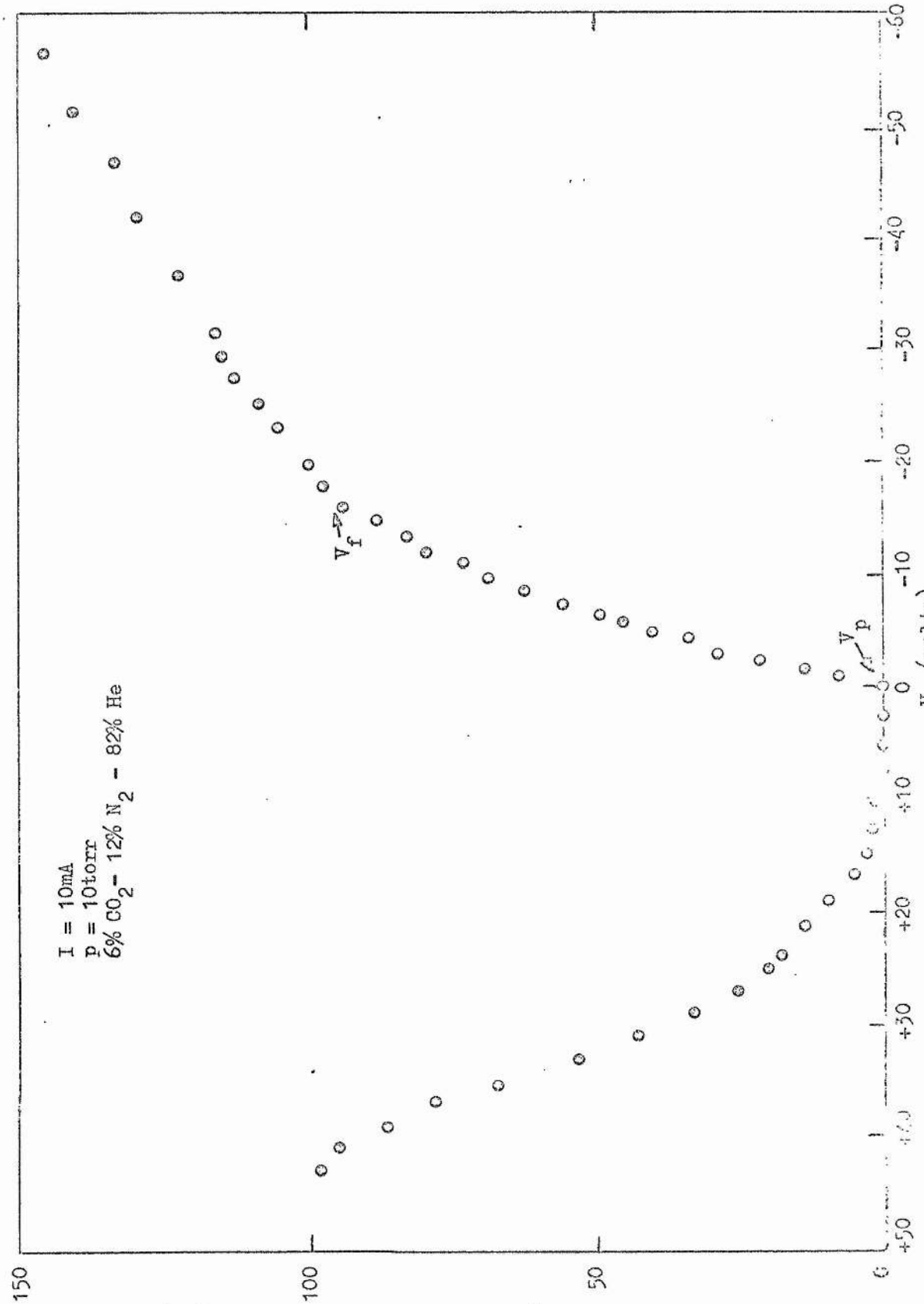


Figure 3.4.2 Sampling probe characteristic for 100 μm diameter orifice in a 3 mm nickel disc.

## References


Austin J M and Smith A L S, 1972, J Phys D, 5, 468.

Bletzinger P, Laborde D A, Bailey W F, Long W H, Tannen P D and Garscadden A, 1975, IEEE J Quantum Electron, QE-11, 317.

Brown S C, 1959, "Basic Data of Plasma Physics", MIT Press, New York.

Corvin K K and Corrigan S J B, 1969, J Chem Phys, 50, 2570.

Dawson P H and Tickner A W, 1963, Proc Int Conf Ionization Phenomena in Gases, 6th Paris, 2, 76.

Egorov N P, Komarov V N, Kupryanov S E, Trubacheev E A and Volchenok V I, 1975, Instrum and Exp Tech (USA), 17, 1743.

Gaur J P and Chanin L M, 1969, Phys Rev, 182, 167.

Hasted J B, 1972, "Physics of Atomic Collisions", Butterworth, London.

Judd O P, 1974, J Appl Phys, 45, 4572.

Keren H, Avivi P and Dothan F, 1976(a), IEEE J Quantum Electron, QE-12, 58.

Keren H, Avivi P and Dothan F, 1976(b), Phys Lett, 56A, 85.

Knewstubb P F and Tickner A W, 1962(a), J Chem Phys, 36, 674.

Knewstubb P F and Tickner A W, 1962(b), J Chem Phys, 36, 684.

Knewstubb P F and Tickner A W, 1962(c), J Chem Phys, 37, 2941.

Knewstubb P F and Tickner A W, 1963, J Chem Phys, 38, 464.

Kuehn D G and Chanin L M, 1972, J Appl Phys, 43, 339.

Kuehn D G and Chanin L M, 1973, J Appl Phys, 44, 5288.

Laderman A J and Byron S R, 1971, J Appl Phys, 42, 3138.

Lowke J J, Phelps A V and Irwin B W, 1973, J Appl Phys, 44, 4644.

Mark T D and Helm H, 1974, Acta Phys Austr, 40, 158.

Nighan W L, 1970, Phys Rev, A2, 1989.

Nighan W L and Wiegand W J, 1974, Phys Rev, A10, 922.

Smith A L S and Austin J M, 1974, J Phys D, 7, 314.

Tannen P D, Bletzinger P and Garscadden A, 1974, IEEE J Quantum Electron, QE-10, 6.

von Engel A, 1965, "Ionized Gases", Oxford University Press, London.

Wiegand W J and Nighan W L, 1973, Appl Phys Lett, 22, 583.

# CHAPTER FOUR

## POSITIVE ION PROCESSES IN THE POSITIVE COLUMN OF $CO_2$ LASER ELECTRICAL DISCHARGES

(Reproduced from 'The Journal of Chemical Physics', Vol 67, pp1594-1604)

# Positive ion processes in the positive column of $CO_2$ laser electrical discharges

A. L. S. Smith and H. Shields

*Department of Physics, University of St. Andrews, St. Andrews, Fife KY16 9SS, Scotland*
(Received 18 October 1976)

A mass spectrometric study of the positive ions in the positive column of dc glow discharges in pure $CO_2$ and $CO_2$ gas laser mixtures has been undertaken to determine the nature of the ions and to elucidate the ion kinetics. Results are presented over the ranges 2–20 torr, 3–15 mA $cm^{-2}$ and for reaction times of 0.1–1.0 s. The nature of the dominant ion species is dependent on the minority neutral species produced in the discharge. $O_2^+$ is the major species in pure $CO_2$, but $NO^+$ accounts for $>70\%$ of the positive ions in a 6% $CO_2$–12% $N_2$–82% He laser mixture and ions of the $H_3O^+$. $(H_2O)_n$ type ($n = 0, 1, 2$) become important in $CO_2$–$N_2$–He–$H_2$ laser mixtures. A semiquantiative reaction kinetic model is developed to explain the formation of these ions and to aid predictive modelling of other $CO_2$ laser systems.

## INTRODUCTION

The $CO_2$ laser is important because it can convert electrical energy to pulsed or cw infrared radiation with greater than 10% efficiency in high power devices. Various other gases are added to the $CO_2$ to improve laser performance and allow devices to be operated with sealed-off gas mixtures. The resulting plasma reaction kinetics, gas vibrational collision processes and charged particle physics are sufficiently complicated to necessitate the use of computer models to obtain detailed insight into the effects of the various processes and to permit device optimization.

Recent models[1–6] have emphasized the effect of electron and ion processes on the discharge $E/P$ (the ratio of electric field to gas pressure) (and hence on the device output power, etc.) and on the discharge stability. Accurate models for systems where several species of positive and negative ions are present require knowledge of the abundance of each ion type.

Several workers have studied the positive ions in glow discharges in $CO_2$ using mass spectrometric techniques. Thus Evans and Jennings[7] and Schildcrout *et al.*[8] have found $O_2^+$ to be the dominant ion in rf discharges in $CO_2$ at pressures of 1–2 torr. Dawson and Tickner[9] have analyzed the ions in dc discharges in $CO_2$ at even lower pressures and Austin and Smith[10] have sampled the ions through the cathode of a dc glow discharge in $CO_2$ at up to 4 torr.

Typically $CO_2$ lasers either work with cw discharges in the 10–20 torr region or with pulsed excitation at atmospheric pressure or above. Likewise pure $CO_2$ is not used, the commonest mixture being one of $CO_2$–$N_2$–He. The only ion mass spectrometry of $CO_2$–$N_2$–He systems has involved sampling from the cathode region of a dc discharge. Austin and Smith[10] sampling through the cathode found the dominant ions to be $CO^+$ and $O_2^+$ in discharges in flowing $CO_2$–$N_2$–He at up to 9 torr total pressure and Tannen *et al.*[11] sampling from "near" the cathode in static $CO_2$–$N_2$–He at up to 8 torr found the dominant ion to be $NO^+$. No sampling from excitation discharges has been reported at higher pressures, nor has there been any reported work on the species in the positive column of a $CO_2$–$N_2$–He mixture. It should be emphasized that sampling from the positive column, as opposed to sampling from at or near the cathode or anode, is important since it is the positive column which provides the stable laser excitation medium.

The addition of small amounts of hydrogen has been found to be beneficial in reducing the long-term degree of dissociation of $CO_2$ in sealed-off, low pressure, cw $CO_2$ lasers.[12,13] This has been shown by Smith and Browne to be due to enhanced reformation of $CO_2$ by the reaction $OH + CO \rightarrow CO_2 + H$.

We have assembled a mass spectrometric system to directly sample the positive ions from the positive column of a dc glow discharge in pure $CO_2$ and in $CO_2$–$N_2$–He and $CO_2$–$N_2$–He–$H_2$ mixtures. We have been able to obtain good spectra for pressures up to 20 torr. Thus our results can be compared with previous work on dc discharges at lower pressures in pure $CO_2$ and can be directly used without any extrapolation to provide quantitative information for low pressure cw discharge lasers and laser models.

All the ion results are presented and expressed as a percentage of the total ion population; this is necessary because of an overall changing efficiency of sampling with several parameters, especially the total gas pressure. This leads to no ambiguity since the total ion density can be determined from the measured discharge current and known drift velocity. No corrections have been made to the ion peaks to allow for changed sensitivity of the sampling and spectrometer with ion species since no standard or reliable technique is available for making such a correction. But the mass to charge range covered is not large and there is some internal evidence to suggest that the errors involved are not large.

## EXPERIMENTAL

Figure 1 shows the experimental system used for both positive ion and neutral particle sampling. The discharge tube is 20 cm long, 2 cm internal diameter Pyrex, with a Pyrex sampling pinhole (120 $\mu$m diam) located approximately halfway along its length. Particles sampled by this pinhole are collimated by a second, metallic pinhole (1 mm diam) before analysis by a "V-G Quadrupoles" Q8K quadrupole mass spectrometer.

 

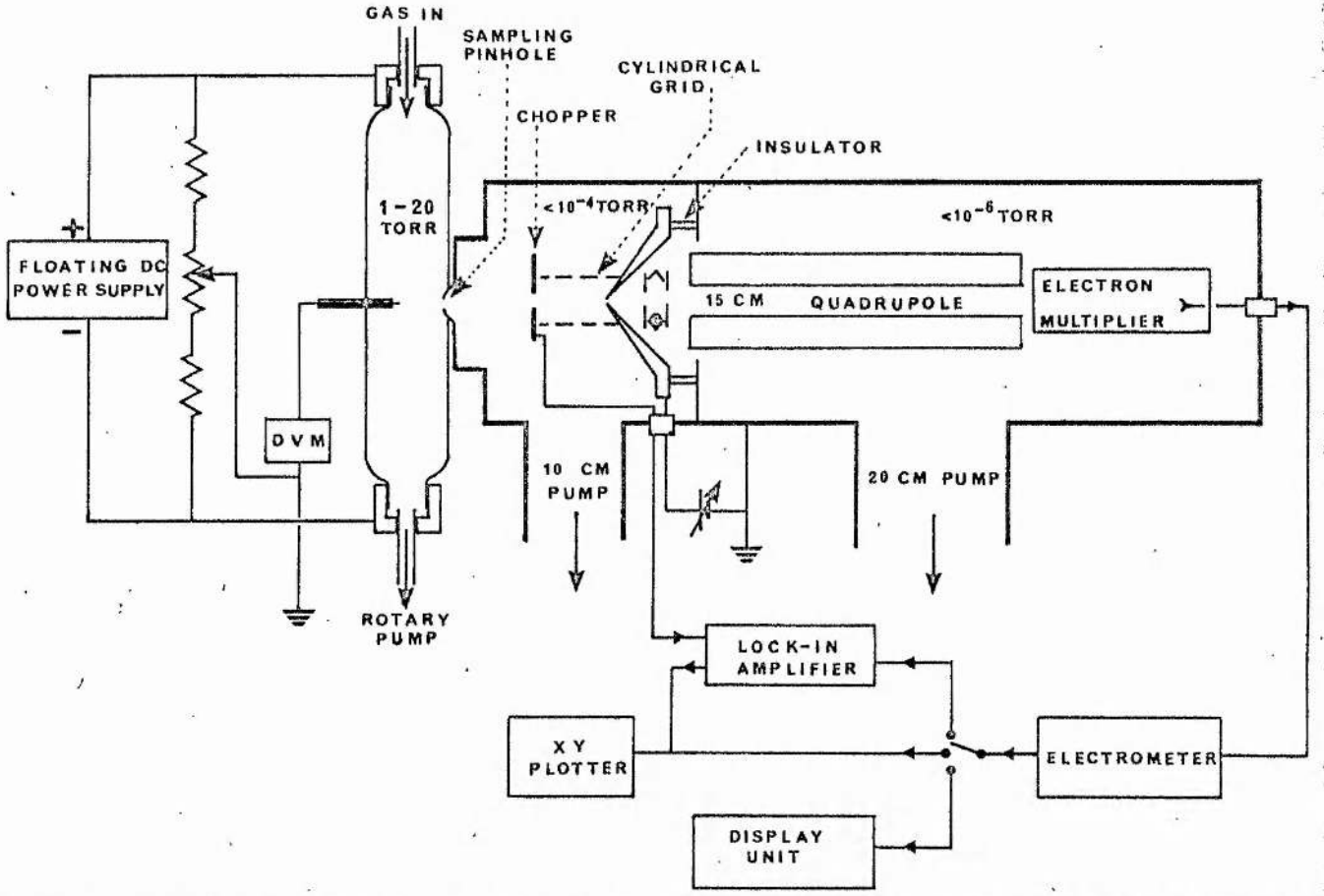


FIG. 1. System for mass spectrometric sampling and analysis of positive ions from the positive column of a dc glow discharge (not to scale).

The use of a differential pumping system allows operation of the discharge tube at pressures of several tens of torr whilst the mass spectrometer chamber pressure is $<10^{-6}$ torr.

The molecular or ionic beam is modulated with a vibrating vane chopper (Brookdeal 9478, 110 Hz) and the output from the anode of the electron multiplier of the Q8K is amplified with a Keithley 428 current amplifier and phase sensitive detected (Brookdeal 9501) at the beam chopping frequency. For most of the neutral spectra and for the larger ion peaks the improvement in the signal to noise produced by the lock-in amplification was unnecessary; and the output of the electrometer was either directly observed on an oscilloscope display unit or recorded on an $X$–$Y$ plotter.

Premixed technical grade gases were used, and no attempt was made to remove any impurity water vapor; thus the gases are typical of those which might be used to fill a laboratory $CO_2$ laser.

Several details of the gas sampling should be noted. Firstly, it is necessary to use a power supply with less than 0.1% ripple to avoid an ac component, at mains frequency, in the ion peak amplitudes due to fluctuations in the potential at the sampling pinhole.

Secondly, when ions effuse through the sampling pinhole there should be no asymmetric electric fields which could deflect them. Thus the high vacuum side of the glass sampling pinhole is coated with a layer of aluminum such that ions are at earth potential and can be drawn to the mass spectrometer by the potential applied to the secondary pinhole. This secondary metallic pinhole is electrically isolated from earth and in order that it have no defocusing effect on the ion beam, a cylindrical grid is used to provide a field free drift region near this pinhole. Positive ions travel along the axis of this cylinder which is electrically connected to the metallic pinhole.

Finally, signal reliability can be improved by careful control of sampling potentials. The axial potential in the discharge tube is monitored using an insulated probe connected to earth via a high impedance digital voltmeter. The potential read by this meter is that between the tube axis and the entrance to the intermediate chamber (earth). Making the axis positive ($0V - +30V$) with respect to earth assists in obtaining stable, repeatable mass spectra. The current drawn by this probe is much less than the discharge current. Additionally, a small negative bias ($0V - -10V$) applied to the secondary pinhole has the effect of pulling ions across the intermediate chamber towards the mass spectrometer.

These refinements introduce no changes in the rela-

tive peak heights of the positive ion species; however, they allow the use of optimum resolution and sensitivity settings of the mass spectrometer and enable a day to day reproducibility of better than ±15%. With careful control of water vapor content, this reproducibility could be improved.

A quantitative model of the kinetic processes leading to the production of the observed positive ion spectra is attempted in the discussion section below. This requires a knowledge of the positive ion spectra as detailed in the next section and also several other systems parameters: gas and electron temperatures together with neutral particle and negative ion densities.

Measurement of the gas temperature $T_g$ using a thermocouple technique shows that for pure $CO_2$, $T_g \sim 500$ K (10 torr, 10 mA), and for the other mixtures investigated $T_g$ is 400–450 K (10 torr, 10 mA) increasing with gas pressure and discharge current. The electron temperature $T_e$ has been calculated for various $CO_2$–$N_2$–He mixtures by Nighan[14] and by Judd.[15] It is estimated to be about 1 eV for the $E/P \sim 10$ V cm$^{-1}$ torr$^{-1}$ in our experiment.

Minority neutral species produced in the gas discharge can be measured using the mass spectrometer with the ionization source switched on. Values of the NO and $O_2$ concentrations are important in the theoretical analysis later. Water vapor concentration is measured with a hygrometer (MCM Model 600) at the gas inlet.

Finally, an estimate of the negative ion density $n_-$ is required to evaluate the importance of positive ion and negative ion recombination. Experimental determination of negative ion densities from an active discharge is not possible with the existing apparatus. However, a comprehensive negative ion model is available to the authors[6] which calculates negative ion species densities in a pulsed atmospheric pressure discharge. This model has been adapted[16] to low pressure discharges in the 1–20 torr region. $CO_3^-$, $NO_2^-$, and $NO_3^-$ are predicted as the major ion species; $NO_2^-$ dominates at the lower pressures (~1 torr) for $NO_2$ concentrations of ≥100 ppm, but at higher gas pressures three body formation of $CO_3^-$ from $O^-$ is considerable. CO detaches[17] from $O^-$, and hence reduces the $CO_3^-$ with a concentration dependent on the amount of CO created in the discharge; actual values are estimated at the appropriate stages of the discussion section.

## RESULTS

### A. Pure $CO_2$

Figure 2 shows typical positive ions in "pure" $CO_2$ as a function of discharge current. Peaks have been identified as $H_3O^+$ (mass 19), $O_2^+$ (mass 32), $CO_2^+$ (mass 44), and $HCO_2^+$ (mass 45). No appreciable clustering was

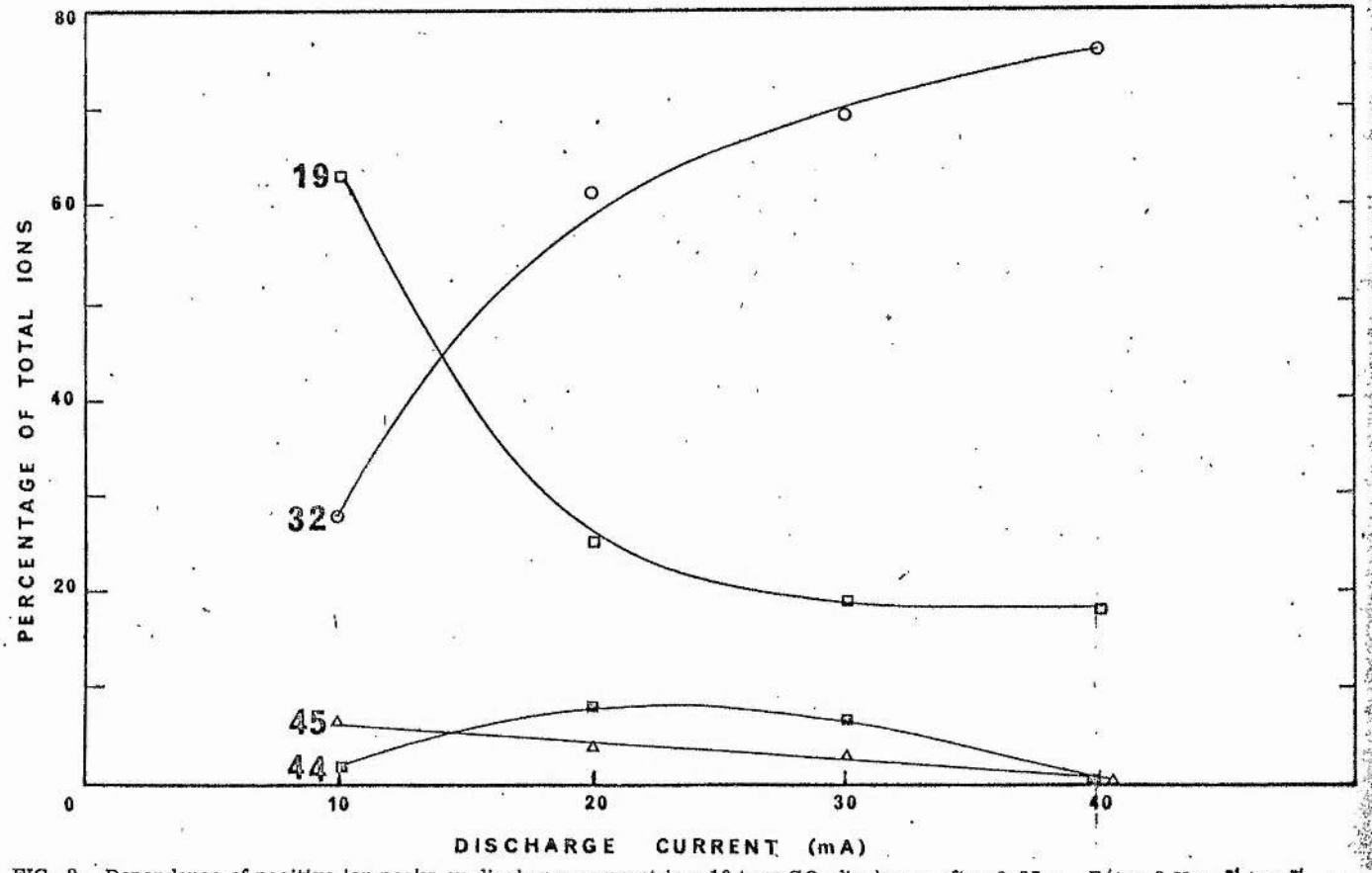


FIG. 2. Dependence of positive ion peaks on discharge current in a 10 torr $CO_2$ discharge after 0.25 s. $E/p \sim 8$ V cm$^{-1}$ torr$^{-1}$. □, $H_3O^+$ (mass 19); ○, $O_2^+$ (mass 32); ■, $CO_2^+$ (mass 44); △, $HCO_2^+$ (mass 45).

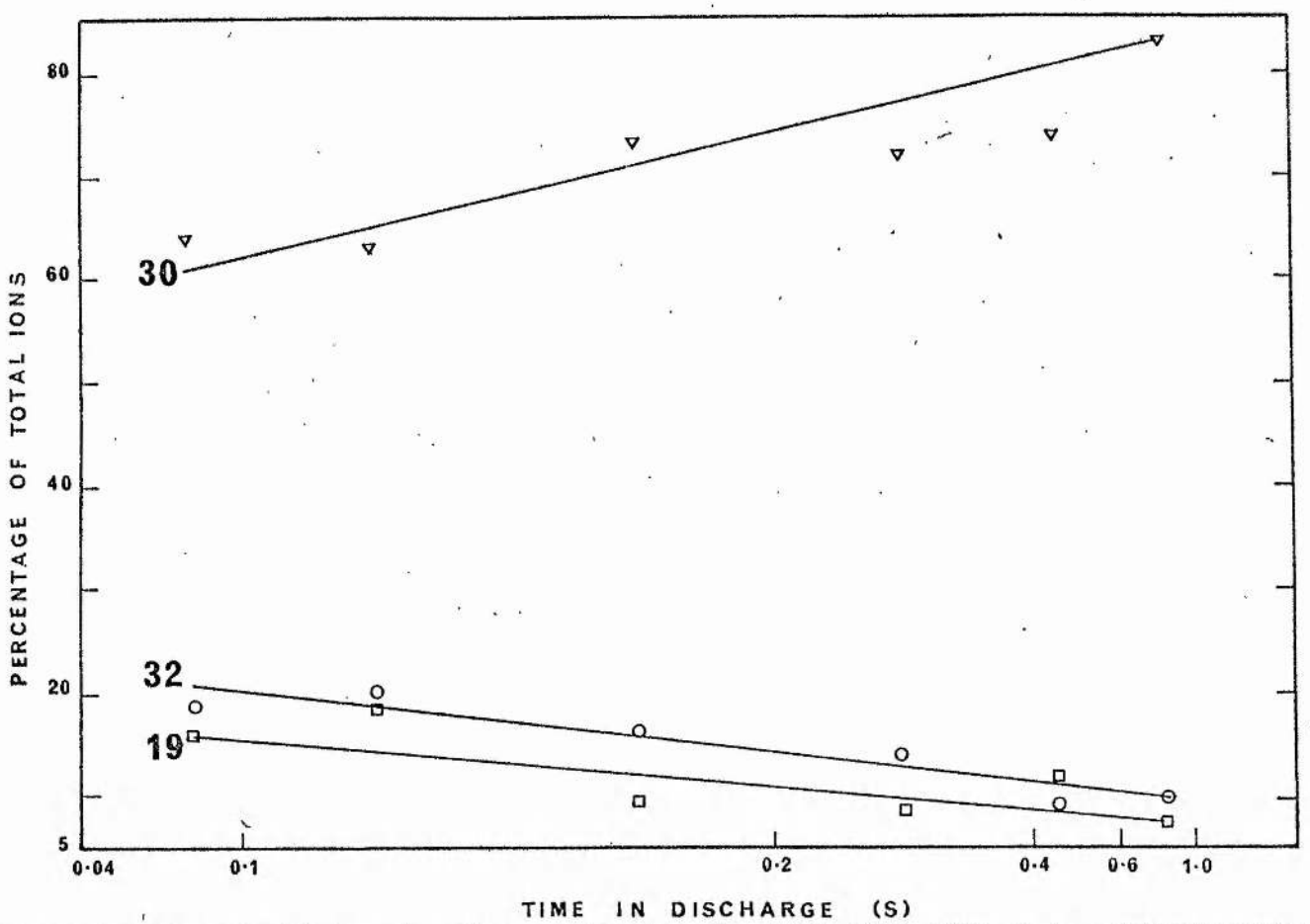


FIG. 3. Dependence of positive ion peaks on time spent in discharge for a 6% $CO_2$–12%$N_2$–82% He discharge at 10 torr and 10 mA. $E/p \sim 10$ V cm$^{-1}$ torr$^{-1}$. □, $H_3O^+$ (mass 19); ▽, $NO^+$ (mass 30); ○, $O_2^+$ (mass 32).

observed at this pressure of 10 torr. However at lower pressure the $H_3O^+ \cdot (H_2O)$ (mass 37) ion was observed, constituting a few percent of the total ion signal. Under most conditions $O_2^+$ was the dominant ion, accounting for 50% to 75% of the total ions present.

The influence of water vapor contamination is suggested by the $H_3O^+$, and $HCO_2^+$ peaks. A hygrometer measurement of the $H_2O$ concentration at the gas inlet gave a value of about 100 ppm.

### B. 6% $CO_2$-12% $N_2$-82% He

Results of analysis of positive ions in a typical gas laser mixture are plotted against time from entry into the discharge region until reaching the sampling point in Fig. 3, and versus total pressure in Fig. 4. These results are dominated by the $NO^+$ (mass 30) peak at pressures above 4 torr. Other ions present are $H_3O^+$ (mass 19), $O_2^+$ (mass 32), and $CO_2^+$ (mass 44).

The $NO^+$ ion constitutes 70%–100% of the total ion signal at pressures above 10 torr (currents from 10–60 mA and flow rates from 0.05 l s$^{-1}$–0.4 l s$^{-1}$).

### C. 6% $CO_2$-12% $N_2$-1.5% $H_2$-80.5% He

Results for this gas mixture are plotted: in Fig. 5 against time in discharge, in Fig. 6 with discharge current, and in Fig. 7 versus total pressure. The spectra are now dominated under all conditions by the $H_3O^+$ (mass 19), and the $H_3O^+ \cdot (H_2O)$ (mass 37) ions. Other ions are $H_2O^+$ (mass 18), $NO^+$ (mass 30), $O_2^+$ (mass 32), $H_3O^+ \cdot (H_2O)_2$ (mass 55), and $NO^+ \cdot (NO)$ (mass 60). In addition, other smaller peaks at masses 44 ($CO_2^+$), 45 ($HCO_2^+$), 48 ($NO^+ \cdot (H_2O)$), and 63 ($H_3O^+ \cdot (CO_2)$) were occasionally observed, always in concentrations <0.5% of the total ion signal. No evidence of cluster ions at mass numbers higher than 63 was found.

## DISCUSSION

### A. Pure $CO_2$

Results of previous experiments in pure $CO_2$[7–9] have indicated a predominance of $O_2^+$ at $CO_2$ pressures of a few torr and less. Although Evans and Jennings,[7] and Schildcrout *et al.*[8] sampled from rf glow discharges, no major qualitative discrepancy exists between their results and our measurements which were obtained under dc glow discharge conditions at higher pressures. The $O_2^+$ is presumed to be formed by the charge exchange reaction[8]

$$CO_2^+ + O_2 \rightarrow O_2^+ + CO_2 , \quad (1)$$

where $O_2$ is produced by dissociation of $CO_2$.[16] The rate

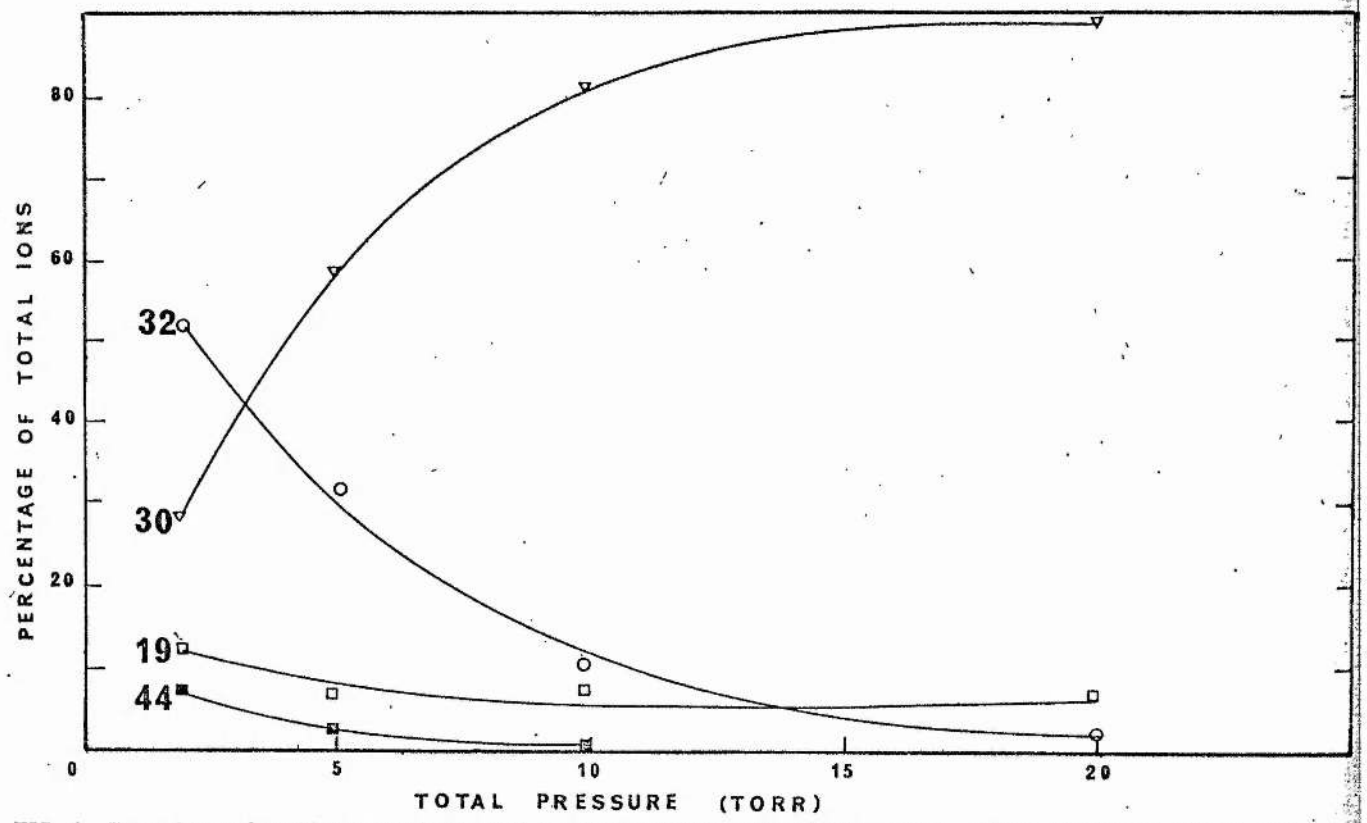


FIG. 4. Dependence of positive ion peaks on total discharge pressure for a 6% $CO_2$–12% $N_2$–82% He discharge at 10 mA after 0.4 s. □, $H_3O^+$ (mass 19); ▽, $NO^+$ (mass 30); ○, $O_2^+$ (mass 32); ■, $CO_2^+$ (mass 44).

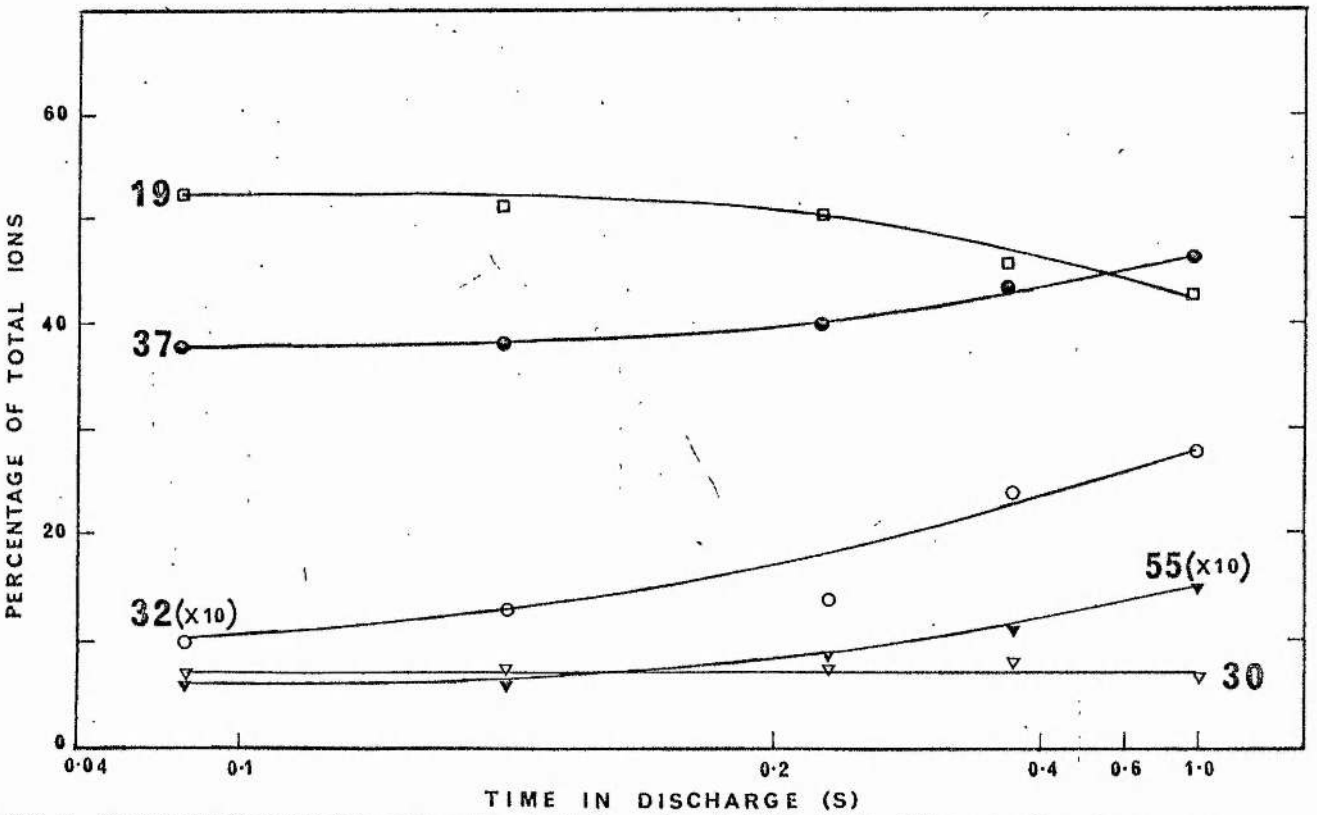


FIG. 5. Dependence of positive ion peaks on time in discharge for a 1.5% $H_2$–6% $CO_2$–12% $N_2$–80.5% He discharge at 10 torr and 10 mA. $E/p \sim 8$ V cm$^{-1}$ torr$^{-1}$. □, $H_3O^+$ (mass 19); ▽, $NO^+$ (mass 30), ○, $O_2^+$ (mass 32); ●, $H_2O^+ \cdot (H_2O)$ (mass 37); ▼, $H_3O^+ \cdot (H_2O)_2$ (mass 55).

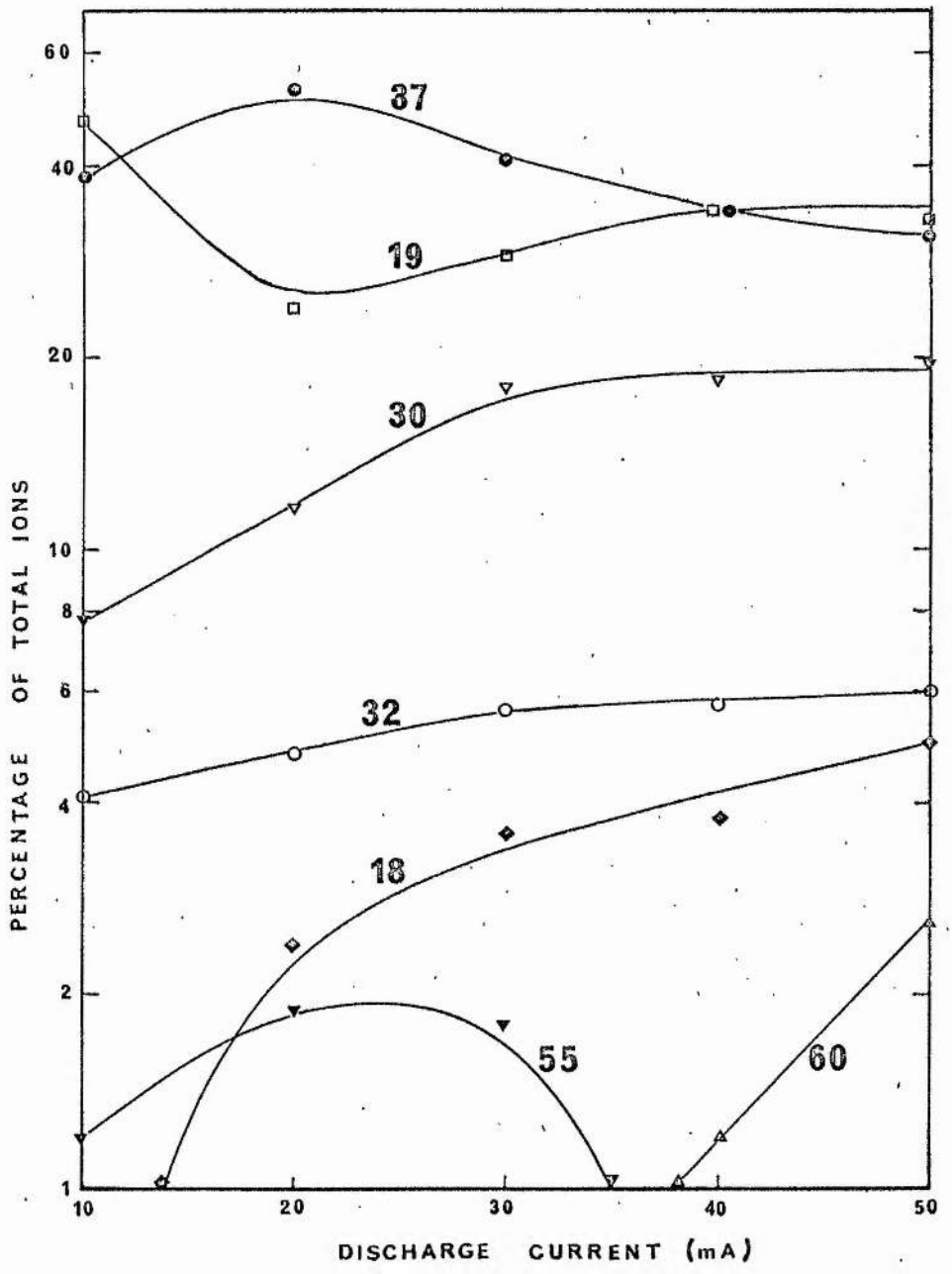


FIG. 6. Dependence of total positive ion peaks on discharge current for a 1.5% $H_2$–6% $CO_2$–12% $N_2$–80.5% He discharge at 10 torr. $E/p$ ~8 V cm$^{-1}$ torr$^{-1}$, discharge time ~0.8 s. ◆, $H_2O^+$ (mass 18); □, $H_3O^+$ (mass 19); ▽, $NO^+$ (mass 30); ○, $O_2^+$ (mass 32); ●, $H_3O^+ \cdot (H_2O)$ (mass 37); ▼, $H_3O^+ \cdot (H_2O)_2$ (mass 55); △, $NO^+ \cdot (NO)$ (mass 60).

constant of Reaction (1), $k_1$, is given by Ferguson[19] as $5\times10^{-11}$ cm$^3$ s$^{-1}$ and this reaction will remove $CO_2^+$ faster than positive ion–electron recombination[20] when there is more than 0.01% $O_2$ present.

The $CO_2^+$ ion is produced by electron impact ionization,

$$e + CO_2 \rightarrow CO_2^+ + 2e \ , \qquad (2)$$

so that this ion will increase with increasing current. However since dissociation of $CO_2$ into CO and O also occurs by electron impact and the degree of dissociation increases with current,[18] the $CO_2^+$ peak begins to decrease as Reaction (1) becomes increasingly effective with more $O_2$ being produced. The increase in the $O_2^+$ with current is similarly explained by the increased abundance of $O_2$ produced by $CO_2$ dissociation.

The electron impact ionization of $O_2$ has a similar rate constant to that for $CO_2$. However, in the conditions of the experiment, less than 1% $O_2$ is produced and the direct production of $O_2^+$ by ionization is not comparable with the charge exchange process (1).

Carbon monoxide and atomic oxygen are produced in the discharge by dissociation of $CO_2$. No charge exchange process is known to exist to produce $CO^+$ or $O^+$ from the ion species present, so $CO^+$ and $O^+$ can only be produced by electron impact ionization. However, these ions are rapidly removed by the charge exchange reactions

$$CO^+ + CO_2 \rightarrow CO_2^+ + CO \ , \qquad (3)$$

and

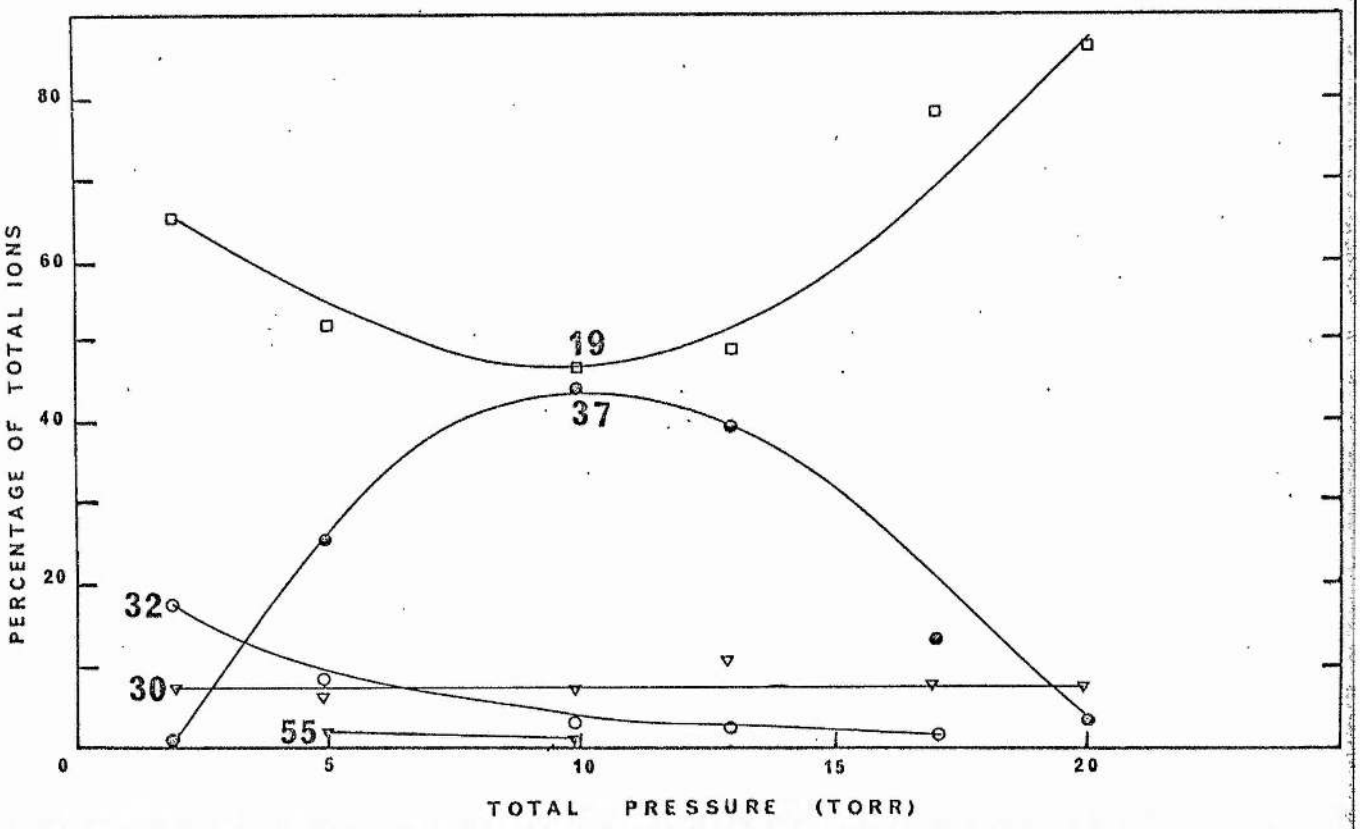


FIG. 7. Dependence of positive ion peaks on total discharge pressure for a 1.5% $H_2$–6% $CO_2$–12% $N_2$–80% He discharge at 10 torr after 0.4 s. □, $H_3O^+$ (mass 19); ▽, $NO^+$ (mass 30); ○, $O_2^+$ (mass 32); ●, $H_3O^+ \cdot (H_2O)_2$ (mass 55).

$$O^+ + CO_2 \rightarrow O_2^+ + CO\,, \tag{4}$$

where[19] $k_3 = 1.1\times10^{-9}$ cm$^3$ s$^{-1}$ and $k_4 = 1.2\times10^{-9}$ cm$^3$ s$^{-1}$. Since these loss rates are much faster than the corresponding ionization rates producing $CO^+$ and $O^+$, these ions are not observed. Reaction (4) is not an important source of $O_2^+$ compared with Reaction (1), even though the ionization rate constant of O is similar to that of $CO_2$, because in our system the concentration of O is very much less than the concentration of $CO_2$.

Three possibilities exist which could explain the production of $H_3O^+$; these are

$$H_3^+ + H_2O \rightarrow H_3O^+ + H_2\,, \tag{5}$$

$$H_2O^+ + H_2O \rightarrow H_3O^+ + OH\,, \tag{6}$$

$$HCO_2^+ + H_2O \rightarrow H_3O^+ + CO_2\,. \tag{7}$$

Reaction (5) can be immediately dismissed since there is insufficient hydrogen present to produce $H_3^+$ in the reaction[21]

$$H_2^+ + H_2 \rightarrow H_3^+ + H\,. \tag{8}$$

The rate constant of (7) has been measured by Betowski *et al.*[22] and was found to be $3\times10^{-9}$ cm$^3$ s$^{-1}$, while Ferguson[19] reports a value of $1.7\times10^{-9}$ cm$^3$ s$^{-1}$ for Reaction (6). This means that the production channels of $H_3O^+$ will depend on the relative concentrations of $H_2O^+$ and $HCO_2^+$. As can be seen from Fig. 2, only $HCO_2^+$ appears in any significant amount; and since $k_7 \approx k_6$, Reaction (7) is suggested as the source of $H_3O^+$.

No reaction has been found in the literature to satisfactorily explain the production of $HCO_2^+$, which appears in the positive ion spectrum. The authors suggest

$$CO_2^+ + H_2O \rightarrow HCO_2^+ + OH \tag{9}$$

as the source of $HCO_2^+$. This is based on literature values of the rates of the reactions

$$CO_2^+ + H_2 \rightarrow HCO_2^+ + H\,, \tag{10}$$

$$O_2^+ + H_2 \rightarrow HO_2^+ + H\,. \tag{11}$$

Fehsenfeld *et al.*[23] have measured $k_{10}$ to be $1.4\times10^{-9}$ cm$^3$ s$^{-1}$ and $k_{11}$ to be $<10^{-11}$ cm$^3$ s$^{-1}$. If corresponding reactions exist between these ions and $H_2O$ (where the H–OH bond is broken instead of the H–H bond) then the considerably faster reaction involving $CO_2^+$ would explain the appearance of $HCO_2^+$, while the nonappearance of $HO_2^+$ would be due to a slower reaction rate constant.

If $HCO_2^+$ is produced by Reaction (9) and lost in Reaction (7) then in the steady state,

$$[HCO_2^+] = k_9[CO_2^+]/k_7\,. \tag{12}$$

Figure 2 shows that $[HCO_2^+] \sim [CO_2^+]$, so that $k_9 \sim 3\times10^{-9}$ cm$^3$ s$^{-1}$. This value is similar to that reported for $k_{10}$ above.[23]

Ion production in $CO_2$ then proceeds by the following channels:

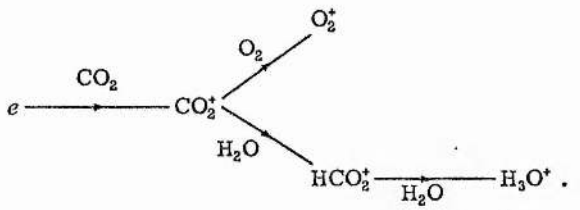


Loss of $O_2^+$ and $H_3O^+$ will be by electron[20,24] and negative ion[25] recombination; diffusion losses are about 10 times less important at the pressure of 10 torr.

With consideration of the appropriate loss reactions, some semiquantitative insight into the plasma chemistry can be gained. These reactions are

$$O_2^+ + e \rightarrow O + O , \tag{13}$$

$$H_3O^+ + e \rightarrow H_2O + H \rightarrow H_2 + OH , \tag{14}$$

$$A^+ + B^- \rightarrow A + B . \tag{15}$$

Assuming a $T_e^{-1/2}$ dependence for Reactions (13) and (14) (where $T_e$ is the electron temperature), from Ref. 20 one can obtain these values for the rate constants: $k_{13} = 4\times10^{-6}$ cm$^3$ s$^{-1}$ and $k_{14} = 3\times10^{-7}$ cm$^3$ s$^{-1}$. Positive ion–negative ion recombination has been little studied, but based on values for $O^-$ (see Ref. 25) one can estimate $k_{15}$ as $\sim 4\times10^{-7}$ cm$^3$ s$^{-1}$.

From Eq. (2) for the ionization production of $CO_2^+$ and Eq. (1) for its charge exchange loss,

$$[CO_2^+] = k_2 n_e [CO_2]/k_1[O_2] , \tag{16}$$

where $n_e$ is the electron density. Likewise from Eqs. (1), (13), and (15):

$$[O_2^+] = k_1[CO_2^+][O_2]/(n_e k_{13} + n_- k_{15}) . \tag{17}$$

Thus with the knowledge of the appropriate rate constants, the electron and negative ion densities and the neutral species concentrations the positive ion concentrations should be calculable. The neutral species concentrations are either known (as in the case of $[CO_2]$) or can be measured (as we have done for $[O_2]$), $n_e$ can be calculated from the discharge current and drift velocity[26] but $k_2$, the ionization rate, is a very rapidly varying function of the discharge reduced field ($E/P$) and electron temperature $T_e$. However, relative peak heights can be estimated; thus from (17) one has

$$\frac{[O_2^+]}{[CO_2^+]} = \frac{k_1[O_2]}{n_e k_{13} + n_- k_{15}} , \tag{18}$$

and from (9), (12), (14), and (15) one has

$$\frac{[H_3O^+]}{[CO_2^+]} = \frac{k_9[H_2O]}{n_e k_{14} + n_- k_{15}} . \tag{19}$$

In (18) and (19) the only unknown quantity is the negative ion concentration, $n_-$. We have computed this from an extensive negative ion model.[6,16] Since several of the parameters, especially $n_-$, $k_9$, and $k_{15}$, are not exact and the values of the charge exchange reactions etc. are those available for room temperature, not the somewhat higher temperature of the glow discharge, it is not appropriate to attempt an exact quantitative fit to the curves of Fig. 2. However, we may compare the situations at, say, 10 mA and 40 mA by substitution of the above quoted numbers, together with $[H_2O]$ as 100 ppm (measured by hygrometry), $[O_2]$ as 2000 ppm at 10 mA and 5000 ppm at 40 mA (measured by mass spectrometry), $n_e$ as $5\times10^9$ cm$^{-3}$ at 10 mA and $2\times10^{10}$ at 40 mA, $n_-$ as $5\times10^9$ cm$^{-3}$ at 10 mA and $2\times10^9$ at 40 mA (the negative ion value falls off with increase in current because of the detaching effect of CO[6,10,17]). We find $[O_2^+]/[CO_2^+] \sim 20$ at 10 mA and $\sim 70$ at 40 mA, and $[H_3O^+]/[CO_2^+] \sim 25$ at 10 mA and $\sim 14$ at 40 mA. Thus $O_2^+$ and $H_3O^+$ are the dominant ions, with $[H_3O^+]$ falling and $[O_2^+]$ increasing as the current increases, as is observed in the experimental results of Fig. 2.

### B. 6% $CO_2$–12% $N_2$–82% He

The 6% $CO_2$–12% $N_2$–82% He mixture studied here is typical of the gas composition used in low pressure, flowing gas cw $CO_2$ lasers. Tannen *et al.*[11] have sampled positive ions from a static 12.7% $CO_2$–15.5% $N_2$–71.8% He mixture in a region of the discharge near the cathode. They find $NO^+$ is the major ion at their pressures of 1–8 torr with $O_2^+$, $CO_2^+$, $O^+$, $N_2^+$ and possibly $CO^+$ also present. No water vapor contamination is evident. In their experiments $NO^+$ takes several seconds to establish itself as the major species. This delay may be due to diffusion of $NO^+$ from the positive column of the discharge to the sampling point. Austin and Smith[10] have sampled ions directly through the cathode with 2–9 torr of a 6% $CO_2$–12% $N_2$–82% He flowing gas mixture and found $CO_2^+$, $O_2^+$, $N_2^+$, $CO^+$, and $H_2O^+$. The correspondence between these species and the neutral gas suggests direct electron impact ionization in the high fields of the cathode region, with ion–molecule processes of secondary importance.

Our results (Figs. 3 and 4) taken directly from the positive column and well removed from cathode influences show spectra which reflect the importance of minor quantities of NO produced in the discharge. Typically NO accounts for less than 0.1% of the gas mixture[11] but, except at the lowest pressures (less than 4 torr), $NO^+$ dominates the positive ion spectrum. There are numerous reactions which could produce $NO^+$ in the discharge, but of these, only three appear to be important in the present case:

$$O_2^+ + NO \rightarrow NO^+ + O_2 , \tag{20}$$

$$CO_2^+ + NO \rightarrow NO^+ + CO_2 , \tag{21}$$

$$e + NO \rightarrow NO^+ + 2e . \tag{22}$$

Ferguson[19] gives the rates $k_{20}$ as $7\times10^{-10}$ cm$^3$ s$^{-1}$ and $k_{21}$ as $1\times10^{-10}$ cm$^3$ s$^{-1}$; values of the ionization rate for Reaction (22) have been calculated as a function of $E/P$ by Bletzinger *et al.*[2] The latter two reactions are only important at low pressure where the ionization rate constant is larger[2] or when there is a few percent $CO_2^+$ present (Fig. 4). This higher percentage of $CO_2^+$ is due to a lower value of $[O_2]$ at low pressure. Under most conditions Reaction (20) accounts for the production of $NO^+$.

The effect of Reaction (20) can be seen in two ways. Figure 3 shows the time development of $NO^+$ where the

gradual increase in $NO^+$ is accompanied by a corresponding drop in $O_2^+$. This can be understood as due to more neutral NO being produced in the discharge as time progresses, so charge exchange with $O_2^+$ becomes more favorable. Figure 4, taken after a 0.4 s discharge time, shows the pressure dependence of the $NO^+$ signal. Mass spectrometry of neutral NO shows that although the relative percentage of NO will decrease as discharge pressure increases—from about 75 ppm at 2 torr to about 30 ppm at 20 torr (for a current density of 2.6 mA/cm$^2$ and flow rate of 0.08 l s$^{-1}$)—the absolute amount of the NO will increase. Thus there is an increase in $NO^+$ accompanied by a drop in $O_2^+$. Since $NO^+$ undergoes no ion–molecule reactions in the discharge, it will be lost mainly by electron and negative ion recombination.

The drop in $H_3O^+$ in Fig. 3 is attributed to some dissociation of $H_2O$ in the discharge, so Reactions (7) and (9) are slightly slower. Charge transfer between $H_3O^+$ and NO is unlikely to occur since no obvious reaction channel exists, so $H_3O^+$ is lost in electron and negative ion recombination.

Smith[27] has shown that $[O_2]$ produced in a 6% $CO_2$–12% $N_2$–82% He mixture increases as the pressure increases. Thus we expect $CO_2^+$ to be removed more rapidly by Reaction (1) as the pressure increases. However, as stated earlier, [NO] also increases with pressure and Reaction (20) rapidly forms $NO^+$ at the expense of $O_2^+$. The net effect is a reduction of $[O_2^+]$.

Thus, in the 6% $CO_2$–12% $N_2$–82% He mixture, ions are produced by the following channels:

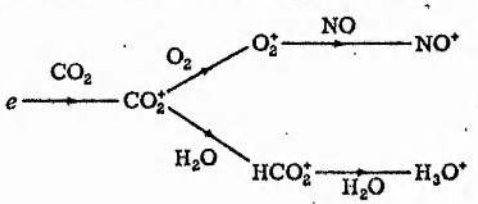


Accounting for the loss of $NO^+$ by positive ion–negative ion recombination [Reaction (15)] and

$$NO^+ + e \rightarrow N + O \tag{23}$$

with the recombination rate[20] $k_{23} = 7\times10^{-8}$ cm$^3$ s$^{-1}$, where a $T_e^{-1/2}$ dependence is again assumed, we get from (15), (20), and (23)

$$[NO^+] = k_{20}[O_2^+][NO]/(n_e k_{23} + n_- k_{15}) . \tag{24}$$

With the additional loss process (20) for $O_2^+$, Eq. (17) becomes

$$[O_2^+] = \frac{k_1[CO_2^+][O_2]}{n_e k_{13} + n_- k_{15} + k_{20}[NO]} . \tag{25}$$

Knowledge of the amount of [NO] present under various conditions enables the positive ion curves of Figs. 3 and 4 to be explained semi-quantitatively. The comments made about $n_-$, $k_{15}$, and the temperature variation of rate constants in the case of pure $CO_2$ still apply; and once again an exact fit to the curves is impossible. However, trends may be clearly illustrated.

From Eq. (24) we have

$$\frac{[NO^+]}{[O_2^+]} = \frac{k_{20}[NO]}{n_e k_{23} + n_- k_{15}} , \tag{26}$$

and from (19) and (25) we have

$$\frac{[H_3O^+]}{[O_2^+]} = \frac{k_9[H_2O](n_e k_{13} + n_- k_{15} + k_{20}[NO])}{k_1[O_2](n_e k_{14} + n_- k_{15})} . \tag{27}$$

The discharge current of 10 mA in Fig. 3 corresponds to $n_e = 5\times10^9$ cm$^{-3}$ (for the drift velocity given by Lowke *et al.*[28]). Taking [NO] as 25 ppm at 0.1 s and 55 ppm at 1.0 s (measured by mass spectrometer) together with $n_-$ as $5\times10^9$ cm$^{-3}$ (as before) we find $[NO^+]/[O_2^+] \sim 2.5$ at 0.1 s flow time and $\sim 5$ at 1.0 s flow time. In the 6% $CO_2$–12% $N_2$–82% He laser gas mixture, $[H_2O]$ measured by hygrometer is 100 ppm, as for pure $CO_2$. Mass spectrometer measurements of $[O_2]$ give values of 0.6% at 0.1 s and 1.1% at 1.0 s which when substituted into (27) results in $[H_3O^+]/[O_2^+] \sim 1$ at both 0.1 s and 1.0 s.

Similarly in Fig. 4, if we assume $n_e \approx n_- \approx 5\times10^9$ cm$^{-3}$ over the pressure range from 2–20 torr, then Eq. (26) predicts $[NO^+]/[O_2^+] \approx 1.5$ at 2 torr and $\approx 6$ at 20 torr. These ratios occur for a concentration of NO of 75 ppm at 2 torr and 30 ppm at 20 torr. When 100 ppm of $H_2O$ and 1% $O_2$ are substituted into Eq. (27), together with the quoted values of $n_e$, $n_-$, and [NO], $[H_3O^+]/[O_2^+] \approx 0.4$ at 2 torr and $\approx 1.2$ at 20 torr. An approximate calculation of diffusion time using a diffusion coefficient[29] of 20 cm$^2$ s$^{-1}$ at 1 torr shows that, for the case of $NO^+$ and $O_2^+$, loss of ions by ambipolar diffusion is equal to loss in electron and negative ion recombination at 1 torr, but a factor of 10 less at 10 torr. It is considerably slower in the case of $H_3O^+$, where the electron recombination rate is large. This correction makes $[NO^+]/[O_2^+] \approx 1$ at 2 torr.

These theoretically predicted ratios and the experimental results presented in Figs. 3 and 4 are in good agreement. Theory predicts a gradual rise in the $[NO^+]/[O_2^+]$ ratio as time progresses while $[O_2^+] \sim [H_3O^+]$ at all times up to 1 s, as observed in Fig. 3. The conversion of $[O_2^+]$ to $[NO^+]$ in Fig. 4 is reflected in Eq. (26) by an increase in $[NO^+]/[O_2^+]$ as pressure increases. The observed increase in $[H_3O^+]/[O_2^+]$ is predicted by (27).

### C. 1.5% $H_2$–6% $CO_2$–12% $N_2$–80.5% He

The addition of 0.1–0.2 torr of hydrogen to the basic $CO_2$–$N_2$–He gas mixture of low pressure cw lasers limits the loss of $CO_2$ by dissociation and allows long life sealed operation.[12,13] Typically these devices work in the 10–20 torr total pressure region, so the amount of added hydrogen is between 0.5 and 2%; we have investigated a mixture with 1.5% added hydrogen.

Figures 5, 6, and 7 show that the ion spectra are now dominated by $H_3O^+$ and $H_3O^+ \cdot (H_2O)$ with a significant contribution from $H_3O^+ \cdot (H_2O)_2$. The most likely reaction sequence begins with the previously mentioned Reaction (10)

$$CO_2^+ + H_2 \rightarrow HCO_2^+ + H ,$$

followed by Reaction (7),

$$HCO_2^+ + H_2O \rightarrow H_3O^+ + CO_2 ,$$

with the $H_3O^+$ being hydrated by

$$H_3O^+ + H_2O + M \rightarrow H_3O^+ \cdot (H_2O) + M , \quad (28)$$

with a similar reaction to form the double hydrate.

Equation (12) for the creation and loss of $HCO_2^+$ is modified in order to allow for Reaction (10):

$$[HCO_2^+] = \frac{k_{10}[CO_2^+][H_2] + k_9[CO_2^+][H_2O]}{k_7[H_2O]} ; \quad (29)$$

and $[H_3O^+]$ is given by

$$[H_3O^+] = \frac{k_7[HCO_2^+][H_2O]}{n_e k_{14} + n_- k_{15} + k_{28}[H_2O][M]} . \quad (30)$$

Provided $[H_2] > [H_2O]$, from (29) and (30) we get

$$\frac{[H_3O^+]}{[CO_2^+]} = \frac{k_{10}[H_2]}{n_e k_{14} + n_- k_{15} + k_{28}[H_2O][M]} . \quad (31)$$

$[CO_2^+]$ is too small to appear on Figs. 5, 6, or 7; but at 10 torr (and with the other conditions of Fig. 5) the ratio $[H_3O^+]/[CO_2^+]$ is about 250. Fehsenfeld *et al.*[23] has measured $k_{10}$ as $1\times10^{-9}$ cm$^3$ s$^{-1}$ and $[H_2]$ is $6\times10^{15}$ cm$^{-3}$; thus the denominator in (31) should be $\sim 2\times10^4$ s$^{-1}$. But $n_e k_{14} + n_- k_{15}$ is only $\sim 3\times10^3$ s$^{-1}$, so $k_{28}[H_2O][M]$ must be $\sim 2\times10^4$ s$^{-1}$ if Eq. (31) is correct. $[H_2O]$ is ~100 ppm and with $[M] = 4\times10^{17}$ cm$^{-3}$, $k_{28}$ becomes $\sim 10^{-27}$ cm$^6$ s$^{-1}$. Good *et al.*[30] have studied the hydration reaction of $H_3O^+$,

$$H_3O^+ \cdot (H_2O)_n + H_2O + M \rightarrow H_3O^+ \cdot (H_2O)_{n+1} + M , \quad (32)$$

and have found a rate constant for the forward reaction of $3.4\times10^{-27}$ cm$^6$ s$^{-1}$ ($n=0$, M = $N_2$, $T_g = 300$ K). This agrees favorably with our derived value of $10^{-27}$ cm$^6$ s$^{-1}$ ($n=0$, M largely He, $T_g \sim 400$–$450$ K). Similarly, the same authors obtain a rate constant of $2.3\times10^{-27}$ cm$^6$ s$^{-1}$ for the forward reaction when $n=1$. They evaluate the rate constants for the reverse reactions as $7\times10^{-26}$ cm$^3$ s$^{-1}$ ($n=0$) and $7\times10^{-18}$ cm$^3$ s$^{-1}$ ($n=1$), respectively, at 300 K. Since the temperature dependence of the equilibrium constant is known,[31] we have calculated the rate constants of the reverse reactions at 400–450 K assuming the forward rate to be approximately constant over the 300–450 K temperature range. We obtain $10^{-17}$ to $10^{-19}$ cm$^3$ s$^{-1}$ ($n=0$) and $10^{-12}$ to $10^{-13}$ cm$^3$ s$^{-1}$ ($n=1$) showing that $H_3O^+ \cdot (H_2O)_n$ hydrates are unstable against thermal dissociation of the cluster bond, and this instability increases very considerably with both the gas temperature and the value of $n$.

Consider the formation and loss of $H_3O^+ \cdot (H_2O)$ from Eq. (28):

$$\frac{[H_3O^+ \cdot (H_2O)]}{[H_3O^+]} = \frac{k_{28}[H_2O][M]}{n_e k_{34} + n_- k_{15} + Y} , \quad (33)$$

where $k_{34}$ is the positive ion–electron recombination rate constant for $H_3O^+ \cdot (H_2O)$, given by Leu *et al.*[32] as $2\times10^{-6}$ cm$^3$ s$^{-1}$ at a gas and electron temperature of 400–500 K. Assuming a $T_e^{-1/2}$ dependence, this gives $k_{34}$ as $6\times10^{-7}$ cm$^3$ s$^{-1}$ at 1 eV. $Y$ represents additional loss processes for $H_3O^+ \cdot (H_2O)$: these include thermal dissociation of the cluster bond in $H_3O^+ \cdot (H_2O)$, the net formation of $H_3O^+ \cdot (H_2O)_2$ by Eq. (32) when $n=1$, and diffusion. Substitution of the previously assumed values in Eq. (33) together with the derived value of $k_{28}$ and the above value of $k_{34}$ yields

$$\frac{[H_3O^+ \cdot (H_2O)]}{[H_3O^+]} = \frac{1.6\times10^4}{3\times10^3 + 2\times10^3 + Y} .$$

This ratio will have a maximum value of about 3 and will be less if $Y$ is significant; from Fig. 5 we see the measured ratio is about 1 at 10 torr. Also from Fig. 5, it can be seen that $H_3O^+ \cdot (H_2O)_2$ is present in rather small amounts, although from Eq. (32), where for $n=1$, $[M] = 4\times10^{17}$ cm$^{-3}$, and $[H_2O] = 4\times10^{13}$ cm$^{-3}$, it will be formed at a considerable rate (contributing $4\times10^4$ to $Y$ above). However, the reformation of $H_3O^+ \cdot (H_2O)$ by the thermal dissociation of the $H_3O^+ \cdot (H_2O)_2$ takes place at a comparable rate (the exact rate is uncertain because of the uncertainty in $k_{-32}$ ($n=1$) due to its rapid variation with gas temperature, as mentioned above). Thus the net contribution of the formation of $H_3O^+ \cdot (H_2O)_2$ to $Y$ may not be great. The most likely explanation for the calculated ratio being somewhat high is that the thermal breakup of $H_3O^+ \cdot (H_2O)$ is significant.

Consider the results of Fig. 7: the ion variations with total pressure. At about 10 torr the value of $[H_3O^+ \cdot (H_2O)]/[H_3O^+]$ is explained as in the previous paragraph; as the pressure is decreased, [M] in Eq. (32) decreases, possibly $Y$ increases (with enhanced diffusion), and possibly $[H_2O]$ decreases, so the ratio decreases as observed. At higher pressures [M] increases, but the gas temperature increases with pressure (for constant current conditions) and so thermal dissociation may be increased, $Y$ increased, and the ion ratio decreased. The behavior of the $NO^+$ and $O_2^+$ is similar to that described in the section above in the three part gas mixture.

The results of Fig. 6 are explicable in a similar manner. As the current is increased and as $[H_2O]$ is increased by neutral reactions, $[H_3O^+ \cdot (H_2O)]/[H_3O^+]$ increases; but at high currents the gas temperature is increased and the value of $Y$ should increase to reduce the ion ratio. It should be noted that the smaller $H_3O^+ \cdot (H_2O)_2$ curve behaves in a similar manner to the single hydrate curve, as would be expected with this explanation.

## CONCLUSIONS

In the positive column of a $CO_2$ laser, the positive ion chemistry can be explained by the scheme

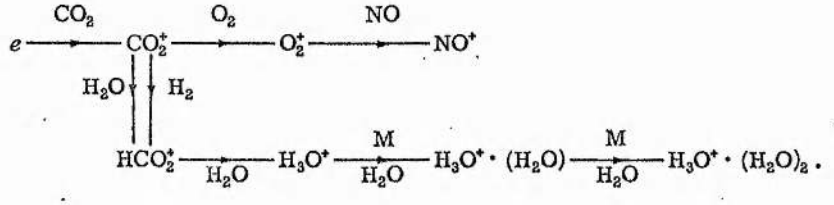

In an initially pure $CO_2$ system there is dissociation of the $CO_2$ and the dominant ion is $O_2^+$; but in a $CO_2$–$N_2$–He mixture this is rapidly converted by reaction with NO—formed from the $CO_2$ and $N_2$ by the discharge—into $NO^+$. However, if $H_2O$ or $H_2$ is present, $H_3O^+$ is formed; and if there is sufficient $H_2O$, $H_3O^+ \cdot (H_2O)$ and a lesser amount of $H_3O^+ \cdot (H_2O)_2$ will also be formed.

This reaction scheme qualitatively explains the observed behavior of the ion peaks over the pressure range 2–20 torr in the positive column of a flowing gas mixture and should describe the ion chemistry of the corresponding sealed system with appropriate adjustment of the composition of the neutral gas.

Satisfactory quantitative agreement is obtained using established values for the various rate constants, etc., together with the determined values of rate constants of about $3\times10^{-9}$ cm$^3$ s$^{-1}$ for Reaction (9),

$$CO_2^+ + H_2O \rightarrow HCO_2^+ + OH\ ,$$

and $10^{-27}$ cm$^6$ s$^{-1}$ for Reaction (28),

$$H_3O^+ + H_2O + M \rightarrow H_2O^+ \cdot (H_2O) + M\ .$$

Quantitative uncertainty arises because of lack of comprehensive values for electron–positive ion and positive ion–negative ion recombination coefficients and to a lesser extent the need to use theoretically calculated values of $k_2$ and $n_-$ and the difficulty in quantitatively calibrating the mass spectrometer for ion peaks. However, in practice the agreement between experimental results and predicted behavior is surprisingly good, except for the situation with added hydrogen, where there is little established data available about the formation and breakup of water vapor clusters; therefore discussion and explanation of the experimental results is somewhat restricted.

## ACKNOWLEDGMENTS

It gives us great pleasure to acknowledge the assistance of Mr. F. Akerboom with the production of the pinholes, and to thank both C. V. D. for equipment support and the Science Research Council for the award of a studentship to H. S.

[1]W. L. Nighan and W. J. Wiegand, Phys. Rev. A 10, 922 (1974).
[2]P. Bletzinger, D. A. Laborde, W. F. Bailey, W. H. Long, P. D. Tannen, and A. Garscadden, IEEE. J. Quantum Electron. QE-11, 317 (1975).
[3]L. J. Denes and J. J. Lowke, Appl. Phys. Lett. 23, 130 (1973).
[4]P. E. Dyer and D. J. James, J. Appl. Phys. 46, 1679 (1975).
[5]D. A. Douglas-Hamilton and S. A. Mani, J. Appl. Phys. 45, 4406 (1974).
[6]H. Shields, A. L. S. Smith, and B. Norris, J. Phys. D 9, 1587 (1976).
[7]H. E. Evans and P. P. Jennings, Trans. Faraday Soc. 61, 2153 (1965).
[8]S. M. Schilderout, J. G. Collins, and J. L. Franklin, J. Chem. Phys. 52, 5767 (1970).
[9]P. H. Dawson and A. W. Tickner, Proc. 6th Int. Conf. Ionization Phenomena Gases, Paris, 2, 79 (1963).
[10]J. M. Austin and A. L. S. Smith, J. Phys. D 5, 468 (1972).
[11]P. D. Tannen, P. Bletzinger, and A. Garscadden, IEEE J. Quantum Electron. QE-10, 6 (1974).
[12]W. J. Witteman and H. W. Werner, Phys. Lett. A 26, 454 (1968).
[13]A. L. S. Smith and P. G. Browne, J. Phys. D 7, 1652 (1974).
[14]W. L. Nighan, Phys. Rev. A2, 1989 (1970).
[15]O. P. Judd, J. Appl. Phys. 45, 4572 (1974).
[16]H. Shields and A. L. S. Smith (to be published).
[17]M. McFarland, D. L. Albritton, F. C. Fehsenfeld, E. E. Ferguson, and A. L. Schmeltekopf, J. Chem. Phys. 59, 6629 (1973).
[18]A. L. S. Smith and J. M. Austin, J. Phys. D 7, 314 (1974).
[19]E. E. Ferguson, N. T. I. S. Rep. No. NBSIR 74-450, edited by D. Garvin and R. F. Hampson (1974).
[20]J. N. Bardsley and M. A. Biondi, *Advances in Atomic and Molecular Physics*, 6, edited by D. R. Bates and I. Esterman (Academic, New York, 1970).
[21]E. Herbst and W. Klemperer, Astrophys. J. 185, 505 (1973).
[22]D. Betowski, J. D. Payzant, G. I. MacKay and D. K. Bohme, Chem. Phys. Lett. 31, 321 (1975).
[23]F. C. Fehsenfeld, A. L. Schmeltekopf and E. E. Ferguson, J. Chem. Phys. 46, 2802 (1967).
[24]R. A. Heppner, F. L. Walls, W. T. Armstrong and G. H. Dunn, Phys. Rev. A 13, 1000 (1976).
[25]R. E. Olsen, J. Chem. Phys. 56, 2979 (1972).
[26]S. C. Brown, *Basic Data of Plasma Physics* (Wiley, New York, 1959), p. 60.
[27]A. L. S. Smith, Br. J. Appl. Phys. 2, 1129 (1969).
[28]J. J. Lowke, A. V. Phelps, and B. W. Irwin, J. Appl. Phys. 44, 4664 (1973).
[29]A. Von Engel, *Ionized Gases* (Oxford University Press, London, 1965), p. 140.
[30]A. Good, D. A. Durden, and P. Kebarle, J. Chem. Phys. 52, 212 (1970).
[31]P. Kebarle, S. K. Searles, A. Zolla, J. Scarborough, and M. Arshadi, J. Am. Chem. Soc. 89, 6393 (1967).
[32]M. T. Leu, M. A. Biondi, and R. Johnsen, Phys. Rev. A7, 292 (1972).

# CHAPTER FIVE

## DETERMINATION OF NEGATIVE IONS IN $CO_2$ LASER DISCHARGES

## 5.1 INTRODUCTION

The present limitation to the achievement of high power output from compact laser devices is the onset of plasma instabilities at high input power densities, as discussed in chapter 1. The theories of ionisation and thermal instabilities (section 1.5) link the stability of $CO_2$ laser discharges to negative ion kinetics under conditions where ambipolar diffusion is a negligible charged particle loss mechanism. However, these theories suffer from lack of experimental determination of the major negative ion species present in the discharge.

Conceivably, this knowledge could be provided by mass-spectrometric identification of the negative ions, as was performed for positive ions in chapters 3 and 4. However there are experimental difficulties involved in measurement of negative ion currents effusing from a dc glow discharge. These difficulties are discussed in section 5.2, and methods of circumventing them are considered. It will be shown that such methods are not relevant to the $CO_2$ laser discharge analysis and an alternative means of determining negative ion densities is desirable.

Section 5.3 shows that sufficient data is available in the literature to allow the densities of negative ion species to be derived computationally. This approach not only predicts the major negative ion species for a particular laser situation, but yields the species densities and temporal evolution after the initiation of the discharge. Conversely, the mass-spectrometric determination of species can only give relative concentrations of ion species, and is unlikely to have sufficient time response to follow the development of ions on a sub-millisecond time scale. Additionally, the versatility of the computational approach allows its adaptation to a variety of laser situations. Section 5.3 gives some general details of the

computational model which is then applied to the $CO_2$ TEA laser discharge in chapter 6, and the EDCL discharge in chapter 7.

## 5.2 MASS-SPECTROMETRIC MEASUREMENT OF NEGATIVE ION SPECIES

As with positive ions, the nature of negative ion species present in a gas discharge may be determined by mass-spectrometric analysis as the ions effuse from the discharge. The theory of positive ion sampling from gas discharge plasmas was extensively treated in chapter 2. Much of this theory is applicable to negative ions, but there are experimental difficulties involved in measurement of negative ion currents effusing from a dc glow discharge plasma. These difficulties are discussed below.

The theory of ambipolar diffusion in an electronegative plasma has been derived by Thompson (1959) and was discussed with relevance to positive ion diffusion in section 2.2.2. The particle fluxes to the dischargewall are given by,

$$\begin{aligned} \underline{\Gamma}_+ &= -D_+ \nabla n_+ + \mu_+ n_+ \underline{E}_s \\ \underline{\Gamma}_- &= -D_- \nabla n_- - \mu_- n_- \underline{E}_s \\ \underline{\Gamma}_e &= -D_e \nabla n_e - \mu_e n_e \underline{E}_s \end{aligned} \qquad (5.2.1)$$

where $\Gamma$ is the particle flux, D is the free diffusion coefficient, $\mu$ is the particle mobility, n is the particle density and $E_s$ is the radial electric field. The subscripts +, −, and e refer to positive ions, negative ions and electrons respectively. Eliminating $\underline{E}_s$, as in chapter 2, yields

$$\begin{aligned} \underline{\Gamma}_+ &= -D_{a+} \nabla n_+ \\ \underline{\Gamma}_- &= -D_{a-} \nabla n_- \\ \underline{\Gamma}_e &= -D_{ae} \nabla n_e \end{aligned} \qquad (5.2.2)$$

The ambipolar diffusion coefficients, $D_a$, are given

$$D_{a\mp} = D_{\mp}\left[\frac{(1\mp\gamma\mp2\alpha\gamma)(1\mp\alpha\mu_-/\mu_e)}{(1\mp\alpha\gamma)\{1\mp\mu_{\mp}(1\mp\alpha)/\mu_e \mp \alpha\mu_-/\mu_e\}}\right]$$

$$D_{a-} = D_{\mp}\left[\frac{\mu_-(1 \mp \gamma \mp 2\alpha\gamma)}{\gamma\mu_e\{1 \mp \mu_{\mp}(1\mp\alpha)/\mu_e \mp \alpha\mu_-/\mu_e\}}\right] \qquad (5.2.3)$$

$$D_{ae} = D_{\mp}\left[\frac{(1 \mp \gamma \mp 2\alpha\gamma)}{1 + \mu_{\mp}(1\mp\alpha)/\mu_e \mp \alpha\mu_-/\mu_e}\right] ,$$

where $\alpha = n_-/n_e$ and $\gamma$ is the ratio of electron to ion temperatures $(T_e/T_{\mp})$.

Calculations of these ambipolar diffusion coefficients and their variation with $\alpha$, have been performed for oxygen by Thompson (1959) ($\gamma \simeq 16$) and for a 5-15-80, $CO_2$-$N_2$-He mixture by Bletzinger et al (1975) ($\gamma \simeq 60$). The results of the latter authors are of relevance to $CO_2$ laser discharges and were previously shown in figure 2.2.2. This figure is reproduced as figure 5.2.1 for convenience. It may be divided into three regimes corresponding to low, moderate and high negative ion densities, for the purposes of discussion.

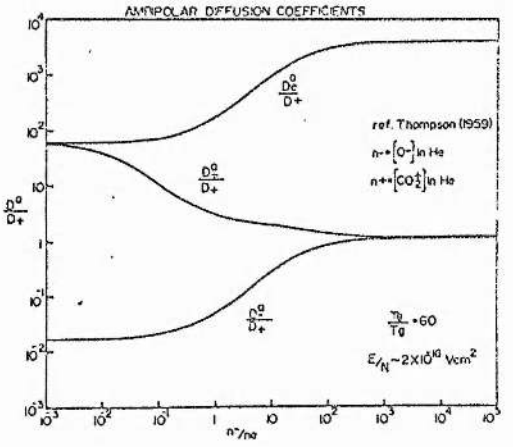


Figure 5.2.1 Variation of ambipolar diffusion coefficients with $n_-/n_e$ in a 5-10-85, $CO_2$-$N_2$-He gas mixture at 300K and 10 torr (as figure 2.2.2).

$\underline{\alpha < 10^{-1}}$ $(n_- << n_e)$

When the negative ion density is appreciably less than the electron density, the plasma may be considered to be approximately a positive ion-electron plasma. Thus $D_{a+} \simeq D_{ae}$, as figure 5.2.1 shows and as was discussed in section 2.2. The negative ion ambipolar diffusion coefficient, $D_{a-}$, is $\sim$ 3 orders of magnitude smaller than $D_{a+}$ and $D_{ae}$ and thus, not only is there a low density of negative ions but those present diffuse slowly to the walls. Thus the current of negative ions effusing through a sampling orifice will be much less than that for positive ions.

$\underline{10^{-1} < \alpha < 10^{2}}$ $(n_- \simeq n_e)$

Although the densities of positive and negative ions are approximately equal in this regime, the coefficient $D_{a-}$ is still $\sim$ 100 times smaller than the corresponding current of positive ions, and a highly sensitive mass-spectrometer system is required.

$\underline{\alpha > 10^{2}}$ $(n_- >> n_e)$

Such a plasma is effectively composed only of positive and negative ions and is typical of a highly electronegative gas (eg $SF_6$). The large electron ambipolar diffusion coefficient results in a high diffusive loss of electrons, so that those electrons not lost in the attachment process rapidly diffuse from discharge. Positive and negative ion effusion currents are approximately equal and mass-spectrometric analysis of negative ions from such a discharge should present no particular difficulties.

The formation of negative ions in a discharge in $CO_2$ gas occurs by the reaction

$$e + CO_2 \longrightarrow O^- + CO$$

The rate at which this dissociative attachment proceeds depends on the E/N of the discharge (see section 1.4). However, a considerable density of

electrons must be present in a $CO_2$ laser discharge since the excitation of the upper laser level is by electron collision (sections 1.1 and 1.3). Thus a value of $\alpha \simeq 1$ (ie $n_- \approx n_e$) may be reasonably assumed for a $CO_2$ laser discharge. The low ambipolar diffusion current of negative ions resulting from this value of $\alpha$ (from figure 5.2.1) makes mass-spectrometric negative ion determination in dc $CO_2$ laser discharges a difficult task.

Furthermore, due to the magnitude of the wall sheath potential and its retarding effect on negatively charged species (section 2.3) only relatively high energy negative ions will be able to escape from the plasma. The magnitude of the wall sheath potential computed for a typical $CO_2$-$N_2$-He gas mixture is $\sim$ 15 - 20V (equation 2.3.2). Thus only negative ions of $\gtrsim$ 15 eV energy will effuse from the discharge. For a Boltzmann distribution of ion energies, with an ion temperature approximately equal to the gas temperature the number of negative ions able to penetrate the sheath will be exceedingly small, resulting in an undetectable ion current for conventional techniques.

The considerations discussed above have virtually eliminated the possibility of direct determination of negative ion densities in dc plasmas. However other techniques have been developed which have enabled mass-spectrometric monitoring of negative ions under conditions similar to those of a dc gas discharge. These techniques have employed afterglow plasmas as the ion source.

An afterglow plasma may be created in two ways, corresponding to pulsed and dc conditions. First, the stationary afterglow is produced in the decay of a pulsed gas discharge. At the termination of the electric field which sustains the discharge, electrons rapidly diffuse from

the plasma by ambipolar diffusion, since $D_{ae} > D_{a+} > D_{a-}$ (figure 5.2.1). Thus as the electron density decreases the value of $\alpha$ increases, with a corresponding increase in $D_{a-}$ predicted by figure 5.2.1. Also, as the electron density decays, so too does the wall sheath since this is maintained by the equality of electron and positive ion currents to the wall. Thus a considerable enhancement of the negative ion effusion current is obtained. However this negative ion current will be decaying with time.

Fite and Rutherford (1964), Puckett et al (1971) and Smith and Plumb (1973) have employed the stationary afterglow technique to study negative ions in atmospheric gases, oxides of nitrogen and krypton-oxygen mixtures, respectively. Each group has observed a considerable enhancement of the negative ion signal (>100) as the electron density decays. In all cases results were reported for gas pressures < 1 torr.

The second technique for observation of negative ions is the flowing afterglow. In this case gas is flowed through a discharge and is observed as the plasma decays, immediately downstream of this discharge. When the gas is flowed continuously and a dc discharge is employed, the negative ion mass spectrum measured at a chosen time in the afterglow will be temporally constant. In the flowing afterglow the negative ions are sampled from a point sufficiently downstream from the discharge that electrons have decayed to a low density by ambipolar diffusion. Thus, $\alpha$ is large and a negative ion effusion current may be detected.

This technique has been applied to a mixture of $CO_2$-$N_2$-He in the proportions 13-15-72 by Prince and Garscadden (1975). This gas mixture is typical of that used in $CO_2$ lasers, but the experiment was performed at a pressure of 1 torr, which is considerably lower than is commonly used in $CO_2$ lasers. No other examples of the application of this technique

to gas discharge generated afterglows have been found in the literature, presumably due to the relatively fast gas flow velocities required to spatially separate the afterglow from the discharge.

Noticeably, all the abovementioned afterglow experiments have been restricted to pressures less than or approximately 1 torr. This is due to the increase in the time for ion diffusion from the afterglow plasma to the sampling orifice as pressure increases. The recombination of positive and negative ions occurs on a time scale of $\sim$ 1 ms for an ion density of $\sim 10^{10}$ $cm^{-3}$ and a two-body recombination coefficient of $10^{-7}$ $cm^3 s^{-1}$. Thus an ambipolar diffusion time of less than a millisecond is required for loss of ions by recombination to be relatively unimportant. This condition is more easily satisfied at low pressure ($p \lesssim 1$ torr) and limits the application of afterglow techniques in negative ion sampling.

More seriously, the afterglow technique necessarily depends on a very low electron density at the sampling point. Thus the plasma is not typical of a laser discharge where an appreciable electron density is essential. The resulting mass spectrum does not represent the negative ion equilibrium in a dc plasma since species initially created by electron attachment will have been converted to other species by ion-molecule reactions. If these ion-molecule reactions are well known, extrapolation to the conditions of a dc discharge may be possible.

Thus, although afterglow techniques may elucidate some of the negative ion plasma chemistry of $CO_2$ laser discharges, unambiguous determination of negative ion species in $CO_2$ laser discharges is not possible.

## 5.3 THEORETICAL PREDICTION OF NEGATIVE ION SPECIES

As discussed in the introduction to this thesis (section 1.6) the reasons for determining negative ion species densities in the $CO_2$ laser

discharge are threefold. First, the ratio of negative ion to electron density ($n_-/n_e$) at the onset of plasma instability in volume-dominated discharges requires comparison with theoretical prediction (section 1.5). Second, the rate of growth of negative ions in the plasma should be compared with the computed and observed onset times of instability (section 1.5). Finally, knowledge of the nature of the negative ions is essential to improve existing models of steady state discharges (section 1.4) and plasma instabilities (section 1.5) by characterising the ion-ion recombination and detachment processes.

In addition to the difficulties in measurement of negative ions discussed in the previous section, the mass-spectrometric approach is incapable of satisfying the first of the requirements mentioned above. In order to determine absolute negative ion densities by mass spectrometer, the sensitivity of the experimental system must be known. This requires knowledge of the transmission efficiency of sampling orifice, ion lenses, mass filter, etc and of the variation of ion effusion currents with discharge parameters. Chapters 2 and 3 have shown that such a calibration is normally not possible and mass-spectrometric results are usually expressed in relative, not absolute, units.

Recent measurements of rate coefficients for ion-electron recombination, ion-ion recombination, detachment and ion-molecule reactions for the gaseous constituents of air have enabled computer models of the earth's ionosphere to be constructed. Much of this data may be applied to the computation of negative ion densities in $CO_2$ laser discharges, where the same gaseous constituents are present, but in different concentrations. The rate coefficients for electron attachment to neutral particles may be obtained from published cross-section data (Rapp and Briglia (1965)) by averaging over the electron energy distribution appropriate to the discharge conditions, as outlined in chapter 1. Thus sufficient information exists,

as will be shown in this section, to form a system of time-dependent equations describing the variation of various negative ion species under $CO_2$ laser discharge conditions.

The feasibility of theoretically modelling ion densities in plasmas has been illustrated by several authors. For example, Niles (1970) has modelled discharges in air intended to simulate ionospheric conditions, computing temporal variation of positive and negative ions and neutral species; Mohnen (1971) has calculated densities of positive ions in the lower atmosphere but has encountered difficulties in the negative ion calculations due to lack of data on negative ion clustering with water molecules; Bastien et al (1975) have simulated the temporal evolution of negative ions in negative corona discharges in air and noted the influence of impurities.

The results of the above studies have been qualitatively verified experimentally by mass-spectrometric techniques. This has been possible since in the plasmas modelled the electron and gas temperatures are approximately equal. Equation (2.3.2) shows that when $T_e=T_g$ no wall sheath exists around a sampling probe in the plasma and no impediment to negative ion mass-spectrometry exists. Thus, ion densities may be confidently predicted in isothermal plasmas (electron temperature ≈ gas temperature), using available data.

Since the electron temperature is $\sim$ 50 times greater than the ion and gas temperatures in a typical $CO_2$ laser discharge, the confidence with which ion densities can be predicted depends on detailed knowledge of relevant electron processes. As discussed in section 1.4, the processes which depend on electron temperature are ionisation, attachment and, to a lesser degree, electron-ion recombination. However, sufficient cross-section data for these processes exists over the range of electron energies

appropriate to a $CO_2$ laser discharge to allow ion densities to be computed with some certainty. Nighan and Wiegand (1974) have computed attachment and ionisation rate coefficients for a variety of molecules in a 5-35-60, $CO_2$-$N_2$-He gas mixture over the range of electron temperature (and E/N) likely to be encountered in these discharges. A comprehensive discussion of electron-ion recombination exists due to Bardsley and Biondi (1970).

The necessary rate coefficients for the ion-molecule reactions occurring in the $CO_2$ laser discharge have been measured for application to the understanding of atmospheric phenomena and are well documented in the literature (eg the reviews of Ferguson (1969), Fite (1969) and Ferguson (1974)). Detachment of electrons from negative ions has also been studied for relevant species (reviewed by McDaniel et al (1970)). However, at present some controversy surrounds measurements of ion-ion recombination rates (Smith and Church (1976)). Nevertheless, adequate order-of-magnitude rate coefficients for two-body and three-body ion-ion recombination processes may be obtained from Olsen (1972), McGowan (1967) and Mahan and Person (1964).

Using information provided from sources such as those above, Wiegand and Nighan (1973) have computed the temporal evolution of negative ion species in a 5-35-60, $CO_2$-$N_2$-He gas mixture at 20 torr pressure and 10 mA $cm^{-2}$ current density over a period of $\sim$ 5 ms. This model predicts $CO_3^-$ as the dominant ion reaching a density of $\sim 10^{11}$ $cm^{-3}$, approximately an order of magnitude greater than the electron density.

A computer model of the temporal evolution of negative ion species, under $CO_2$ laser discharge conditions, has been developed along the same principles as that of Wiegand and Nighan (1973), but in greater detail. This model traces the time development of nine negative ion species

($O^-$, $O_2^-$, $NO^-$, $NO_2^-$, $NO_3^-$, $CO_3^-$, $CO_4^-$, $H^-$ and $OH^-$) and takes account of the possible presence of eleven impurity neutral particles (CO, O, $O_2$, $O_3$, $H_2$, $H_2O$, H, OH, $NO_2$, NO, $N_2O$) in addition to the major constituents of $CO_2$, $N_2$ and He. The formation of the negative ion species is described by the appropriate attachment reactions while ion loss occurs by detachment and ion-ion-recombination. Interchange of negative ion species is represented by ion-molecule reactions. (Full details of all reactions are given in chapter 6.) Thus a system of coupled, first-order, non-linear differential equations has been constructed to follow the development of the negative ions. (These equations are presented in an appendix to chapter 6.) This system has been solved using the Runge-Kutta iterative integration procedure (eg Fox (1962)) on an IBM 360/44 computer.

The model has been adapted to predict negative ion densities in two laser situations. Chapter 6 describes the application of the model to a sealed-off $CO_2$ TEA laser, while the negative ion densities in an EDCL are computed in chapter 7. Both these situations have the common feature that diffusive loss of charged particles occurs on a longer time scale than the duration of gas in the discharge, and thus may be neglected in comparison with other loss processes (see section 1.4).

Details of the constraints on the model, as applied to each situation, are given in the appropriate chapters. However a few general remarks are required at this stage.

Due to the low degree of fractional ionisation in a $CO_2$ laser discharge ($n_e/N \sim 10^{-7}$) the effects of impurity species on plasma kinetics may be considerable when only a few parts per million of these species are present (ie impurity density approximately equal to the electron density). Such impurities may be CO, O and $O_2$ formed in $CO_2$ dissociation (Smith and

Austin (1974)), oxides of nitrogen formed in the discharge (Tannen et al (1974)), or H, OH, $H_2$ and $H_2O$ due to residual water vapour. Also some species may be added in quantities of a few percent to perform a specific function. For example, $H_2$ or $H_2O$ addition, or CO addition, is known to improve the life of sealed-off systems (Witteman and Werner (1968), Smith and Browne (1974)).

The effects on contaminants and/or additives on the plasma chemistry are difficult to evaluate when several are present in the gas, as will be the case in a laser discharge. Using the computational approach it is possible to consider the individual role of each impurity species in a basic $CO_2$-$N_2$-He mixture, under typical discharge conditions. In this way the analysis of negative ion processes in a typical laser mixture where several minority species are present can be simplified. This approach has been adopted, to a large extent, in the analyses of chapters 6 and 7.

Lack of detailed information in two particular directions has imposed some limitation on the application of the model to laser discharges. Firstly, the rate coefficients of many ion-molecule reactions have only been measured at 300K. Rate coefficients which have been measured at higher temperatures suggest that little variation occurs over the range 300-600K. However the rate coefficients for detachment of electrons from negative ions is likely to be temperature sensitive, although little data is available (see section 1.5.2). This confines the model to laser discharges where there is little gas heating.

Second, many negative ions are known to form clusters with other molecules (water vapour, especially, forms clusters such as $CO_3^-.(H_2O)$, $NO_2^-.(H_2O)$, etc). Information on the loss processes and ion-molecule

reactions for such cluster species is insufficient to allow their inclusion in the model. Thus, where detailed measurements of reaction rates are unavailable, such clustered species are assumed not to be formed.

While the above considerations impose limits on the applicability of the negative ion model, computations may be confidently performed for two laser types. The TEA laser and the EDCL are treated in chapters 6 and 7 respectively, and computations of negative ion species densities are correlated with experimentally observed plasma instabilities.

## References


Bardsley J N and Biondi M A, 1970, in "Advances in Atomic and Molecular Physics", 6, (ed. D R Bates, Academic Press, New York).

Bastien F, Haug R and Lecuiller M, 1975, J Chimie Physique, 72, 105.

Bletzinger P, Laborde D A, Bailey W F, Long W H, Tannen P D and Garscadden A, 1975, IEEE J Quantum Electron, QE-11, 317.

Ferguson E E, 1969, Can J Chem, 47, 1815.

Ferguson E E, 1974, in "Chemical Kinetics Data Survey", ed D Garvin and R F Hampson, NTIS Report no.NBSIR 74-450.

Fite W L, 1969, Can J Chem, 47, 1797.

Fite W L and Rutherford J A, 1964, Discuss Faraday Soc, 37, 192.

Fox, L, 1962, "Numerical Solution of Ordinary and Partial Differential Equations" (Pergamon Press, Oxford).

Mahan B H and Person J C, 1964, J Chem Phys, 40, 392.

Mohnen V A, 1971, Pure and Appl Geoph, 84, 141.

McDaniel E W, Cermak V, Dalgarno A, Ferguson E E and Friedman L, 1970, "Ion-Molecule Reactions", (Wiley, New York).

McGowan S, 1967, Can J Phys, 45, 439.

Nighan W L and Wiegand W J, 1974, Phys Rev, A10, 922.

Niles F E, 1970, J Chem Phys, 52, 408.

Olsen R E, 1972, J Chem Phys, 56, 2979.

Prince J F and Garscadden A, 1975, Appl Phys Lett, 27, 13.

Puckett L J, Kregel M D and Teague M W, 1971, Phys Rev, A4, 1659.

Rapp D and Briglia D D, 1965, J Chem Phys, 43, 1480.

Smith A L S and Austin J M, 1974, J Phys D, 7, 314.

Smith A L S and Browne P G, 1974, J Phys D, 7, 1652.

Smith D and Church M J, 1976, Int J Mass Spectrom and Ion Phys, 19, 185.

Smith D and Plumb I C, 1973, J Phys D, 6, 1431.

Tannen P D, Bletzinger P and Garscadden A, 1974, IEEE J Quantum Electron, QE-10, 6.

Thompson J B, 1959, Proc Roy Soc, 73, 818.

Wiegand W J and Nighan W L, 1973, Appl Phys Lett, 22, 583.

Witteman W J and Werner H W, 1968, Phys Lett, 27A, 454.

# CHAPTER SIX

## NEGATIVE ION EFFECTS IN TEA $CO_2$ LASERS

(Reproduced from 'Journal of Physics D: Applied Physics', Vol 9, pp1587-1603)

J. Phys. D: Appl. Phys., Vol. 9, 1976. Printed in Great Britain. 

# Negative ion effects in TEA $CO_2$ lasers

H Shields, A L S Smith and B Norris
Department of Physics, University of St Andrews, St Andrews, Fife KY16 9SS

Received 23 February 1976

**Abstract.** Using sealed and flowing-gas TEA $CO_2$ lasers we have determined that long-life arc-free operation can be obtained in sealed $CO_2$–$N_2$–He–$O_2$–CO–$H_2$–$H_2O$ mixtures provided the $O_2$ concentration is less than ½–2%, depending on the particular laser, and the $H_2O$ concentration less than 1–3%.

With a computer model of 63 neutral and negative ion processes we have calculated that the negative ion population is significantly increased with these amounts of added $O_2$ and $H_2O$ and that $CO_4^-$ and $H^-$ respectively become large compared with $CO_3^-$ (the dominant ion in systems with little $O_2$ or $H_2O$). The beneficial effect of CO in suppressing negative ion formation is explained and the ratio of negative ions to electrons $N_n/N_e$ is determined to be between 0·05 and 1·0 for a wide range of gas mixtures used in trigger-wire and UV pre-ionized TEA lasers.

## 1. Introduction

In 1973 Nighan *et al* (1973) suggested that negative ions could play an important role in ionization instabilities in low-pressure gas dynamic lasers. Wiegand and Nighan (1973) computed that in a CW $CO_2$–$N_2$–He laser the dominant ion species should be $CO_3^-$ and its population could be greater than the electron concentration. Johns and Nation (1972), Douglas-Hamilton and Mani (1973, 1974) and Kovalev *et al* (1974) have suggested that similar processes are important in atmospheric-pressure plasmas. Several other authors (Stark *et al* 1975a, Dyer and James 1975, Smith *et al* 1975) have invoked such processes to explain their TEA laser results, but no one has reported any actual measurements of negative ions in TEA lasers or at atmospheric pressure.

Recently Prince and Garscadden (1975) have reported the detection of negative ions in the flowing afterglow of a CW discharge in a low-pressure (~1 Torr) $CO_2$–$N_2$–He mixture. Only relative concentration information is given, but they find not $CO_3^-$ as predicted, but $NO_2^-$ and $NO_3^-$ as the principle ions.

In this paper we seek to calculate the negative ion populations in a typical TEA laser and also at low pressures. The latter enables comparisons to be made with both the predictions of Wiegand and Nighan and the results of Prince and Garscadden. We use the negative ion model in conjunction with mass spectrometric results to show how both gaseous dissociation products of the $CO_2$–$N_2$–He mixture and additive gases can sufficiently change the discharge negative ion concentration balance in a typical sealed TEA laser so as to inhibit or permit the transition from diffuse to arc-like operation.

## 2. The model

### *2.1. Discharge*

The negative ions in the positive column of a glow discharge arise from the production of electrons by electron–molecule collisions and subsequent attachment reactions. The model describes the attachment, detachment and ion–molecule reactions occurring in an atmospheric-pressure discharge typical of either sealed or flowing pulsed $CO_2$ lasers. It also considers positive ion–negative ion recombination, the dissociation of neutral species by electron–molecule collisions and some molecule–molecule reactions.

The electrical excitation in the model is of the form of a square pulse of electrons of density $10^{13}$ cm$^{-3}$ for time $t=0$ to $t=300$ ns with a mean electron energy of 1 eV. This roughly corresponds to the situation in a pre-ionized parallel-plate-electrode transverse-discharge TEA laser with the discharge of 0·5 nF (at $\sim$25 kV) per cm$^2$ of electrode. It is assumed that the discharge reduced field $E/N$ is $\sim 2\times10^{-16}$ V cm$^2$ and does not vary with the gas mixture. For the low-pressure calculations (1–20 Torr) the electron density is $10^{10}$ cm$^{-3}$ for $t=0$ to $t\sim10$ ms, with the same discharge $E/N$ and mean energy. (This corresponds to a CW discharge of 10–15 mA cm$^{-2}$ in a $CO_2$–$N_2$–He mixture.) The gas temperature is assumed to be 300 K and unaltered by the discharge. This is a good approximation for a pre-ionized TEA laser, but would not be so for a TEA laser externally sustained for $\gtrsim1$ μs. At low pressures the gas will be significantly heated for $t\gtrsim10$ ms and this is one of the reasons for the computation being limited to the first 10 ms after switch-on (see also §§2.2 and 2.3 below).

### *2.2. Negative ions*

The initial negative ions are created either by two-body dissociative attachment reactions or by three-body attachment reactions. The most important of these are listed as reactions 1–11 in table 1: we have included those with the largest rate constants involving $CO_2$, CO, O, $O_2$, NO, $N_2O$, $NO_2$, $H_2$ and $H_2O$.

The negative ions undergo various ion–molecule reactions with the various neutral gaseous constituents, both two-body and three-body; these reactions are listed in table 2.

The loss of negative ions is assumed to be by homogeneous processes and no wall reactions are considered. This is a good approximation at atmospheric pressure and should be true at low pressures for $t<10$ ms, provided the discharge tube is of a reasonable diameter ($\gtrsim1$ cm). The homogeneous loss processes considered are the detachment reactions listed in table 1 and two- and three-body positive-ion–negative-ion recombination. Exact values for many of these recombination reactions are not available, but since all the known two-body rates are similar we assume a mean value of the recombination coefficient $k_{2R}=2\times10^{-7}$ cm$^3$ s$^{-1}$ and likewise for the three-body processes $k_{3R}=10^{-25}$ cm$^6$ s$^{-1}$ (Olsen 1972, McGowan 1967, Mahan and Person 1964).

### *2.3. Molecular dissociation and neutral reactions*

In a $CO_2$–$N_2$–He mixture the $CO_2$ is dissociated by the dissociative attachment reaction 1, but this rate is small compared with the electron–molecule neutral reaction

$$e+CO_2 \xrightarrow{k_{20}} e+O+CO.$$

**Table 1.** Electron attachment and detachment; neutral dissociation and recombination processes

| No. | Reaction | Rate constant (300 K) | Reference |
|---|---|---|---|
| Dissociative attachment: | | | |
| 1. | $e+CO_2 \rightarrow CO+O^-$ | $5\times10^{-13}$ cm$^3$ s$^{-1}$† | Nighan and Wiegand (1974) |
| 2. | $e+CO \rightarrow C+O^-$ | $3\times10^{-14}$ cm$^3$ s$^{-1}$ | Nighan and Wiegand (1974) |
| 3. | $e+O_2 \rightarrow O+O^-$ | $3\times10^{-12}$ cm$^3$ s$^{-1}$ | Nighan and Wiegand (1974) |
| 4. | $e+N_2O \rightarrow N_2+O^-$ | $2\times10^{-10}$ cm$^3$ s$^{-1}$ | Nighan and Wiegand (1974) |
| 5. | $e+NO \rightarrow N+O^-$ | $1\times10^{-12}$ cm$^3$ s$^{-1}$ | Nighan and Wiegand (1974) |
| 6. | $e+NO_2 \rightarrow NO+O^-$ | $1\times10^{-11}$ cm$^3$ s$^{-1}$ | Nighan and Wiegand (1974) |
| 7. | $e+H_2O \rightarrow H^-+OH$ | $5\times10^{-12}$ | Nighan and Wiegand (1974) |
| 8. | $e+H_2 \rightarrow H^-+H$ | $1\times10^{-13}$ | Rapp and Briglia (1965) |
| Three-body attachment: | | | |
| 9. | $e+O_2+M \rightarrow O_2^-+M$ | $2\times10^{-30}$ cm$^6$ s$^{-1}$ (M=$O_2$) | Phelps (1969) |
| | | $1\times10^{-31}$ cm$^6$ s$^{-1}$ (M=$N_2$) | Phelps (1969) |
| | | $3\times10^{-30}$ cm$^6$ s$^{-1}$ (M=$CO_2$) | Phelps (1969) |
| | | $2\times10^{-30}$ cm$^6$ s$^{-1}$ (M=He) | Chanin *et al* (1962) |
| 10. | $e+O+M \rightarrow O^-+M$ | $1\times10^{-31}$ cm$^6$ s$^{-1}$ (M=$O_2$) | Bastien *et al* (1975) |
| | | $1\times10^{-31}$ cm$^6$ s$^{-1}$ (M=$N_2$) | Bastien *et al* (1975) |
| 11. | $e+NO_2+M \rightarrow NO_2^-+M$ | $2\times10^{-11}$ cm$^3$ s$^{-1}$ (M=He) | Mahan and Walker (1967b)‡ |
| | | $4\times10^{-11}$ cm$^3$ s$^{-1}$ (M=$N_2$) | Mahan and Walker (1967b)‡ |
| Associative detachment: | | | |
| 12. | $O^-+CO \rightarrow CO_2+e$ | $7\times10^{-10}$ cm$^3$ s$^{-1}$ | McFarland *et al* (1973) Moruzzi and Phelps (1966) |
| 13. | $O^-+O \rightarrow O_2+e$ | $2\times10^{-10}$ cm$^3$ s$^{-1}$ | Niles (1970), Melton (1970) |
| 14. | $O^-+O_2(^1\Delta_g) \rightarrow O_3+e$ | $1\times10^{-10}$ cm$^3$ s$^{-1}$ | Niles (1970) |
| 15. | $O^-+NO \rightarrow NO_2+3$ | $2\times10^{-10}$ cm$^3$ s$^{-1}$ | McFarland *et al* (1973) Niles (1970) |
| 16. | $O^-+H_2 \rightarrow H_2O+e$ | $8\times10^{-10}$ cm$^3$ s$^{-1}$ | Phelps (1969) |
| 17. | $CO_3^-+CO \rightarrow 2CO_2+e$ | $5\times10^{-13}$ cm$^3$ s$^{-1}$ | D A Price and J L Moruzzi (1974 private communication) |
| 18. | $O_2^-+O \rightarrow O_3+e$ | $3\times10^{-10}$ cm$^3$ s$^{-1}$ | Niles (1970), Melton (1970) |
| 19. | $O_2^-+O_2(^1\Delta_g) \rightarrow 2O_2+e$ | $2\times10^{-10}$ cm$^3$ s$^{-1}$ | Fehsenfeld *et al* (1966) |
| 20. | $O_2^-+H \rightarrow HO_2+e$ | $1\times10^{-9}$ cm$^3$ s$^{-1}$ | Fehsenfeld (1975) |
| 21. | $H^-+H \rightarrow H_2+e$ | $1\times10^{-9}$ cm$^3$ s$^{-1}$ | McDaniel *et al* (1970) |
| 22. | $H^-+O_2 \rightarrow HO_2+e$ | $1\times10^{-9}$ cm$^3$ s$^{-1}$ | McDaniel *et al* (1970) |
| 23. | $OH^-+O \rightarrow HO_2+e$ | $2\times10^{-10}$ cm$^3$ s$^{-1}$ | Melton (1970) |
| 24. | $OH^-+H \rightarrow H_2O+e$ | $1\times10^{-9}$ cm$^3$ s$^{-1}$ | Melton (1970) |
| Collisional detachment: | | | |
| 25. | $NO^-+M \rightarrow NO+M+e$ | $5\times10^{-10}$ cm$^3$ s$^{-1}$ | Bastien *et al* (1975) |
| Neutral dissociation: | | | |
| 26. | $e+CO_2 \rightarrow CO+O+e$ | $1\times10^{-9}$ cm$^3$ s$^{-1}$ | Smith and Austin (1974) |
| 27. | $e+O_2 \rightarrow O+O+e$ | $1\times10^{-9}$ cm$^3$ s$^{-1}$ | see text |
| 28. | $e+H_2 \rightarrow H+H+e$ | $4\times10^{-9}$ cm$^3$ s$^{-1}$ | see text |
| 29 | $e+H_2O \rightarrow H+OH+e$ | $2\times10^{-9}$ cm$^3$ s$^{-1}$ | see text |
| Neutral recombination: | | | |
| 30. | $O+CO+M \rightarrow CO_2+M$ | $2\times10^{-36}$ cm$^6$ s$^{-1}$ | Stuhl and Niki (1971) |
| 31. | $O+O+M \rightarrow O_2+M$ | $3\times10^{-33}$ cm$^6$ s$^{-1}$ | Niles (1970) |
| 32. | $O+O_2+M \rightarrow O_3+M$ | $5\times10^{-34}$ cm$^6$ s$^{-1}$ | Niles (1970) |
| 33. | $O+O_3 \rightarrow O_2+O_2$ | $9\times10^{-15}$ cm$^3$ s$^{-1}$ | Niles (1970) |

† For a mean electron energy of 1 eV.
‡ This is a saturated three-body reaction, hence the rate constant is in units of cm$^3$ s$^{-1}$.

**Table 2.** Negative-ion–molecule reactions

| No. | Reaction | Rate constant (300 K) | Reference |
|---|---|---|---|
| Two-body processes: | | | |
| 34. | $O^- + O_2(^1\Delta_g) \rightarrow O_2^- + O$ | $1 \times 10^{-9}$ cm$^3$ s$^{-1}$ | Niles (1970) |
| 35. | $O^- + NO_2 \rightarrow NO_2^- + O$ | $1 \times 10^{-9}$ cm$^3$ s$^{-1}$ | Niles (1970), Melton (1970) |
| 36. | $O^- + NO_2 \rightarrow O_2^- + NO$ | $1 \times 10^{-10}$ cm$^3$ s$^{-1}$ | McDaniel *et al* (1970) |
| 37. | $O^- + N_2O \rightarrow NO^- + NO$ | $2 \times 10^{-10}$ cm$^3$ s$^{-1}$ | Melton (1970) Bastien *et al* (1975) |
| 38. | $O^- + H_2 \rightarrow OH^- + H$ | $3 \times 10^{-11}$ cm$^3$ s$^{-1}$ | McFarland *et al* (1973) |
| 39. | $O_2^- + O \rightarrow O_2 + O^-$ | $1 \times 10^{-11}$ cm$^3$ s$^{-1}$ | Niles (1970) |
| 40. | $O_2^- + O_3 \rightarrow O_2 + O_3^-$ | $4 \times 10^{-10}$ cm$^3$ s$^{-1}$ | Niles (1970), Melton (1970) |
| | | $3 \times 10^{-10}$ cm$^3$ s$^{-1}$ | Fehsenfeld and Ferguson (1974) |
| 41. | $O_2^- + NO_2 \rightarrow O_2 + NO_2^-$ | $2 \times 10^{-9}$ cm$^3$ s$^{-1}$ | Niles (1970) |
| 42. | $O_2^- + H \rightarrow H^- + O_2$ | $2 \times 10^{-9}$ cm$^3$ s$^{-1}$ | Fehsenfeld (1975) |
| 43. | $CO_3^- + O \rightarrow O_2^- + CO_2$ | $8 \times 10^{-11}$ cm$^3$ s$^{-1}$ | Niles (1970), Melton (1970) |
| 44. | $CO_3^- + NO \rightarrow CO_2 + NO_2^-$ | $9 \times 10^{-12}$ cm$^3$ s$^{-1}$ | Niles (1970), Melton (1970) |
| 45. | $CO_3^- + NO_2 \rightarrow CO_2 + NO_3^-$ | $1 \times 10^{-10}$ cm$^3$ s$^{-1}$ | Niles (1970), Fehsenfeld and Ferguson (1974) |
| 46. | $CO_3^- + H \rightarrow OH^- + CO_2$ | $2 \times 10^{-10}$ cm$^3$ s$^{-1}$ | Fehsenfeld (1975) |
| 47. | $CO_4^- + O \rightarrow CO_3^- + O_2$ | $2 \times 10^{-10}$ cm$^3$ s$^{-1}$ | McDaniel *et al* (1970) |
| 48. | $CO_4^- + NO \rightarrow (NO_3^-)^* + CO_2$ | $5 \times 10^{-11}$ cm$^3$ s$^{-1}$ | McDaniel *et al* (1970) † |
| 49. | $CO_4^- + O_3 \rightarrow O_3^- + CO_2 + O_2$ | $1 \times 10^{-10}$ cm$^3$ s$^{-1}$ | Bastien *et al* (1975), Fehsenfeld and Ferguson (1974) |
| 50. | $CO_4^- + H \rightarrow CO_3^- + OH$ | $2 \times 10^{-10}$ cm$^3$ s$^{-1}$ | Fehsenfeld (1975) |
| 51. | $H^- + NO_2 \rightarrow NO_2^- + H$ | $3 \times 10^{-9}$ cm$^3$ s$^{-1}$ | Venugopalan (1971) |
| 52. | $OH^- + NO_2 \rightarrow NO_2^- + OH$ | $1 \times 10^{-9}$ cm$^3$ s$^{-1}$ | Melton (1970) |
| 53. | $NO^- + O_3 \rightarrow O_2^- + NO$ | $9 \times 10^{-10}$ cm$^3$ s$^{-1}$ | Fehsenfeld *et al* (1966) |
| 54. | $NO_2^- + NO_3 \rightarrow NO_3^- + NO$ | $4 \times 10^{-12}$ cm$^3$ s$^{-1}$ | Bastien *et al* (1975) |
| 55. | $NO_3^- + H \rightarrow OH^- + NO$ | $4 \times 10^{-10}$ cm$^3$ s$^{-1}$ | Fehsenfeld (1975) |
| 56. | $(NO_3^-)^* + H \rightarrow NO_2^- + OH$ | $7 \times 10^{-10}$ cm$^3$ s$^{-1}$ | Fehsenfeld (1975)† |
| 57. | $(NO_3^-)^* + NO \rightarrow NO_2^- + NO_2$ | $2 \times 10^{-11}$ cm$^3$ s$^{-1}$ | Adams *et al* (1970)† |
| Three-body processes: | | | |
| 58. | $O^- + CO_2 + M \rightarrow CO_3^- + M$ | $9 \times 10^{-29}$ cm$^6$ s$^{-1}$ (M = $CO_2$) | Moruzzi and Phelps (1966) |
| | | $2 \times 10^{-28}$ cm$^6$ s$^{-1}$ (M = He) | Fehsenfeld and Ferguson (1974) |
| | | $3 \times 10^{-28}$ cm$^6$ s$^{-1}$ (M = $O_2$) | Fehsenfeld and Ferguson (1974) |
| 59. | $O^- + NO + M \rightarrow NO_2^- + M$ | $1 \times 10^{-29}$ cm$^6$ s$^{-1}$ | Bastien *et al* (1975) |
| 60. | $O_2^- + CO_2 + M \rightarrow CO_4^- + M$ | $1 \times 10^{-29}$ cm$^6$ s$^{-1}$ (M = $CO_2$) | Melton (1970) |
| | | $1 \times 10^{-29}$ cm$^6$ s$^{-1}$ (M = $O_2$) | Melton (1970) |
| | | $5 \times 10^{-29}$ cm$^6$ s$^{-1}$ (M = $O_2$) | Fehsenfeld and Ferguson (1974) |
| 61. | $CO_3^- + H_2O + M \rightarrow CO_3^-(H_2O) + M$ | $1 \times 10^{-28}$ cm$^6$ s$^{-1}$ (M = $O_2$) | Fehsenfeld and Ferguson (1974) |
| 62. | $O_2^- + H_2O + M \rightarrow O_2^-(H_2O) + M$ | $2 \times 10^{-28}$ cm$^6$ s$^{-1}$ (M = $O_2$) | Fehsenfeld and Ferguson (1974) |
| 63. | $NO_2^- + H_2O + M \rightarrow NO_2^-(H_2O) + M$ | $1 \times 10^{-28}$ cm$^6$ s$^{-1}$ (M = $O_2$) | Niles (1970) |
| | | $1 \times 10^{-28}$ cm$^6$ s$^{-1}$ (M = $N_2$) | Niles (1970) |

† Some $NO_3^-$ is produced in a reactive form (Fehsenfeld 1975). This occurs when $O_2^-$ is transferred to NO, but not when $O^-$ is transferred to $NO_2$. We have indicated this reactive form by $(NO_3^-)^*$.

The dissociation coefficient $\alpha/P$ for this reaction has been measured by Smith and Austin (1974) for typical laser mixtures; its value varies with the discharge $E/N$. The rate constant $k$ can be obtained from the dissociation coefficient from the relation

$$(\alpha/P)_{E/N}=\frac{3{\cdot}6\times10^{16}}{v_d}(k)_{E/N}$$

where $v_d$ is the electron drift velocity (assumed to be $5\times10^6$ cm s$^{-1}$ for $E/N=2\times10^{-16}$ V cm$^2$, Lowke *et al* 1973). $\alpha/P$ is in units of electron$^{-1}$ cm$^{-1}$ Torr$^{-1}$, and $k$ is in units of cm$^3$ s$^{-1}$. The value obtained for $k_{26}$ is $1\times10^{-9}$ cm$^3$ s$^{-1}$, which is only $\sim0{\cdot}2\%$ dissociation per TEA discharge pulse, so we assume in the model the $CO_2$ population is constant over any one discharge pulse. At low pressures this approximation is also valid for discharge periods $<10$ ms.

No reliable data is available for the dissociation rate of $N_2$, CO, $O_2$, $H_2O$ or $H_2$ in a typical $CO_2$–$N_2$–He mixture. Since $N_2$ and CO are certainly dissociated at a considerably slower rate than $CO_2$ in a typical glow discharge we assume that they are undissociated and hence that any oxides of nitrogen in the model have to be added as empirical constants. The dissociation rate of oxygen is very similar to that of $CO_2$ (based on the 'pure' gas results of Smith and Austin 1976), and the dissociation rate of hydrogen is about four times as great (based on the 'pure' gas results of Corrigan and von Engel 1958). We assume the dissociation rate of $H_2O$ to be twice as great as that of $CO_2$ (unpublished). These dissociation processes are tabulated in table 1.

On the time scale of the TEA laser discharge pulse, neutral–neutral reactions will be unimportant, but over the longer period of some of the low-pressure discharges they become significant. We have included in the model four atomic oxygen homogeneous neutral loss mechanisms; these are listed in table 1.

### *2.4. Computation procedure*

Equations expressing the time development of five neutral species (CO, O, $O_2$, $O_3$, H) and nine negative ion species ($O^-$, $O_2^-$, $NO^-$, $NO_2^-$, $NO_3^-$, $CO_3^-$, $CO_4^-$, $H^-$, $OH^-$) during the discharge have been solved iteratively using the Runge-Kutta technique with an IBM 360/44 computer. The full equations are listed in the Appendix. The time development of the other neutral species is not considered because their populations are considered constant (see §2.3 above).

Because the reactions of hydrated cluster ions such as $CO_3^-(H_2O)$ are not known in any detail we have assumed that reactions of the type 61, 62 and 63 do not occur. Thus where $CO_3^-$ and $O_2^-$ etc are referred to it must be taken that they may be present in a hydrated form. The results will need to be modified if the reaction rates of the hydrates are significantly different from those of the parent ions.

## 3. Negative ion predictions

### *3.1. The flowing-gas* TEA *model predictions*

We first consider the TEA laser situation where the gas in the laser is completely replaced between discharge pulses and there is no accumulation of dissociation products over several pulses. Figure 1 shows the computed development of the main negative ion concentrations with time during and immediately subsequent to the discharge pulse in a

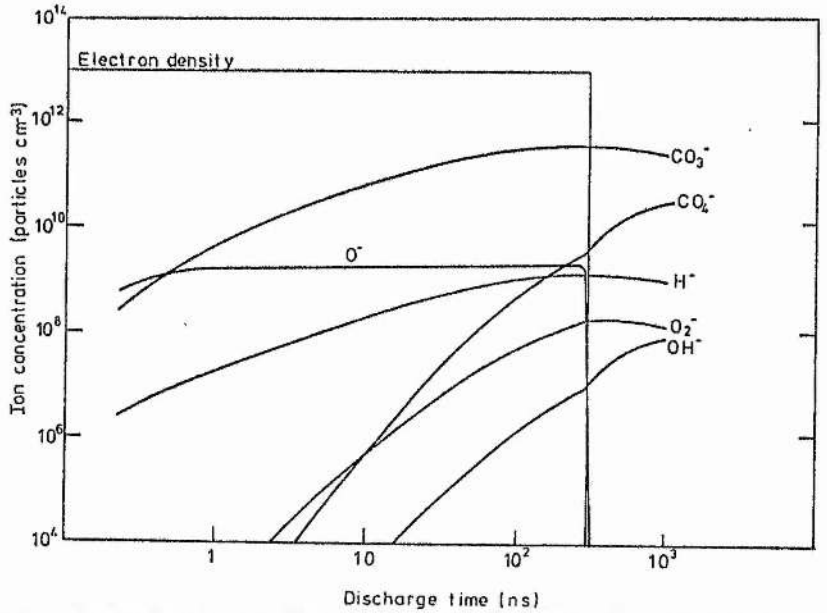


**Figure 1.** Variation with time of the main negative ions species with a 300 ns discharge in a flowing gas 10–10–80 $CO_2$–$N_2$–He atmospheric-pressure mixture.

10–10–80, $CO_2$–$N_2$–He atmospheric pressure mixture. The chief peak is $CO_3^-$, other peaks being $CO_4^-$, $O^-$, $O_2^-$, $H^-$ and $OH^-$. The $H^-$ and $OH^-$ arise because in all computed mixtures we assume an impurity level of 30 ppm of water vapour. The $O^-$ is mainly formed by dissociative attachment of $CO_2$ (reaction 1), but it rapidly reacts with $CO_2$ in the three-body reaction 58 to form $CO_3^-$ and thence $O_2^-$ and $CO_4^-$ by reactions 43 and 60. The $H^-$ is mainly formed by dissociative attachment of $H_2O$ (reaction 7) and the $OH^-$ is formed in reactions 38 and 46. It should be noted that the $CO_3^-$ reaches an approximate equilibrium value after about 100 ns with a population of about $5 \times 10^{11}$ ions cm$^{-3}$, giving a negative ion to electron ratio $N_n/N_e$ of $\sim 0{\cdot}05$. This equilibrium is caused by the loss of negative ions by three-body recombination with positive ions, which at this pressure is faster than both two-body recombination and detachment. In the afterglow the total negative ion population decays by both recombination and detachment, but individual peaks may continue to increase in magnitude for a time because ion–molecule processes produce these species faster than the corresponding ion loss processes remove them.

If a substantial amount of molecular oxygen is added to the $CO_2$–$N_2$–He mixture reaction 9 becomes significant in directly creating $O_2^-$ by three-body attachment. Thus in figure 2 with 10% $O_2$ added to the 10–10–80 mixture $O_2^-$ is the dominant peak, but later in the pulse $CO_4^-$ is dominant, being formed by reaction 60. The total negative ion population is also increased such that after about 50 ns it is constant with $N_n/N_e \sim 1$. Figure 3 is a plot of the concentrations of $CO_3^-$, $CO_4^-$ and $O_2^-$ after 100 ns for varying amounts of added oxygen. Results are plotted for three basic $CO_2$–$N_2$–He mixtures, 10–10–80 and 20–20–60 which are typical of those used in non-pre-ionized and trigger-wire pre-ionized devices and 60–20–20 which is typical of those used in UV pre-ionized devices. Clearly the $CO_4^-$ becomes dominant and the total negative ion population is

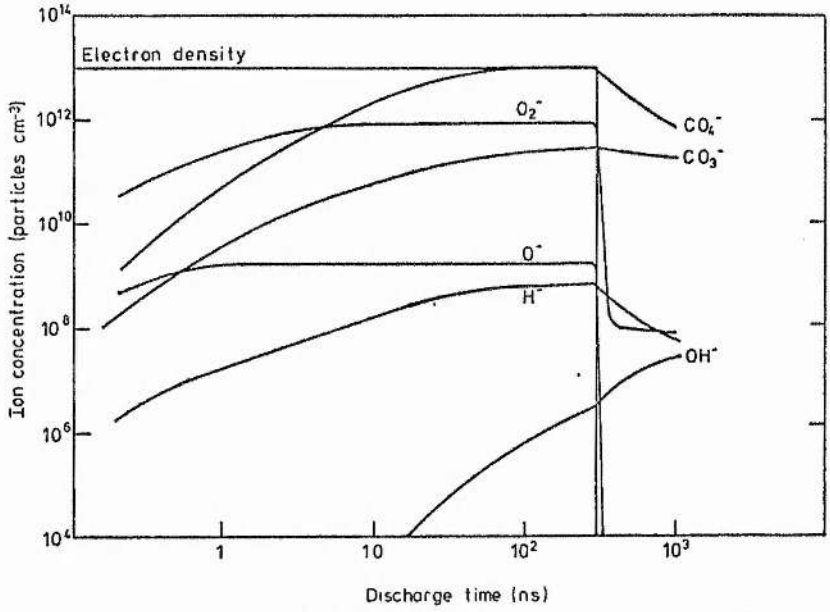


**Figure 2.** Variation with time of the main negative ion species with a 300 ns discharge in a flowing gas 10–10–80 $CO_2$–$N_2$–He atmospheric-pressure mixture with 10% added $O_2$.

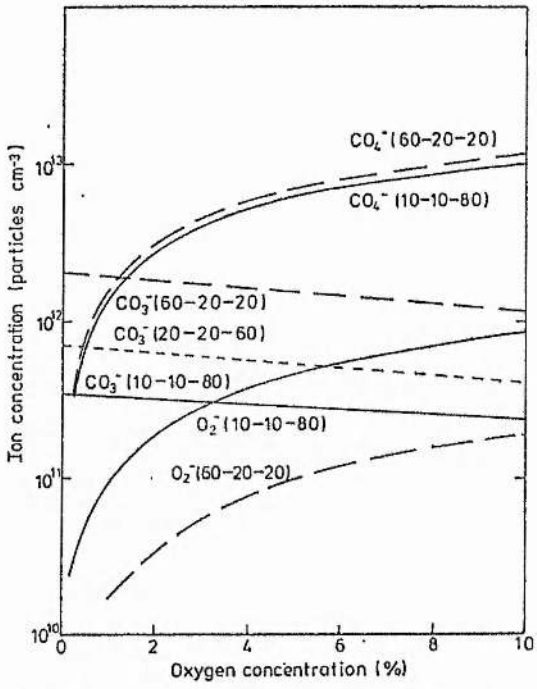


**Figure 3.** Variation with amount of added $O_2$ of the main negative ion species at $t$= 100 ns in atmospheric pressure discharges in three $CO_2$–$N_2$–He mixtures.

significantly increased with between ¼ and 2% of added $O_2$ depending on the original gas mixture.

The effect of the addition of CO to the $CO_2$–$N_2$–He mixture is insignificant (but see §3.2 below) and likewise the addition of hydrogen (in quantities up to 10%) does not significantly affect the dominant $CO_3^-$ ion, but the secondary peaks $H^-$ and $OH^-$ are increased. But the addition of $H_2O$ produces $H^-$ as the dominant ion (reaction 7); thus figure 4 shows that the total negative ion population is significantly increased and $H^-$ can become dominant when 1 to 5% of $H_2O$ is added, the percentage depending on the particular $CO_2$–$N_2$–He mixture.

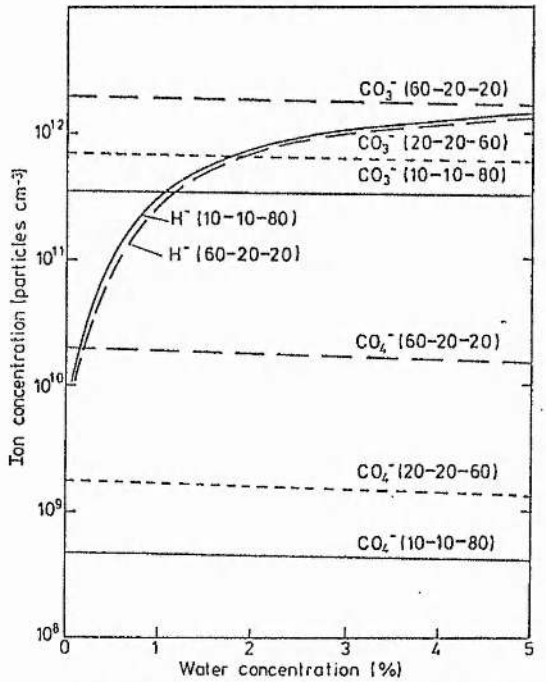


**Figure 4.** Variation with amount of added $H_2O$ of the main negative ion species at $t = 100$ ns in atmospheric pressure discharges in three $CO_2$–$N_2$–He mixtures.

Above we have mentioned briefly some of the most important reactions, there are more completely summarized in figure 5, which is a reaction path chart for the various negative ion processes excluding recombination. The thicker lines indicate the more important paths. The dotted line linking $O^-$ and $O_3^-$ is important in the atmosphere, but not in our system. The closed loop

$$CO_3^- \xrightarrow{(O)} O_2^- \xrightarrow{(M+CO)} CO_4^- \xrightarrow{(O \text{ or } H)} CO_3^-$$

is very significant both during the discharge pulse and in the afterglow.

### *3.2. The effect of carbon monoxide*

We have previously (Smith *et al* 1975) roughly calculated that the direct effect of carbon monoxide on the negative ion population in a TEA laser is only significant if a large

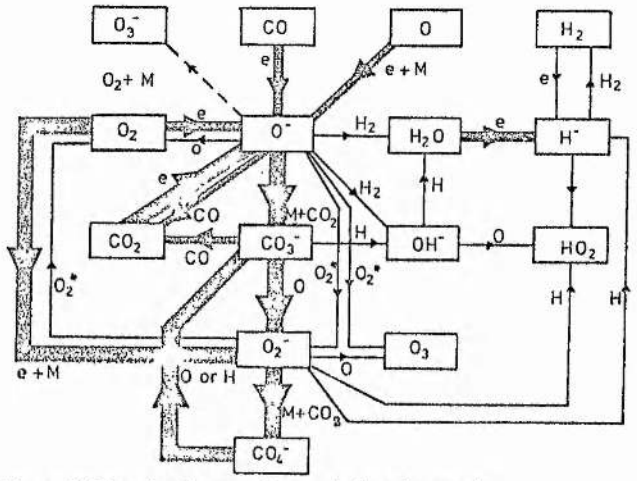


**Figure 5.** Negative ion reaction path chart (see text).

amount (~20%) is added to the $CO_2$–$N_2$–He. But Stark *et al* (1975a) have suggested that the effect on a TEA laser is considerable and Nighan *et al* (1973) have shown that at low pressures electron detachment by CO controls the $N_n/N_e$ ratio. In figure 6 we show the computed effect of the addition of CO on the dominant $CO_3^-$ ion in the 10–10–80

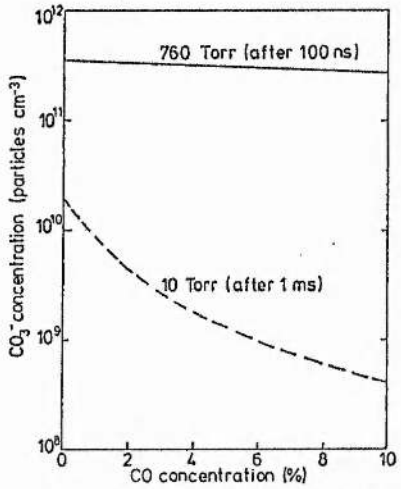


**Figure 6.** Effect of the addition of CO on the $CO_3^-$ in atmospheric-pressure ($N_e$= $10^{13}$ cm$^{-3}$) and low-pressure ($N_e = 10^{10}$ cm$^{-3}$) discharges in 10–10–80 $CO_2$–$N_2$–He.

mixture for the TEA laser ($10^{13}$ electrons cm$^{-3}$, after 100 ns) and at 10 Torr ($10^{10}$ electrons cm$^{-3}$, after 1 ms). The effect of even 10% added CO is small in the TEA case, but at 10 Torr the $CO_3^-$ is reduced by a factor of about 50. This difference can be understood by reference to the $CO_3^- \rightarrow O_2^- \rightarrow CO_4^- \rightarrow CO_3^-$ rapid cycle in figure 5. At low pressures the dominant reaction of $O^-$ is the detachment with CO to form neutral $CO_2$ (reaction 12)

$$O^- + CO \rightarrow CO_2 + e$$

but at the much higher pressure of the TEA laser the three-body reaction 58

$$O^- + CO_2 + M \rightarrow CO_3^- + M$$

becomes faster and the ion population is recycled.

It should also be noted that at 10 Torr when little CO is present $N_n/N_e > 1$.

### *3.3. The effects of oxides of nitrogen*

The computer programme includes numerous reactions involving the oxides of nitrogen (see tables 1 and 2), but these have not led to any negative ions in §§3.1 and 3.2 above because as mentioned earlier the oxides of nitrogen have to be added as empirically determined amounts. We have experimentally determined that there is less than 25 ppm of NO and $NO_2$ and less than 75 ppm of $N_2O$ in a flowing or sealed TEA laser. With these maximum amounts of the oxides of nitrogen, $NO_2^-$ and $NO_3^-$ peaks are produced but they are small compared with the principal negative ion peaks.

At low pressures (1–8 Torr) Tannen *et al* (1974) have used mass spectrometry to measure the concentrations of NO, $NO_2$ and $N_2O$. Extrapolation from their results would suggest about 1000 ppm NO and $NO_2$, and 300 ppm $N_2O$ in a $CO_2$–$N_2$–He mixture at 1 Torr with a discharge dwell time of ~60 ms. Prince and Garscadden (1975) have measured the negative ions in a flowing afterglow system (dwell time 62 ms) in an initial mixture of 12·7% $CO_2$, 15·5% $N_2$, 71·8% He. We have computed the negative ions in this mixture, assuming the $CO_2$ is dissociated by a discharge of 60 ms. The results of this computation are given in figure 7, together with Prince and Garscadden's results corresponding to $10^{10}$ electron $cm^{-3}$: since Prince and Garscadden's results are only relative we have normalized their $O^-$ peak to our $O^-$ peak. Our model

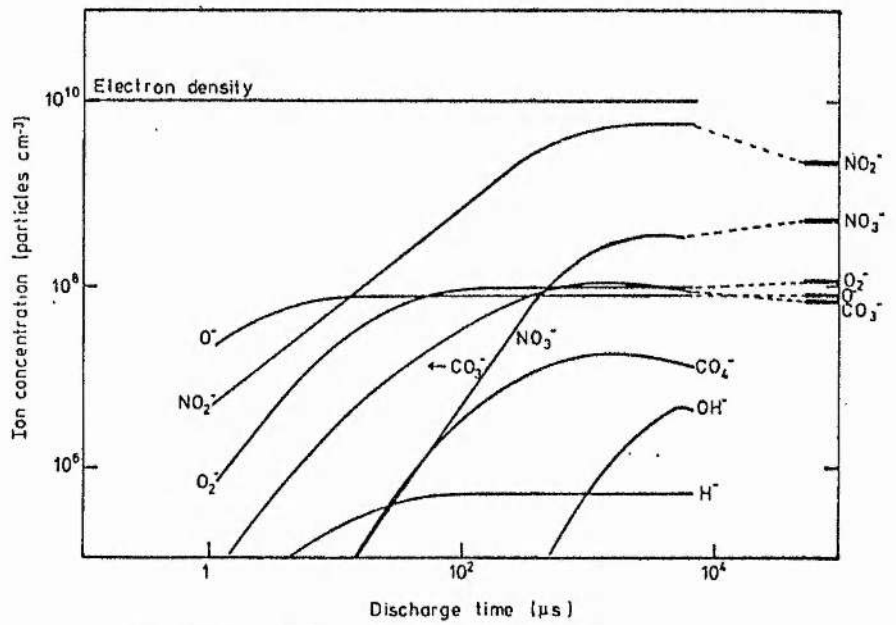


Figure 7. Variation with time of the main negative ion species with a discharge at 1 Torr in a gas mixture similar to that of Prince and Garscadden (1975). Prince and Garscadden's experimental peaks (after 60 ms) are shown on the right of the figure (normalized to $O^-$).

predicts the largest peak to be $NO_2^-$ followed by $NO_3^-$ and then $CO_3^-$, $O_2^-$ and $O^-$ close together, whereas Prince and Garscadden measure $NO_2^-$ to be the largest peak, followed by $NO_3^-$ and then likewise $O_2^-$, $O^-$ and $CO_3^-$ close together. Given the approximation involved in determining the concentration of the neutral oxides of nitrogen and the extent of knowledge of ion–molecule processes this agreement seems very satisfactory and gives some confidence that the high-pressure predictions are acceptably accurate.

## 4. Comparison with experimental TEA laser results

### *4.1. Experimental system*

The experimental results have been obtained with a Pearson and Lamberton (1972) trigger-wire TEA laser similar to that described by Stark *et al* (1975a). This is constructed with a glass envelope and metal vacuum seals so that it can be operated for long periods of time without any significant surface outgassing or gas leakage; our version can either be operated sealed-off or with a flowing gas mixture. The main discharge is between two 20 cm by 1 cm Rogowski profile electrodes separated by 1 cm. The composition of either flowing or sealed-off mixtures could be measured with an AEI MS10 mass spectrometer and gas flow rates measured with calibrated flow meters.

### *4.2. Dissociation equilibrium in a sealed* TEA *laser*

The sealed laser with a static mixture of 20–20–60 $CO_2$–$N_2$–He was pulsed at a rate of about 2 pps with the main 12 nF capacitor charged to 25 kV. A uniform discharge was obtained and after 1000 pulses, the dissociation within the vacuum envelope was measured to be about 6½% (i.e. ~0·0065% per discharge pulse over all the gas). The laser was refilled and pulsed for 8000 shots and the dissociation measured to be 28%. This was repeated for several other sets of pulses and the results are plotted in figure 8. Diffuse discharges were obtained on all occasions up to 5000 pulses, after which the discharge occasionally became erratic and arced: on these occasions the tube was refilled and the

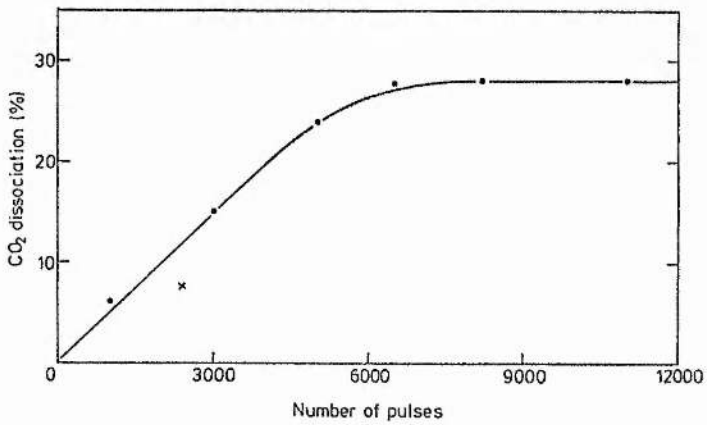


**Figure 8.** Variation of the dissociation of $CO_2$ in a 20–20–60 $CO_2$–$N_2$–He mixture with number of discharge pulses in a sealed TEA laser.

pulsing repeated. From figure 8 it is clear that the tube reaches a dissociation equilibrium with about 28% dissociation after 6000–7000 pulses.

We investigated the effect of the addition of CO on this dissociation equilibrium by adding varying amounts of CO to the original 20–20–60 mixture and determining the dissociation after 8200 discharge pulses for each gas mixture. The results are presented in figure 9: the dissociation equilibrium falls to 10% with 5% added CO and 3% with 10% added CO. We will explain the neutral dissociation equilibrium and its variation with added CO elsewhere.

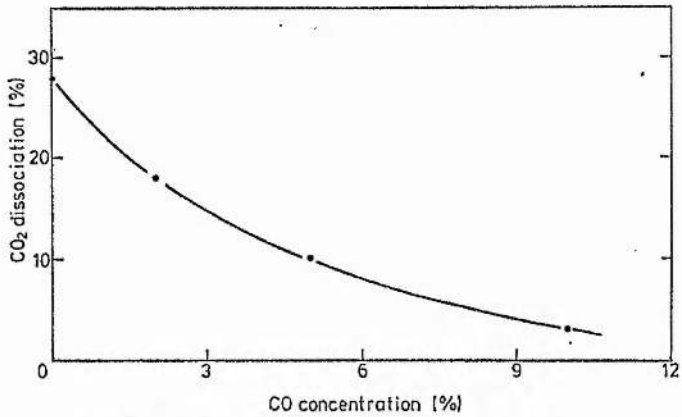


**Figure 9.** Effect of the addition of CO on the dissociation of $CO_2$ in a 20–20–60 $CO_2$–$N_2$–He mixture after 8200 pulses in a sealed TEA laser.

### *4.3. Effect of hydrogen*

The addition of hydrogen also reduces the $CO_2$ dissociation in the $CO_2$–$N_2$–He mixture, but its exact effect is difficult to measure because it can lead to discharge arcing. Thus in figure 8 the point X represents the $CO_2$ dissociation after 2400 pulses in the 20–20–60 mixture with 6% added hydrogen: there is a reduction of about 35%. Points could not be obtained for any larger number of pulses because after 2400 pulses the discharge arced. This can be contrasted with the result reported in an earlier paper (Smith *et al* 1975) when 25% hydrogen could be added without arcing: but in that case the addition was made to a flowing gas laser, so no dissociation products were accumulated. In the present situation dissociation of the hydrogen will be about 0·025% per pulse (reaction 28) so considerable amounts of water vapour will be formed by reactions of H and $H_2$ with other dissociation products such as O and OH and after $10^3$–$10^4$ pulses the $H_2O$ concentration will be 1–3%.

Figure 4 predicts that the negative ion concentration will be doubled in a 20–20–60 mixture with the addition of about 2% $H_2O$. Thus in a sealed TEA laser with the added $H_2$ the negative ion population will have been doubled after $10^3$–$10^4$ pulses, whilst it is observed that the discharge arcs after $2{\cdot}4 \times 10^3$ pulses.

That this effect of $H_2$ is due to the formation of $H_2O$ by the discharge is supported by the observation that if the gases in a flowing gas TEA laser are passed through a water-saturated alumina column before entering the laser the discharge arcs and this arcing continues for a considerable time after the addition of $H_2O$ has ceased.

*4.4. Effect of oxygen*

Previously we have reported (Smith *et al* 1975) that several percent of oxygen could be added to a flowing gas trigger-wire TEA laser before it started to arc, whereas Stark *et al* (1975a) have reported that less than 1% could be added to a similar device prior to arcing. We have measured the arcing threshold in the TEA laser with the gas flowing sufficiently fast so as to be completely replaced between pulses: figure 10 summarizes the

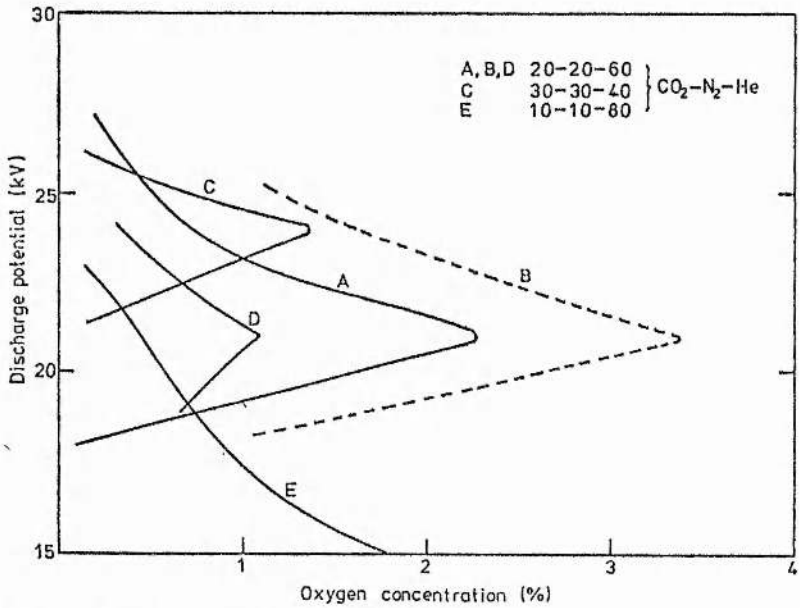


**Figure 10.** Effect of the addition of $O_2$ on the arcing threshold in various $CO_2$–$N_2$–He mixtures. The dashed curve B is for 50% of pulses arcing. Results obtained after the laser had discharged about $10^5$ times (curve D after $2\times10^6$ times).

results. The solid curves (A, C, D, E) represent the variation of arcing threshold with added $O_2$ for several different gas mixtures at different discharge voltages. The dashed curve (B) represents the same situation as curve A except that the arcing limit has been measured for 50% of the pulses arcing, rather than arcing threshold. Curves A, B, C and E were measured after the laser had discharged about $10^5$ times, curve D after $2\times10^6$ times. Clearly the arcing situation changes from pulse to pulse (A and B) and this is presumably due to slight variations in the discharge pulse and electrode surfaces. The arcing threshold also decreases with number of pulses (A and D), but since the neutral gas composition has not changed significantly between the situations of curves A and D the effect must be due to a change of surface condition. Thus one has a situation that where the surface condition has changed (deteriorated with time) so the threshold for arcing with added amounts of $O_2$ changes. Also it may be observed that a higher helium content at low voltages is more tolerant of added $O_2$, but the operating potential must be carefully chosen for any given mixture. In a sealed device with a reasonable power output the maximum permissible $O_2$ is $\frac{1}{2}$–2%. This measured amount can be compared with the computed amount of about $\frac{1}{2}$% which doubles the negative ion concentration in a 20–20–60 mixture (figure 3).

*4.5. Long-life sealed* TEA *laser*

Carbon monoxide and hydrogen have been successfully used to produce long-life sealed TEA lasers (Stark *et al* 1975a). The effect of the CO addition on the negative ions is relatively insignificant (figure 6), however it does reduce the $CO_2$ dissociation (figure 9) and hence the amount of $O_2$, and so the negative ion population will be reduced (figure 3). $\frac{1}{2}$% $O_2$ doubles the negative ion concentration, with $CO_4^-$ then comparable with $CO_3^-$, so it is important that the oxygen concentration is limited.

Addition of $H_2$ has three effects: (*a*) it aids the pre-ionization of the discharge (Smith *et al* 1975); (*b*) together with CO it limits $CO_2$ dissociation (§4.2 above); (*c*) after a succession of pulses $H_2O$ is formed in the discharge. The model predicts that about 1% $H_2O$ will produce sufficient $H^-$ to double the negative ion density in the pulse ($H^-$ comparable with $CO_3^-$). Thus, although the first two effects of $H_2$ addition are beneficial to sealed operation, the third is detrimental and limits $H_2$ addition to small amounts. $H^-$ is produced from $H_2$ at a much slower rate than from $H_2O$, thus allowing the addition of $H_2$ to flowing lasers in larger amounts.

We have operated a sealed laser with a $CO_2$–$N_2$–He–CO–$H_2$ mixture for $10^6$ pulses with a diffuse discharge at all times and reduction of only about 15% of the peak pulse power and pulse energy over this period. After $10^6$ pulses the $CO_2$ loss was 12%, which would correspond to a maximum $O_2$ of $1\frac{1}{4}$%, and there would be less if some of it had been absorbed on the electrode surfaces.

## 5. Conclusions

We have experimentally determined that stable long-life sealed diffuse discharge TEA laser operation can be obtained in a $CO_2$–$N_2$–He laser mixture provided the oxygen concentration is less than $\frac{1}{2}$–2%, depending on the particular laser, and the water vapour concentration is less than 1–3%. Theoretically we have determined that $\frac{1}{2}$% $O_2$ or 2% $H_2O$ will double the negative ion population. Several authors (Douglas-Hamilton and Mani 1974, Kovalev *et al* 1974, Dyer and James 1975, Velikhov *et al* 1975) have attributed discharge instability to negative ion processes and suggested that these can produce arcing in TEA lasers. Quantitative verification of this requires the accurate determination of the variation of ionization and attachment coefficients with the discharge $E/N$ for individual $CO_2$–$N_2$–He–CO–$O_2$–$H_2$–$H_2O$ mixtures, something which has yet to be attempted. Extrapolation from results or calculations for 'similar' $CO_2$–$N_2$–He mixtures is not satisfactory because of the rapidity with which the ionization and attachment coefficients vary with the discharge parameters in typical laser discharges. But one can conclude from our work that the TEA lasers become unstable and arc under the conditions when the negative ion population has been calculated to have been significantly increased.

In a $CO_2$–$N_2$–He mixture the dominant negative ion is predicted to be $CO_3^-$ with $N_n/N_e \sim \frac{1}{10}$, depending on the gas mixture, being greatest in mixtures with a high $CO_2$ concentration. In a sealed $CO_2$–$N_2$–He mixture when there are also dissociation products CO and $O_2$ the dominant ion is $CO_4^-$ and $N_n/N_e$ is increased and will be $\sim 1$ for a mixture rich in $CO_2$, such as that used in UV pre-ionized lasers. The presence of CO reduces the $CO_2$ dissociation such that in the trigger-wire laser with about 20% initial fill of $CO_2$ the negative ion population is only slightly increased, but it is not clear that in the UV pre-ionized laser with a high $CO_2$ concentration the oxygen will be similarly successfully controlled.

The presence of NO, $N_2O$ and $NO_2$ in densities typical of sealed TEA lasers ($<25$ ppm NO and $NO_2$, $<75$ ppm $N_2O$) has no serious effect on the negative ion chemistry, but at low pressures (1–20 Torr) $NO_2^-$ becomes the dominant ion and $N_n/N_e \sim 1$.

The addition of $H_2$ leads to the production of $H^-$ in insignificant amounts, but $H_2O$ is also created in the discharge which attaches and produces $H^-$ in significant quantities.

Stark *et al* (1975b) have shown that one advantage of UV pre-ionization is that greater peak powers are obtained because the amount of $CO_2$ in a flowing gas mixture can be increased without discharge arcing. However, when such devices are sealed the larger amounts of $CO_2$ may lead to more $O_2$ being produced by dissociation, with a consequent increase in $CO_4^-$. The main loss process for this ion is three-body recombination with positive ions. This process has similar reaction rates for most ion pairs, so it is unlikely that the $CO_4^-$ can be suppressed by addition of a suitable additive (unless the $CO_2$ dissociation is further reduced). However, the negative ion population takes 50–100 ns to reach its equilibrium value, so, if the electrical discharge can take place in less than 50 ns, the $N_n/N_e$ ratio will be relatively small during the discharge and the susceptibility to arcing will be reduced.

**Acknowledgments**

We would like to thank Mr D Stark and Mr H Foster for useful discussions and encouragement in this work, SERL, Baldock for the loan of the sealed laser assembly and CVD for financial support.

**Appendix**

A summary of the rate equations, describing the time development of the various negative ion and neutral species is given below. Rate coefficients are denoted by $k$, with a subscript referring to the corresponding reaction in table 1 or table 2.

$n_e$ is the electron density. $n_p$ is the positive ion density. The fraction of molecular oxygen in the $(^1\Delta_g)$ state is denoted by $F$. $k_{2R}$ and $k_{3R}$ are the two-body and three-body negative-ion/positive-ion recombination coefficients.

$$\frac{d[CO_3^-]}{dt} = k_{58}[M][CO_2][O^-] + k_{47}[CO_4^-][O] + k_{50}[CO_4^-][H] - (k_{17}[CO] + k_{43}[O] + k_{44}[NO] + k_{45}[NO_2] + k_{46}[H] + k_{2R}n_p + k_{3R}[M]n_p) \times [CO_3^-]$$

$$\frac{d[O^-]}{dt} = n_e(k_1[CO_2] + k_2[CO] + k_3[O_2] + k_4[N_2O] + k_5[NO] + k_6[NO_2]) + k_{39}[O][O_2^-] + n_e k_{10}[M][O] - (k_{58}[M][CO_2] + k_{12}[CO] + k_{13}[O] + k_{14}F[O_2] + k_{15}[NO] + k_{34}F[O_2] + k_{35}[NO_2] + k_{36}[NO_2] + k_{37}[N_2O] + k_{38}[H_2] + k_{16}[H_2] + k_{2R}n_p + k_{3R}[M]n_p)[O^-]$$

$$\frac{d[O_2^-]}{dt} = k_{34}F[O_2][O^-] + k_{43}[CO_3^-][O] + k_9 n_e[O_2][M]$$
$$+ k_{36}[O^-][NO_2] + k_{53}[NO^-][O_2] - (k_{18}[O] + k_{19}F[O_2]$$
$$+ k_{20}[H] + k_{39}[O] + k_{40}[O_3] + k_{41}[NO_2] + k_{60}[CO_2][M]$$
$$+ k_{2R}n_p + k_{3R}[M]n_p)[O_2^-]$$

$$\frac{d[NO^-]}{dt} = k_{37}[O^-][N_2O] + (k_{53}[O_2] + k_{25}[M] + k_{2R}n_p + k_{3R}[M]n_p)[NO^-]$$

$$\frac{d[NO_2^-]}{dt} = k_{11}n_e[NO_2] + k_{35}[NO_2][O^-] + k_{41}[NO_2][O_2^-]$$
$$+ k_{44}[NO][CO_3^-] + k_{59}[O^-][NO][M] + k_{51}[H^-][NO_2]$$
$$+ k_{52}[OH^-][NO_2] + k_{56}[(NO_3^-)^*][H]$$
$$+ k_{57}[(NO_3^-)^*][NO] - (k_{54}[NO_2] + k_{55}[H] + k_{2R}n_p + k_{3R}[M]n_p)[NO_2^-]$$

$$\frac{d[NO_3^-]}{dt} = k_{45}[CO_3^-][NO_2] + k_{54}[NO_2^-][NO_2] + k_{48}[NO][CO_4^-]$$
$$- (k_{2R}n_p + k_{3R}[M]n_p)[NO_3^-] - (k_{56}[H] - k_{57}[NO])[(NO_3^-)^*]$$

$$\frac{d[CO_4^-]}{dt} = k_{60}[O_2^-][CO_2][M] - (k_{47}[O] + k_{48}[NO] + k_{49}[O_3]$$
$$+ k_{50}[H] + k_{2R}n_p + k_{3R}n_p[M])[CO_4^-]$$

$$\frac{d[H^-]}{dt} = n_e(k_7[H_2O] + k_8[H_2]) + k_{42}[O_2^-][H] - (k_{21}[H] + k_{22}[O_2] + k_{51}[NO_2]$$
$$+ k_{2R}n_p + k_{3R}[M]n_p)[H^-]$$

$$\frac{d[OH^-]}{dt} = k_{38}[O^-][H_2] + k_{55}[NO_2^-][H] + k_{46}[CO_3^-][H]$$
$$- (k_{23}[O] + k_{24}[H] + k_{52}[NO_2] + k_{2R}n_p + k_{3R}[M]n_p)[OH^-]$$

$$\frac{d[CO]}{dt} = k_{26}n_e[CO_2] - k_{30}[O][M][CO]$$

$$\frac{d[O]}{dt} = 2k_{27}n_e[O_2] + k_{26}n_e[CO_2] - (k_{30}[CO][M] + k_{31}[O][M]$$
$$+ k_{32}[O_2][M] + k_{33}[O_3])[O]$$

$$\frac{d[O_2]}{dt} = k_{31}[O][O][M] + 2k_{33}[O][O_3] - (k_{32}[O][M] + k_{27}n_e)[O_2]$$

$$\frac{d[O_3]}{dt} = k_{32}[O][O_2][M] - k_{33}[O][O_3]$$

$$\frac{d[H]}{dt} = 2k_{28}n_e[H_2] + k_{29}n_e[H_2O]$$

## References

Adams N G, Bohme D K, Dunkin D B, Fehsenfeld F C and Ferguson E E 1970 *J. Chem. Phys.* **52** 3133–40
Austin J M, Smith A L S and Browne P G 1974 *Phys. Lett.* 46A 427–8
Bastien F, Haug R and Lecuiller M 1975 *J. Chim. Phys.* **72** 105–12

Chanin L M, Phelps A V and Biondi M A 1962 *Phys. Rev.* **128** 219–30
Corrigan S J B and Von Engel A 1958 *Proc. R. Soc.* **245** 335–51
Douglas-Hamilton D A and Mani S A 1973 *Appl. Phys. Lett.* **23** 508–10
—— 1974 *J. Appl. Phys.* **45** 4406–15
Dyer P E and James D J 1975 *J. Appl. Phys.* **46** 1679–83
Fehsenfeld F C 1975 *J. Chem. Phys.* **63** 1686–7
Fehsenfeld F C and Ferguson E E 1974 *J. Chem. Phys.* **61** 3181–93
Fehsenfeld F C, Ferguson E E and Schmeltekopf A L 1966 *J. Chem. Phys.* **45** 1844–5
Johns T W and Nation J A 1972 *Appl. Phys. Lett.* **20** 495–6
Kovalev A A, Persiantsev I G, Pismenny V D and Rakhimov A T 1974 *Phys. Lett.* **49A** 29–30
Lowke J J, Phelps A V and Irwin B W 1973 *J. Appl. Phys.* **44** 4664–71
McDaniel E W, Cermak V, Dalgarno A, Ferguson E E and Friedman L 1970 *Ion–Molecule Reactions* (New York: Wiley)
McFarland M, Albritton D L, Fehsenfeld F C, Ferguson E E and Schmeltekopf A L 1973 *J. Chem. Phys.* **59** 6629–35
McGowan S 1967 *Can. J. Phys.* **45** 439–48
Mahan B H and Person J C 1964 *J. Chem. Phys.* **40** 392–401
Mahan B H and Walker I C 1967 *J. Chem. Phys.* **47** 3780–2
Melton C E 1970 *Principles of Mass Spectrometry and Negative Ions* (New York: Dekker)
Moruzzi J L and Phelps A V 1966 *J. Chem. Phys.* **45** 4617–27
Nighan W L and Wiegand W J 1974 *Phys. Rev. A.* **10** 922–45
Nighan W L, Wiegand W J and Haas R A 1973 *Appl. Phys. Lett.* **22** 579–82
Niles F E 1970 *J. Chem. Phys.* **52** 408–24
Olsen R E 1972 *J. Chem. Phys.* **56** 2979–84
Pearson P R and Lamberton H M 1972 *IEEE J. Quantum Electron.* **QE-8** 145–9
Phelps A V 1969 *Can. J. Chem.* **47** 1783–93
Prince J F and Garscadden A 1975 *Appl. Phys. Lett.* **27** 13–5
Rapp D and Briglia D D 1965 *J. Chem. Phys.* **43** 1480–9
Smith A L S and Austin J M 1974 *J. Phys. D: Appl. Phys.* **7** 314–22
—— 1976 *Dynamic Mass Spectrometry* vol. 4 (London: Heyden and Sons) pp 211–6
Smith A L S, Bett T H and Browne P G 1975 *IEEE J. Quantum Electron.* **QE-11** 335–40
Stark D S, Cross P H and Foster H 1975a *IEEE J. Quantum Electron.* **QE-11** 774–8
Stark D S, Cross P H, Harris M J and Foster H 1975b *2nd Br. Nat. Quantum Electron. Conf., Oxford*
Stuhl F and Niki H 1971 *J. Chem. Phys.* **55** 3943–53
Tannen P D, Bletzinger A and Garscadden A 1974 *IEEE J. Quantum Electron.* **QE-10** 6–11
Velikhov E P, Zemstov Yu K, Kovalev A S, Persantsev I G, Pismenny V D and Rakhimov A T 1975 *Sov. Phys.–JETP* **40** 837–40
Venugopalan M 1971 *Reactions Under Plasma Conditions* vol. 2 (New York: Wiley)
Wiegand W J and Nighan W L 1973 *Appl. Phys. Lett.* **22** 583–6

# CHAPTER SEVEN

## NEGATIVE ION EFFECTS IN $CO_2$ CONVECTION LASER DISCHARGES

(Reproduced from 'Applied Physics', Vol 16, pp111-118)

Appl. Phys. 16, 111—118 (1978)

Applied Physics



# Negative Ion Effects in $CO_2$ Convection Laser Discharges

*H. Shields* and *A. L. S. Smith*
Physics Department, University of St. Andrews, St. Andrews, Fife, Scotland KY16 9SS

Received 1 August 1977/Accepted 28 October 1977

**Abstract.** Negative ions are computed to be formed on a time scale and in quantities such that they may be a cause of plasma instability observed in low pressure electrical discharge convection $CO_2$ lasers. In a typical $CO_2$-$N_2$-He-$H_2O$ laser mixture the principal ions are $CO_3^-$, $CO_4^-$ and $H^-$ with the total negative ion density $n_-$ given by $0.1\, n_e < n_- < n_e$, where $n_e$ is the electron density: but if the gases are re-cycled or if there is an air leak $NO_2^-$ and $NO_3^-$ are formed in significant amounts and $n_-$ can become greater than $n_e$ in a time considerably less than the gas dwell time in the electrical excitation discharge. CO is effective in reducing $n_-$ in a system without re-cycling, but is ineffective in a re-cycled system with the oxides of nitrogen present.

**PACS:** 42.55D.

In recent years $CO_2$ electric discharge convection lasers (EDCL's) have become important as $>5$ kW sources of cw power for welding, cutting, heat treatment etc. The $CO_2$ is usually mixed with He and $N_2$ at a total pressure of 10–50 Torr. When the energy deposited in the gas, the Discharge Specific Power (DSP) is $\sim$200–600 kW per kg per s, it is found that the excitation discharge tends to become unstable and constrict to an arc and the gas dwell time in the discharge must be kept less than 1–3 ms. The exact dwell times and DSP's for instability depend on gas turbulence and flow conditioning, but are less for a re-cycled gas mixture than for a mixture discharged only once.

Possible modes of instability have been extensively investigated theoretically [1–5]. Experimentally instabilities may be initiated at an electrode or in the bulk of the gas: but for a local instability to develop and cause plasma collapse there must be a positive feedback mechanism in the bulk medium operative over a time as short as the gas dwell time. Nighan [1, 3, 4] has analysed a range of 'thermal instabilities' and has shown in particular that negative ion species significantly affect the growth rate of thermal instabilities by way of their influence on electron density fluctuations. Computed instability growth times agree with the observed times for diffuse-discharge-to-arc-collapse times observed in EDCL's. However before this type of 'thermal instability' can occur it is clearly necessary both to have a significant density of negative ions present and that these ions should be created in a time considerably less than the gas dwell time in the discharge.

Comparatively little work has been done on investigating the creation and development of the negative ion species, either experimentally or theoretically. Wiegand and Nighan [6] developed a negative ion computer model to show that the principle negative ion in 20 torr of $CO_2$-$N_2$-He would be $CO_3^-$ and that the total negative ion density could be greater than the electron density. Prince and Garscadden [7] measured the principle negative ions in the flowing afterglow of a discharge at very low pressures ($\sim$1 Torr) of $CO_2$-$N_2$-He to be $NO_2^-$ and $NO_3^-$, but did not determine the absolute concentrations. Shields et al. [8] constructed an extensive negative ion model to simulate TEA laser instability conditions and correlated the measured discharge instability in a TEA laser with the enhancement of the negative ion density predicted by the model for contamination by neutral reaction products or for additive gases: they also showed that for the conditions of Prince and Garscadden [7] $NO_2^-$ and $NO_3^-$ would be expected to be the principle negative ion

0340-3793/78/0016/0111/$01.60

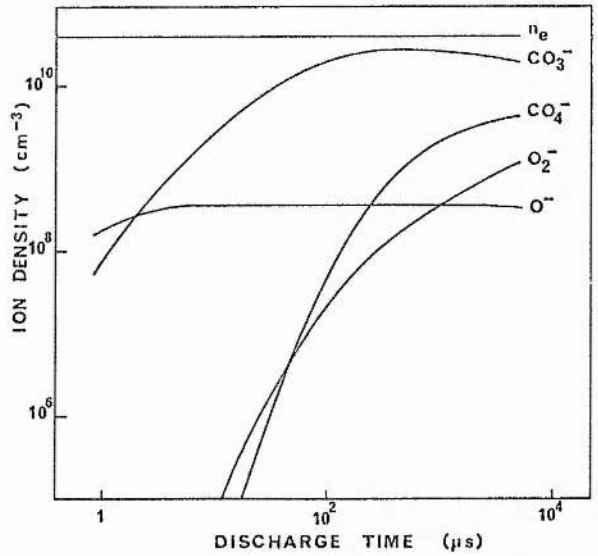


Fig. 1. Variation with time of the main negative ion species in a flowing gas 5-15-80, $CO_2$–$N_2$–He discharge at 15 torr pressure ($E/P = 5\,V\,cm^{-1}\,torr^{-1}$)

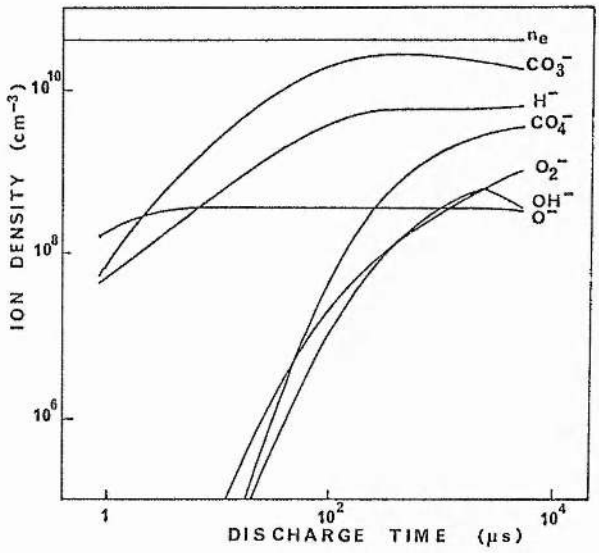


Fig. 2. Variation with time of the main negative ion species in a flowing gas 5-15-80, $CO_2$–$N_2$–He discharge with 1000 ppm $H_2O$ at 15 torr pressure ($E/P = 5\,V\,cm^{-1}\,torr^{-1}$)

species. Bletzinger et al. [9] have shown that a low pressure discharge becomes unstable with the selective addition of the oxides of nitrogen ($\sim$100–500 ppm $NO_2$ or $N_2O$, $\sim$1000 ppm NO).

We have modified our negative ion TEA laser model [8] to the typical rapid gas transport low pressure cw discharge situation and examined the time development of the various negative ion species from entry into the discharge, and the changes in the main species as various additional gases (which are or might be expected to be found in significant amounts in a re-cycled gas device) are selectively considered. Thus we determine the time development of negative ions and compare it with the known range of instability times for similar rapid gas transport discharges ($10^3$–$3 \times 10^3$ μs) and we compare the total negative ion density in various situations with the electron density: but we do not attempt to show how the negative ions may actually bring about the plasma instability: for this see [1–5].

## 1. The Negative Ion Model

Unless otherwise stated we assume 15 Torr total pressure of a 5-15-80, $CO_2$-$N_2$-He mixture in a steady electrical discharge environment described by a constant electron density $n_e$ of $4 \times 10^{10}\,cm^{-3}$ and a reduced field $E/P$ of 5 volt $cm^{-1}\,Torr^{-1}$ ($E$ is the electric field and $P$ is the gas pressure). Individual neutral and negative ion peaks are appropriately designated and $n_-$ represents the total negative ion density.

The model has been extensively described in Shields et al. [8] and the homogeneous reactions below are labelled as in [Ref. 8, Tables 1 and 2]. Heterogeneous processes can be ignored since EDCL laser dimensions and the gas pressures are such that diffusion to the walls of the laser vessel is negligible for the period of the gas dwell time used. Equations expressing the time development of neutral species CO, O, $O_2$, $O_3$, H and negative ions $O^-$, $O_2^-$, $NO^-$, $NO_2^-$, $NO_3^-$, $CO_3^-$, $CO_4^-$, $H^-$ and $OH^-$ have been solved iteratively using the Runge-Kutta technique with an IBM 360/44 computer and a step length of 10–100 ns as appropriate. $T$ is used to represent the time delay from the start of the discharge (or entry of a flowing gas into the discharge) until the negative ion density $n_-$ reaches a specific magnitude, in particular $T(n_e)$ and $T(0.1\,n_e)$ are used to designate the time for $n_-$ to reach 100% and 10% of $n_e$, respectively. Large values of $T(n_e)$ and $T(0.1\,n_e)$ will result in the ratio $n_-/n_e$ remaining small throughout most of the time spent by the gas in the discharge, delaying the influence of negative ion effects on discharge stability. The maximum discharge period used in the computation was between $10^3$ and $10^4$ μs, being limited by the availability of computation time and the need to avoid any complications due to significant gas heating by the excitation discharge.

## 2. EDCL without Gas Re-Cycling

Negative ions are formed by several attachment reactions, the most important being

$$e + CO_2 \rightarrow CO + O^- . \qquad (1)$$

Figure 1 shows the formation of the $O^-$ and the subsequence development with time of other ions by ion-neutral reactions

$$O^- + CO_2 + M \rightarrow CO_3^- + M \quad (58)$$

$$CO_3^- + O \rightarrow O_2^- + CO_2 \quad (43)$$

$$O_2^- + CO_2 + M \rightarrow CO_4^- + M \quad (60)$$

with $CO_3^-$ becoming dominant and $n_- \sim 0.7\, n_e$ after $\sim 100\,\mu s$. The quasi-equilibrium situation is due to a balance between the creation of negative ions by (1) and their loss by two-body recombination.

Any realistic laser system will be contamined with water vapour and Fig. 2 illustrates the negative ion temporal development with 1000 ppm $H_2O$ present. The $H^-$ is created when $t$ is small by the dissociative attachment reaction

$$e + H_2O \rightarrow H^- + OH \quad (7)$$

and the $OH^-$ is formed later by

$$CO_3^- + H \rightarrow OH^- + CO_2 \quad (46)$$

when the discharge has had time to form sufficient atomic hydrogen by neutral dissociation of $H_2O$ (or $H_2$).

Both Fig. 1 and 2 show that the total negative ion density $n_-$, reaches a value almost equal to the electron density, $n_e$. However the precise ratio of $n_-/n_e$ achieved depends on the prevailing gas discharge conditions, i.e. $E/P$, $n_e$, gas pressure and gas mixture. First consider varying $E/P$ and hence the discharge attachment rates without altering the gas pressure $P$ or the current (and hence $n_e$): in practice this could only be done by some form of external discharge control, such as electron beam or uv radiation ionisation. Figure 3 shows that as $E/P$ increases so $n_-$ increases, becoming greater than $n_e$, and $T(0.1\, n_e)$ decreases. This is a reflection of the strong dependence of attachment rates on $E/P$. Also in Fig. 3 the effect of changing the gas mixture is shown, as $[CO_2]$ increases and so the production of $O^-$ by (1), so the negative ion peaks become larger and the equilibrium values are reached faster ($n_-$ increases, $T(0.1\, n_e)$ decreases). If the total pressure $P$ is increased but the gas mixture and $E/P$ are kept constant there is similar behaviour ($n_-$ increases, $T(0.1\, n_e)$ decreases), since the amount of $CO_2$ is increased.

If $n_e$ is varied (keeping $E/P$ constant) there is little change in $n_-$ or the main negative ion peaks but $T(0.1\, n_e)$ does increase slowly as $n_e$ increases.

To summarize, in an EDCL discharge where the $CO_2$-$N_2$-He gas mixture is not re-cycled the initial $O^-$ is formed by dissociative attachment from $CO_2$, and $CO_3^-$ becomes the dominant ion by the ion molecule reaction (58). Exact composition is not important, unless $[CO_2]$ or the discharge $E/P$ is changed. When the $E/P$ is increased, $n_-$ increases and $T$ decreases due to an increase in the rate constant of reaction (1). Increasing $[CO_2]$ either by increasing its relative concentration or by increasing the total gas pressure (assuming $E/P$ and $n_e$ constant) increases $n_-$ and decreases $T$.

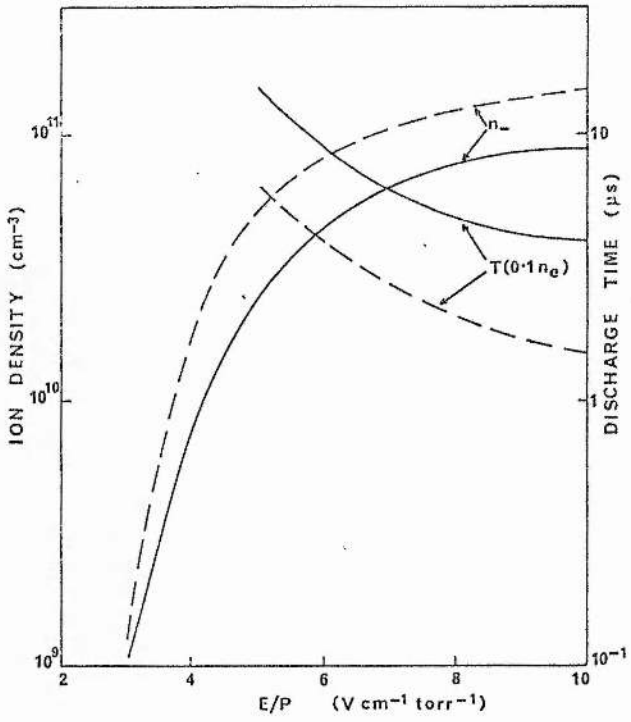


Fig. 3. Dependence of total negative ion density and the time for $n_-$ to reach 10% of the electron density on discharge $E/P$ in 5-15-80, $CO_2$-$N_2$-He (solid lines) and 13-9-78, $CO_2$-$N_2$-He (broken lines)

## 3. EDCL with Re-Cycled Gas

With convection lasers there is need to re-cycle the gas mixture if enormous quantities are not to be consumed. On any one cycle through the electrical discharge there will only be a small amount of $CO_2$ dissociation but over many cycles a considerable amount of $O_2$ and CO will be created and a dissociation equilibrium will be established. Figure 4 illustrates the situation for an arbitrarily assumed 50% dissociation equilibrium, the $CO_3^-$ is suppressed and $H^-$ is now dominant and there is an overall $n_-$ decrease. The detailed individual effects of the CO and $O_2$ are discussed in Section 4 below.

It is known that small amounts of the oxides of nitrogen $NO_2$, $N_2O$ and NO will be formed by the discharge [11, 12] but the exact amounts are very uncertain. We assume $NO_2$, NO and $N_2O$ are always present in amounts $Y : Y : Y/2$ ppm and in Fig. 5, $Y$ is taken to be 1000 ppm. There is a change from $CO_3^-$ to $NO_2^-$ and

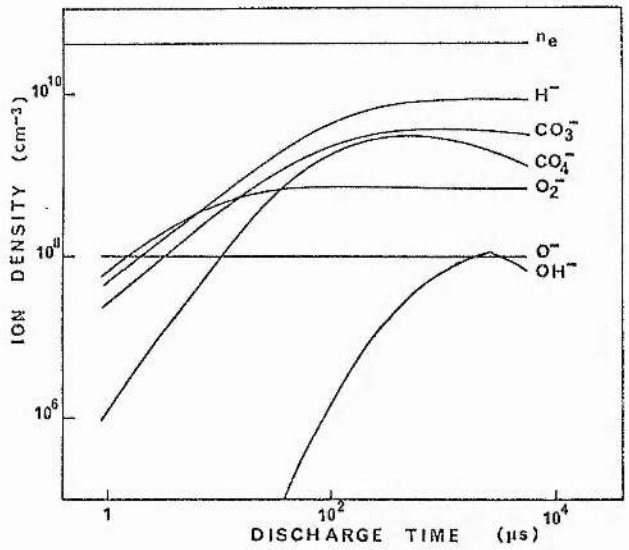


Fig. 4. Variation with time of the main negative ion species in a re-cycled gas assuming 50% dissociation of $CO_2$ (i.e. $2\frac{1}{2}$% $CO_2$, $2\frac{1}{2}$% CO, $1\frac{1}{4}$% $O_2$, 15% $N_2$, 79% He and 1000 ppm $H_2O$) at 15 Torr pressure ($E/P = 5\ V\ cm^{-1}\ torr^{-1}$)

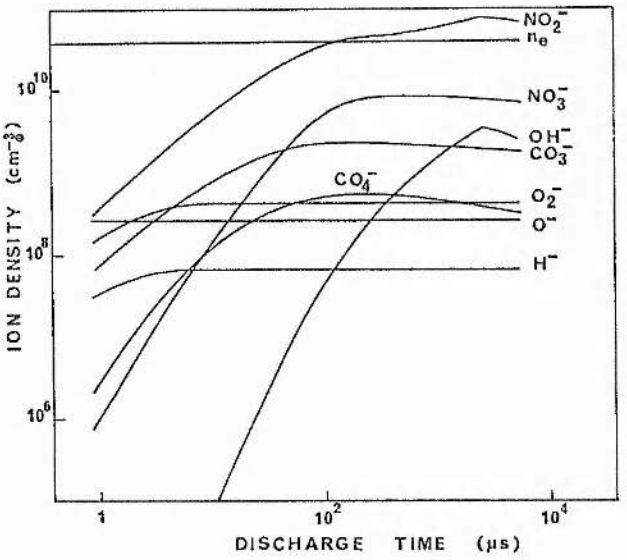


Fig. 5. Variation with time of the main negative ion species in a re-cycled gas. Conditions are as in Fig. 4 with the addition of 1000 ppm NO, $NO_2$ and 500 ppm $N_2O$

$NO_3^-$ as the principle species and $[NO_2^-] > n_e$ when $t \gtrsim 100\ \mu s$.

Several attachment and ion-molecule reactions are involved, the main ones being the very fast dissociative attachment

$$e + N_2O \rightarrow N_2 + O^- \quad (4)$$

and the somewhat slower attachment reactions

$$e + NO_2 \rightarrow NO + O^- \quad (6)$$

$$e + NO_2 + M \rightarrow NO_2^- + M \quad (11)$$

together with the charge exchange processes

$$O^- + NO_2 \rightarrow NO_2^- + O \quad (35)$$

$$O_2^- + NO_2 \rightarrow O_2 + NO_2^- \quad (41)$$

and

$$CO_3^- + NO \rightarrow CO_2 + NO_2^- \quad (44)$$

$$CO_3^- + NO_2 \rightarrow CO_2 + NO_3^- . \quad (45)$$

The $CO_4^-$ and $H^-$ are strongly suppressed by

$$CO_4^- + NO \rightarrow NO_3^- + CO_2 \quad (48)$$

$$H^- + NO_2 \rightarrow NO_2^- + H . \quad (51)$$

Thus it is clear that all three oxides have a role to play, the chief ones being the increase in $n_-$ with dissociative attachment of $N_2O$ and the selective production of $NO_2^-$ and $NO_3^-$ with $NO_2$ and NO.

The exact amounts of the oxides present is crucial. Fig. 6 is a plot of the variation of $n_-$ wirh the amount of $NO_x$, plotted for $t = 100\ \mu s$ and 50% $CO_2$ dissociation: but note that with only 10% dissociation, and the same $NO_x$ amount, there is little difference. $[NO_x] = 250$ ppm produces a significant increase in $n_-$ and when $[NO_x] = 1000$ ppm, $n_- > n_e$. From Fig. 7 it can be seen that, for the same dissociation situations, the negative ion concentration builds up much faster as the oxides of nitrogen are added, so the delay time $T(0.1\ n_e)$ decreases from about 100 μs to less than 10 μs and likewise $T(n_e)$ decreases rapidly. To summarise: oxides of nitrogen with $[NO_x] = 100 - 1000$ ppm will have a strong effect on both the total negative ion population and the rate of rise of the negative ion population. These amounts are typical of those observed to cause instability by Bletzinger et al. [9]. From the limited literature available [11, 12] it is possible that these amounts of oxides of nitrogen may be produced in a re-cycled system but the evidence is inadequate and direct and systematic measurements are required.

## 4. Addition of CO and $O_2$

In Sec. 3 it was noted that dissociation of $CO_2$ and the formation of CO and $O_2$ led to the suppression of $CO_3^-$ and $H^-$ became the main peak if sufficient $H_2O$ was present. Consider the action of CO and $O_2$ separately: first CO.

Fast associative detachment of $O^-$

$$O^- + CO \rightarrow CO_2 + e \quad (12)$$

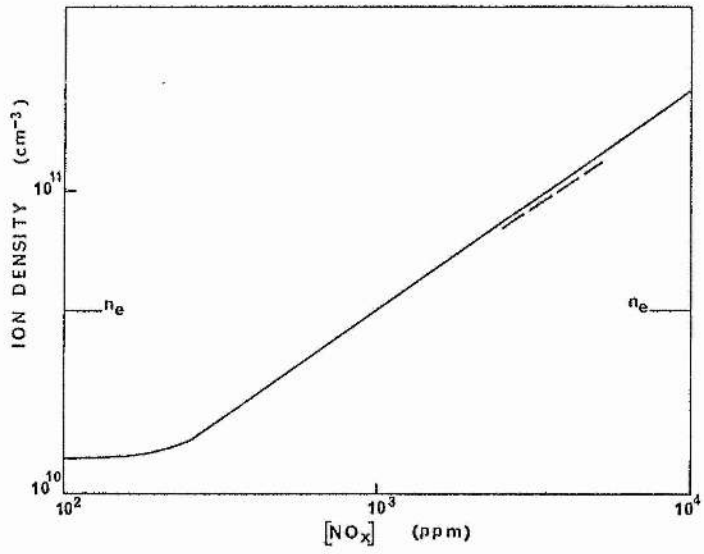


Fig. 6. Dependence of negative ion density on $NO_x$ concentration in a recycled system; ——— 50% $CO_2$ dissociation; ——— 10% $CO_2$ dissociation (assuming $NO_2:NO:N_2O=2:2:1$)

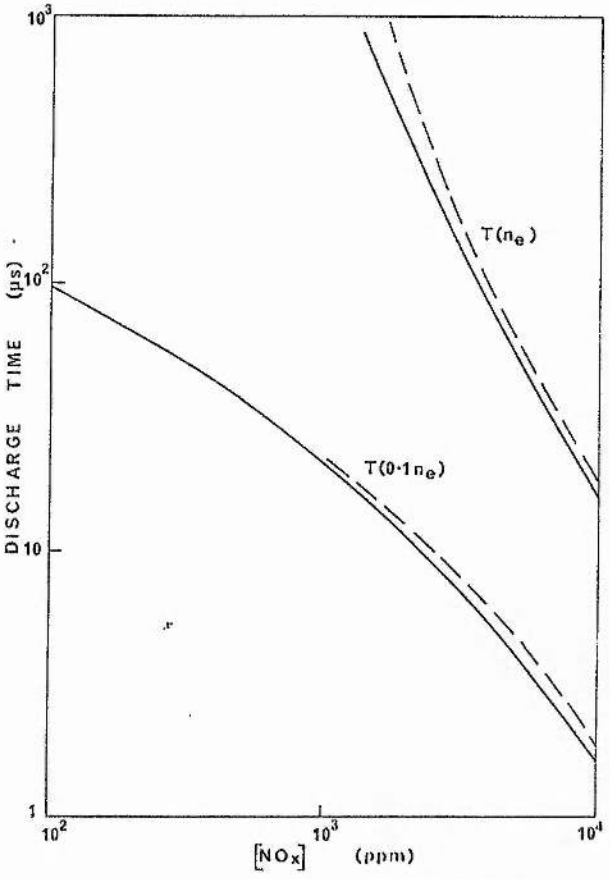


Fig. 7. Dependence of discharge time required for $n_e$ to reach 10% and 100% of the electron density on $NO_x$ concentration in a re-cycled system; ——— 50% $CO_2$ dissociation; ——— 10% $CO_2$ dissociation (assuming $NO_2:NO:NO_2=2:2:1$)

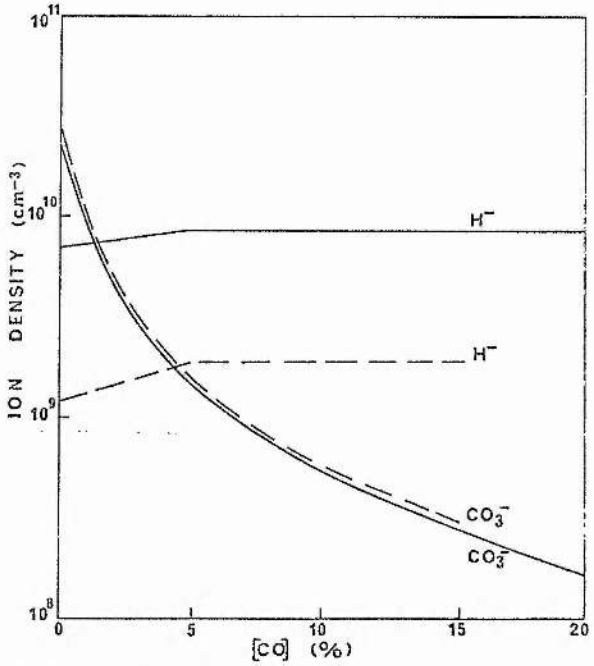


Fig. 8. Dependence of main negative ion species on CO concentration in a 5% $CO_2$, 15% $N_2$, (80 [CO])% He mixture; - - —— 1000 ppm $H_2O$; ---- 200 ppm $H_2O$

together with the slower

$$CO_3^- + CO \rightarrow 2CO_2 + e \qquad (17)$$

leads to the rapid decrease of $CO_3^-$ as CO is added. Fig. 8 shows the behaviour of the two principle peaks, $CO_3^-$ and $H^-$, for a fresh undissociated $CO_2$ gas mixture and

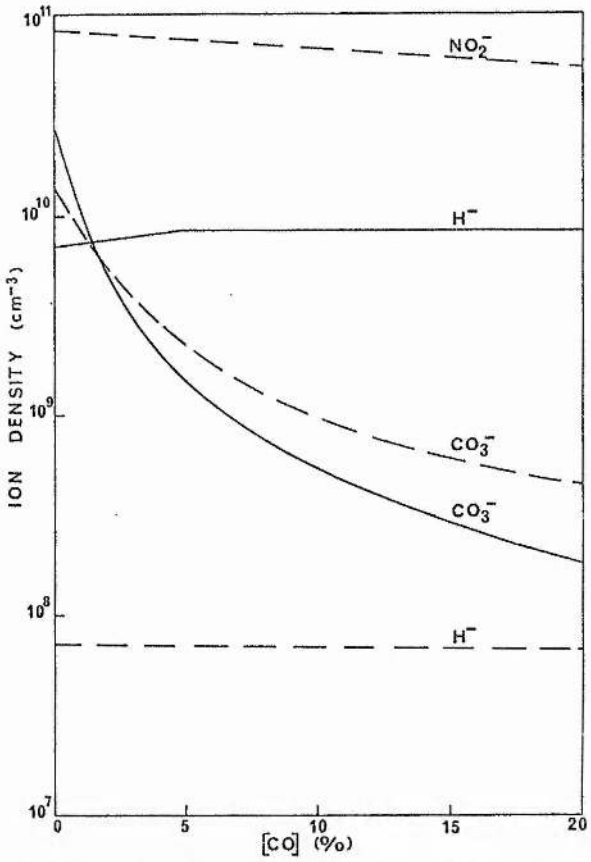


Fig. 9. Dependence of main negative ion species on CO concentration in a 5% $CO_2$, 15% $N_2$, (80–[CO])% He mixture; ——— 1000 ppm $H_2O$, NO, $NO_2$, 500 ppm $N_2O$; —— 1000 ppm $H_2O$

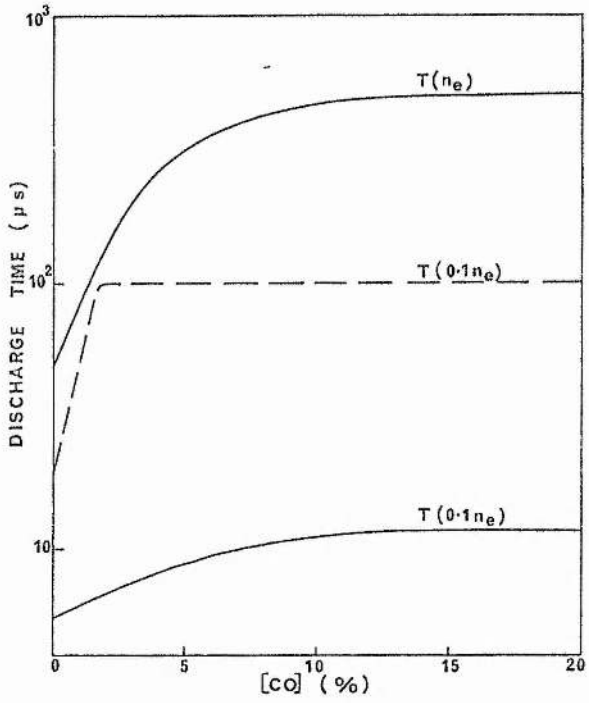


Fig. 10. Dependence of discharge time required for $n_-$ to reach 10% and 100% of the electron density on CO concentration in a 5% $CO_2$, 15% $N_2$, (80–[CO])% He mixture; ——— 1000 ppm $H_2O$, NO, $NO_2$, 500 ppm $N_2O$; —— 1000 ppm $H_2O$

$H_2O$ impurity levels of 200 and 1000 ppm. $H^-$ becomes dominant when ~1% (1000 ppm $H_2O$) or ~4½% (200 ppm $H_2O$) CO is added, and clearly CO is very effective in reducing the total negative ion population. But with the presence of $NO_x$ although $CO_3^-$ is still reduced the effect is unimportant since $NO_2^-$ is the dominant ion and it is only slightly affected, see Fig. 9. This is because the detachment of an electron from $O^-$ by CO is slower than the conversion of $O^-$ to $NO_2^-$ and $NO_3^-$ in reactions with the oxides of nitrogen. Since CO is not known to have any detaching effect on these negative ions, no significant change in $n_-$ or $T$ with CO addition is observed. Likewise the delay times are affected differently, see Fig. 10: when there is no $NO_x$ the addition of a small amount of CO significantly increases $T(0.1\,n_e)$, but with more than ~1% CO there is little change in $n_-$ because $[H^-] > [CO_3^-]$. Whereas, with $NO_x$ present $T(0.1n_e)$ and $T(n_e)$ both increase steadily as CO is added.

Thus in a $NO_x$ free system the addition of CO significantly decreases $n_-$ and increases $T$. It was this detaching effect which Wiegand and Nighan [6] noted and hence they used the amount of $CO_2$ dissociation (and hence CO produced) as a stability parameter, but both oxygen and the oxides of nitrogen are also present in a recycled system. In a $NO_x$ contaminated system the effect of the addition of CO is different, $n_-$ is little affected although $T$ is increased considerably, so the overall effect will be to only delay the onset of instability: this effect may well be small compared to the direct harmful effects of the $NO_x$ (Sec. 3).

Figure 11 shows the effect of the addition of oxygen on the principle negative ion peaks in systems with (dashed lines) and without (solid lines) $NO_x$. Without $NO_x$ there is a general increase in the peak heights ($CO_3^-$, $CO_4^-$, $O_2^-$) due to the additional fast attachment reaction

$$e + O_2 \rightarrow O + O^- \qquad (3)$$

and subsequent ion-molecule reactions. $H^-$ decreases due to the associative detachment process

$$H^- + O_2 \rightarrow HO_2 + e. \qquad (22)$$

But with $NO_x$ the chief peaks, $NO_2^-$ and $NO_3^-$, are little altered as $O_2$ is added, since

$$e + N_2O \rightarrow N_2 + O^- \qquad (20)$$

is about two orders of magnitude faster than the additional attachment reaction (3), for similar $O_2$ and $N_2O$ concentrations.

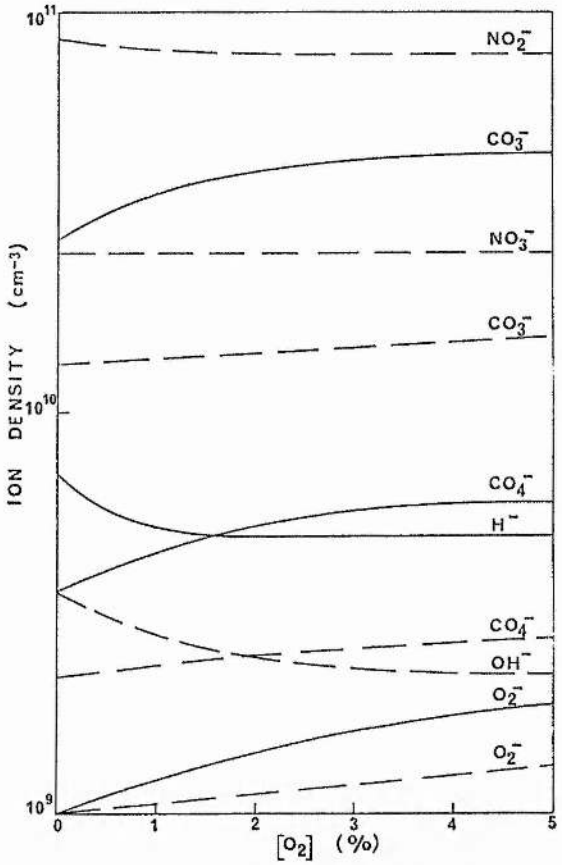


Fig. 11. Dependence of main negative ion species on $O_2$ concentration in a 5% $CO_2$, 15% $N_2$, (80–[$O_2$])% He mixture; ——— 1000 ppm $H_2O$; —— 1000 ppm $H_2O$, NO, $NO_2$, 500 ppm $N_2O$

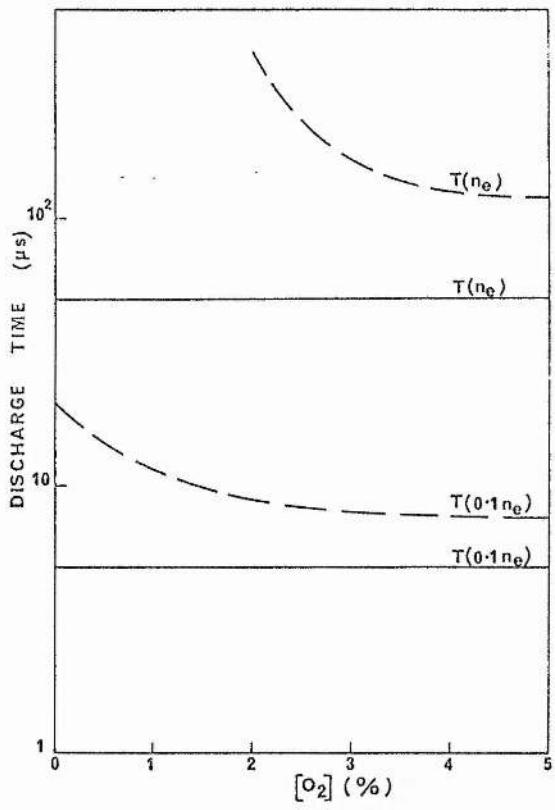


Fig. 12. Dependence of discharge time required for $n_-$ to reach 10% and 100% of the electron density on $O_2$ concentration in a 5% $CO_2$, 15% $N_2$, (80–[$O_2$])% He mixture; ——— 1000 ppm $H_2O$, NO, $NO_2$ 500 ppm $N_2O$; ———— 1000 ppm $H_2O$

Likewise as might be expected the negative ion rise times are affected differently. From Fig. 12, without $NO_x$ $T(0.1n_e)$ and $T(n_e)$ are significantly reduced whereas with $NO_x$ they are unaffected.

## 5. General Discussion

Negative ions are created in quantities comparable with the electron density in times of 100 to 1000 μs in EDCL conditions. Such times are about an order of magnitude less than experimental gas residence times in the discharge region of these convection lasers. Thus conditions exist, especially in the downstream discharge region, where plasma non-uniformities could lead to the thermal instability predicted by Nighan [1]. The negative ion densities and their rate of production are strongly dependent on the gas composition. The situations with and without $CO_2$ dissociation are considerably different and the formation of oxides of nitrogen and presence of water vapour complicate the analysis.

The complexity of modelling a multi-component gas mixture, such as that existing after gas re-cycling, is indicated in Fig. 13, which summarises the attachment and ion-molecule reaction channels of importance: negative ion-positive ion recombination is represented by grey-shading.

While operation of EDCL's at high $E/P$ will cause high ratios of $n_-/n_e$ in both fresh gas and re-cycled gas systems, the $E/P$ can be reduced if some form of external ionisation is provided. The increase in the negative ion density due to accumulation of oxides of nitrogen in a re-cycled system is a more serious problem. Although the negative ion density can be controlled in an uncontaminated gas mixture, where $CO_3^-$ dominates, by the detaching effect of CO addition, this is not the case when oxides of nitrogen are present (see Sec. 4). The accumulation of the oxides of nitrogen may result from plasma chemical reactions of the nitrogen in a recycled $CO_2$–$N_2$–He gas mixture of from air leaks into an initially nitrogen free laser mixture.

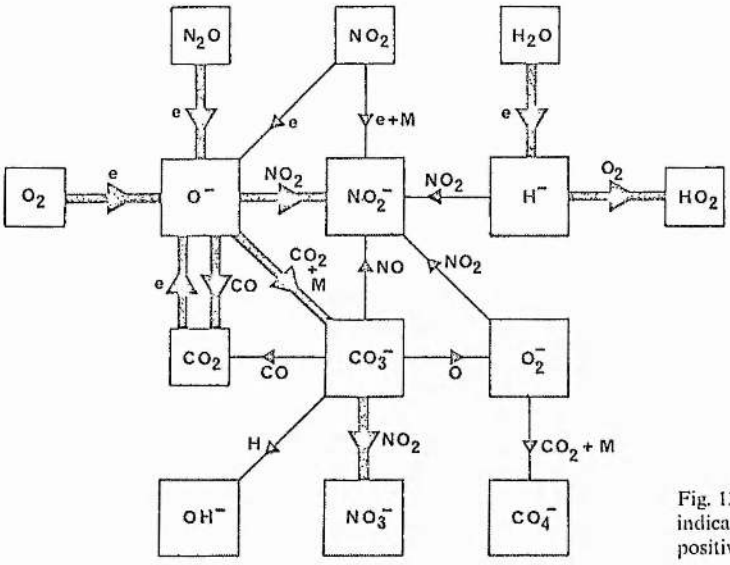


Fig. 13. Negative ion reaction path chart. Dominant reactions are indicated by heavy lines and shading indicates species undergoing positive ion-negative ion recombination

An air leak will contaminate a system with nitrogen, water vapour and oxygen. The harmful effects of nitrogen have been discussed above, but water vapour will lead to $H^-$ and $OH^-$ in insignificant amounts, even though the 1000 ppm addition of $H_2O$ we have considered is rather more than might be expected in an experimental system. Also it is possible that cluster hydrate ions may be formed [13], but at our relatively low pressures their formation will be slow and within the electrical discharge they will be quickly broken-up. With a $NO_x$ free system oxygen would produce an increase in $n_-$ and reduce $T$, but in a $NO_x$ contaminated system both $n_-$ and $T$ are little affected. Thus an air leak will always increase $n_-$ and reduce $T$, either because of the direct effect of the oxygen or because of the subsequent formation of the oxides of nitrogen.

## Conclusions

Negative ions are formed on a time scale and in quantities such that they may influence the plasma stability in EDCL's. The presence of an air leak, or the formation of the oxides of nitrogen in a recycled system increases both the total negative ion concentration and its rate of formation. Thus it is desirable to eliminate vacuum system leaks and to either operate with a nitrogen free mixture or to selectively remove any oxides of nitrogen formed. Dissociation of $CO_2$ with the formation of oxygen and carbon monoxide will only significantly affect the negative ions in a $NO_x$ free situation. Substitution of CO for $N_2$ in recycled gas EDCL's will eliminate the presence of $NO_x$, maintain a low $CO_2$ dissociation loss [14], and still allow efficient near-resonant pumping of the $CO_2(001)$ upper laser level.

## References

1. W. L. Nighan: Phys. Rev. 15A, 1701—1720 (1977)
2. W. P. Allis: Physica 82C, 43—51 (1976)
3. W. L. Nighan, W. J. Wiegand: Appl. Phys. Lett. 25, 633—636 (1974)
4. W. L. Nighan: In *Principles of Laser Plasmas*, ed. by G. Bekefi (Wiley, New York 1976)
5. L. E. Kline: J. Appl. Phys. 46, 1994—2000 (1975)
6. W. J. Wiegand, W. L. Nighan: Appl. Phys. Lett. 22, 583—586 (1973)
7. J. F. Prince, A. Garscadden: Appl. Phys. Lett. 27, 13—15 (1975)
8. H. Shields, A. L. S. Smith, B. Norris: J. Phys. D (Appl. Phys.) 9, 1587—1603 (1976)
9. P. Bletzinger, D. A. La Borde, W. F. Bailey, W. H. Long, P. D. Tannen, A. Garscadden: IEEE J. QE-11, 317—323 (1975)
10. Attachment rates as a function of $E/N$ for the 5-15-80 $CO_2$–$N_2$–He mixture are obtained from [9], while those for the 13-9-78, $CO_2$–$N_2$–He mixture have been kindly provided by K. Smith and R. M. Thomson of the Centre for Computer Studies, Leeds University
11. A. L. S. Smith, H. Shields: J. Chem. Phys. 67, 1594—1604 (1977)
12. P. D. Tannen, P. Bletzinger, A. Garscadden: IEEE J. QE-10, 6—11 (1974)
13. H. W. Ellis, R. Y. Pai, I. R. Gatland, E. W. McDaniel, R. Wernlund, M. J. Cohen: J. Chem. Phys. 64, 3935—3941 (1976)
14. A. L. S. Smith: unpublished

# CHAPTER EIGHT

## SUMMARY OF RESULTS

## 8.1 SUMMARY

The advancement of plasma kinetic modelling of $CO_2$ laser discharges is restricted at present by the unavailability of essential data. In particular, a reliable, comprehensive determination of the positive and negative ion processes operating in the laser discharge and the major ion species resulting from these processes is required. This thesis has examined these ion processes and major ion species densities in detail for conditions typical of practical $CO_2$ lasers.

Positive ion species in a $CO_2$ laser discharge of the conventional axial flow type have been measured using mass-spectrometric techniques. These ions have been sampled directly from the positive column of the discharge. Results presented in chapter 4 have shown that $NO^+$ is the dominant positive ion in a 6-12-82, $CO_2$-$N_2$-He mixture over the 2-20 torr pressure range, for a gas residence time in the discharge of greater than 100 ms. However, when a small amount of hydrogen is present (1.5%), ions of the $H_3O^+.(H_2O)_n$ (n=0,1,2) series dominate under most conditions.

Analysis of the variation of positive ion species in the discharge with current, pressure and gas flow rate has led to the following reaction scheme,

$$e \xrightarrow{CO_2} CO_2^+ \xrightarrow{O_2} O_2^+ \xrightarrow{NO} NO^+$$

$$CO_2^+ \xrightarrow[H_2]{H_2O} HCO_2^+ \xrightarrow[H_2O]{} H_3O^+ \xrightarrow[H_2O]{M} H_3O^+.(H_2O) \xrightarrow[H_2O]{M} H_3O^+.(H_2O)_2$$

This scheme indicates the importance of residual impurities ($H_2O$) and discharge-produced impurities ($O_2$,NO) on the ion chemistry. Also, the resultant ion species ($NO^+$ and $H_3O^+.(H_2O)_n$) are produced from a series of

rapid ion-molecule reactions rather than from direct ionisation of impurities.

Negative ion species and their densities in $CO_2$ TEA laser and EDCL discharges have been determined computationally. Results for the TEA laser show that the ratio of negative ion density to electron density reaches $\sim$ 0.05 for a 10-10-80, $CO_2$-$N_2$-He gas mixture. The presence of greater than 0.5% $O_2$ or 2% $H_2O$ in the gas mixture significantly increases the negative ion density (by at least a factor of two). Dominant negative ions are $CO_3^-$ for a "clean" gas, $CO_4^-$ for greater than 0.5% $O_2$ contamination, and $H^-$ and $CO_3^-$ for 2% water vapour contamination.

The theoretical calculations of negative ion densities have been compared with experimental results obtained in a $CO_2$ TEA laser. Oxygen addition to a flowing $CO_2$-$N_2$-He gas mix where the gas is completely replaced between pulses, has shown that arcing (ie discharge instability) commences when 0.5 - 2% $O_2$ is present, the exact amount depending on the $CO_2$:$N_2$:He ratios in the mixture. This correlates well with calculated increases in the negative ion density with $O_2$ present, and confirms the influence of negative ions on plasma stability.

The effect of $H_2O$ addition to an experimental system has been determined by adding $H_2$ to a sealed laser. The $H_2O$ is formed by plasma-chemical reaction and has been calculated to constitute $\sim$ 1-3% of the gas mix when arcing commences. As for $O_2$, the exact amount depends on the gas mixture.

Since the formation of negative ions, and the associated discharge arcing, is enhanced by the presence of $O_2$, for a long-life, arc-free, sealed $CO_2$ TEA the amount of $O_2$ formed from $CO_2$ dissociation must be limited to $\lesssim$ 1%. This may be achieved by judicial addition of CO and $H_2$ as discussed in chapter 6.

Negative ion densities in an EDCL discharge have been calculated for a 5-15-80, $CO_2$-$N_2$-He gas mixture at 15 torr and 20 mA $cm^{-2}$. When fresh gas is flowed through the laser the dominant negative ion is $CO_3^-$, with a peak density of $\sim$ 0.5 times the electron density. When the gas is recirculated, and contaminants such as $O_2$, CO and oxides of nitrogen have accumulated due to plasma-chemical reactions, the ions $NO_2^-$ and $NO_3^-$ dominate. In this case the negative ion density exceeds the electron density for $\gtrsim$ 0.1% oxides of nitrogen in the gas.

The negative ions are formed on a time scale which correlates with the onset of plasma stabilities in experimental devices, as reported in the literature. Also, the faster development of negative ions in a recirculated-gas system is consistent with the more rapid instability growth rate observed in experimental devices employing recirculation.

An important feature of both the positive and negative results is the influence of impurity neutral species. In particular, $O_2$, $H_2O$ and the oxides of nitrogen play important roles in the ion chemistry of the discharge. Oxygen and oxides of nitrogen are formed by plasma chemical processes in sealed laser systems. Water vapour may be an additive to the basic $CO_2$-$N_2$-He mix or may be a residual impurity. Other impurity species which may exist in a practical laser system, due to residual pump oil vapour, outgassing from components, leaks, etc, may considerably alter the ion species. However, the reported results are believed to be representative of an initially clean system.

The results of experiments and analyses of ion production and loss processes reported in this thesis allow the inclusion of realistic ion species and densities in $CO_2$ laser models with greater certainty than has hitherto been possible. The general principles for determining positive

ions by mass spectrometry and negative ions by computation can be applied to other discharge-pumped gas laser systems.

Appendix I - The Ionisation Instability Criterion

The instability criterion for the occurrence of ionisation instability is derived in this appendix. The derivation is closely based on that of Nighan (1976), but the mathematics is presented in greater detail.

The conservation equations for electrons and negative ions are

$$\begin{aligned} \frac{dn_e}{dt} &= k_i N n_e - k_a N n_e + k_d N n_- - k_r^e n_e n_+ + NS \\ \frac{dn_-}{dt} &= k_a N n_e - k_d N n_- - k_r^i n_+ n_- \end{aligned} \qquad (A.1)$$

Assuming small fluctuations in the electron and negative ion densities of the form $\delta n_{e,-} = n_{e,-k} e^{i\omega t}$ and quasineutrality in the plasma ($n_+ = n_e + n_-$), the perturbed form of (A.1) is

$$\begin{aligned} \delta n_e(i\omega) &= \delta n_e\left[k_i N - k_a N - k_r^e n_+ - k_r^e n_e\right] + \delta n_-\left[k_d N - k_r^e n_e\right] \\ &\quad + N n_e\left[\frac{\partial k_i}{\partial E} - \frac{\partial k_a}{\partial E}\right]\delta E \\ \delta n_-(i\omega) &= \delta n_e\left[k_a N - k_r^i n_-\right] - \delta n_-\left[k_d N + k_r^i n_- + k_r^i n_+\right] \\ &\quad + N n_e \frac{\partial k_a}{\partial E}\delta E \end{aligned} \qquad (A.2)$$

$\delta E$ is the fluctuation in electric field associated with the charge density fluctuation.

Several manipulations are necessary to equation (A.2) to yield a simpler form. The first involves the steady state form of equations (A.1), ie equating time derivatives to zero. Thus,

$$\begin{aligned} k_i N - k_a N - k_r^e n_+ &= -\frac{1}{n_e}\left[k_d N n_- + NS\right] \\ \text{and} \qquad k_d N + k_r^i n_+ &= \frac{1}{n_-}\left[k_a N n_e\right] \end{aligned} \qquad (A.3)$$

The second simplification involves the partial derivatives, $\frac{\partial k}{\partial E}$.

Putting,

$$u = \ell n\ k, \quad \frac{du}{dk} = \frac{1}{k}$$
$$\text{and} \quad v = \ell n\ E, \quad \frac{dv}{dE} = \frac{1}{E} \tag{A.4}$$

$$\text{then} \quad \frac{dk}{dE} = \frac{dk}{du} \cdot \frac{du}{dv} \cdot \frac{dv}{dE}$$
$$= \frac{k}{E} \frac{d(\ell n\ k)}{d(\ell n\ E)}$$
$$= \frac{k \hat{k}}{E} \ .$$

The notation $\hat{k}$ is thus used to indicate a logarithmic derivative.

Equations (A.2) then become

$$\begin{aligned}
\frac{\delta n_e}{n_e}(i\omega) = &- \frac{\delta n_e}{n_e} \left[ \frac{n_e}{n_+} n_+ k_r^e + \frac{n_+}{n_e} N k_d + \frac{NS}{n_e} \right] \\
&+ \frac{\delta n_-}{n_-} \left[ \frac{n_-}{n_e} N k_d - \frac{n_-}{n_+} n_+ k_r^e \right] \\
&+ N \left[ k_i \hat{k}_i - k_a \hat{k}_a \right] \frac{\delta E}{E}
\end{aligned} \tag{A.5}$$

$$\begin{aligned}
\frac{\delta n_-}{n_-}(i\omega) = &\frac{\delta n_e}{n_e} \left[ \frac{n_e}{n_-} N k_a - \frac{n_e}{n_+} n_+ k_r^i \right] \\
&- \frac{\delta n_-}{n_-} \left[ \frac{n_-}{n_+} n_+ k_r^i + \frac{n_e}{n_-} N k_a \right] \\
&+ \left[ N \frac{n_e}{n_-} k_a \hat{k}_a \right] \frac{\delta E}{E}
\end{aligned}$$

The coefficients in equations (A.5) are written in terms of the characteristic times for the various processes. Thus $\tau_a = (N k_a)^{-1}$, $\tau_d = (N k_d)^{-1}$, $\tau_r^e = (n_+ k_r^e)^{-1}$, and $\tau_r^i = (n_+ k_r^i)^{-1}$ are the typical time scales of the attachment, detachment, electron-ion recombination and ion-ion recombination processes (Haas (1973)).

To simplify the subsequent algebra it is convenient to represent the coefficients of the perturbed quantities in equation (A.5) by

$$A_1 = \left[\frac{n_e}{n_+} n_+ k_r^e + \frac{n_-}{n_e} N k_d + \frac{NS}{n_e}\right]$$

$$A_2 = \left[\frac{n_-}{n_e} N k_d - \frac{n_-}{n_+} n_+ k_r^e\right]$$

$$A_3 = N\left[k_i \hat{k}_i - k_a \hat{k}_a\right] \qquad (A.6)$$

$$A_4 = \left[\frac{n_e}{n_-} N k_a - \frac{n_e}{n_+} n_+ k_r^i\right]$$

$$A_5 = \left[\frac{n_-}{n_+} n_+ k_r^i + \frac{n_e}{n_-} N k_a\right]$$

$$A_6 = \left[N \frac{n_e}{n_-} k_a \hat{k}_a\right].$$

Thus, equations (A.5) become,

$$\frac{\delta n_e}{n_e}(i\omega) = -A_1 \frac{\delta n_e}{n_e} + A_2 \frac{\delta n_-}{n_-} + A_3 \frac{\delta E}{E}$$

$$\frac{\delta n_-}{n_-}(i\omega) = A_4 \frac{\delta n_e}{n_e} - A_5 \frac{\delta n_-}{n_-} + A_6 \frac{\delta E}{E}. \qquad (A.7)$$

Substitution, for $\frac{\delta n_-}{n_-}$, from the second equation into the first, and solving in terms of $(i\omega)$ yields,

$$(i\omega)^2 + \left[A_5 + A_1 - A_3 \frac{\delta E}{E} \cdot \frac{n_e}{\delta n_e}\right](i\omega) + \left[A_1 A_5 - A_2 A_4 - (A_2 A_6 + A_3 A_5)\frac{\delta E}{E} \cdot \frac{n_e}{\delta n_e}\right] = 0 \qquad (A.8)$$

Noting that the perturbation was assumed to have the form $\sim e^{i\omega t}$, then a positive $(i\omega)$ will result in temporal amplification of a disturbance. The roots of equation (A.8) are given by

$$(i\omega) = \tfrac{1}{2}(-b \pm \sqrt{b^2 - 4c}) \qquad (A.9)$$

where

$$b = A_5 + A_1 - A_3 \frac{\delta E}{E} \cdot \frac{n_e}{\delta n_e} \qquad (A.10)$$

and $$c = A_1 A_5 - A_2 A_4 - (A_2 A_6 + A_3 A_5) \frac{\delta E}{E} \cdot \frac{n_e}{\delta n_e}$$

Several possible situations exist where instability may occur, ie $(i\omega) > 0$ (For example, when $b < 0$, or when b and c are of opposite sign). Having assumed perturbations in both electron and negative ion densities, the roots of equation (A.9) will correspond to instability in electron density (ionisation instability) or instability in negative ion density (negative ion instability) or instability in both densities simultaneously. The root corresponding to a temporal growth in electron density (ie that causing ionisation instability) may be identified by considering a plasma with no negative ions present. Thus $n_- = k_a = k_r^i = 0$, and equations (A.6) yield

$$A_1 = \frac{n_e}{n_+} n_+ k_r^e + \frac{NS}{n_e}$$

$$A_3 = N k_i \hat{k}_i \qquad (A.11)$$

$$A_2 = A_4 = A_5 = A_6 = 0 .$$

Substitution from (A.11) into (A.10) gives

$$b = \left[ \frac{n_e}{n_+} n_+ k_r^e + \frac{NS}{n_e} - N k_i \hat{k}_i \frac{\delta E}{E} \cdot \frac{n_e}{\delta n_e} \right]$$

and $c = 0$.

Thus, from equation (A.9) the roots are $(i\omega) = 0$ (no instability) or $(i\omega) = -b$. The condition for instability is then that $-b > 0$, and the ionisation instability mode is then identified with the condition $b < 0$.

Returning to the case where negative ions are present, the condition for instability that $b < 0$, yields, from (A.10)

$$-A_5 - A_1 + A_3 \frac{\delta E}{E} \cdot \frac{n_e}{\delta n_e} > 0$$

ie from equations (A.6)

$$\frac{\delta E}{E} \cdot \frac{n_e}{\delta n_e} N \left[ k_i \hat{k}_i - k_a \hat{k}_a \right] - \left[ \frac{n_e}{n_+} n_+ k_r^e + \frac{n_-}{n_e} N k_d + \frac{NS}{n_e} \right.$$

$$\left. + \frac{n_-}{n_+} n_+ k_r^i + \frac{n_e}{n_-} N k_a \right] > 0 \qquad (A.12)$$

Equation (A.12) presents the criterion for the occurrence of ionisation instability. The conditions under which such an instability may manifest itself in a $CO_2$ laser discharge are discussed in detail in section 1.5.1.

References

Haas R A, 1973, Phys Rev, A8, 1017.

Nighan W L, 1976, in "Principles of Laser Plasmas", ed Bekefi, Wiley, New York.

Appendix 2 - The Thermal Instability Criterion

The hydrodynamic equations describing neutral particle conservation and conservation of translational and vibrational energy density in a mixture of diatomic molecular and atomic gases are (Nighan (1976)),

$$\frac{DN}{Dt} + N\ \nabla.\underline{u} = 0 \qquad (B.1)$$

$$\frac{D(N\epsilon_T)}{Dt} + (N\epsilon_T + P)\nabla.\underline{u} = K\ \nabla^2 T + \frac{N_m}{\tau_{VT}}\left[\epsilon_V(T_V) - \epsilon_V(T)\right] + F_T JE \qquad (B.2)$$

$$\frac{D(N_m\epsilon_V)}{Dt} + (N_m\ \epsilon_V)\nabla.\underline{u} = F_V JE - \frac{N_m}{\tau_{VT}}\left[\epsilon_V(T_V) - \epsilon_V(T)\right] \qquad (B.3)$$

In the equations (B.1) - (B.3) $D/Dt = \partial/\partial t + \underline{u}.\nabla$ is the convective derivative (see for example Pao (1967)). The neutral particle density is N, u is the mass averaged gas flow velocity, P is the gas pressure, K is the coefficient of thermal conductivity, T is the gas temperature, $N_m$ is the density of molecular species in the gas, $\tau_{VT}$ is the characteristic time of vibrational-translational energy relaxation, $F_T$ and $F_V$ are the fractions of input power density (JE) coupled to translational and vibrational heating of the gas. The vibrational population of the molecular species is assumed to have a Boltzmann distribution amongst the vibrational energy levels, characterised by a vibrational temperature $T_V$. Thus the average vibrational energy per molecule is given by (Nighan (1977))

$$\epsilon_V = \frac{\in}{\exp(\in/kT_V)-1}\ , \qquad (B.4)$$

where $\in$ is the vibrational energy quantum. The average translational-rotational energy per particle is

$$\epsilon_T = \left(\frac{3}{2}X_a + \frac{5}{2}X_m\right)kT. \qquad (B.5)$$

Translational and rotational energies are assumed to be in

equilibrium at the gas temperature T. $X_a$ and $X_m$ are fractions of atomic and molecular species and k is Boltzmann's constant.

In equation (B.1) the derivative may be expanded so that the equation becomes

$$\frac{\partial N}{\partial t} + \underline{u}.\nabla N + N\nabla.u = 0,$$

or

$$\frac{\partial N}{\partial t} + \nabla.(N\underline{u}) = 0 \qquad (B.6)$$

The first term in (B.6) represents the temporal rate of change of the density of gas particles while the second describes the net change in particle flux into the volume. With no sources or sinks of particles in the volume, and no change in flow of particles into the discharge volume, the density of particles in the volume is constant.

Similarly, the net rate of change of translational-rotational energy and vibrational energy is given by the left hand sides in equations (B.2) and (B.3). In equation (B.2), the term $K\nabla^2 T$ represents the conduction of heat from the discharge by thermal diffusion. The terms $F_T JE$ and $F_V JE$ represent the fractional volumetric rate of energy input into gas heating and vibrational excitation, respectively. The quantity $\left[\varepsilon_V(T_V)-\varepsilon_V(T)\right]$ represents the average energy difference per molecule between a vibrationally excited and a ground state molecule; thus $N_m\left[\varepsilon_V(T_V)-\varepsilon_V(T)\right]/\tau_{VT}$ represents the rate of energy transfer between vibrational and translational motion. Hence, terms on the right hand sides of equations (B.2) and (B.3) describe the means by which gas heating and vibrational excitation are produced and dissipated.

Before considering the effect of coupled perturbations in gas density, translational and vibrational temperatures and their effect on the electron density, several comments are required. First, the gas pressure

($P = NkT$) will be assumed to remain constant during the perturbation (Haas (1973)). Thus density and gas temperature perturbations are related by $\delta N/N = -\delta T/T$. Second, the vibrational relaxation time $\tau_{VT}$ is assumed to be inversely proportional to gas density and to depend, in some way, on gas temperature ie $\tau_{VT}^{-1} = N\, f(T)$. Third, the fractions of input power density into translational heating ($F_T JE$) and vibrational heating ($F_V JE$) are assumed to depend on collisions between electrons and neutral particles. In this way energy from the electric field is coupled into translational and vibrational excitation, and the effect of ion-neutral particle collisions is neglected. Thus $F_T JE$ and $F_V JE$ are proportional to $n_e N$ and depend on the discharge E/N ratio (see figure 3.1 and section 1.3.1). Finally since electrons may gain energy from the electric field and lose energy in collisions on a time scale which is rapid in comparison with neutral particle processes, the mean electron energy (ie the discharge E/N) is assumed to adjust itself to any small change in N, T or $T_V$ sufficiently quickly that it may be regarded as having corrected itself before any significant growth or damping of the density or temperature fluctuation occurs. Thus the electron energy is considered constant during gas density or temperature fluctuations (Haas (1973)).

Considering a perturbation in gas density $\delta N$, and a resultant flow velocity perturbation $\delta u$, the particle conservation equation (B.1) yields the perturbed form

$$\frac{D(\delta N)}{Dt} + N\, \nabla.\underline{\delta u} = 0 \quad , \qquad (B.7)$$

The velocity profile is assumed uniform (ie $\nabla.\underline{u} = 0$) for volume-dominated discharges typical of high power molecular lasers.

Proceeding to treat fluctuations in gas density, electron density, gas temperature and vibrational temperature in the same way, equations (B.2) and (B.3) yield,

$$N\frac{D(\delta\varepsilon_T)}{Dt} + \varepsilon_T \frac{D(\delta N)}{Dt} + (N\,\varepsilon_T + N\,kT)\nabla.\underline{\delta u}$$

$$= K\,\nabla^2(\delta T) + \frac{\delta N_m}{\tau_{VT}}\left[\varepsilon_V(T_V) - \varepsilon_V(T)\right] + \frac{N_m}{\delta\tau_{VT}}\left[\varepsilon_V(T_V) - \varepsilon_V(T)\right]$$

$$+ \frac{N_m}{\tau_{VT}}\,\delta\left[\varepsilon_V(T_V) - \varepsilon_V(T)\right] + \delta(F_T JE) \qquad (B.8)$$

$$N_m\frac{D(\delta\varepsilon_V)}{Dt} + \varepsilon_V \frac{D(\delta N_m)}{Dt} + N_m\,\varepsilon_V\,\nabla.\underline{\delta u} = \delta(F_V JE)$$

$$- \frac{\delta N_m}{\tau_{VT}}\left[\varepsilon_V(T_V) - \varepsilon_V(T)\right] - \frac{N_m}{\delta\tau_{VT}}\left[\varepsilon_V(T_V) - \varepsilon_V(T)\right]$$

$$- \frac{N_m}{\tau_{VT}}\,\delta\left[\varepsilon_V(T_V) - \varepsilon_V(T)\right] \qquad (B.9)$$

It is now assumed that any fractional perturbation in molecular density is equal to that in total gas density, ie $\delta N_m/N_m = \delta N/N$. Also, the specific heats, $C_V$, $C_V^V$ and $C_P$ are introduced where

$$C_V = \frac{\partial\varepsilon_T}{\partial T} \qquad \text{(thus } \varepsilon_T = C_V T \text{ from equation (B.5))}$$

$$C_V^V = \frac{\partial\varepsilon_V}{\partial T_V}$$

and $$C_P = \gamma\,C_V = C_V + k$$

(where $\gamma$ is the ratio of specific heats and k is Boltzmann's constant). From equation (B.7) the substitution $\nabla.\underline{\delta u} = -\frac{1}{N}\frac{D(\delta N)}{Dt}$ may be made in (B.8) and (B.9) and since it is assumed that $\tau_{VT}^{-1} = Nf(T)$, then $\frac{1}{\delta\tau_{VT}} = \delta\,N\,f(T) + N\,\delta\,f(T)$. Finally since the energy fractions input to translation and vibration are proportional to the gas number density and electron density, then

$$\frac{\delta(F_V JE)}{(F_V JE)} = \frac{\delta(F_T JE)}{(F_T JE)} = \frac{\delta N}{N} + \frac{\delta n_e}{n_e} .$$

With these substitutions, equations (B.8) and (B.9) become

$$\frac{NC_P}{\gamma}\frac{D(\delta T)}{Dt} - \frac{(\gamma-1)}{\gamma}TC_P\frac{D(\delta N)}{Dt} = K\nabla^2(\delta T)$$
$$+ \frac{N_m}{\tau_{VT}}\left[\varepsilon_V(T_V) - \varepsilon_V(T)\right](2\frac{\delta N}{N} - \hat{\tau}_{VT}\frac{\delta T}{T}) + \frac{N_m}{\tau_{VT}}\left[C_V^V(T_V)\delta T_V - C_V^V(T)\delta T\right]$$
$$+ (F_T JE)(\frac{\delta N}{N} + \frac{\delta n_e}{n_e}) \qquad (B.10)$$

$$N_m C_V^V(T_V)\frac{D(\delta T_V)}{Dt} = -\frac{N_m}{\tau_{VT}}\left[\varepsilon_V(T_V) - \varepsilon_V(T)\right](2\frac{\delta N}{N} - \hat{\tau}_{VT}\frac{\delta T}{T})$$
$$- \frac{N_m}{\tau_{VT}}\left[C_V^V(T_V)\delta T_V - C_V^V(T)\delta T\right] + (F_V JE)(\frac{\delta N}{N} + \frac{\delta n_e}{n_e}) \quad (B.11)$$

In the above equations (B.10) and (B.11) the notation

$$\hat{\tau}_{VT} = \frac{d(\ell n\, \tau_{VT})}{d(\ell n T)} = \frac{T}{\tau_{VT}}\frac{d\tau_{VT}}{dT}$$

is used to indicate the logarithmic derivative of $\tau_{VT}$ with respect to gas temperature. Thus $\hat{\tau}_{VT}$ indicates the gas temperature dependence of the vibrational relaxation rate (eg $\tau_{VT} \propto T^{-3}$ gives $\hat{\tau}_{VT} = -3$).

Assuming perturbations in the gas temperature are related to gas density perturbations by $\delta N/N = -\delta T/T$ (ie constant pressure), the equations (B.10) and (B.11) may be linearised by taking perturbations of the form $e^{i(\omega t - k'x)}$ (see Appendix 1). Thus equations (B.10) and (B.11) yield, after some simplification,

$$\frac{\delta T}{T}(i\omega) = -\frac{Kk'^2}{NC_P}\frac{\delta T}{T} - \frac{N_m\left[\varepsilon_V(T_V) - \varepsilon_V(T)\right]}{\tau_{VT}\, N\, C_P\, T}(2 + \hat{\tau}_{VT})\frac{\delta T}{T}$$
$$+ \frac{N_m}{NC_P T\,\tau_{VT}}\left[C_V^V(T_V)\delta T_V - C_V^V(T)\delta T\right] - \frac{(F_V JE)}{NC_P T}(\frac{\delta n_e}{n_e}\frac{N}{\delta N} + 1)\frac{\delta T}{T} \qquad (B.12)$$

$$\frac{\delta T_V}{T_y}(i\omega) = \frac{N_m\left[\varepsilon_y(T_V) - \varepsilon_y(T)\right]}{\tau_{VT} n_m C_V^V(T_V) T_V}(2 + \hat{\tau}_{VT})\frac{\delta T}{T}$$

$$- \frac{N_m\left[C_y^V(T_y)\,\delta T_V - C_V^V(T)\,\delta T\right]}{\tau_{yT} T_y\, N_m\, C_y^V(T_y)} - \frac{F_V JE}{N_m C_y^V(T_y) T_y}\left(\frac{\delta n_e}{n_e}\frac{N}{\delta N} + 1\right)\frac{\delta T}{T}. \quad (B.13)$$

These equations may be further simplified by making use of the steady state form of the vibrational energy equation (B.3) (ie left hand side set equal to zero),

$$\frac{N_m}{\tau_{yT}}\left[\varepsilon_y(T_y) - \varepsilon_y(T)\right] = F_y JE. \quad (B.14)$$

Also, since the vibrational temperature $T_y$ is much greater than the gas temperature T, for the non-equilibrium conditions of a molecular gas discharge, from equation (B.4) $\varepsilon_y(T_y)$ is much greater than $\varepsilon_y(T)$. Thus $C_y^V(T)$ may be neglected in comparison with $C_y^V(T_y)$.

Equations (B.12) and (B.13) become

$$\frac{\delta T}{T}(i\omega) = A_1\frac{\delta T}{T} + A_2\frac{\delta T}{T} + A_3\frac{\delta T_y}{T_y} + A_4\frac{\delta T}{T}$$

$$\frac{\delta T_y}{T_y}(i\omega) = B_1\frac{\delta T}{T} + B_2\frac{\delta T_y}{T_y} + B_3\frac{\delta T}{T} \quad (B.15)$$

where

$$A_1 = -\frac{Kk}{N C_p}$$

$$A_2 = -\frac{\left[F_y JE(2 + \hat{\tau}_{yT}) + C_y^V(T)\frac{N_m}{\tau_{VT}} T\right]}{NC_pT}$$

$$A_3 = \frac{N_m C_y^V(T_y) T_y}{NC_pT\,\tau_{yT}}$$

$$A_4 = -\frac{F_T JE}{NC_pT}\left(\frac{\delta n_e}{n_e}\cdot\frac{N}{\delta N}\right) \quad (B.16)$$

$$B_1 = \frac{\left[F_y JE(2 + \hat{\tau}_{yT}) + \frac{C_y^V(T)\, N_m T}{\tau_{yT}}\right]}{N_m\, C_y^V(T_y) T_y}$$

$$B_2 = -\frac{1}{\tau_{yT}}$$

$$B_3 = - \frac{F_V JE}{N_m C_y^V(T_y) T_y} \left( \frac{\delta n_e}{n_e} \cdot \frac{N}{\delta N} \right)$$

(It is assumed in deriving the coefficients $A_4$ and $B_3$ that any instability will be such that the maximum fractional change in electron density ($\delta n_e / n_e$) will accompany a change in gas number density ($\delta N/N$) and the term $\left( \frac{\delta n_e}{n_e} \frac{N}{\delta N} \right) > 1$.)

The fractional temperature perturbations $\delta T/T$ and $\delta T_y/T_y$ may be eliminated from equations (B.15) to yield a quadratic equation for the instability growth rate, $\omega$ (see Appendix 1). Thus the roots are

$$\omega = - \frac{b}{2} \pm \tfrac{1}{2} \sqrt{b^2 - 4c} \tag{B.17}$$

where
$$b = A_1 + A_2 + A_4 + B_2 \tag{B.18}$$

and
$$c = B_2(A_1 + A_2 + A_4) - A_3(B_1 + B_3)$$

Assuming almost all input power is dissipated as gas heating or vibrational excitation (ie $F_T + F_y \simeq 1$) then the coefficients b and c are

$$b = (NC_pT)^{-1} \left[ Kk'^2 T + \frac{NC_pT}{\tau_{yT}} + F_y JE(2 + \hat{\tau}_{yT}) + F_T JE \left( \frac{\delta n_e}{n_e} \cdot \frac{N}{\delta N} \right) \right] \tag{B.19}$$

$$c = \frac{(NC_pT)^{-1}}{\tau_{yT}} \left[ Kk'^2 T + JE \left( \frac{\delta n_e}{n_e} \cdot \frac{N}{\delta N} \right) \right] \tag{B.20}$$

Conditions corresponding to temporal growth of an initial disturbance in gas density or temperature ($\omega > 0$) are such that either $b<0$, or b and c are of opposite sign (see Appendix 1). These two instability modes may be identified by setting the input power density (JE) equal to zero. Thus, equations (B.19) and (B.20) yield

$$b = \frac{Kk'^2}{NC_p} + \frac{1}{\tau_{yT}}$$

$$c = \frac{Kk'^2}{NC_p \tau_{yT}} \tag{B.21}$$

Substitution of (B.21) into (B.17) shows that the two roots when JE = 0 are $-Kk'^2/NC_p$ and $-1/\tau_{VT}$. The first root ($-Kk'^2/NC_p$) is the rate at which thermal disturbances are damped by heat conduction. The second root ($-1/\tau_{VT}$) is the rate at which perturbations in the vibrational equilibrium are damped by vibrational-translational relaxation. Thus, when JE $\neq$ 0, the roots of equation (B.17) correspond to either growth ($\omega>0$) or damping ($\omega<0$) of thermal or vibrational disturbances.

Thermal instability (temporal growth of T) and vibrational instability (temporal growth of $T_V$) may occur individually or simultaneously. When b is negative and c is positive then both roots of equation (B.17) will be positive (simultaneous instabilities), but when b and c are both negative, or b is positive and c is negative, only one instability occurs. By considering the case of an atomic gas only ($F_V \to 0$, $\tau_{VT} \to \infty$) then equation (B.20) shows that c = 0 when no vibrational excitation can occur. Thus, since only thermal instability is possible, this instability must correspond to the case when $b < 0$. Hence, when $b < 0$, the thermal instability grows; when $b > 0$, $c < 0$, the vibrational instability grows and when $b < 0$, $c > 0$, both instabilities can occur simultaneously.

As is discussed in section 1.5.2, the occurrence of the thermal instability requires that $(\frac{\delta n_e}{n_e} \cdot \frac{N}{\delta N}) < 0$, otherwise the condition $b < 0$ cannot be fulfilled. Calculations (Nighan and Wiegand, (1974)) have shown that such a requirement may be readily satisfied for $CO_2$ laser discharges. Indeed the response of the electron density to gas density perturbations is so great ($\frac{dn_e}{n_e} \cdot \frac{N}{\delta N} \sim -100$) that the value of c in equation (B.20) is almost always negative. Similarly the effect of the $(\frac{\delta n_e}{n_e} \cdot \frac{N}{\delta N})$ term in equation (B.19) is such that $b < 0$, thus satisfying the criterion for thermal instability. Hence the thermal instability is of

particular relevance to $CO_2$ lasers and is discussed in detail in section 1.5.2.

References

Haas R A, 1973, Phys Rev, A8, 1017.

Nighan W L, 1976, in "Principles of Laser Plasmas", ed Bekefi, Wiley, New York.

Nighan W L, 1977, Phys Rev, A15, 1701.

Nighan W L and Wiegand W J, 1974, Appl Phys Lett, 25, 633.

Pao R H F, 1967, "Fluid Dynamics", Merrill, Columbus, Ohio.